Gallium-essential applications of Gallium-67 and Gallium-68

Darwesh, Afnan

Awarding institution:
King's College London

Gallium-Essential Applications of Gallium-67 and Gallium-68

A thesis submitted by

Afnan Darwesh

PhD in Molecular Imaging

2021

School of Biomedical Engineering and Imaging Sciences

King's College London

Abstract

Over the past decades, Ga^{3+} application in medicine has become significant, based in many respects on its similarity in some aspects to Fe^{3+}. The difference between the two metals renders gallium interesting as potential therapeutic agent to disturb iron demand in cells and pathogens. The availability of radioactive gallium (^{68}Ga and ^{67}Ga) helps facilitate the use of gallium as an iron mimic for radionuclide imaging purposes. The current work is composed of two main projects dealing with different aspects of ^{68}Ga/^{67}Ga in medical imaging, with the common theme of involving gallium-specific biology.

Fe^{3+} siderophore complexes are taken up by bacteria making their isostructural Ga^{3+} complexes applicable, in principle, for imaging infection. Desferrioxamine-B (DFO) is a siderophore and a clinically accepted drug, hence, it can be radiolabelled with ^{68}Ga and tested clinically for imaging graft infection with low regulatory barriers for use in humans. In the first part of this project, [^{68}Ga]Ga-DFO was radiolabelled using GMP-graded reagents. [^{68}Ga]Ga-DFO stability in human serum and urine was assessed *in vitro*. [^{68}Ga]Ga-DFO *in vivo* biodistribution was studied in healthy animal models after i.v. injection. [^{68}Ga]Ga-DFO was labelled with high radiochemical purity (≥ 95%). [^{68}Ga]Ga-DFO demonstrated no binding to serum proteins *in vitro* and rapid renal excretion and low blood retention *in vivo*. *Ex vivo* biodistribution showed most of the activity resided in urine. However, incubating [^{68}Ga]Ga-DFO in urine samples *in vitro* showed formation of metabolites which increase with time. We concluded that [^{68}Ga]Ga-DFO is stable in blood during the timescale investigated and degradation occurred in urine. Overall, [^{68}Ga]Ga-DFO can be easily radiolabelled for evaluation clinically as infection imaging agent.

Tris(8-hydroxyquinoline) gallium (III) (KP46) has been investigated as an orally administered anti-cancer drug. KP46 was developed on the rationale of better gut absorption and tumour effect compared to orally administered gallium salts. Despite preclinical and clinical evaluation of its efficacy, its trafficking to tumours remains poorly understood. In the second part of this project, [^{68}Ga/^{67}Ga]KP46 was used to elucidate the biological behaviour of KP46 *in vivo* post oral and i.v. administration as tracer or combined with a pharmacologically relevant dose of KP46. [^{68}Ga/^{67}Ga]KP46 was synthesised and its binding to apo-transferrin and albumin was measured *in vitro* by size exclusion chromatography. [$^{68/67}$Ga]KP46 was giving i.v. or orally, as a tracer or combined with KP46. Mice were PET/CT scanned and culled for *ex-vivo* biodistribution. Octanol extraction and tissue digestion was performed on tissue samples to determine the form of $^{68/67}$Ga and to measure stable ^{69}Ga by ICP-MS. [$^{68/67}$Ga]KP46 showed no binding to apo-transferrin and minimal binding to albumin indicating the stability of [$^{68/67}$Ga]KP46. Post i.v. injection of [^{68}Ga]KP46 as tracer, most of the activity was seen in the liver, owing to its lipophilicity. Post oral administration of [$^{68/67}$Ga]KP46 as tracer or with KP46, radioactivity remained in the large

intestine with minimal trafficking to other tissues at 4 hours. At 24 hours post oral administration, the group administered with [^{67}Ga]KP46 combined with KP46 showed better gut absorption compared to the group administered with [^{67}Ga]KP46 as a tracer. However, delivery of ^{67}Ga to tumour and other tissues was still low. All measurable radioactivity in tissue samples was no longer in the form of [$^{68/67}$Ga]KP46. ICP-MS measurement of ^{69}Ga in tissue samples was consistent with $^{68/67}$Ga trafficking results. We concluded that KP46 does not enhance gallium gut absorption compared to gallium salts after single oral dose and does not deliver gallium significantly to tumour. However, KP46 trafficking could be further investigated in the future after prolonged oral administration. In addition, the delivery of 8-hydroxyquinoline to tumour cells could be investigated as an active component to KP46 mode of action.

Finally, in the third part of this project, we investigated multiple conditions for radiolabelling ^{68}Ga with 8-hydroxyquinoline and some of its derivatives aiming to find the best chemical form to deliver ^{67}Ga into cells and study its radiobiology as an Auger electron emitter therapeutic radionuclide. Among ligands investigated, thiooxine complex of ^{68}Ga showed the highest cellular uptake. However, more studies such as protein binding and cellular efflux should be conducted to understand the complex biological behaviour.

Declaration

I Afnan Darwesh confirm that no part of this thesis has been submitted in support of any other application for a degree or qualification of King's College London, or any other university or institute of learning. I confirm that this work is my own. Where information has been derived from other sources it has been indicated in this thesis.

Acknowledgments

First and foremost, my deepest gratitude goes to my supervisor Professor Phil Blower, who, over the past three years, not only guided me through my PhD journey but also taught me how to be a better scientist, enabling me to produce work that I am proud of. Thank you for your feedback, patience, and encouragement during my research and the writing of my thesis. I am privileged to have had the opportunity to work under your supervision. Finally, thank you for creating the best and most collaborative work environment that I have ever been a part of.

I would also like to thank my second supervisor, Dr Michelle Ma, who has always been supportive and provided the necessary resources for me to accomplish my work. Thank you for giving me the opportunity to be a part of your wonderful group. Thank you for all your chemistry lessons and inspiring discussions.

I would like to thank Dr Kavitha Sunassee, Dr Jayanta Bordoloy, Dr Jana Kim, Dr Francis Man, and Dr Fahad Al-Salemee for the help they provided during the preclinical studies. I am incredibly grateful for your support and advice. Special thanks go to Dr Julia Blower, who helped me so much during the beginning of my PhD journey. I still remember my first day in the labs and how you were so patient in teaching me, even though I was incredibly nervous. Your help and time were much appreciated. To Dr Cinzia Imberti, thank you for always being available to answer my many questions (especially chemistry related). Thank you for proofreading my writing and for giving me feedback. I am also thankful to Dr Margaret Cooper and Dr Ruslan Cusnir for their help with radiolabelling and HPLC. My sincere thanks to the lab management team Dr David Thakor, Dr Matthew Hutchings, Dr Maxwell Handley and Dr Lisa Sanderson for their support and effort to make the labs run smoothly.

Thank you to my colleagues George Firth, Alex Rigby, Joanna Bartnicka, Matthew Farleigh, George Keeling, Azalea Khan, Ingebjorg Hungnes, Jessica Jackson, Dr Elise Verger and Dr Mauricio Da Silva Morais. I could not have asked for a better team to work with and share my science passion. Thank you for helping me get through long days of experiments with such enjoyable conversations and laughs.

A special thanks to my flatmate Sabrina Semidei. Thank you for making our home a quiet (ish) and nice environment for me to write my thesis. Thank you for the pizza and movie nights you created to cheer me up. To my friend Afnan Malaih, who has been with me every step of the way. You have supported me even when I was at my worst. You were an exceptionally good listener and knew how to make me laugh. Thank you for the long walks and endless coffee breaks you had to take with me.

To my parents, no words can describe the love and support you have given me throughout my life. Thank you both for giving me the strength to chase my dream, I could not have done this without you. I'm so sorry for answering 'I cannot' whenever you asked me to come home. However, I am so excited to have more time to spend with you again.

I would also like to thank my sister Dalya, who encouraged me with her kind words and supported me throughout. To my sister Reem, thank you for knowing exactly what to say to get me through difficult times. To my best friend, sister and role model, Bayan, I don't think I can thank you enough for being my rock and standing by my side no matter what. Thank you for answering my daily phone calls (well, sometimes more than once a day).

To my husband, Amr, thank you for encouraging me to chase my dream even though we would be exactly 2948 miles apart. Thank you for being selfless and putting up with me through this tough period of my life. I cannot wait to start new adventures with you, and I know that I will be OK facing whatever difficulties arise throughout my life if we face them together.

Finally, I would like to acknowledge the Saudi Arabian Cultural Bureau for the funding that supported this work.

Table of Contents

List of Abbreviations

Abbreviation	Meaning
µ-XAS	X-ray absorption spectroscopy
18F-FDG	Fluorine-18-fluorodeoxyglucose
8HQ	8-hydroxyquinoline
A427	Non-small lung carcinoma cells
ATCC	American type cancer collection
BAX	Bcl-2-associated X (BAX) protein
Bfr	Bacterioferritin
BPS	Bathophenanthroline sulfonate
CaCo-2	Human intestinal cells
CCRF-CEM	T-cell lymphoma
CFU	Colony forming unit
CHO	Chinese hamster ovary cells
Cp	Ceruloplasmin
CT	Computed tomography
DcytB	Duodenal cytochrome B
DFO	Desferrioxamine-B
DMT1	Divalent metal transporter 1
DoHH2	B-cell lymphoma
EMT-6/UW	Mouse sarcoma cells
Fbp	Ferric-binding protein
FBS	Fetal bovine serum
FDA	Food and drug administration
Fep	Ferric enterobactin permease
FPN1	Ferroportin
Ftn	Ferritin

Abbreviation	Meaning
FUO	Fever of unknown origin
Ganite	FDA approved gallium nitrate
GMP	Good manufacturing practice
H1299	Non-small lung carcinoma cells
HCP1	Haem-carrier protein 1
HCT-116	Human colon cancer
HeLa	Human cervical cancer cells
Heph	Hephaestin
HL60	Human leukemic cells
HMPAO	Hexamethylpropylene-amine oxime
HO-1	Haem oxygenase 1
HPLC	High-performance liquid chromograph
IC50	Half-maximum inhibitory concentration
ICP-MS	Inductively coupled plasma mass spectrometry
Isd	Iron regulated surface determinant
iTLC	Instant thin-layer chromatography
KP46	Tris (8-hydroxyquinolinato) gallium (III)
Lbp	Lactoferrin-binding proteins
LC/MS	Liquid chromatography/ mass spectrometry
Lcn2	Lipocalin 2
LD50	Median lethal dose
LF	Lactoferrin
LGP	Labile gallium pool
LIP	Labile iron pool
MCF-7	Human breast cancer cells
MDA-MB-231	Human breast cancer cells

Abbreviation	Meaning
MIP	Maximum intensity projection
MoAb	Monoclonal antibody
MRI	Magnetic resonance imaging
MTD	Maximum tolerated dose
NCI	National Cancer Institute
NMR	Nuclear magnetic resonance
NTBI	Non-transferring-bound iron
PBMCs	Human peripheral blood mononuclear cells
PBP	Periplasmic binding proteins
PBS	Phosphate buffered saline
PC3	Human prostatic adenocarcinoma cells
PET	Positron emission tomography
RBC	Red blood cells
RCP	Radiochemical purity
ROS	Reactive oxygen species
siRNA	Short-interfering RNA
SPECT	Single photon emission computed tomography
SUV	Standardised uptake value
Tbp	Transferrin-binding proteins
Tf	Transferrin
TfR1	Transferring receptor 1
THP	Tris (hydroxypyridinone)
TRPC6	Transient receptor potential cation channel
UIBC	Unsaturated iron-binding capacity
WBC	White blood cells
XANES	X-ray absorption near edge structure

1 Gallium: chemistry, radiochemistry, and bio-similarity to iron

1.1 Introduction

Gallium (Ga) is a non-physiological metal that belongs to group 13, in the 4th period of the periodic table with atomic number 31.[1] Over the past three decades, gallium compounds have become significant for their application in medicine.[2] Many of these applications are driven by some similarities of Ga^{3+} to ferric iron (Fe^{3+}) in chemistry and biology.[3] Research has demonstrated that the ionic radius of Ga^{3+} is similar to that of Fe^{3+}: 0.620 Å for its octahedral ionic radius and 0.47 Å for its tetrahedral ionic radius. The octahedral ionic radius of high spin Fe^{3+} is 0.645 Å and its tetrahedral ionic radius is 0.49 Å. The ionisation potential for Ga^{3+} is 64 eV and for Fe^{3+} is 54.8 eV. The electron affinity values of Ga^{3+} are 30.71 eV and are 30.65 eV for high spin Fe^{3+}.[4] The similarities between the two metals has influenced the diagnostic application of gallium-67 (^{67}Ga) for tumours (especially lymphomas) and infections, and encouraged the investigation of non-radioactive gallium compounds as therapeutic agents against cancers.[5] Ongoing studies have revealed potential linkages between gallium and iron in cellular metabolism, and contributed to the investigation of gallium binding to iron-binding proteins and chelators, including siderophores.[3,5]

Although Fe^{3+} and Ga^{3+} share some similarities, they differ in other aspects. Unlike Fe^{3+}, Ga^{3+} is not reduced to Ga^{2+} under physiological conditions, and it does not undergo redox chemistry within the cell.[6] The inability of Ga^{3+} to be reduced to Ga^{2+} prevents its participation to binding to molecules such as haem and haemoglobin, as Fe^{2+} does.[3] In addition, gallium is typically found in its Ga^{3+} oxidation state, which dominates its aqueous chemistry. Free hydrated Ga^{3+} cations in aqueous solution are stable, but only under acidic conditions.[1] Between pH values of 3–7, hydrated Ga^{3+} undergoes hydrolysis to insoluble gallium hydroxide [$Ga(OH)_3$] when stabilising ligands are not present. Within the basic pH range, [$Ga(OH)_3$] is re-solubilised as gallate [$Ga(OH)_4$]$^{-1}$. For example, at physiological pH (7.4), Ga^{3+} has a solubility of 1 µM as [$Ga(OH)_4$]$^{-1}$, with a small amount of [$Ga(OH)_3$] (< 2%).[3,7–10] On the contrary, Fe^{3+} has low solubility at physiological pH (10^{-6}–10^{-12} µM) indicating the absence of biomedical reactions of Fe^{3+} which can only exist when bound with a protein or chelate. Unlike Fe^{3+}, the solubility of Ga^{3+} at physiological pH allows some concentration of unbound gallate to exist in plasma, which may allow some biomedical reactions that are not possible for Fe^{3+}.[3,7,9,11]

Gallium *in vivo* trafficking is fundamentally important to this research. To understand the *in vivo* biodistribution and pharmacokinetics of gallium, and its mechanism of tissue uptake, it is critical to explore its mechanism of delivery and trafficking at the cellular level. The availability of radioactive gallium has facilitated the knowledge of gallium biodistribution and trafficking. This

chapter will briefly review the most common gallium radioisotopes and the types of tomography used to scan them. This chapter will also review the current understanding of gallium and the nature of its competition with iron as it occurs in biologic systems, including transferrin binding, cellular uptake, pharmacokinetics and biodistribution.

1.2 The isotopes of gallium

There are large number of gallium isotopes. ^{69}Ga and ^{71}Ga are the two stable and naturally occurring nonradioactive isotopes with naturally occurring abundances of 60.11% and 39.89%, respectively. ^{66}Ga, ^{67}Ga, ^{72}Ga and ^{68}Ga are the most common radionuclides prepared by either cyclotron production or generator elution. Table 1.1 contains additional information about the most common radionuclides. Gallium radionuclides possess decay properties suitable for performing studies related to clinical positron emission tomography (PET) and single photon emission computed tomography (SPECT) imaging.[1] Among the previously mentioned radioisotopes, ^{67}Ga and ^{68}Ga will be discussed in this chapter, due to their relevance to the overall research project. However, PET and SPECT imaging will be addressed briefly before discussing the different gallium radioisotopes.

Radioisotope	Half-life	Decay method	Abundant Decay energy (keV)	Daughter product	Preparation	Reference
^{66}Ga	9.5 hours	43 % EC 57 % β+	4153 (β+) 511 (γ)	Stable ^{66}Zn	cyclotron	12,13
^{67}Ga	78.3 hours (3.3 days)	Electron capture (EC)	(γ): 91 (2.9%), 93 (36%), 185 (20%), 209 (2.2%), 300 (16%), and 394 (5%) Auger electron: 7.4, 8.4, and 9.4	stable ^{67}Zn	cyclotron	1,10,14
^{68}Ga	67.71 minutes (1.13 hours)	11 % EC 89 % β+	1899 (β+) 511 (γ)	stable ^{68}Zn	^{68}Ge/^{68}Ga generator	1,14
^{72}Ga	14.25 hours	β-	β-: 640 and 950 γ: 840, 2210, 2510, and 630	Stable ^{72}Ge	cyclotron	15

Table 1.1: The most common radioisotopes of Ga.

1.3 SPECT vs PET

SPECT and PET are tomographic radionuclide imaging modalities that have contributed considerably to the field of nuclear medicine and molecular imaging by representing the distribution and accumulation of gamma and positron emitter radionuclides. After administering to patients, gamma emitter isotopes can be detected by SPECT using an external gamma camera. Positron emitter isotopes have different decay properties, yet have some similarity in imaging to gamma emitter isotopes.[16] PET radioisotopes emit positrons that travel small distances (a few millimetres) before interacting with electrons where they are annihilated. When positrons and electrons interact, their mass is converted into two 511 keV gamma photons at an approximately 180° angle. Gamma photons can then be detected by PET external ring-shaped detectors (Figure 1.1).[16,17]

SPECT and PET have higher sensitivity than other contrast agent-based imaging modalities based on their ability to detect the biodistribution of radiotracer concentration (at pM or nM concentrations) and provide functional information at the physiological or biochemical level.[17,18] However, the low resolution of anatomical information (not related to the radiotracer) revealed in SPECT and PET images is considered a limitation in both imaging modalities.[19] Anatomical modalities such as computed tomography (CT) and magnetic resonance imaging (MRI), based on their high spatial resolution, can provide the morphological precision that SPECT and PET lack.[18] Combining morphological and functional imaging modalities in hybrid scanners such as SPECT/CT, PET/CT and PET/MRI has allowed improvement in diagnostic process and outcomes.[18,20]

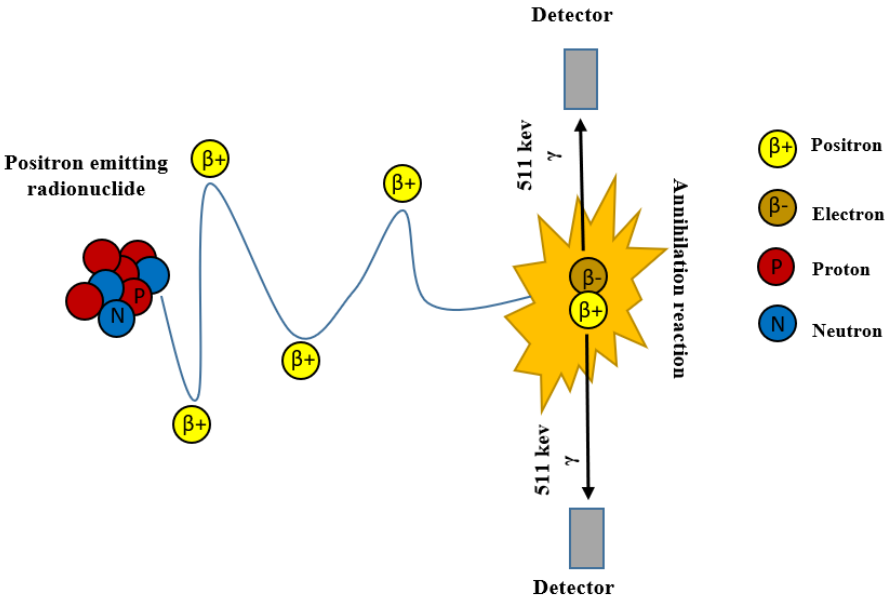

Figure 1.1: A positron is emitted from an atomic nucleus and interacts with an electron. The annihilation reaction causes the creation of two opposite direction 511 keV gamma rays that are detected by detectors on the opposite sides of the object (grey rectangles).

1.3.1 Gallium-67

^{67}Ga is cyclotron-produced and has a half-life of 78.3 hours. It decays by electron capture to stable ^{67}Zn, and during this decay process it emits multiple gamma rays to reach its stable state (Table 1.1).[1,10,14] As a gamma photon emitter, ^{67}Ga can be used for multiple diagnostic applications with planar and SPECT imaging. The earliest reported medical application of ^{67}Ga compounds was during the 1960s when ^{67}Ga (as a carrier free ^{67}Ga citrate) was injected intravenously (i.v.) into laboratory animals and found to concentrate in tumours.[2,5,21] This observation subsequently led to a nuclear medicine procedure for lymphoma and inflammation imaging.[2,5]

However, the multiple gamma photons produced by ^{67}Ga can limit image quality when compared to other SPECT metal radioisotopes, such as technetium-99m (^{99m}Tc), that emit a single 140 keV gamma photon.[14,22] During a ^{67}Ga scan, an energy window is set on the wide range of ^{67}Ga predominant gamma energies (93, 185, and 300 keV), causing detection of down-scattered high energy photons falling into a lower energy photopeak. Scatter photons in the imaging projection can decrease the resolution and contrast in the region of interest.[22–25]

In addition to ^{67}Ga gamma emission for planar and SPECT imaging, ^{67}Ga emits Auger electrons and thus has potential as a therapeutic radionuclide.[26] Most of Auger electrons are < 25 keV in energy and travel only short ranges (μm to nm distances) in tissues. The short distance travelled by these electrons allow high linear energy deposition in tumours, especially if they are internalised or in a close proximity to the target.[14,27] Although ^{67}Ga emits Auger electrons, its application as a therapeutic radionuclide is minimal due to its low incorporation into most cells in uncomplexed form. It has been suggested that ^{67}Ga may provide higher cytotoxic effect if internalised within cells. The recent developments of multiple chelators, including tris(hydroxypyridinone) (THP), allow simple kit-based radiolabelling with gallium radionuclides at high specific activity, and renew the opportunities for ^{67}Ga as a therapeutic radionuclide.[26,28] Attempts have been made to test the cytotoxic effect of ^{67}Ga as an Auger electron-emitting radionuclide after attaching it to the antibody trastuzumab by conjugation to THP, to target HER2 receptors in the breast cancer cell line, and with 8-hydroxyquinoline (oxine) in multiple cancer cell lines. ^{67}Ga showed higher cytotoxic effect when incorporated into cells when presented as [^{67}Ga]Ga-THP- trastuzumab or [^{67}Ga]Ga-oxine, compared to [^{67}Ga]Ga-THP and ^{67}Ga citrate which did not significantly bind to cells [26,28] (more details in chapter 4).

1.3.2 Gallium-68

Over the past two decades, clinical interest in ^{68}Ga has grown. This has largely been due to ^{68}Ga generator production, the availability of commercial generators, and its relatively short half-life of 68 minutes.[29] ^{68}Ga is produced from germanium-68/gallium-68 generators that have a long half-life ($t_{½}$ (^{68}Ge) = 270.95 days), allowing one to two years of shelf life depending on the amount of radioactivity loaded. ^{68}Ge decays by electron capture to ^{68}Ga, which in turn decays by positron emission (89%, E_{max} = 1899 keV) to stable ^{68}Zn.[12] As a positron emitter, ^{68}Ga can be used for multiple imaging application with PET imaging. Although ^{68}Ga generator production is quite convenient, allowing for continuous presence of radionuclides and on-site radiolabelling, the presence of trace metal impurities in the elution (such as natural titanium, aluminium, iron, and impurities from the parent and daughter radionuclide, ^{68}Ge and ^{68}Zn, respectively) are a disadvantage. The presence of impurities in the elution can compete with ^{68}Ga in radiolabelling and consequently reduce ^{68}Ga radiolabelling yields or molar activity.[1,30] Although the short half-life of ^{68}Ga makes it inconvenient for widespread shipping, and it is almost compulsory to possess a local generator, its half-life is long enough for preparation, purification and imaging of molecular probes as long as their pharmacokinetics are relatively fast. For example, ^{68}Ga is well-suited for the fast pharmacokinetics of peptides and can be used to radiolabel peptides through bifunctional chelators for receptor targeting imaging.[29,31,32,33]

1.4 The similarities and differences of Fe^{3+} and Ga^{3+}

Gallium shares some properties with iron, permitting it to bind to some iron-binding proteins and biomolecules and be taken up by tumours and microorganisms as an iron mimic. As such, it is plausible for gallium to disrupt the requirement of iron in cancer cells and bacteria as a potential therapeutic approach (when administered in therapeutic doses). In addition, radioactive ^{67}Ga and ^{68}Ga can be used as an iron analogue for imaging purposes. The use of gallium as an iron analogue for infection imaging, and its mechanism of action as anti-cancer drug, will be discussed in subsequent chapters. The rest of this chapter discusses, supported by available evidence, some of the similarities and differences between gallium and iron in cellular uptake based on transferrin and non-transferrin mediated mechanisms. In addition, the biodistribution and pharmacokinetics of iron and gallium *in vivo* will be discussed. Although gallium is a non-physiological metal, iron can enter the body through different dietary sources. The following section discusses the different sources of oral iron intake and absorption and provides a brief introduction to orally administered gallium compounds as anti-cancer drugs, which will be discussed in detail in chapter 3.

1.4.1 Iron and gallium gut absorption

Iron enters the body through different dietary sources. These sources are either plant or dairy products (which are sources of non-haem iron), or food obtained from animal tissue (which contains haem iron).[34] Haem and non-haem iron absorption take place in the duodenum and proximal jejunum. The amount of iron intake from these sources is regulated by a variety of factors, including type of iron present (haem vs. non-haem) and body demands.[34] Although both haem and non-haem iron sources are taken up by the proximal part of the small intestine, they possess different absorption pathways.[34]

It is believed that haem is released from haemoglobin or haemoproteins in the stomach and absorbed by the apical membrane of the enterocytes as an intact molecule. The exact mechanism of haem absorption by enterocytes is not fully elucidated.[35] However, the haem-carrier protein 1 (HCP1) is identified as the most likely receptor to be involved in haem iron uptake.[36] The role of HCP1 in haem iron absorption was studied in HeLa (cervical cancer) and CaCo-2 (human intestinal) cell lines. Cells were incubated at different time points with either ^{55}Fe-haem or ^{59}Fe citrate and the results were compared to other cells that were infected with HCP1 adenovirus that causes significant increase in HCP1 expression. Infected cells showed a two to three-fold increase in ^{55}Fe-haem uptake compared to non-infected cells. However, ^{59}Fe uptake was similar in infected and non-infected cells.[37,38] In addition, incubating the CaCo-2 cells with Desferrioxamine (DFO, binds iron in the form of Fe^{3+}-DFO) had no effect on either HCP1 expression nor ^{55}Fe-haem uptake. This indicates that HCP1 plays a role in iron porphyrin ring uptake (but not $^{59}Fe^{3+}$), but its precise role has not fully been explored.[34,37,38] In addition, research strongly suggests that once

haem is absorbed into enterocytes, it is broken down by haem oxygenase-1 (HO-1) to release iron in its ferrous form (Fe^{2+}).[34,35,39] Studies have showed that HCP1 and ^{55}Fe-haem uptake increased significantly post-incubation with cadmium chloride (an inducer of HO-1) indicating that over expressing HO-1 increased the transcellular haem uptake. HO-1 expression was increased upon incubation of CaCo-2 cells with haem (especially cells infected with adenovirus) compared to a control group (no haem added). However, no change in HO-1 expression was observed after ferric citrate incubation (Figure 1.2).[38,40]

In comparison, the iron absorption and cellular uptake of non-haem iron are well-defined.[39,41] The body is the recipient of non-haem iron when the iron is in its Fe^{3+} state , Fe^{3+} is reduced to Fe^{2+} to allow absorption by enterocytes. The membrane-bound ferric reductase duodenal cytochrome B (DcytB) facilitates iron reduction at the apical membrane. The divalent metal transporter 1 (DMT1) transfers Fe^{2+} over the border of the apical membrane. Fe^{2+} from haem and non-haem sources joins the labile iron pool (LIP) in the cytoplasm. In accordance with the body's iron needs, Fe^{2+} is then either stored in the iron storage protein ferritin (Ftn) in a process that involves Fe^{2+} oxidation to Fe^{3+}, or guided to the basolateral membrane of the enterocyte.[34,36,42,43] The basolateral membranes of the enterocytes express ferroportin (Fpn1, a transmembrane protein) that transfers Fe^{2+} across to the basolateral membrane to the extracellular compartment where Fe^{2+} is oxidised by hephaestin (Heph) and ceruloplasmin (Cp) (Figure 1.2).[36,42,43]

Studies have been conducted to investigate iron absorption after oral administration of radioactive iron (^{59}Fe), aiming to understand iron trafficking in hemochromatosis (iron overload) patients. Preclinical and clinical studies showed between 1.5–7% of injected dose (%ID) of iron was absorbed 3 to 7 days after oral administration of $^{59}FeCl_3$ in healthy groups. However, hemochromatosis groups showed a range between 20–45% ID.[44,45]The difference in absorption rate in each group and between groups is not surprising since iron absorption depends largely on the condition of the body and its need for iron.

On the contrary, gallium, cannot enter the body orally through dietary sources. However, gallium salts have been investigated for decades in clinical trials as an anti-cancer drug via oral administration due to the high risk of renal toxicity following intravenous injection of gallium nitrate. However, poor gut absorption and minimal tumour effect limited their use.[4,46] Gallium compounds have been developed, from simple gallium salts to a range of gallium-bound ligands, on the rationale for better gut absorption and tumour effect following oral administration (more details in chapter 3).[46]

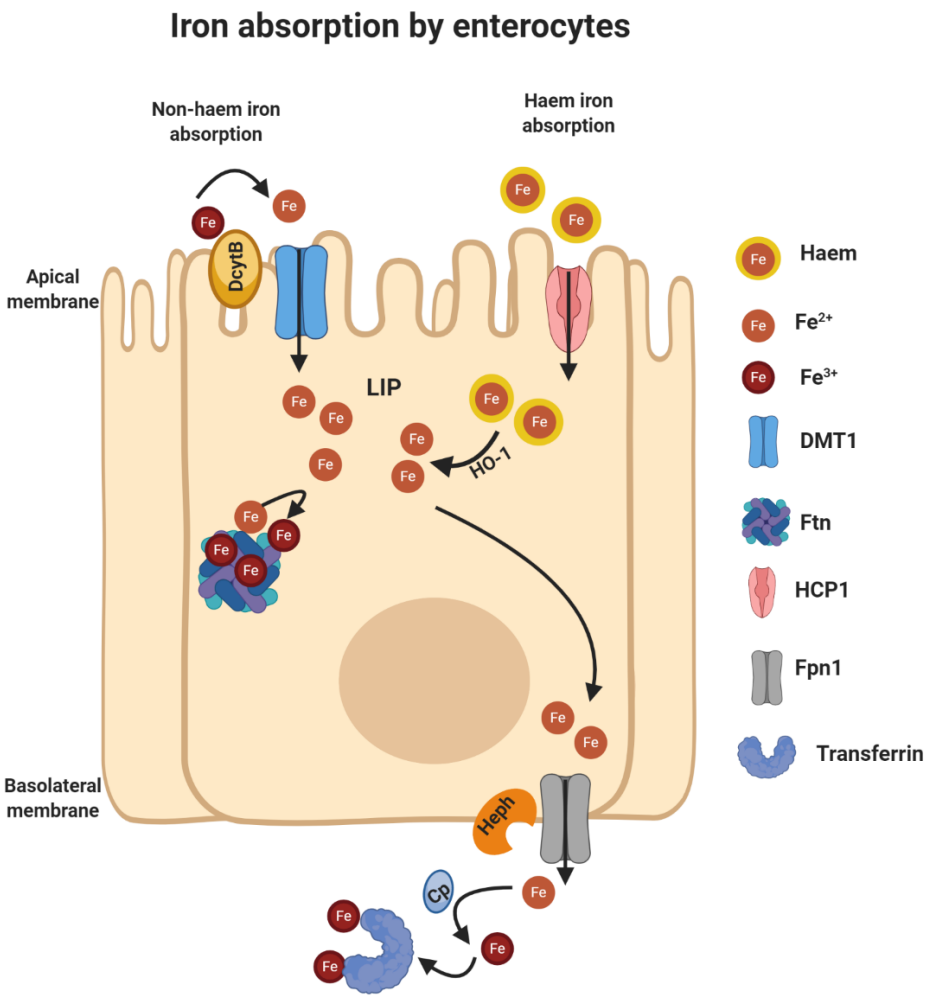

Figure 1.2: Haem and non-haem iron absorption by enterocytes. Haem is transported as an intact form through HCP1 and dissociated by HO-1 to release iron in its Fe^{2+} form. Non-haem iron (in Fe^{3+} form) is reduced by DcytB at the apical membrane and transported via DMT1. Fe^{2+} in the cytoplasm either gets stored in Ftn (involves an introductory step of Fe^{2+} oxidation) or transported out of the cells by Fpn1. On the extracellular side of the basolateral membrane, Fe^{2+} is oxidised by Heph and Cp. Created with BioRender.com.

1.4.2 Iron and gallium cellular trafficking

In this section, iron cellular trafficking (in conjunction with its transferrin and non-transferrin uptake mechanisms) will be discussed briefly prior to discussing gallium cellular uptake and trafficking. Gallium, as an iron analogue, shares its ability to bind to some iron-binding proteins and biomolecules and enters cells following, at some level, similar uptake mechanisms. Gallium cellular trafficking, its binding to the plasma protein transferrin and its cellular uptake by transferrin and non-transferrin mechanisms will be discussed in this section.

1.4.2.1 Cellular trafficking of iron and gallium by transferrin-dependant mechanisms

Once Fe^{3+} is transported to the plasma by enterocytes Fpn1, it binds to transferrin (Tf), the main iron-binding protein in plasma.[47] Transferrin binds to two Fe^{3+} atoms with high affinity (binding constants are log K_1 = 22.8 and log K_2 = 21.5) when bicarbonate binding takes place simultaneously (serum bicarbonate concentration = 27 mM).[8,47,48] In physiological conditions, 30% of transferrin is saturated by Fe^{3+}.[43,49] Transferrin-bound iron is then delivered and bound to transferrin receptors (TfR) at the cellular membrane, which are then internalised through receptor-mediated endocytosis, and the endocytosed Fe^{3+}-Tf-TfR complex is trafficked to an endosome.[47] The endosome pH is reduced to 5.5 by the introduction of H^+ by an ATP-dependent proton pump. This causes the release of Fe^{3+}, although apo-transferrin (apo-Tf, transferrin with no iron bound) remains TfR1 bound.[47,50] The enzyme ferrireductase Steap3 then acts as an electron donor to reduce Fe^{3+} to Fe^{2+}. The Tf–TfR complex is propelled toward the exterior of the cell, where the apo-Tf is discharged into the plasma. Fe^{2+} is transported via DMT1 from the endosome to the cytosol where it forms LIP. Fe^{2+} in the LIP is either delivered to the mitochondria for metabolic utilisation, including synthesis of haem and iron–sulfur clusters, stored in Ftn (involved Fe^{2+} oxidation step), or exported from the cells through Fpn1 (Figure 1.3).[43,50,51,52]

The ability of gallium to bind to transferrin was researched extensively in literature using the radiometal ^{67}Ga citrate.[8,53,54,55] Gallium can bind to unoccupied transferrin, however its transferrin binding affinity is less than that of iron (binding constants are log K_1 = 20.3 and log K_2 = 19.3) at a serum bicarbonate concentration of 27 mM.[8] Incubating ^{67}Ga citrate with transferrin *in vitro* showed that almost all the ^{67}Ga was found to be associated with transferrin.[56,57] The presence of transferrin was also found to stimulate the cellular uptake of ^{67}Ga compared to its uptake in media with no transferrin.[55] The ability of ^{67}Ga to bind to transferrin was tested preclinically in rabbits after intramuscular injection of apo-Tf. Intravenously injected ^{67}Ga citrate was bound to apo-Tf injection sites but did not bind to sites injected with normal saline.[58] However, *in vitro* and *in vivo* studies have shown that saturating transferrin with Fe^{3+} diminishes ^{67}Ga cellular uptake indicating a competition over transferrin binding.[55,58]

As mentioned previously, transferrin is partially occupied by Fe^{3+} and retains a relatively high capacity for binding to other metals.[8] Carrier free ^{67}Ga is usually administered intravenously for imaging purposes, and it is expected to mostly bind to transferrin and get delivered to cells via transferrin-mediated mechanisms.[56] Studies have demonstrated the role of TfR in gallium cellular uptake. However, the gallium transferrin complex has a lower affinity to TfR compared to the iron transferrin complex (equilibrium constant = 1.1 μM for gallium and 0.5 μM-2.3 nM for iron).[59,60]

It is worth noting that most of the *in vitro* studies investigating cellular gallium trafficking were performed using ^{67}Ga citrate in cancer cells based on its main role as cancer imaging agent. An *in vitro* study on a human leukaemia cell line (where transferrin was present in the media) showed that ^{67}Ga citrate uptake was significantly decreased from 10% to 1% of the administered dose after adding anti-human transferrin receptor monoclonal antibodies (MoAb), indicating that MoAb prevents ^{67}Ga cell internalisation by transferrin mediated uptake.[61] Another study supported the role of TfR in cellular uptake of gallium by demonstrating that ^{67}Ga citrate uptake in mutant Chinese hamster ovary (CHO) cell lines, that do not express TfR, increased significantly after transfecting these cells to overexpress TfR. These results were confirmed *in vivo* in the same study after intravenous injection of ^{67}Ga citrate. Transfected cells showed 10 times more ^{67}Ga uptake compared to non-transfected cells.[5,62] In another preclinical study, an intravenous injection of MoAb, 24 hours prior to ^{67}Ga citrate administration, decreased tumour uptake from 21.4% ID/g to 5.12% ID/g, suggesting the involvement of TfR in ^{67}Ga cancer cell uptake. Although transferrin and TfR provide the majority of ^{67}Ga uptake, *in vitro* and *in vivo* studies still show some uptake even after blocking TfR indicate some uptake by non-transferrin mechanisms (more detail in 1.4.2.2 section).[63]

Although both gallium and iron compete for the same transferrin binding sites, bind to TfR, and are internalised through receptor-mediated endocytosis, their intracellular trafficking is expected to be different based on their different chemical properties. The exact mechanism of gallium cellular trafficking is not fully understood. However, some insights into the possible pathways of intracellular gallium trafficking have been demonstrated in studies. *In vitro* studies have shown that the stability of the ^{67}Ga-Tf complex decreases when the pH of the incubation solution decreases.[64,65] This might indicate that the low pH of endosomes might facilitate the dissociation of the Ga-Tf complex, like iron. However, DMT1 was shown to not be able to facilitate gallium transport from endosomes to the cytoplasm, because unlike Fe^{3+}, it cannot be reduced to the divalent state.[66] Studies have shown the presence of a labile gallium pool (LGP) in the cytoplasm of multiple cancer cell lines using autoradiography, but the mechanism by which gallium is transported from the endosomes to the cytoplasm is not fully understood.[67,68] Although Ga^{3+} does not undergo reduction within the cell, it is plausible that it binds to ferritin (Fe^{2+} undergoes oxidation before being incorporated into ferritin). In fact, some data suggest that ^{67}Ga binds to

ferritin, but it is not yet demonstrated whether it is incorporated into ferritin or bound to the external surface of the protein (Figure 1.3).[5,61,68] In addition, *in vitro* studies on the mechanism of action of gallium (as a therapeutic dose) showed a cytotoxic effect through the mitochondrial pathway, but it is not yet clear whether gallium's cytotoxic effect is related to its storage in mitochondria or in the external pathway [4,5] (more details in chapter 3).

1.4.2.2 Cellular trafficking of iron and gallium by transferrin-independent mechanisms

Typically, the transferrin-independent system is utilised in abnormal situations such as hemochromatosis where a high concentration of non-transferrin bound iron (NTBI) exists.[69] While the nature of NTBI in plasma is not fully understood, some studies have suggested that NTBI is possibly bound to albumin or present in the form of a Fe^{3+}-citrate complex. Although cellular iron trafficking by transferrin-independent mechanisms remains poorly understood, the most agreed upon pathway is this: iron is involved in a reduction step (by an unknown pathway) before being transported via DMT1 and the zinc transporter Zrt/Irt-like protein 14 (ZIP14).[69–73]

Studies have shown that gallium, like iron, can be taken up by cells through transferrin independent mechanisms.[7] An *in vitro* study investigating gallium non-transferrin-mediated cellular uptake in HL60 (human leukemic) cells showed that, in the absence of transferrin, ^{67}Ga citrate cellular uptake was only 10% of that in the presence of transferrin. Blocking TfR did not affect ^{67}Ga uptake in transferrin-free media, indicating its uptake by non-transferrin mechanisms, while it significantly decreased ^{67}Ga uptake in media containing transferrin.[62] Consistently, ^{67}Ga citrate showed similar uptake *in vitro* in TfR+ or TfR- CHO cells in serum free media, indicating uptake by a transferrin-independent mechanism.[61] An *in vivo* study utilising the same cells following subcutaneous inoculation showed that although higher ^{67}Ga accumulation in TfR+ than TfR- was observed, ^{67}Ga uptake in the absence of TfR indicated a non-transferrin uptake pathway.[61] Although *in vitro* and *in vivo* studies suggested gallium uptake by transferrin-independent mechanisms, the exact pathway is poorly understood. Multiple studies showed that although gallium and iron are expected to have different transferrin-independent pathways (due to gallium's inability to be reduced under physiological conditions), their transferrin-independent uptake is influenced by each other. For example, an *in vitro* study of HL60 cells showed that ^{67}Ga citrate and iron-nitrilotriacetic acid (^{59}Fe-NTA) uptake (incubated in serum free media) enhanced post-incubation of ferric chloride and gallium nitrate respectively in a dose related manner.[74] Another study showed higher ^{67}Ga uptake in CHO (TfR-) cells post-incubation of iron tricine ascorbate (FeTA), but adding holo-transferrin did not influence the uptake, indicating that only free iron can influence gallium transferrin-independent mechanisms.[62] Although the results from these studies might suggest that both metals share the same transferrin-independent uptake mechanism, this is unlikely considering gallium's inability to be reduced under physiological conditions; its transferrin-independent mechanism is likely to be different than that of iron.[7,62] In

fact, studies have demonstrated inhibition of transferrin-independent iron uptake post-incubation of multiple divalent metals including zinc (Zn^{2+}), manganese (Mn^{2+}), copper (Cu^{2+}), and cadmium (Cd^{2+}). This may support the iron reduction step theory prior to cell internalisation and suggest a possible competition of previously mentioned divalent metals over ferrous iron transporting systems.[75,76] Studies have failed to explain the mechanism of transferrin-independent gallium uptake increasing in the presence of iron and the converse: that transferrin-independent iron uptake increases in the presence of gallium. However, the results clearly indicate that transferrin-independent gallium and iron uptake are connected at some level, and the presence of one metal might increase or induce cellular binding sites/transporters of the other.[74,77]

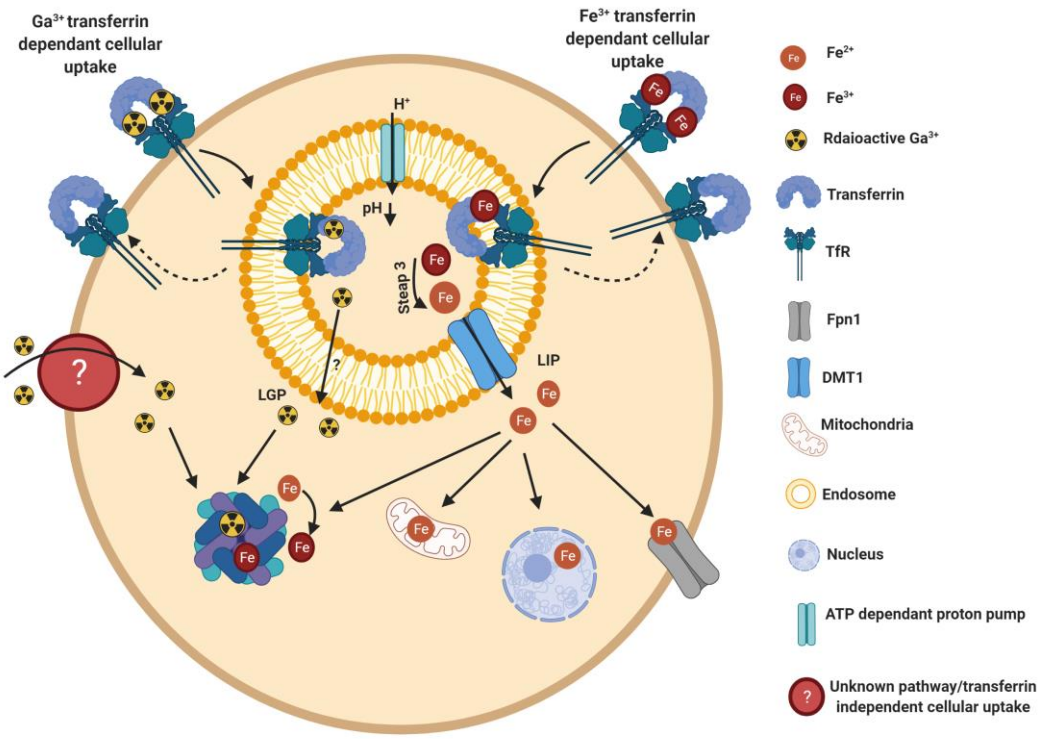

Figure 1.3: Cellular iron and gallium trafficking. Fe^{3+} and Ga^{3+} transferrin complexes bind to TfR and are internalised through receptor mediated endocytosis. Fe^{3+} and Ga^{3+} are released from the transferrin by the low pH of the endosomes. While Fe^{3+} is reduced to Fe^{2+} in the endosome by the enzyme ferrireductase Steap3 and transported to the cytoplasm by DMT1, Ga^{3+} is transported to the cytoplasm by an unknown pathway. Fe^{2+} is delivered to the mitochondria for haem and iron-sulfur cluster synthesis, stored in Ftn (involves an introductory step of Fe^{2+} oxidation), or exported through Fpn1. Like Fe^{3+}, Ga^{3+} can be stored in Ftn, but the mechanism of its delivery to the mitochondria (if any) is unknown. Created with BioRender.com

1.4.3 Pharmacokinetics and biodistribution of iron and gallium

Despite the circulation of both gallium and iron as Tf-bound complexes in blood and the uptake of each by cells via transferrin-dependant or transferrin-independent mechanisms, the metals display different pharmacokinetics *in vivo.* The previous section addressed the similarities and differences of iron and gallium at cellular level, while this section will focus on their pharmacokinetics and biodistribution *in vivo*. The availability of radioactive iron and gallium facilitated the understanding of their biodistribution, however, therapeutic/high doses, or carrier added radiopharmaceuticals might have different pharmacokinetics and biodistribution compared to trace amounts of the same compounds. In this section, the pharmacokinetics and biodistribution of both metals as a tracer or with carrier added will be explored.

A preclinical study in mice showed marked differences between ^{67}Ga citrate and ^{59}Fe citrate tissue distributions.[78] ^{67}Ga citrate distribution in normal mice showed the highest accumulation in the blood and kidneys at 1 hour after injection. Uptake in the blood and kidneys decreased over time while gradually increasing in other tissues including the liver, small intestine, and bones (but not bone marrow) indicating the slow blood clearance of ^{67}Ga. Minimal uptake was noticed in the spleen (~2% ID/g) during the 72 hours after injection. Blood sample analysis showed that ^{67}Ga uptake is incorporated into the plasma and decreased over time with negligible incorporation into red blood cells (RBC). For example, at one hour following the injection, 21% ID/g was found in the plasma versus 0.9% ID/g in cells. The absence of activity in the spleen, bone marrow, and RBC suggest no affinity of ^{67}Ga for hematopoietic tissues.[78] In contrast, ^{59}Fe citrate biodistribution varied over time with the highest concentration found in RBC, the spleen, and bone marrow indicating the transfer of ^{59}Fe between circulation and hematopoietic tissues. Additionally, tracer distributions of both isotopes in tumour hosts were found to be similar to that of a healthy host. However, ^{67}Ga accumulated in the tumour tissue gradually while there was no evidence of ^{59}Fe uptake by the tumours.[78] Preclinical studies in mice and rats using $^{67/68}$Ga citrate,[79,80] ^{68}Ga acetate[80] and ^{67}Ga chloride buffered in sodium hydroxide or phosphate buffered saline (PBS)[81,82] showed similar biodistribution data of gallium regardless of the formulation.

Although the difference in ^{67}Ga and ^{59}Fe biodistribution is easily understood based on the limitation of ^{59}Fe to hematopoietic tissues for the production of haemoglobin,[53] their difference in tumour uptake needs additional explanation. The first hypothesis was based on the rationale that gallium accumulation in tumours is related to the tumour's increased need for iron, which consequently increases TfR expression followed by accumulation of gallium as gallium-transferrin complex, indicating that tumour uptake is largely based on accumulation by transferrin-dependant mechanisms.[83] However, this hypothesis failed to explain the difference in gallium and iron tumour uptake.

Sephton[84] hypothesised that the difference in gallium and iron tumour uptake is based on the presence of free ^{67}Ga (soluble gallate) in plasma and its binding to extravascular transferrin (especially at early time points) rather than the transport of Ga-Tf from plasma to tumour.[84] Sephton considered that the extravasation of a large molecule such as Ga-Tf is slow and might contribute to tumour uptake at later time points. However, free gallium can diffuse from plasma and quickly bind to extravascular transferrin which contributes to tumour uptake at an early time point.[84] The exchange between free and transferrin-bound gallium in plasma is continuous until an equilibrium is reached. This could explain the progressive tumour accumulation of ^{67}Ga post-intravenous injection. In contrast, soluble free iron does not exist, and iron travels only in the form of Fe-Tf which favours hematopoietic tissues rather than tumour extravasation.[84] In fact, Sephton's hypothesis could explain the preclinical study that showed no change in ^{67}Ga tumour accumulation post-intravenous injection of ferric citrate. A preclinical study on rats showed that an intravenous injection of ferric citrate 10 minutes prior to ^{67}Ga citrate injection caused no change in tumour uptake, but uptake in normal tissue (liver, spleen, lung and muscle) significantly decreased, while uptake in bone increased, but not significantly.[85] These results can be interpreted based on Sephton's hypothesis. Although the presence of excess iron decreased the level of unsaturated iron-binding capacity (UIBC), causing less available transferrin to bind to gallium, more free gallium (gallate) would be available and binding to extravascular transferrin. This resulted in no change in tumour uptake. The uptake by normal tissue might be dependent on the Ga-Tf complex as their ^{67}Ga accumulation decreased when less transferrin was available to bind to gallium.[85,86] These results suggest that ^{67}Ga has two separate routes for tumour and normal tissue uptake.[85] Other preclinical studies confirmed these results but in an opposing manner. Rats with experimentally induced anaemia showed an increase in ^{67}Ga uptake in the liver and spleen, indicating that prolonged blood loss lowers serum iron levels and increases the transferrin pool to bind ^{67}Ga. In iron deficient situations, TfR increases in many tissues causing increases in ^{67}Ga uptake.[85,87] However, studies have shown conflicting results regarding ^{67}Ga tumour uptake in anaemic animal models. The first preclinical study by Hayes et al. [85] showed lower ^{67}Ga uptake in anaemic (anaemia induced by multiple heart puncture bleedings) rats bearing 5123C hepatoma xenografts compared to the control group (3.0 ± 0.2 in hepatoma vs 7.5 ± 0.8 in control, % ID/g).[85] In contrast, the preclinical study by Bradley et al.[87] showed unchanged ^{67}Ga tumour uptake in anaemic (anaemia induced through a no-iron diet) rats bearing Walker-256 carcinosarcoma xenografts compared to the control group (0.7 ± 0.1 in control vs 0.95 ± 0.2 in tumour, % ID/g).[87] A reason for this discrepancy may be the different methods used for inducing anaemia, which may have caused differences in anaemic state, and consequently affected the availability of the transferrin pool. Another reason might be the use of different tumour types, resulting in different ^{67}Ga uptake mechanisms in iron deficient conditions. Lower bone uptake in the anaemic animal models was noticed in both studies, but it was not significant compared to the control groups.[85,87]

The same effect of ferric citrate on ^{67}Ga biodistribution was seen in other preclinical studies using high therapeutic doses of Ga citrate.[15,88,89] Pre-saturating transferrin with intravenously injected Ga-citrate (carrier added) showed an alteration in ^{67}Ga biodistribution. ^{67}Ga uptake was decreased in the liver, spleen, and muscles while uptake in the bones and urine increased. In the absence of carrier added gallium, the liver, spleen, and bones showed 3.06, 7.9, and 5.45% ID respectively. However, post-intravenous injection of 25 mg/kg Ga-citrate, the liver, spleen, and bones showed 1.4, 2.1, and 12.4%ID respectively.[15,88] This indicates that when less transferrin is available for ^{67}Ga binding, there is less ^{67}Ga uptake in normal tissues. However, the elevated uptake of ^{67}Ga in the bones indicates a different mechanism of accumulation compared to soft tissues, which appear to be non-transferrin dependant.[9] In fact, a preclinical study on hypotransferrinemia in mice showed higher, but not significant, ^{67}Ga bone uptake compared to healthy Balb/C mice indicating that ^{67}Ga bone uptake is likely transferrin-independent.[90] In addition, an increase in ^{67}Ga renal excretion was noticed when high doses of stable Ga-citrate were injected prior to ^{67}Ga administration. With the absence of a carrier added dose, 43% ID was excreted in the urine, while 81% ID was excreted during the same time when a high dose of Ga-citrate was used.[15] This higher level of ^{67}Ga excretion may be related to the saturation of transferrin and the increase in levels of small charged gallate in the plasma which is expected to be renally eliminated.[9] Additionally, the effects on ^{67}Ga biodistribution were not limited to high doses of iron and gallium. Scandium (Sc^{3+}) can also modify the biodistribution of gallium based on its binding to transferrin. In rats and mice, an intravenous injection of Sc^{3+}-citrate prior to that of ^{67}Ga increases ^{67}Ga renal excretion and bone uptake, and lower uptake of ^{67}Ga in the soft tissue. These effects are a result of Sc^{3+} binding to ^{67}Ga transferrin binding sites and preventing ^{67}Ga uptake in soft tissues.[91,92]

In addition to transferrin, other Fe^{3+}-binding proteins (lactoferrin and ferritin) and siderophores are potential Ga^{3+} carriers.[93] ^{67}Ga citrate has been extensively studied as an infection imaging agent.[94,95,96] However, ^{67}Ga has similar uptake mechanisms in infection and inflammation based on its binding to the high transferrin receptors expressed at sites of infection and inflammation, and its binding to lactoferrin and ferritin in leukocytes and macrophages. Due to this, ^{67}Ga cannot be considered as a specific infection imaging agent.[9,96] However, microorganisms have the ability to produce siderophores and acquire iron from the resulting Fe^{3+}–siderophore complexes.[97] Thus, gallium can radiolabel siderophores and thus be used as a specific infection imaging agent.[98] Recent studies using a variety of siderophores radiolabelled with $^{67/68}$Ga showed promising results *in vitro* and *in vivo* suggesting the specificity of $^{67/68}$Ga siderophores in imaging infection (more details in chapter 2).[97–103]

Overall, although gallium shares some properties with iron that allow it to bind to iron-binding proteins and siderophores, it possesses different cellular trafficking, *in vivo* biodistribution and pharmacokinetics. ^{68}Ga and ^{67}Ga can be used to an extent as iron analogues for imaging purposes, including cancer and infection imaging. Unlike iron, the inability of Ga^{3+} to be reduced to Ga^{2+}

under physiological conditions or to undergo reduction within cells may facilitate its role as an anti-cancer or anti-infection therapeutic agent when it is administered in therapeutic dose concentration.[6,9] In addition, gallium can exist in a form of soluble gallate which permits some biomedical reactions that are not possible for iron.[9] The biodistribution of gallium is not fully understood. However, studies have shown some important insights and possible gallium uptake pathways. While gallium uptake in normal tissue might be largely dependent on the Ga-Tf complex, its uptake in tumours might be dependent on the binding of free gallium (gallate) to extravascular transferrin.[84] Unlike soft tissue uptake, the increased level of radioactive gallium in bone in transferrin-saturated conditions indicate different mechanisms of accumulation, probably non-transferrin mediated.[9] Evidence from literature exhibited alteration in carrier free gallium biodistribution when co-administered with carrier added elements such as Fe^{3+}, Ga^{3+} and Sc^{3+}.[15,85,88,89,91,92]

1.5 Thesis statements

This chapter has discussed the general current understanding of gallium and its analogy with iron in biological systems. The following chapters will specifically explore how the literature relates to the main questions of this research project. This thesis is composed of two main projects, each dealing with different aspects of ^{68}Ga and ^{67}Ga in medical imaging, with the common theme of involving gallium-specific biology.

^{68}Ga and ^{67}Ga siderophore complexes have shown promising results, indicating their specificity as infection imaging agents.[97–103] Among the siderophores tested in literature, a clinically-approved siderophore DFO for treating iron overload diseases[104] was investigated *in vitro* and *in vivo* and showed specificity in imaging *Staphylococcus aureus (S. aureus)* and *Pseudomonas aeruginosa* (*P. aeruginosa).*[99,100] The fact that DFO is a clinically-accepted drug renders its ^{68}Ga complex amenable to clinical translation with low regulatory barriers. The following chapter (chapter 2) will briefly introduce bacterial iron trafficking, followed by the trafficking and application of unchelated ^{68}Ga and ^{67}Ga, and ^{68}Ga/^{67}Ga radiolabelled with siderophores as analogues of iron siderophore complexes for infection imaging. Following the introductory section, chapter 2 will be dedicated to developing good manufacturing practice (GMP)-compatible [^{68}Ga]Ga-DFO complex that can be investigated clinically as a specific infection imaging agent.

When administered intravenously, gallium nitrate showed promising results as an anti-cancer drug against lymphoma and bladder cancer in phase I and II clinical trials.[105,106] However, due to its high renal toxicity, attempts have been made to investigate gallium salts as anti-cancer drugs post-oral administration as an alternative method to avoid renal toxicity.[107] Although poor gut absorption of gallium salts post-oral administration might limit their use as anti-cancer drugs, gallium bound to multiple ligands were developed to overcome the poor absorption of gallium salts. Among them, tris(8-hydroxyquinolinato) gallium (III) (KP46) was developed with the rationale of making a more efficiently absorbed drug.[4,108] Despite ongoing research, KP46 pharmacokinetics are not fully understood. KP46 will be the focus of chapter 3. Its protein binding, mechanism of action, *in vitro* and *in vivo* studies will be extensively discussed in the introductory section. Following the introductory section, chapter 3 will be dedicated to study KP46 trafficking in cancer models (*in vitro* and *in vivo*) using [$^{68/67}$Ga]KP46 post-intravenous and oral administration as a tracer or combined with a pharmacologically relevant dose of KP46.

As mentioned previously, although ^{67}Ga emits auger electrons, its application as a therapeutic radionuclide is undeveloped due to its low incorporation into cells. It has been suggested that ^{67}Ga provides better cytotoxic effects when incorporated into cells.[26,28] An attempt has been made to investigate ^{67}Ga cytotoxic effects using 8-hydroxyquinoline (8HQ) as a chelator.[26] In chapter 4,

the therapeutic applications of 8HQ and its derivatives will be introduced in the introductory chapter. Chapter 4 will then focus on radiolabelling ^{68}Ga with 8HQ and its derivatives to find the best chemical form to deliver gallium to tumour cells while aiming to radiolabel selected 8HQ derivatives with ^{67}Ga to study its radiobiology as an Auger electron emitter radionuclide.

2 Simple radiosynthesis of GMP-compatible [^{68}Ga]Ga-DFO for infection imaging

2.1 Introduction to bacterial iron trafficking

Iron is not only an essential nutrient for humans; bacteria that infect humans also require iron for host colonisation and survival. In oxygen-rich conditions, iron exists in the form of insoluble iron hydroxide, $Fe(OH)_3$, creating an obstacle for microorganisms to absorb and use it. Furthermore, most of the total body iron is intracellular (haemoglobin, myoglobin, ferritin, ~ 4 g); thus, it is not readily available to microorganisms.[93,109,110] Extracellular iron is either bound to transferrin (3 mg), found in haemoglobin as an effect of simple haemolysis (small amount, 5–50 mg/L), or bound in haem molecules (small amount).[93,109,110] Haemoglobin is considered the major haem source for bacteria. Hence, some bacteria secrete haemolysins to lyse red blood cells and release haemoglobin for easier uptake.[111]

Bacterial pathogens differ with respect to the iron sources they favour. Generally, most bacterial iron uptake involves haem uptake by direct contact between bacteria and haem sources (haem and haemoglobin) or by production of haemophores - proteins that bind haem and deliver it back to bacterial cells.[109,112] Bacteria are also able to secrete siderophores - small ferric iron chelators that have a higher affinity for iron compared to that of transferrin and lactoferrin. With binding constant (log *K*) between 29 and 50 (depending on the siderophore), siderophores can outcompete transferrin and lactoferrin which have binding constants of 20-21 and 22-24 respectively.[109,113–117]

Given the ability of siderophores to hijack iron from transferrin and lactoferrin, it is not surprising that host cells have developed a mechanism to overcome bacterial invasion. Lipocalin 2 (Lcn2), also known as siderocalin, is a protein expressed by the host's immune cells (macrophages and neutrophils) and which, when complexed with Fe^{3+} siderophores, prevents reuptake by microorganisms.[109,118] Some pathogens in turn have evolved specific mechanisms to overcome the host's defences. One such mechanism is the development of a modified Lcn2-resistant siderophore (stealth siderophore) that prevents Lcn2 binding. For instance, Lcn2 can easily bind enterobactin, a siderophore secreted by *Escherichia coli (E.coli)*; however, glycosylated enterobactin (salmochelin) precludes Lcn2 binding.[109,118] Another mechanism is the development of a siderophore that cannot be natively recognised by Lcn2 (Figure 2.1).[118]

Gram-positive and gram-negative bacteria have different iron-capturing mechanisms. Due to their outer membranes and large periplasmic spaces (which contain approximately 20% of the total cell water), gram-negative bacteria have iron uptake mechanisms that are more complicated than those of gram-positive bacteria.[109,118] In gram-negative bacteria, haem, haemoglobin and haemophores

are delivered to specific outer membrane receptors. While free haem is transported directly to the periplasmic space, haem in haemoglobin and haemophores must be unloaded at the receptors, although the exact mechanism of haem extraction in not fully understood. Once in the periplasmic space, haem binds to specific periplasmic binding proteins (PBP) and is transported to cytoplasm by adenosine triphosphate (ATP)-binding cassette (ABC) transporters, which are driven by ATP hydrolysis.[109,110,117] In addition, Fe^{3+}-siderophore complexes are taken up directly by specific outer membrane receptors (different siderophores are recognised by different receptors) and are transported to the periplasmic space, where they bind to PBP. They are then shuttled to the inner membrane and transported to the cytoplasm by ABC transporters.[109,110,118,117] For example, Fe^{3+}-enterobactin binds to the outer membrane ferric enterobactin permease (FepA) receptor, and is then transported to the FepB protein in the periplasmic space, before being transported into the cytoplasm by ABC transporters.[109,110,117,118] In addition to secreting siderophores to hijack ferric iron from transferrin and lactoferrin, selected gram-negative bacteria can evolve a mechanism of direct holo-transferrin/lactoferrin uptake by producing specific transferrin-binding proteins A and B (TbpA and TbpB) and lactoferrin-binding proteins A and B (LbpA and LbpB) receptors.[109,119] Ferric iron is released from the transferrin or lactoferrin protein receptors and binds to a periplasmic ferric-binding protein (Fbp) before entering the cytoplasm via ABC transporters.[120] The mechanism of Fe^{3+} transport and storage in the cytoplasm, however, is unknown.[121] In almost all gram-negative bacteria, cytoplasmic membrane energy-transducing proteins TonB, ExbB, and ExbD (producing energy from proton motive force) interact with outer membrane receptors to facilitate the iron uptake mechanism from the outer membrane to the cytoplasm.[109,110,117,118]

Unlike gram-negative bacteria, gram-positive bacteria only possess a cytoplasmic membrane (inner membrane), making the process of delivering iron easier.[118] However, they are protected from the environment by a thick cell wall. They follow the same haem uptake system as gram-negative bacteria. However, haem, haemoglobin and haemophores are taken up by specific cell wall receptors and transported to the cytoplasm by the iron regulated surface determinant (Isd) system and then enter the cytoplasm by ABC transporters.[109,111,117] Fe^{3+} siderophores are delivered directly to specific inner membrane receptors and enter the cytoplasm via ABC transporters without the need to bind to periplasmic proteins. For example, *S. aureus* secretes staphyloferrin A and staphyloferrin B, which are recognised at the inner membrane by HtsA and SirA receptors, respectively. HtsBC and SirBC permeases are then activated to allow Fe^{3+} siderophores to cross the inner membrane and enter the cytoplasm. No energy-transducing proteins are involved in gram-positive bacteria iron transport.[109,111,117,118]

Once inside the cytoplasm of either gram-positive or gram-negative bacteria, haem is broken down by oxygenase enzymes to release Fe^{2+}. Bacteria utilise two types of iron storage proteins, Ftn and the ferritin-like protein bacterioferritin (Bfr). The uptake of iron by ferritin and bacterioferritin involves an introductory step of Fe^{2+} oxidation at the ferroxidase centre, and iron

is then stored as Fe^{3+}.[122,123,124] In the cytoplasm, iron is released from the Fe^{3+}-siderophore complex by an unknown mechanism. However, some studies suggest that the reduction of Fe^{3+} to Fe^{2+}, which destabilises the siderophore complex and releases ferrous iron destined for storage, is the most adopted method for iron release (Figure 2.2).[117,120,125,126,127]

2.2 Mechanism of gallium localisation in infection and inflammation

Several non-invasive radiological techniques, including CT and MRI, are used to identify infection; however, they are only able to detect structural abnormalities related to the infectious disease. Thus, they possess limitations in identifying an infection in its early stages, especially in cases where abnormal structures develop only at a later stage in the disease process. Furthermore, they lack the specificity to differentiate between infection and inflammation and can present major artefacts in patients with prosthesis.[128–131] Nevertheless, structural modalities still play an important role in identifying infection sites for biopsies and as a back-up technique to molecular imaging for confirming infection diagnosis.[128,129,130]

Because of the structural similarity between Fe^{3+} and Ga^{3+}, Fe^{3+}-binding proteins (including transferrin, lactoferrin and ferritin but not haem) and siderophores are potential Ga^{3+}carriers.[93] Bacterial transporters involved in iron uptake may not be sufficiently able to distinguish iron from relevant gallium complexes and, therefore, might also take up the corresponding gallium complexes.[94] Unlike Fe^{3+}, Ga^{3+} cannot be reduced under physiological conditions to Ga^{2+}. Thus, gallium binding to iron proteins and siderophore sites might disturb the biological processes of bacteria and function as an anti-infective agent.[5,93] In addition, unchelated radioactive ^{67}Ga or ^{68}Ga, or siderophores labelled with $^{67/68}$Ga, can be used as an iron analogues for imaging infection.[93]

SPECT using ^{67}Ga-citrate has been extensively studied for imaging infection;[94,95,96] however, ^{67}Ga citrate is a non-specific infection imaging agent due to the similarities in its uptake mechanisms in infection and inflammation.[96] The exact uptake mechanism of $^{67/68}$Ga citrate in infection and inflammation in not fully understood. Many studies have suggested that, due to the weak chelation of citrate, radioactive gallium can be distributed in the blood as free $^{67/68}$Ga (probably in small amounts) or as $^{67/68}$Ga bound to Tf (Ga–Tf binding constant is log K_1 = 20.3 and log K_2 = 19.3). Sites of infection and inflammation often show high uptake of $^{67/68}$Ga due to the higher amount of transferrin receptor expressed and the uptake by transferrin-mediated mechanisms.[9,95,132] In addition to binding to transferrin, $^{67/68}$Ga binds avidly to lactoferrin (LF), a related protein that has been observed at infection and inflammation sites, especially in neutrophil leukocytes (Ga–LF binding constant is log K_1 = 21.43 and log K_2 = 20.57).[9,95,132,133,134] One question that needs to be asked, however, is whether selected gram-negative bacteria can directly take up gallium bound to

transferrin/lactoferrin by their specific transferrin/lactoferrin receptors, similarly to iron (Figure 2.2).

In addition to binding to Tf and LF, it has been suggested that $^{67/68}$Ga uptake in infection/inflammation might also be related to its accumulation in macrophage ferritin.[9] Macrophages play an important role in host immune defence and exist in sites of infection and inflammation. Several early studies showed uptake of ^{67}Ga citrate in macrophages using autoradiography; however, the exact mechanism of radioactive $^{67/68}$Ga accumulation in macrophages has not been experimentally addressed.[135,136] Moreover, it is possible that $^{67/68}$Ga could also be stored in bacterial ferritin (at sites of infection) when it is transferred to the cytoplasm,[95] but information about the fate of gallium in bacterial cells is lacking and further experimental studies are required to fill the current knowledge gap.

In addition, uptake of $^{67/68}$Ga in infection (not sterile inflammation) sites can be through binding to bacterial siderophores. Like iron, gallium has a high affinity for siderophores compared with transferrin or lactoferrin. For instance, Ga-DFO has a stability constant of log K = 28.1 and consequently can "steal" Ga from Lf or Tf and enter the bacterial cells as Ga^{3+}-siderophore complex (Figure 2.1 and 2.2).[9,94,132,134,137]

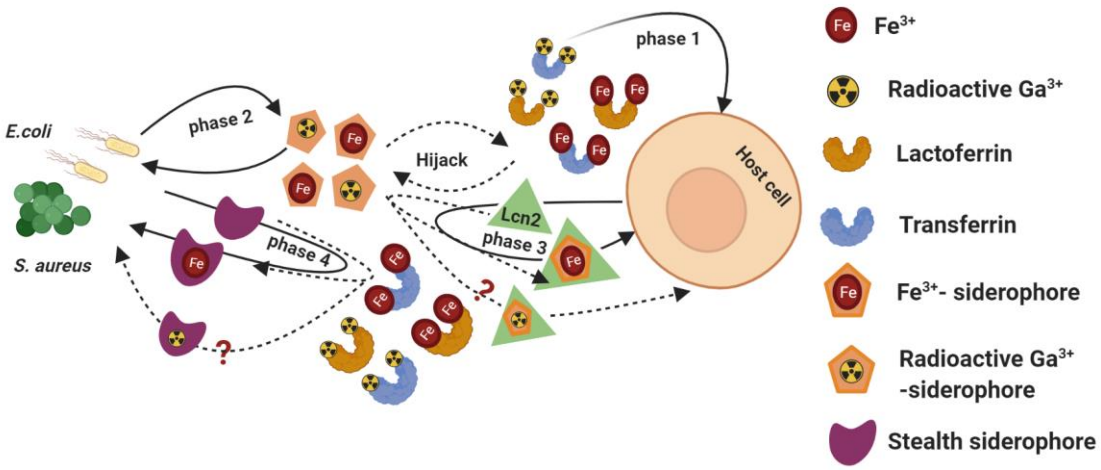

Figure 2.1: The battle for iron and gallium between bacterial pathogens and host cells. Bacterial pathogens produce siderophores to steal Fe^{3+} and Ga^{3+} from transferrin and lactoferrin. To overcome this invasion, host cells secrete Lcn2 that can bind to Fe^{3+} and possibly Ga^{3+}-siderophores complexes. Selected pathogens can produce stealth siderophores as a defence mechanism to block Lcn2 binding. Created with BioRender.com

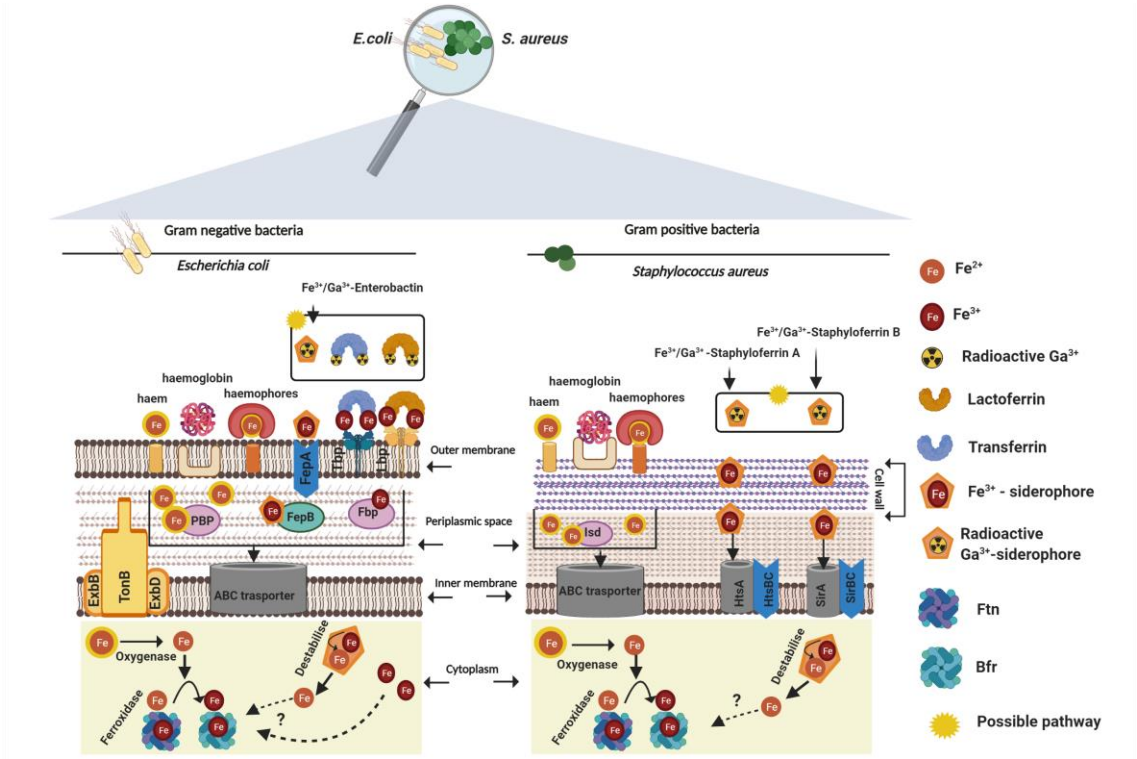

Figure 2.2: Bacterial iron trafficking in gram negative (left) and gram positive (right) bacteria. In gram negative bacteria, haem sources are recognised by specific outer membrane receptors, and transported to the cytoplasm by PBP where they enter by ABC transporter. Fe^{3+}-siderophore, -transferrin, and -lactoferrin complexes are recognised by specific outer membrane receptors. Fe^{3+}-siderophores and Fe^{3+} (released from transferrin and lactoferrin) are transported via specific proteins in the periplasmic space to the cytoplasm where they enter by ABC transporters. In gram positive bacteria, haem sources are recognised by specific cell wall receptors. Haem is transported by Isd system in the periplasmic space and enters the cytoplasm via ABC transporters. Fe^{3+}-siderophores shuttle directly to the cytoplasm where they enter via ABC transporters. Once in the cytoplasm of gram negative and positive bacteria, haem is broken down to release Fe^{2+} which is stored in Ftn or Bfr (involving oxidation of Fe^{2+}). Fe^{3+} is released from Fe^{3+}-siderophores complexes possibly by reduction of Fe^{3+} to Fe^{2+}. It is likely that Ga^{3+} (released from siderophores, transferrin, or lactoferrin) follows similar uptake mechanism as Fe^{3+} and is stored in Ftn or Bfr once transported to the cytoplasm; however, information about the fate of gallium in bacterial cells is lacking. Created with BioRender.com

2.3 Application of unchelated ^{67}Ga/^{68}Ga in infection and inflammation

The role of ^{67}Ga citrate in infection and inflammation imaging has changed considerably over the past years. Although ^{67}Ga citrate scans are to this day considered useful for imaging infection and inflammation, they still present many disadvantages. First, ^{67}Ga is not readily available, based on its production from high energy cyclotrons. Due to its slow blood clearance, 48 hours waiting time is needed before imaging. This makes the diagnostic process time-consuming and exposes patients to relatively high radiation doses. Second, it has high background uptake and interference from the intestine and liver.[95,131,138]

To overcome the disadvantages of ^{67}Ga citrate, the positron-emitter ^{68}Ga citrate has been tested for imaging infection and inflammation. Although there are no chemical differences between the two tracers, major advantages of ^{68}Ga citrate compared with ^{67}Ga citrate are its relatively short half-life (68 minutes) providing low radiation dose to patients and the fact that it is generator produced.[131] ^{68}Ga citrate was tested preclinically in *S. aureus* myositis rat models. Activity was detected at infected sites from 10 minutes (standardised uptake value $(SUV)_{max} = 3.5$) and an intense focal spot was seen from 60 minutes ($SUV_{max} = 4.5$) up to 4 hours ($SUV_{max} = 5.5$), with a decrease in tissues activity including heart, liver, and bowel.[139] Another study on rat models with right osteomyelitis tibia confirmed the ability of ^{68}Ga citrate to image infection. Uptake at the infection site was significantly higher ($SUV_{max} = 4.7 \pm 1.5$) compared to that at the left normal tibia ($SUV_{max} = 2.5 \pm 0.49$).[132] However, these preclinical studies failed to demonstrate the difference between ^{68}Ga citrate uptake in infection and sterile inflammation models (for example, turpentine oil injection) to show the specificity of ^{68}Ga citrate to image infection.

A case study on a patient with intra-abdominal infection showed ^{68}Ga citrate uptake at the infection sites from 30 minutes post injection ($SUV_{max} = 5.2$), further increasing by 60 minutes post injection ($SUV_{max} = 6.7$).[139] Another larger sample size clinical study, conducted on 31 patients with suspected osteomyelitis and discitis, showed high ^{68}Ga citrate sensitivity with no false-negative results. However, two patients with positive scans were later diagnosed with lymphoma, which indicates the low specificity of ^{68}Ga citrate.[140] In addition, this study did not provide evidence on the specificity of ^{68}Ga citrate to differentiate between infection and inflammation sites.

Although the short half-life of ^{68}Ga citrate is effective for overcoming some of the limitations of ^{67}Ga citrate, it might be unfavourable for delayed imaging in low-grade infection cases. In some cases, the guaranteed background reduction caused by delayed images can be useful for better contrast of the lesion.[94,95,131] It is reasonable to conclude that ^{68}Ga citrate is able to image infection; however, it cannot be considered as a specific infection imaging agent.[131]

Fluorine-18-fluorodeoxyglucose (^{18}F-FDG) is another PET imaging agent that has proven its efficiency in imaging infection and inflammation. Nonetheless, ^{18}F-FDG can be stored in cells with high glycolysis for many reasons[94,141] and is, therefore, not specific for imaging infection.[134] Head-to-head comparisons of ^{18}F-FDG and ^{68}Ga citrate in imaging infection were performed in preclinical and clinical studies. A preclinical study in four *S. aureus* osteomyelitis juvenile pig models with 10 infectious lesions (5 osteomyelitis and 5 soft tissue abscesses) showed that ^{18}F-FDG had better ability to detect osteomyelitis (4 lesions) and soft tissue abscesses (5 lesions) peripheral to bones compared to ^{68}Ga citrate (3 soft tissue abscesses and 1 osteomyelitis lesion).[141] A further clinical study on four patients with *S. aureus* bacteraemia contradicted the preclinical findings by demonstrating similar sensitivity of both tracers in imaging osteomyelitis patients (SUV_{max} average was 6.0 ± 1.0 for ^{18}F-FDG and 6.8 ± 3.5 for ^{68}Ga citrate). Consistent with the preclinical study, ^{18}F-FDG uptake (SUV_{max} average 6.5 ± 2.5) was significantly higher in soft tissue lesions compared to ^{68}Ga citrate uptake (SUV_{max} average 3.9 ± 1.2).[134]

It is difficult to conclude the superiority of ^{18}F-FDG over ^{68}Ga citrate in detecting infection lesions due to the very limited sample sizes in both studies. A possible explanation of the low sensitivity of ^{68}Ga citrate might be related to the biodistribution difference between the two tracers.[134,141] Unlike the homogeneous and slight uptake of ^{18}F-FDG in bones in the animal study, ^{68}Ga citrate showed extensive accumulation in the growth zones (metaphyses) of the bones, which might prevent identification of some bone or attached soft tissue lesions. In addition, the clinical study showed that ^{68}Ga citrate images have higher blood background activity (SUV_{mean} 2.9 ± 0.88) compared to ^{18}F-FDG images (SUV_{mean} 1.4 ± 0.05). High background noise might decrease lesion to background ratio and make diagnoses more challenging.[134,141]

The non-specific activity of $^{67/68}$Ga citrate can be considered an advantage in identifying infection sites in fever of unknown origin (FUO) based on the broad spectrum diseases causing FUO.[96,142] Although ^{67}Ga citrate has limitations, it remains the most widely used radioisotope for identifying infection sites in FUO patients.[96,142] Similar to ^{67}Ga citrate, the low specificity of ^{18}F-FDG can be an advantage in FUO diagnosis.

Overall, ^{18}F-FDG and $^{67/68}$Ga citrate play an important role in imaging infection. However, as mentioned previously, $^{67/68}$Ga citrate and ^{18}F-FDG are unable to discriminate between sites of infection and inflammation. Hence, ^{18}F-FDG and $^{67/68}$Ga citrate are not specific radiotracers for imaging infection.[94,128,129] Distinguishing between inflammation and infection remains one of the greatest challenges in modern medicine. Thus, there is an urgent need for specific and sensitive infection imaging tools that localise pathogen sites and quantify treatment responses.[131]

2.4 Gallium labelled siderophores

A considerable amount of research has focused on studying the uptake and transport of siderophores during infection. The application of siderophore molecules has had a progressing history since the 1960s.[128] The continued research on clinical application of siderophores has led to the development of the use of the clinically-approved siderophore DFO for treating iron overload diseases.[104] As highlighted previously, pathogens use different approaches to sequester iron. One of these approaches is the iron–siderophore uptake mechanism that depends on Fe^{3+}–siderophore complexes.[97] The fact that Fe^{3+} siderophores are taken up by bacteria makes their isostructural $^{67/68}$Ga complexes applicable, in principle, for imaging infection. Gallium uptake mechanisms other than by siderophores may contribute to the retention of $^{67/68}$Ga in both infection and inflammation sites, which makes $^{67/68}$Ga citrate unspecific for infection imaging.[94,95,131] However, due to the ability of microorganism to secrete siderophores and acquire gallium, siderophores radiolabelled with gallium radionuclides can be used as specific infection imaging agents.[98]

Ioppolo et al.[99] radiolabelled DFO with ^{67}Ga. The complex showed high stability in mouse serum (> 97%) after 3-hours incubation. An *in vitro* study of [^{67}Ga]Ga-DFO uptake by *S. aureus* in culture showed 25% uptake post 6-hours' incubation, with no change in uptake percentage after 24 hours.[99] In the same study, [^{67}Ga]Ga-DFO was tested *in vivo* in a *S. aureus* (ATCC 25293) myositis model (1×10^8 colony forming unit (CFU), 50 μL PBS) and compared with another group of mice who received a PBS injection in the left thigh as a control. After 20 hours of infection induction, [^{67}Ga]Ga-DFO was injected intravenously. *Ex vivo* biodistribution at 1 hour post injection exhibited higher but modest uptake in the infected (~ 0.5%ID/g) compared to the non-infected thighs (~ 0.1%ID/g) and demonstrated that the majority of the uptake occurs in the bladder, with minimal uptake in the kidneys. To test the viability and ability of bacteria to grow, abscesses from infected muscles were collected using aseptic technique and cultured for 24 hours. After incubation, *S. aureus* from the infected muscles showed growth of colonies indicating viable bacteria at the site of infection.[99]

Due to the higher sensitivity of PET over SPECT, the commercially available germanium-68/gallium-68 generator and the relatively short half-life of ^{68}Ga, ^{68}Ga-labelled siderophores have been investigated as a specific infection imaging agent.[95] A study testing [^{68}Ga]Ga-DFO as an infection imaging agent *in vitro* and *in vivo* confirmed previous research results and showed uptake of [^{68}Ga]Ga-DFO in different strains of *S. aureus* and *P. aeruginosa in vitro* in iron-deficient conditions. Unlike in *S. aureus* and *P. aeruginosa*, [^{68}Ga]Ga-DFO showed no uptake in any *E. coli* strains *in vitro*.[100] The difference in [^{68}Ga]Ga-DFO uptake between microorganism species might be related to the ability of different strains to utilise DFO as a xenosiderophore (a

siderophore that is not produced by the same microorganism) or to use different iron-scavenging mechanisms in iron-deficient conditions.[100,109]

In the same study, [^{68}Ga]Ga-DFO was tested *in vivo* in *S. aureus* (CCM 5971, 5 x 10^8 CFU) and *P. aeruginosa* (ATCC 15692, 5 x10^7 CFU) myositis models. *S. aureus* or *P. aeruginosa* live bacteria was injected into the left leg of each mouse, while heated killed bacteria, turpentine oil (sterile inflammation) or 5 x 10^8 CFU of live *E. coli* were injected into the right leg. Bacterial infections were allowed to grow for 5 hours and sterile inflammations for 24 hours.[100] PET/CT images showed high uptake in *S. aureus* and *P. aeruginosa* infection sites compared to minimal uptake in sterile inflammation sites and no uptake in *E. coli* or heated killed bacteria injection sites. *Ex vivo* biodistribution confirmed PET/CT results and demonstrated a significant difference in uptake between legs infected with *S. aureus* (1.27 ± 0.34%ID/g) and non-infected legs (heated killed bacteria and sterile inflammation) (0.13 ± 0.02%ID/g). No *ex vivo* data were presented regarding the *P. aeruginosa* and *E. coli* infectious myositis models.[100] A higher uptake of [^{68}Ga]Ga-DFO (1.27 ± 0.34%ID/g) was observed in *S. aureus*-infected sites compared to the uptake of [^{67}Ga]Ga-DFO recorded by Ioppolo et al.[99] (~ 0.5%ID/g). This discrepancy could be attributed to differences in the *S. aureus* strains used and in the number of bacteria present at the time of imaging. In agreement with the findings of Ioppolo et al., [^{68}Ga]Ga-DFO showed 98.4 ± 0.46% stability in human serum *in vitro* after 120 minutes incubation and no [^{68}Ga]Ga-DFO uptake was seen in normal tissues *in vivo* at 30 minutes, except in the kidneys and bladder.[99,100] Although the *ex vivo* data from the previously mentioned preclinical studies of [$^{68/67}$Ga]Ga-DFO showed modest uptake in the infected sites, the rapid renal excretion and low blood pool of [$^{68/67}$Ga]Ga-DFO renders infection sites higher uptake than the surrounding tissues. In addition, [^{68}Ga]Ga-DFO showed a specific property in imaging *S. aureus* and *P. aeruginosa* infection over inflammation making it a possible specific infection imaging agent.

Over the past few years, the siderophore compounds [^{68}Ga]Ga-triacetylfusarinine C ([^{68}Ga]Ga-TAFC), [^{68}Ga]Ga-ferrioxamine E ([^{68}Ga]Ga-FOXE), and [^{68}Ga]Ga-desferriferricrocin ([^{68}Ga]Ga-FC) have been studied preclinically in *Aspergillus fumigatus* (*A. fumigatus*) fungal infections,[97,98,101,102] with [^{68}Ga]Ga-TAFC in particular showing stability and low protein binding *in vitro* (< 2%). It showed no uptake *in vitro* in iron-sufficient conditions and high uptake in iron-deficient conditions which can be blocked by Fe-TAFC, indicating specific binding and competition over siderophore transporters.[97,98,101,102] Moreover, it showed low blood pool activity (1.6 ± 0.37%ID/g), with uptake only in the kidneys and bladder at 30 minutes *in vivo* in healthy BALB/c mice, indicating its stability and ability to not release ^{68}Ga to blood proteins.[97,98]

In contrast, [^{68}Ga]Ga-FC showed instability and high protein binding (64.36%) *in vitro*. [^{68}Ga]Ga-FC showed high uptake in iron deficient conditions which can only be partially blocked by Fe-FC indicating the instability of [^{68}Ga]Ga-FC and a possible non-specific binding probably by

trans-chelation of ^{68}Ga to transferrin. In addition, unlike [^{68}Ga]Ga-TAFC, [^{68}Ga]Ga-FC showed minimal uptake (~20% of that in iron deficient condition) in iron sufficient conditions confirming the possibility of non-specific binding.[97,98] In the same study, [^{68}Ga]Ga-FC showed high blood pool activity *in vivo* even at 90 minutes post-injection (16.1 ± 1.07%ID/g). In addition, uptake was also seen in kidneys (~ 8%ID/g), liver (~ 7%ID/g), heart (~ 6%ID/g), lungs (~ 10%ID/g), spleen and intestine (< 2%ID/g). No *ex vivo* data or PET images of the bladder were presented.[97,98] The high blood pool activity and tissue uptake of [^{68}Ga]Ga-FC might suggest its instability *in vivo*, however, this must be demonstrated experimentally.[97,98]

[^{68}Ga]Ga-FOXE is another siderophore compound that was tested preclinically in *A. fumigatus.* [^{68}Ga]Ga-FOXE showed high uptake in iron-deficient conditions and minimal uptake in iron-sufficient conditions, as well as high stability and low protein binding (0.53%) *in vitro*. The minimal uptake of [^{68}Ga]Ga-FOXE in iron-sufficient conditions might indicate non-specific binding and/or the different mechanisms of *A. fumigatus* to accumulate xenosiderophores when iron is sufficiently present. Unlike TAFC and FC, which are natural siderophores for *A. fumigatus*, FOXE is a siderophore produced by bacteria (*Streptomyces spp*.).[98,101,102,143] *Ex vivo* biodistribution of [^{68}Ga]Ga-FOXE in healthy animals confirmed the stability of the tracer with low blood pool activity (< 0.5%ID/g) at 90 minutes and rapid renal excretion.[98] PET images of [^{68}Ga]Ga-FOXE in healthy rats showed that only the kidneys and bladder were visible at 1 hour post injection.[102]

Preclinical studies in rats showed accumulation of [^{68}Ga]Ga-TAFC and [^{68}Ga]Ga-FOXE in infected sites in proportion to severity (1–3%ID/g for severe infections and 0.3–1%ID/g for mild infections), with negligible uptake in control (healthy) models (0.04%ID/g) 2 hours post injection. Signals from imaging infection sites were minimal but detectable due to the fast clearance and low blood pool activity of [^{68}Ga]Ga-TAFC and [^{68}Ga]Ga-FOXE.[97,101,102] A preclinical study in a rat myositis model injected with *S. aureus* on one side and turpentine oil on the other side was performed to test the specificity of [^{68}Ga]Ga-TAFC and [^{68}Ga]Ga-FOXE in imaging infection and to compare the result with ^{18}F-FDG. PET images after ^{18}F-FDG showed high uptake in both infection and inflammation sites, indicating ^{18}F-FDG's lack of ability to differentiate between infection and inflammation. However, [^{68}Ga]Ga-TAFC and [^{68}Ga]Ga-FOXE showed no uptake at the infection sites which might indicate that *S. aureus* probably does not utilise TAFC and FOXE as xenosiderophores. [^{68}Ga]Ga-TAFC and [^{68}Ga]Ga-FOXE showed detectable signals at the inflammation sites, which might be related to the severity of infection and some level of non-specific extravasation.[102] To address this knowledge gap, the specificity of [^{68}Ga]Ga-TAFC and [^{68}Ga]Ga-FOXE must be tested in a myositis model infected with a fungal strain (for example *A. fumigatus),* that is known to take up TAFC and FOXE, and the results compared to a control group with sterile inflammation. Although non-specific binding of [^{68}Ga]Ga-TAFC and [^{68}Ga]Ga-FOXE is unlikely to be due to the ability of siderophores to be taken up selectively by live

microorganisms, it is important to experimentally study and test the specificity of ^{68}Ga siderophores and their ability to distinguish between infection and inflammation.

Specific imaging of *P. aeruginosa* was studied using pyoverdine PAO1 (PVD-PAO1, a *P. aeruginosa* natural siderophore) radiolabelled with ^{68}Ga. Compared to other ^{68}Ga siderophores used such as [^{68}Ga]Ga-FOXE and [^{68}Ga]Ga-TAFC for bacterial screening, [^{68}Ga]Ga-PVD-PAO1 showed the highest *in vitro* uptake.[103] In *P. aeruginosa* lung infection rat models, PET/CT imaging of [^{68}Ga]Ga-PVD-PAO1 showed focal accumulation in infected lungs compared to no uptake in the control group. *Ex vivo* biodistribution confirmed the imaging results, with significant difference in lung uptake between infected (1.35 ± 0.23%ID/g) and non-infected lungs (0.23 ± 0.03%ID/g). To test the specificity of [^{68}Ga]Ga-PVD-PAO1 in imaging *P. aeruginosa* infection, two myositis mouse models bearing either *P. aeruginosa* and sterile inflammation (induced by turpentine oil) or *P. aeruginosa* and *E. coli* were tested. PET/CT imaging of [^{68}Ga]Ga-PVD-PAO1 showed high uptake in *P. aeruginosa* compared to no obvious uptake in sterile inflammation and *E. coli*.[103] Overall, there seems to be evidence indicating the specificity and sensitivity of [^{68}Ga]Ga-PVD-PAO1 in detecting *P. aeruginosa* infection. However, no *ex vivo* biodistribution data were presented.[103] Unlike [^{68}Ga]Ga-PVD-PAO1, PET/CT images of ^{68}Ga citrate and ^{18}F-FDG showed uptake in *P. aeruginosa* and sterile inflammation. Due to fast renal excretion of ^{68}Ga siderophores, [^{68}Ga]Ga-PVD-PAO1 images showed low background uptake and better infection visualisation compared to uptake of ^{68}Ga citrate and ^{18}F-FDG.[103] Findings from previous $^{67/68}$Ga siderophore studies suggest the specificity of $^{67/68}$Ga siderophore compounds for imaging infection. Performing bacterial culture on infected muscle tissues (in myositis models) after *ex vivo* biodistribution could be added to *in vivo* experimental planning as it would be a key analysis to confirm the viability and ability of the bacteria to grow or to indicate an active infection.

2.5 Graft infection imaging

In addition to its use in diagnosing soft tissue and bone infection, radionuclide imaging is emerging as a major tool for detecting post-operative graft infection. Progress in medicine has made the use of grafts in blood vessels, bile ducts, bronchi, and ureters an option. Nevertheless, any external material in the body can be a nest for infection. Although infection is not a very common complication after graft implantation (0.5–6%), a delay in diagnosis could increase morbidity and mortality.[144,145,146] Diagnosis and treatment of graft infection remains a challenge, even in modern medicine.[144,147] CT scanning is an imaging approach for detecting graft infection; however, results are often inconclusive as CT detects anatomical changes in the area surrounding the graft that could be related to either infection abscesses or other conditions, such as haematomas.[145] Current gold standard for graft infection diagnosis includes surgical intervention, with positive microorganism cultures taken directly from a biopsy sample or surgically-removed

tissue specimen. Unfortunately, this approach is clinically often difficult to implement on a regular basis, and is invasive and dangerous.[148,149,150]

Molecular imaging studies can contribute to the detection of graft infection, either by using labelled white blood cells (WBC), ^{67}Ga citrate, or ^{18}F-FDG. Early clinical studies on imaging of graft infection showed that ^{99m}Tc-hexamethylpropylene-amine oxime (HMPAO)-labelled WBC scintigraphy (planar imaging) has high sensitivity and specificity in detecting aortofemoral graft infection in patients who develop specific graft infection symptoms, such as groin abscesses, gastrointestinal bleeding, persistent abdominal or back pain and high fever. ^{99m}Tc-HMPAO-labelled WBC scintigraphy showed no false-positive or false-negative scans.[151,152] Conversely, in patients who showed non-specific signs and symptoms, such as low-grade fever, vague abdominal pain and leukocytosis, the specificity of ^{99m}Tc-HMPAO-labelled WBC scintigraphy decreased as it presented patients with false-positive results indicating its low specificity. The reliability of ^{99m}Tc-HMPAO-labelled WBC scintigraphy was assessed by microbiological tests and cultures on surgically removed stents.[151,152] The sensitivity and specificity of ^{99m}Tc-HMPAO-labelled WBC scintigraphy were tested in a more recent clinical study on patients with different graft infection locations who developed specific graft infection symptoms. Results were compared with ^{99m}Tc-HMPAO-labelled WBC SPECT/CT. ^{99m}Tc-HMPAO-labelled WBC SPECT/CT recognised 4 false-positive and 9 false-negative scans out of 55 scans on planar imaging. The final graft infection diagnoses were confirmed by surgically removing the stents and performing microbiological tests.[153] The superiority of SPECT/CT over planar imaging might be related to the ability of tomographic imaging to anatomically localise the precise infection site and minimise tissue superimposition.[153,154]

Indium (^{111}In)-oxine is another WBC tracer that has been tested for detecting graft infection. An early clinical study on patients with suspected aortic graft infection based on specific signs and symptoms showed that ^{111}In-oxine-labelled WBC scintigraphy was able to detect 5 out of 5 positive groin infections in patients but failed to detect 2 out of 3 extended retroperitoneum infections. Graft infection was confirmed by CT scan, surgical removal of stents and bacterial culture.[155] Retrospective studies using autopsy reports and operation records of patients with multiple prosthetic graft infection sites and specific symptoms showed the ability of ^{111}In-oxine-labelled WBC scintigraphy and SPECT/CT to detect graft infection. However, the results of these retrospective studies provided false-positive/negative results or indefinite diagnoses.[156,157,158]

Clinical studies have also examined the ability of ^{67}Ga citrate to diagnose graft infection. Research on patients with specific graft infection symptoms reported that ^{67}Ga citrate correctly identified infected grafts (confirmed by graft culture and CT scan), with no uptake seen in non-infected cases.[159,160,161] An isolated case report confirmed the sensitivity and specificity of ^{67}Ga citrate in detecting graft infection.[162] One of the limitations of these studies, however, is the patient sample

size used (≤ 11 patients). Moreover, in all cases, patients developed specific signs and symptoms of graft infection, but the specificity of ^{67}Ga citrate in patients with less specific symptoms was not studied.[159,160,161,162] Another case study offered a contradictory finding on ^{67}Ga citrate sensitivity by demonstrating a false-negative result in a confirmed graft infection case.[163]

In addition to WBC tracers and ^{67}Ga citrate, ^{18}F-FDG specificity and sensitivity in detecting graft infection have been tested clinically. Prospective clinical studies on patients with suspected graft infection based on clinical signs and symptoms (such as fluid formation, cellulitis, local pain, swelling and fever) have shown false-positive ^{18}F-FDG PET/CT scans in graft infection cases confirmed with either surgery and microbiology tests or with follow-up scans and contrast-enhanced high-resolution CT (in patients with contraindications to surgery).[164,165,166] Although ^{18}F-FDG showed high sensitivity, the false-positive results indicate its questionable specificity. False-positive ^{18}F-FDG scans might be related to the presence of haematomas or lymphoceles adjacent to the infected graft.[164,165] In patients with no signs of infection, ^{18}F-FDG PET/CT scans also showed mild increased activity in grafts, which might be related to post-operative inflammation in newly implanted grafts and this was the case in some patients (grafts were implanted 1–24 months before the PET/CT scan).[164] Other prospective clinical studies contradicted the high sensitivity of ^{18}F-FDG[166,167]. The authors initially assumed a high-rate sensitivity of ^{18}F-FDG in diagnosing graft infection based on the appearance of a focal uptake at the infected graft site because most of the focal ^{18}F-FDG uptake graft infection suspected cases were later confirmed to be infection. However, ^{18}F-FDG showed false-negative (no focal uptake) results in cases confirmed to be graft infections. These studies also showed diffuse (not focal) ^{18}F-FDG uptake in graft areas that were later confirmed to be either positive or negative results.[166,167] Although ^{18}F-FDG is reasonably able to detect graft infection, ^{18}F-FDG distribution can be very similar in both infected and non-infected grafts, making diagnosis very challenging. Another study aiming to assess the uptake patterns of infected and non-infected grafts showed considerable overlap between the two in terms of maximum SUV distribution, focal/homogeneous uptake and infected/non-infected graft to background ratio.[168]

While current imaging agents, such as ^{67}Ga citrate, ^{111}In-oxine- and ^{99m}Tc-HMPAO-labelled WBCs, and ^{18}F-FDG, showed feasibility in detecting graft infection, most of their study results were confirmed with other structural imaging modalities, such as CT or microbiology tests. However, microbiology tests in particular are invasive and often not possible for patients with contraindications to surgery as they require obtaining a specimen or surgically removing part of the stent.[164,169] In addition, most of the previously mentioned studies using ^{67}Ga citrate, WBC tracers and ^{18}F-FDG were based on patients who developed specific signs of graft infection and who, therefore, are likely to have infection present, leading to positive results. However, patients might develop specific symptoms at a later stage of the infection, when therapy is more challenging and morbidity and mortality are increased.[151,169] Thus, it is desirable to find a specific

imaging agent that is capable of accurately assessing graft infection even in the absence of specific clinical signs and symptoms aiming to detect infections at early stage.

Accumulation of ^{67}Ga citrate is based on transferrin, lactoferrin, ferritin and siderophores, while accumulation of WBC tracers and ^{18}F-FDG is based on WBCs and glycolysis, respectively, regardless of the underlying pathology. All uptake mechanisms (except siderophores) are part of the inflammatory process and the host's response to infection rather than to the infectious pathogen itself which makes these mechanisms non-specific for infection imaging, which is unable to reliably distinguish infection from other diseases.[144,149] Due to their non-specific properties for infection imaging, ^{67}Ga citrate, labelled WBC tracers and ^{18}F-FDG might have less sensitivity and specificity in detecting graft infection in patients with non-specific graft infection signs and symptoms or in patients with altered responses to infection due to other underlying diseases, such as cancer, immunosuppression or diabetes.[169,149] False-positive results in graft infection patients can be caused by accumulation of ^{67}Ga citrate, labelled WBC tracers or ^{18}F-FDG in both infection and inflammation sites, while false-negative results can be the result of low-grade infection limitations (especially in inhomogeneous biodistribution) or of overlapping of the graft and normal tissue uptake.[153,165] False-positive results could lead to unnecessary surgery, and false-negative results to high morbidity.[164] The current limitations in assessing graft infection, especially in the absence of specific signs and symptoms, makes therapy more challenging. Non-definitive diagnosis remains a major barrier that can lead to invasive procedures, such as biopsies and surgical removal of stents, as well as indiscriminate use of antibiotics, antibiotic resistance, and drug toxicity. Thus, there is an urgent need to find a specific graft infection imaging agent based on the infectious pathogen to detect graft infection at an early stage and improve patient outcomes.[149,151] Small molecules, such as siderophores, that are selectively secreted by bacteria could help these agents to accurately distinguish infections from inflammations, such as haematomas or scar tissues.[149] As mentioned previously, $^{68/67}$Ga-labelled siderophores are non-invasive specific infection imaging agents that can also play a major role in graft infection imaging. Previously mentioned preclinical studies of $^{68/67}$Ga siderophores in infection (other than graft infection) imaging showed that they favour bacterial accumulation over background signal (low blood pool activity), making these agents adequate for infection imaging.[149] Due to the rapid renal excretion of $^{68/67}$Ga siderophores, imaging using them would likely not require a prolonged delay between administration and imaging, in contrast to using ^{67}Ga citrate (6–97 hours), ^{111}In-oxine- (18–24 hours) and ^{99m}Tc-HMPAO-labelled WBCs (30 minutes to 24 hours) or ^{18}F-FDG (≥ 45 minutes), or fasting for several hours like when using ^{18}F-FDG.[151,153,155,159,160,161,166] To the best of our knowledge, no studies have been conducted to test the effectiveness of $^{68/67}$Ga siderophores in imaging graft infection in humans.

Overall, $^{67/68}$Ga siderophores showed promising results *in vitro* and *in vivo* indicating their specificity for imaging infection. The specificity of $^{67/68}$Ga siderophores for imaging infection can

be investigated clinically. DFO is a good candidate that can be radiolabelled with ^{68}Ga and tested clinically for imaging graft infection. The advantages of investigating [^{68}Ga]Ga-DFO clinically is that DFO is a well-established clinical drug with a modest cost. In addition, ^{68}Ga eluted from a clinically approved ^{68}Ge/^{68}Ga generator can provide easy access and simple on-site radiolabelling. [^{68}Ga]Ga-DFO would have a low regulatory barrier to clinical translation and could be investigated clinically as a specific infection imaging agent for selected bacteria such as *P. aeruginosa* and *S. aureus* (but probably not *E.coli*), which was previously shown to take up [^{68}Ga]Ga-DFO.[99,100,170,171] In addition, other bacterial and fungal species that can utilise the Fe^{3+} complex of DFO (ferrioxamine), such as the *Yersinia enterocolitica* bacterium, *A. fumigatus* and *Cryptococcus neoformans* fungus, could also be investigated.[172,173,174]

2.6 Proof of principle

A proof of principle study was performed in our department by M. Cooper and R. Cusnir (un-published work), to assess the sensitivity and specificity of [^{68}Ga]Ga-DFO for imaging graft infection *in vitro*. Infected stents were generously provided by A. Patel, Department of Infectious Diseases, St Thomas' Hospital. Infected stents were placed in 50 ml Falcon tubes and inoculated with 9 ml of brain heart infusion (BHI) broth and 1 ml of > 10^6 CFU of *S. aureus*, *E. coli*, *P. aeruginosa*, or *Candida albicans* (*C. albicans*). Controls including an organism-free stent in PBS, and organism free stents in BHI broth were also provided. Stents were incubated for 24 hours and then washed three times with sterile PBS. Stents were then resuspended in 7.5 ml of sterile PBS and sent to our department. Upon arrival, PBS from stent tubes was carefully discarded and stents were resuspended in 10 ml of Davies minimal broth. [^{68}Ga]Ga-DFO was radiolabelled by mixing 20 µl of DFO dissolved in water, 500 µl of $NaHCO_3$ (0.2 M), an 1 ml of ^{68}Ga in 0.1 M HCl. The reaction was incubated for 10 minutes at room temperature. 50 µl of [^{68}Ga]Ga-DFO was added to each sample tube (10 µg of DFO, 5-6 MBq), and tubes were incubated at 37°C while shaking for 30 minutes (70 rpm). After incubation, broth was discarded, and stents were washed three times with sterile PBS. The fraction of [^{68}Ga]Ga-DFO bound to the infected stents and controls was measured using a gamma counter (Figure 2.3) and imaged with a phosphor imager (Figure 2.4).

Figures 2.3 showed that among different strains of bacteria and fungi, [^{68}Ga]Ga-DFO showed the highest uptake in *S. aureus* (8.77 ± 1.5 % administered dose (% AD)) and *P. aeruginosa* (12.9 ± 4.07 % AD), while uptake in *E. coli* and *C. albicans* was similar to controls. The results from the phosphor imager (Figure 2.4) were in consistent with gamma counter results. These results confirm previous studies from literature that showed [$^{68/67}$Ga]Ga-DFO is taken up by *S. aureus* and *P. aeruginosa* but not by *E. coli* [99,100] (see section 2.4).

The proof of principle study suggested the potential of [^{68}Ga]Ga-DFO as an imaging agent for grafts infected with selected microorganisms. Based on the evidence from literature and the proof

of principle study, and the prospects for low regulatory barriers to clinical evaluation, it was decided to develop a GMP-compatible [^{68}Ga]Ga-DFO complex in preparation for evaluation of graft infection imaging in humans. This chapter is dedicated to developing simple radiosynthesis of [^{68}Ga]Ga-DFO using GMP grade reagents.

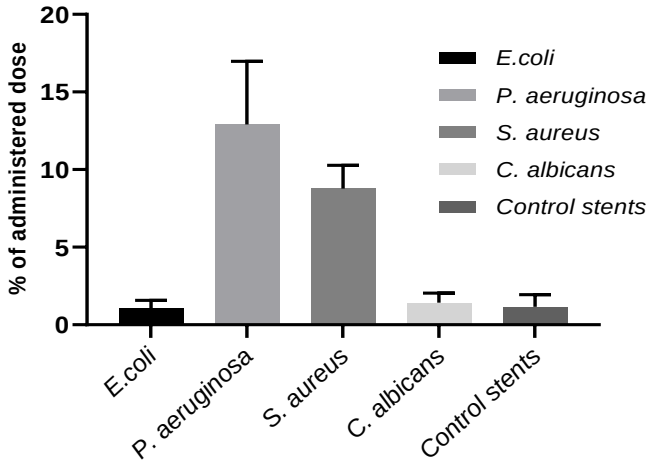

Figure 2.3: [^{68}Ga]Ga-DFO uptake in stents infected with four different strains of bacteria and fungi. Uptake is expressed as mean of % of administered dose ± SD (quadruplets). Control samples are represented as the mean of % of administered dose of three different microorganism-free stents in PBS and broth. Stents were analysed by gamma counter.

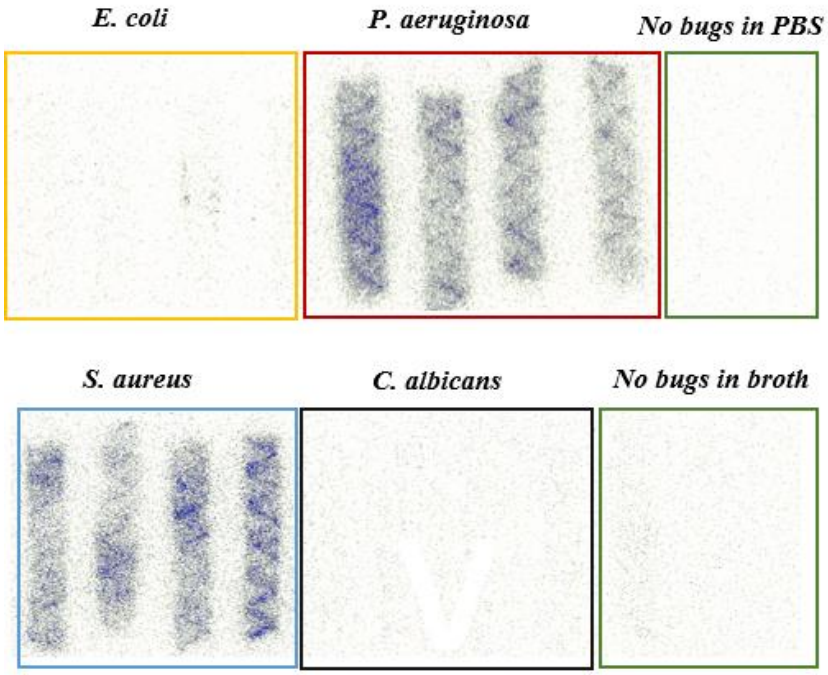

Figure 2.4: [^{68}Ga]Ga-DFO uptake in stents infected with *E. coli* (yellow), *P. aeruginosa* (red), *S. aureus* (blue), *C. albicans* (black), and control microorganism-free stents in PBS and broth (green). Stents were imaged by phosphor imager.

2.7 Aims

The experimental aims of this chapter are to:

- Synthesise a GMP-compatible [^{68}Ga]Ga-DFO complex suitable for use in humans using a simple and quick method.
- Assess radiolabelling of [^{68}Ga]Ga-DFO by iTLC and HPLC.
- Investigate [^{68}Ga]Ga-DFO *in vitro* chemical characteristics including stoichiometry/structure, log *D* value and stability in human serum and urine.
- Evaluate the biodistribution of [^{68}Ga]Ga-DFO in healthy animal models.

2.8 Experimental

2.8.1 Equipment and consumables

All reagents and consumables were purchased from Sigma Aldrich and Thermo Fisher Scientific unless specified otherwise. ^{68}Ga was obtained from a ^{68}Ge/^{68}Ga generator (Eckert & Ziegler) and eluted with 5 ml of 0.1 M ultrapure HCl and collected in 5 x 1 ml fractions. Instant thin layer chromatography (iTLC) was carried out using Agilent technologies silica gel impregnated glass microfiber strips (10 cm length), scanned by a LabLogic mini scan TLC reader with positron (β^+) detector and analysed with Laura software. High-performance liquid chromatography (HPLC) was implemented using an Agilent Eclipse XDB C_{18} 5 µm 4.6 × 150 mm reversed phase (RP) column and Agilent technologies 1200 series with in-line ultraviolet (UV) detection (220 nm) with Gina Star ™ software version 5.8. Liquid chromatography-mass spectrometry (LC/MS) was acquired by using an Agilent Eclipse XDB C_{18} 5 µm 4.6 × 150 mm RP column on an Agilent Liquid Chromatograph (1200 Series) with UV detection at 230 nm, connected with Advion Expression LCMS mass spectrometer with electrospray ionisation source. Analysis was performed by Advion Mass Express software (version, 6.4.16.1). Gamma counting was performed by LKB Wallac 1282 CompuGamma Gamma Counter. PET/CT images were acquired with nanoScan® PET/CT (Mediso Medical Imaging Systems, Budapest, Hungary). Images were reconstructed using Nucline software (version 2.00) and analysed using VivoQuant software (version 1.23).

2.8.2 Developing a GMP-compatible radiolabelling method for [^{68}Ga]Ga-DFO

Multiple radiolabelling methods were evaluated using GMP grade DFO with different GMP grade buffers to find the easiest and fastest radiolabelling method. The details of each radiolabelling method are listed in the following sections.

2.8.3 Radiolabelling of [^{68}Ga]Ga-DFO using sodium bicarbonate buffer

[^{68}Ga]Ga-DFO was radiolabelled by mixing low and high concentrations of GMP-grade DFO (5 or 150 µl) (DEMO S.A, product licence number: PL 24598/0020) dissolved in water (1 µg/µl), 50 µl of GMP-grade sodium bicarbonate (1 M, contain 0.01 w/v EDTA, Martindale Pharmaceuticals, product licence number: PL 01883/0023) and 500 µl ^{68}Ga chloride. The sample was diluted with water to bring the final volume to 1 ml. The final concentration of EDTA in the samples was 7.25 nM to 7.60 µM (for 5 µg) or 22.8 µM (for 150 µg) of DFO. An unchelated ^{68}Ga (control) was prepared following the same methods, with the aqueous solution of DFO replaced with only water. [^{68}Ga]Ga-DFO and unchelated ^{68}Ga radiolabelled in reagent grade (EDTA free) sodium bicarbonate buffer (1 M, pH=9, Sigma Aldrich 71631) were evaluated for comparison following the same method. In addition, radiolabelling of unchelated ^{68}Ga (as a control) in an

aqueous solution of EDTA (50 mM) was also evaluated following the same method. Radiochemical purity (RCP) was evaluated by iTLC and RP-HPLC after 10 minutes of incubation at room temperature (pH= 6-6.5). An elution profile of the aqueous solution of DFO was obtained by RP-HPLC. iTLC mobile phase: 1 M ammonium acetate in 1:1 v/v H_2O and methanol (pH=7). RP-HPLC mobile phase: water (A) and acetonitrile (B), each containing 0.1%TFA. Gradient: (0–2 min: 0 % B, 2–24 min: 0-60 % B, 24–26 min: 60 % B, 26–28: min: 60-0% B).

2.8.4 Radiolabelling of [^{68}Ga]Ga-DFO using sodium bicarbonate buffer with a heating step

To further investigate the thermodynamic preference between EDTA and DFO binding to ^{68}Ga, an extra step of incubation at 80°C was added to the radiolabelling method of [^{68}Ga]Ga-DFO prepared in GMP-grade sodium bicarbonate to assess whether EDTA and ^{68}Ga binding is a kinetic rather than thermodynamic effect. [^{68}Ga]Ga-DFO was radiolabelled following the previously mentioned method (5 µg/ml of DFO was used). However, instead of incubating for 10 minutes at room temperature, [^{68}Ga]Ga-DFO was heated at 80°C for 10 minutes. RCP was evaluated by RP-HPLC, mobile phase and gradient as before (section 2.8.3).

2.8.5 Radiolabelling of [^{68}Ga]Ga-DFO using sodium acetate buffer

After several attempts to optimise the radiolabelling methods, it was decided (see discussion section) to investigate another GMP-grade buffer for a simple and quick radiolabelling method. [^{68}Ga]Ga-DFO was radiolabelled by mixing GMP-grade DFO (20 µl) dissolved in water (1 µg/µl), 50–100 µl of GMP-grade sodium acetate (EDTA free, 3.6 M, pH=9, Torbay Pharmaceuticals, product code Y8247C) and 500 µl ^{68}Ga chloride. The sample was diluted with water to bring the final volume to 1 ml. [^{68}Ga]Ga-acetate (control) was radiolabelled following the same method, however, the aqueous solution of DFO was replaced with water. RCP was evaluated by iTLC and RP-HPLC after 10 minutes of incubation at room temperature (pH= 5.5/6). The elution profile of the aqueous solution of DFO was obtained by RP-HPLC UV detection (220 nm). iTLC mobile phase: 1 M ammonium acetate in 1:1 v/v H_2O and methanol (pH=7). RP-HPLC mobile phase and gradient as before (section 2.8.3). Due to the presence of some apparent impurities during the RP-HPLC analysis (between 3 to 6 minutes) of [^{68}Ga]Ga-DFO, which was also seen when sodium bicarbonate was used as a buffer but was not visible in the iTLC analysis, it was suggested that these might be artefacts caused by the presence of TFA and low pH in the mobile phase. To test this suggestion, a RP-HPLC analysis of [^{68}Ga]Ga-DFO was performed by radiolabelling [^{68}Ga]Ga-DFO with GMP sodium acetate buffer as previously mentioned. However, post incubation, 20 µl of TFA (2% of the sample volume) was added to the sample preparation (pH=2) and incubated for 1 minute at room temperature. RP-HPLC mobile phase: water (A) and acetonitrile (B), each containing 0.1%TFA. In addition, a RP-HPLC analysis of

[^{68}Ga]Ga-DFO and [^{68}Ga]Ga-acetate (control) was performed with no TFA in the mobile phase, followed by 50 µl of an aqueous solution of EDTA (50 mM) to elute ^{68}Ga trapped in the column (if any). Decay correction was used to normalise the EDTA radioactivity measurement to the time of the HPLC analysis of the relevant sample.

2.8.6 Octanol extraction/ log$D_{7.4}$ (octanol/PBS)

Determination of hydrophilicity was performed by the shake flask method. 0.3–0.5 MBq of the [^{68}Ga]Ga-DFO and [^{68}Ga]Ga-acetate mixtures was added to a pre-equilibrated mixture of equal volumes of octanol and PBS (500 µl/500µl). Samples were vortexed for 2 minutes with a Multi Vortex Mixer V-32 (Grant Bio) to obtain a good separation between the two layers. 200 µl was taken from each layer and analysed separately with a gamma counter.

2.8.7 LC/MS of ^{nat}Ga-DFO and [^{68}Ga]Ga-DFO

^{nat}Ga-DFO was prepared by mixing an aqueous solution of GMP-grade DFO (10 mM), GMP-grade sodium acetate (3.6 M) and an aqueous solution of gallium nitrate (10 mM) (Thermo Fisher Scientific 32116). The mixture was diluted 10-fold with water to bring the final concentration to 1 mM. 20 µl of [^{68}Ga]Ga-DFO (2 MBq) and ^{nat}Ga-DFO were used for LC/MS analysis. LC/MS mobile phase: water (A) and acetonitrile (B), each containing 0.1%TFA. Gradient as before (section 2.8.3).

2.8.8 Serum stability study of [^{68}Ga]Ga-DFO

[^{68}Ga]Ga-DFO was radiolabelled by mixing GMP-grade DFO (10 µl) dissolved in water (1 µg/µl), 10 µl of GMP-grade sodium acetate and 100 µl of ^{68}Ga chloride. After 10 minutes of incubation at room temperature, the mixture was diluted (1:1 v/v) with either human serum (Sigma Aldrich, H4522) or PBS (control) and incubated for 5 and 60 minutes at 37°C. [^{68}Ga]Ga-acetate was incubated in human serum for 5 minutes (control) using the same method. Ice-cold acetonitrile was added (1:1 v/v) and samples were vortexed for 1 minute followed by centrifugation at 13,000 rpm for 5 minutes. Following centrifugation, supernatant was removed and activity in the supernatant and precipitate were counted using a gamma counter. Aliquots from the supernatant were used for iTLC and RP-HPLC analysis after being diluted five times with water (0.3–0.5 MBq). iTLC mobile phase: 1M ammonium acetate in 1:1 v/v H_2O and methanol (pH=7). RP-HPLC mobile phase and gradient as before (section 2.8.3).

2.8.9 *In vivo* study of [^{68}Ga]Ga-DFO after intravenous injection

An animal experiment was completed in accordance with the project and a personal licence approved by British Home Office regulations governing animal experimentation. The animal experiment was performed on healthy female Balb/C mice (6–9 weeks old) purchased from

Charles River UK Ltd. To evaluate the biodistribution and pharmacokinetics of [^{68}Ga]Ga-DFO prepared by the above-described method (see section 2.8.5, with GMP grade sodium acetate buffer), mice (n=3) were intravenously injected with [^{68}Ga]Ga-DFO diluted in PBS (150–200 µl, 1.2–1.5 MBq and 0.2–0.3 µg DFO per mouse) and passed through a sterile Millex-LG 0.20 µm filter before injection. Mice were PET/CT scanned dynamically for 60 minutes and sacrificed for organ harvesting at 60 minutes. Organs were weighed and counted in a gamma counter. To assess the stability of [^{68}Ga]Ga-DFO in urine, a mouse urine sample taken from the excised bladder was injected directly (100 µl) into HPLC for analysis. HPLC mobile phase: water (A) and acetonitrile (B), each containing 0.1%TFA, gradient as before (section 2.8.3). PET/CT static images were generated from the dynamic acquired data and were reconstructed at 1-minute time bins for the first 5 minutes of scanning, at 5-minute time bins from 5 to 30 minutes of scanning, and at 10-minute time bins from 30 to 60 minutes of scanning. PET/CT images were used for the delineation of the region of interest (ROI) and quantification of distributed activity in selected organs. The time-activity curves were obtained from the generated ROIs within the selected organs.

2.8.10 Stability of [^{68}Ga]Ga-DFO in human urine

To further investigate the stability of [^{68}Ga]Ga-DFO in human urine, [^{68}Ga]Ga-DFO was incubated in human urine (Lee BioSolutions, 991-03-P) *in vitro* to assess whether [^{68}Ga]Ga-DFO metabolism occurs in serum prior to reaching urine or in the urine. [^{68}Ga]Ga-DFO was radiolabelled by mixing GMP-grade DFO (20 µl) dissolved in water (1 µg/µl), 20 µl of GMP-grade sodium acetate and 200 µl ^{68}Ga chloride. After 10 minutes of incubation at room temperature, the mixture was diluted (1:1 v/v) with either human urine and incubated for 5, 30 and 60 minutes or diluted with PBS (control) and incubated for 60 minutes. [^{68}Ga]Ga-acetate (control) was radiolabelled following the same method and incubated with human urine for 30 minutes. After incubation, the mixtures were diluted with water (1:1 v/v) and centrifuged for 10 minutes at 13,000 rpm. Before injecting into the HPLC, mixtures were passed through a MF-Millipore membrane filter (33 mm with 0.45 µm pore size, Merck Millipore, SLHA033SS) to remove any particles. 100 µL of the filtered sample (0.4–0.8 MBq) was injected into the HPLC. HPLC mobile phase: water (A) and acetonitrile (B), each containing 0.1%TFA, gradient as before (section 2.8.3).

2.9 Results

2.9.1 Radiolabelling of [^{68}Ga]Ga-DFO using sodium bicarbonate buffer

Mixing GMP-grade DFO using both tested concentrations with ^{68}Ga chloride in reagent grade sodium bicarbonate buffer results in a product with ≥ 95% RCP. While [^{68}Ga]Ga-DFO moved to the solvent front with retention factor (Rf) = 0.7/0.9, unchelated ^{68}Ga remained in the origin as shown by iTLC analysis (Figure 2.5 A and B). On the contrary, using the same conditions, iTLC analysis showed that unchelated ^{68}Ga moved to the solvent front with Rf= 0.86 when prepared with GMP-grade sodium bicarbonate buffer (containing EDTA), indicating EDTA and ^{68}Ga binding (Figure 2.5 C). iTLC analysis of unchelated ^{68}Ga prepared with an aqueous solution of EDTA (control) showed a Rf =0.9, similar to the sample prepared with GMP-grade sodium bicarbonate, confirming ^{68}Ga and EDTA binding (Figure 2.5 D).

RP-HPLC analysis of all unchelated ^{68}Ga samples showed the same retention time at 2:30 min:s (Figure 2.6 A). Figure 2.6 B represents the UV chromatogram of DFO, eluting at 11:50 min:s using ultraviolet (UV) detection (220 nm). The RP-HPLC analysis of [^{68}Ga]Ga-DFO prepared with reagent grade sodium bicarbonate showed that at both DFO concentrations used (5 and 150 µg), a single peak was seen at 10:30/10:50 min:s (Figure 2.6 C and D). On the contrary, the [^{68}Ga]Ga-DFO (5 µg/ml of DFO) sample prepared with GMP-grade sodium bicarbonate (which contains 7.25 nM EDTA) showed 95% of activity eluting at 2:10 min:s, indicating competition between DFO and EDTA for ^{68}Ga binding. Although the presence of a higher concentration of DFO in the sample (150 µg/ml) decreased the amount of ^{68}Ga bound to EDTA to 38%, it did not remove it completely (Figure 2.6 C and D). In addition, some early-eluting radioactivity was seen in the HPLC analysis of [^{68}Ga]Ga-DFO between 3 and 6 minutes, an artefact which will be discussed later.

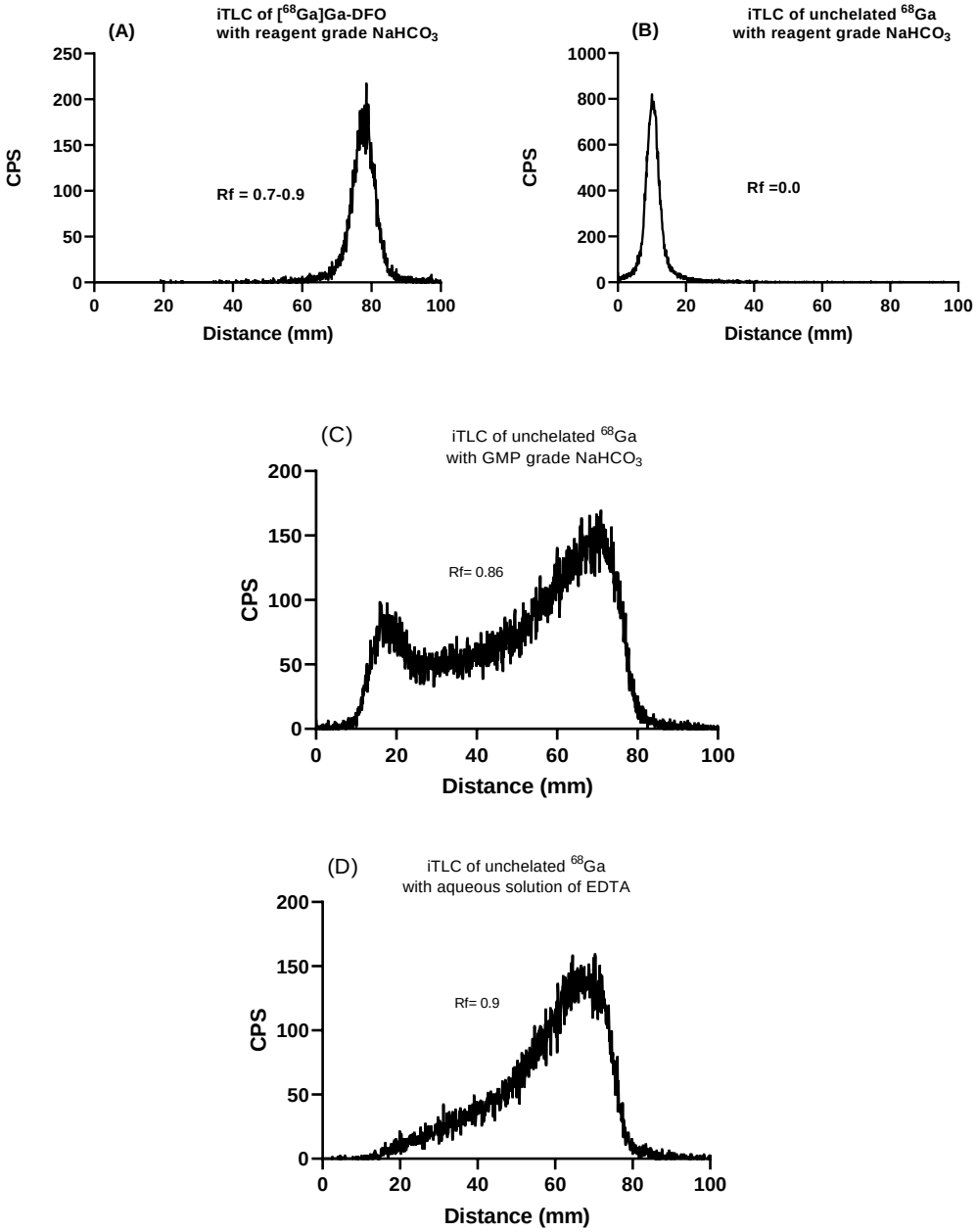

Figure 2.5: Radioactivity distribution pattern on silica gel impregnated glass microfiber strips of [^{68}Ga]Ga-DFO (A) and unchelated ^{68}Ga (B) prepared with reagent grade (EDTA free) sodium bicarbonate buffer shows that [^{68}Ga]Ga-DFO moved to the solvent front while unchelated ^{68}Ga remained in the origin. Panel C and D represent the radioactivity distribution pattern on silica gel impregnated glass microfiber strips of unchelated ^{68}Ga prepared with GMP-grade sodium bicarbonate buffer (contain EDTA) and an aqueous solution of EDTA respectively. Panel C and D shows that unchelated ^{68}Ga moved to the solvent front indicating ^{68}Ga and EDTA binding. Mixtures incubated for 10 minutes at room temperature. Mobile phase: 1M ammonium acetate in 1:1 v/v H_2O and methanol (pH=7).

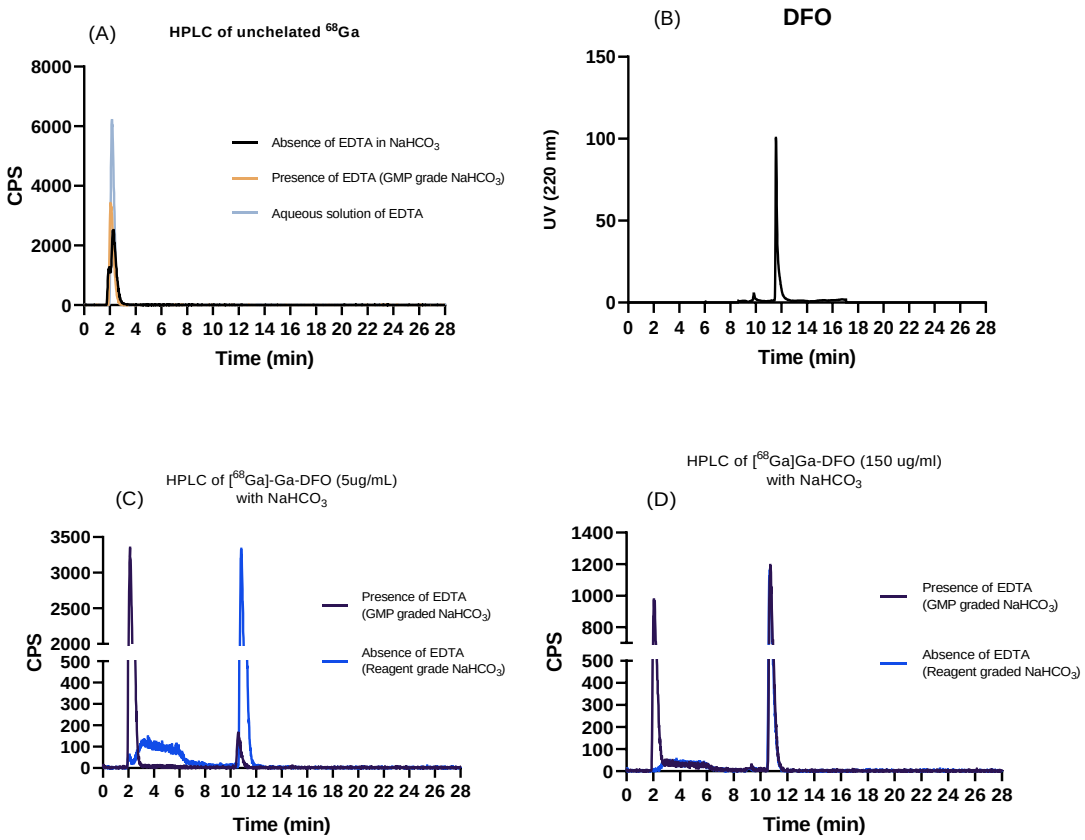

Figure 2.6: Panel A represents a RP-HPLC analysis of unchelated ^{68}Ga samples prepared with reagent, GMP-grade sodium bicarbonate buffer, or aqueous solution of EDTA. Panel B represents the UV chromatogram of an aqueous solution of DFO. Panels C and D represent the RP-HPLC analysis of [^{68}Ga]Ga-DFO prepared with 5 µg/ml or 150 µg/ml of DFO concentration respectively in the presence (GMP-grade) and absence (reagent grade) of EDTA in sodium bicarbonate buffer. Panel C and D show the presence of a single peak at 10:30/10:50 min:s (represent [^{68}Ga]Ga-DFO) when samples were prepared with reagent grade buffer while additional peak was seen at 2:10 min:s in samples prepared with GMP-grade buffer (contain EDTA) indicating ^{68}Ga and EDTA binding. Mixtures were incubated for 10 minutes at room temperature. Mobile phase: water (A) and acetonitrile (B), each containing 0.1%TFA.

2.9.2 Radiolabelling of [^{68}Ga]Ga-DFO using sodium bicarbonate buffer with a heating step

Adding a heating step for only 10 minutes during the [^{68}Ga]Ga-DFO preparation showed less activity (~ 25%) eluted at 2:20 min:s (Figure 2.7) compared to 95% when incubating at room temperature (Figure 2.6 C). This indicates that EDTA might bind to ^{68}Ga faster. However, adding a heating step allows equilibrium to be reached more quickly, favouring DFO binding. Although adding a heating step did indeed improve the RCP, ^{68}Ga-bound EDTA was still present. Due to the desire for a simple and fast radiolabelling process with the greatest RCP possible, it was decided to use GMP grade sodium acetate (EDTA free) instead of GMP grade sodium bicarbonate buffer (0.01 w/v EDTA) (see discussion section for more detail).

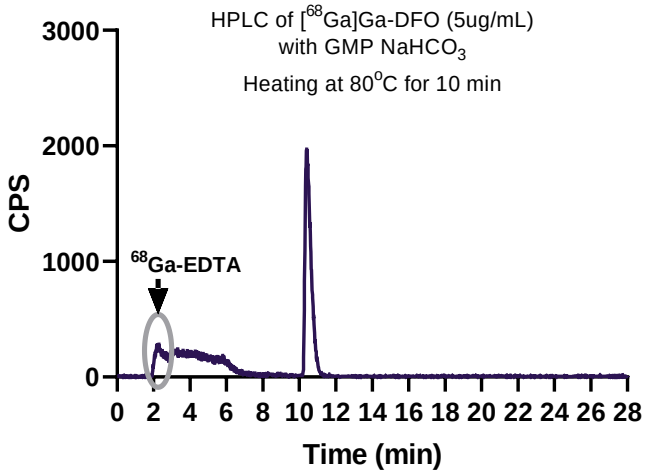

Figure 2.7: RP-HPLC analysis of [^{68}Ga]Ga-DFO prepared with 5 µg/ml of DFO, GMP-grade sodium bicarbonate, and a heating step of 80°C for 10 minutes shows that ^{68}Ga-bound EDTA was still present at 2:20 min:s. Mobile phase: water (A) and acetonitrile (B), each containing 0.1%TFA.

2.9.3 Radiolabelling of [^{68}Ga]Ga-DFO using sodium acetate buffer

Mixing GMP-grade DFO and sodium acetate with ^{68}Ga chloride (pH= 5.5/6) results in RCP ≥ 95% with Rf= 0.86 (Figure 2.8 A). The RP-HPLC analysis exhibited [^{68}Ga]Ga-DFO with one peak at 11:50 min:s (Figure 2.8 B), while the TLC and RP-HPLC analysis of [^{68}Ga]Ga-acetate showed Rf= 0.03 and an elution time at 2:50 min:s, respectively (Figure 2.9). DFO eluted at 13:50 min:s as shown by RP-HPLC with UV detection (Figure 2.8 B). Adding TFA to a [^{68}Ga]Ga-DFO sample preparation after 10 minutes of incubation (pH=2) showed 80% of activity eluted at 2:50 min:s (Figure 2.10). However, a RP-HPLC analysis of [^{68}Ga]Ga-DFO in the absence of TFA in the mobile phase showed a single peak at 8:0 min:s with no visible artefacts between 3 and 6 minutes (Figure 2.11 A), indicating that the presence of TFA in the sample preparation or mobile phase might cause some level of dissociation or possibly a secondary reaction occurring between [^{68}Ga]Ga-DFO and TFA, causing peak tailing during RP-HPLC analysis. The subsequent EDTA run (to elute ^{68}Ga trapped in the column, if any) showed negligible activity eluted from the column at 2:30 min:s (Figure 2.11 B). Unlike [^{68}Ga]Ga-DFO, [^{68}Ga]Ga-acetate was trapped in the column with negligible activity eluted as seen in figure 2.11 C. This behaviour is commonly observed for unchelated ^{68}Ga at neutral pH. However, when 50 µl of EDTA was injected into the HPLC, trapped activity was eluted at 2:30 min:s (Figure 2.11 D). This indicates that in the absence of TFA, unchelated ^{68}Ga remains bound to the HPLC stationary phase, probably as gallium hydroxide which is subsequently eluted with a bolus of EDTA. On the contrary, figure 2.11 A and B showed that > 95% of ^{68}Ga is chelated by DFO and does not get trapped in HPLC column.

Moving forward, it was decided to use GMP-grade sodium acetate buffer (EDTA free) instead of GMP grade sodium bicarbonate (0.01 w/v EDTA) (see discussion section for more detail). In addition, although the presence of TFA in the mobile caused artefacts during HPLC analysis, HPLC analysis with TFA present in the mobile phase was adopted for following experiments for reproducibility.

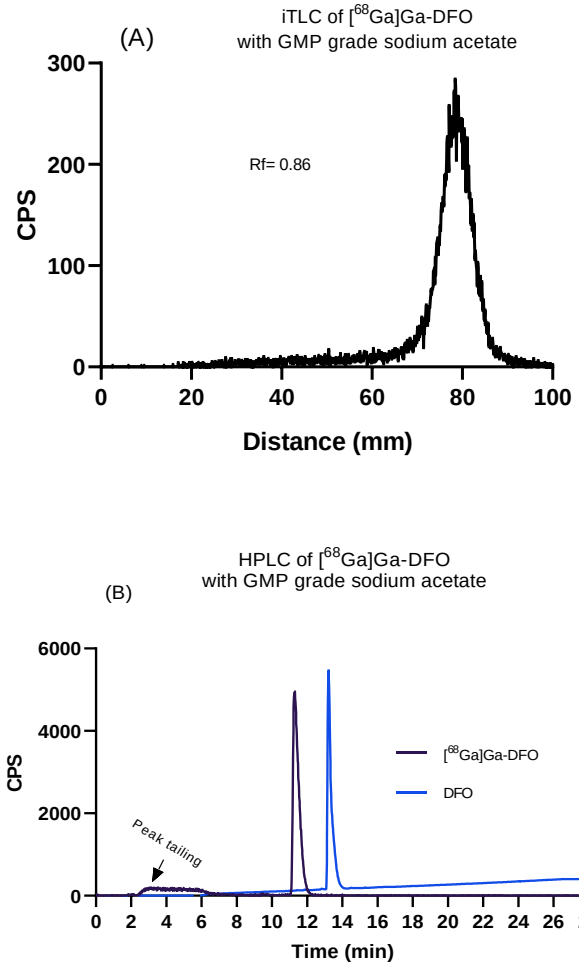

Figure 2.8: (A) Radioactivity distribution of [^{68}Ga]Ga-DFO (prepared with GMP-grade sodium acetate buffer) on silica gel impregnated glass microfiber strips shows that [^{68}Ga]Ga-DFO moved to the solvent front. iTLC mobile phase; 1 M ammonium acetate in 1:1 v/v H_2O and methanol (pH=7). (B) Radioactive chromatogram and UV absorbance of [^{68}Ga]Ga-DFO and DFO using RP-HPLC analysis shows a single peak at 11:50 and 13:50 min:s respectively. RP-HPLC mobile phase; water (A) and acetonitrile (B), each containing 0.1%TFA.

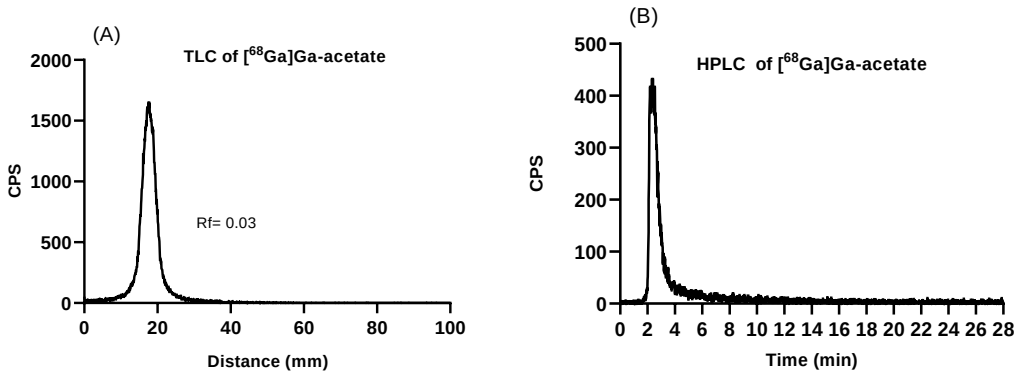

Figure 2.9: Radioactivity distribution of [^{68}Ga]Ga-acetate (prepared with GMP-grade sodium acetate buffer) on silica gel impregnated glass microfiber strips (A) shows that [^{68}Ga]Ga-acetate remained in the origin. B represents RP-HPLC analysis of [^{68}Ga]Ga-acetate with an elution time of 2:50 min:s. iTLC mobile phase; 1 M ammonium acetate in 1:1 v/v H_2O and methanol (pH=7). RP-HPLC mobile phase; water (A) and acetonitrile (B), each containing 0.1%TFA.

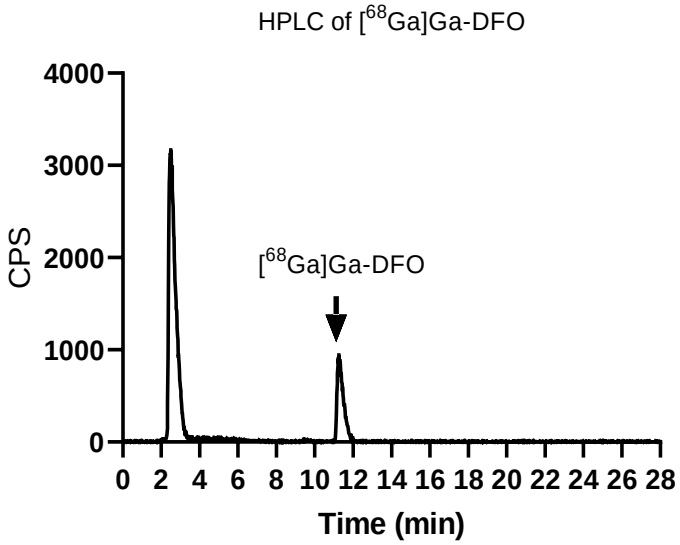

Figure 2.10: RP-HPLC analysis of [^{68}Ga]Ga-DFO prepared with GMP-grade sodium acetate buffer and incubated for 10 minutes at room temperature before 20 µl of TFA (2% of the sample volume) was added. The chromatogram shows that the majority of activity was eluted at 2:50 min:s, indicating some level of dissociation or possibly a secondary reaction occurring between [^{68}Ga]Ga-DFO and TFA. Mobile phase: water (A) and acetonitrile (B), each containing 0.1%TFA.

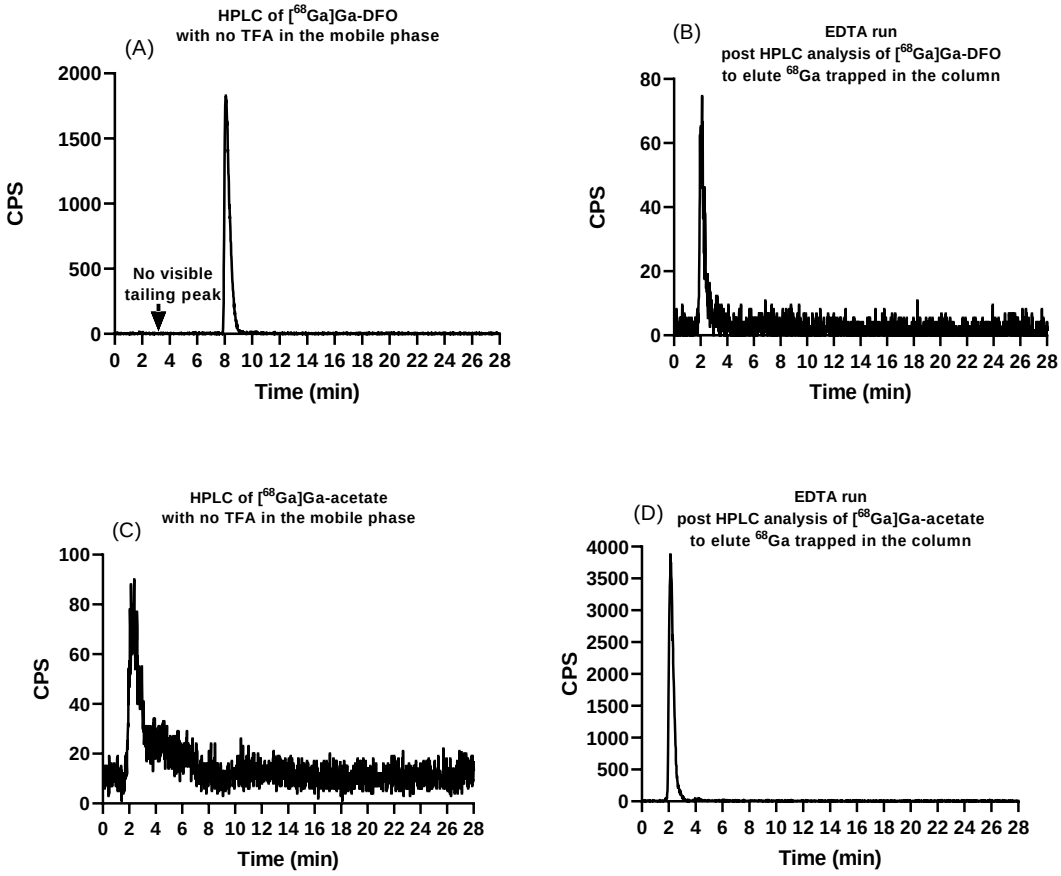

Figure 2.11: RP-HPLC analysis of [^{68}Ga]Ga-DFO (A and B) and [^{68}Ga]Ga-acetate (C and D) prepared with GMP-grade sodium acetate followed by EDTA run (no TFA was used in the mobile phase). Panel A shows no visible tailing peak in the HPLC analysis of [^{68}Ga]Ga-DFO sample when TFA was absent from the mobile phase (see figure 2.8 B for the elution profile of [^{68}Ga]Ga-DFO in the presence of TFA in the mobile phase). EDTA run after HPLC analysis of [^{68}Ga]Ga-DFO (B) shows negligible activity eluted at 2:30 min:s. HPLC analysis of [^{68}Ga]Ga-acetate (control) shows that negligible activity eluted when TFA was absent from the mobile phase (C). However, following EDTA injection into the HPLC, trapped activity was eluted at 2:30 min:s (D). Mobile phase: water (A) and acetonitrile (B).

2.9.4 Octanol extraction/ logD7.4 (octanol/PBS) of [^{68}Ga]Ga-DFO

Both [^{68}Ga]Ga-DFO and [^{68}Ga]Ga-acetate showed similar hydrophilic properties with $logD_{(octanol/PBS)}$ values of -2.9 ± 0.4 and -2.8 ± 0.6 respectively as shown by octanol extraction (Figure 2.12).

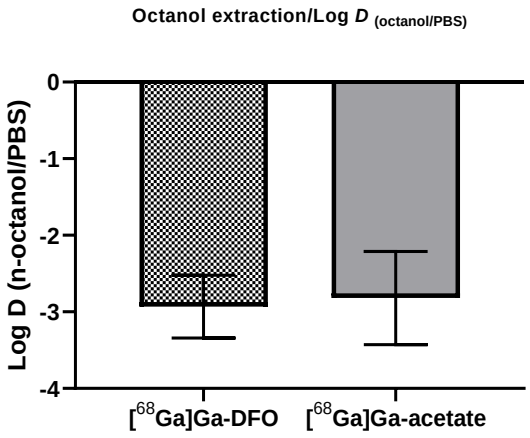

Figure 2.12: Log $D_{7.4\ (octanol/PBS)}$ of [^{68}Ga]Ga-DFO and [^{68}Ga]Ga-acetate (control) using the shake flask method. Values are reported as mean ± SD.

2.9.5 LC/MS of ^{nat}Ga-DFO and [^{68}Ga]Ga-DFO

A LC/MS analysis of ^{nat}Ga-DFO showed a peak at 8:20 min:s that corresponds to the ^{nat}Ga-DFO mass seen in the mass spectrometry analysis at 627.1 and 629.1 m/z $[M+H]^+$ (natural abundance isotopic pattern of gallium) (Figure 2.13 A and B). Another low abundant peak was seen at 10:21 min:s that correlated to the DFO mass seen in the mass spectrometry at 561.1 m/z $[M+H]^+$ (Figure 2.13 A and C). LC/MS coupled with the radiation detector showed a similar elution time of [^{68}Ga]Ga-DFO (9:20 min:s) to that of ^{nat}Ga-DFO (Figure 2.13 D). The serial configuration between the UV and radiation detectors accounts for the 60-second delay.

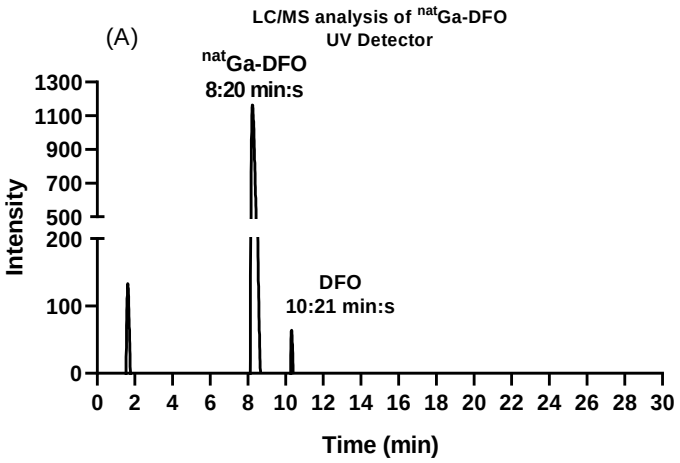
(A)
LC/MS analysis of natGa-DFO
UV Detector
natGa-DFO
8:20 min:s
DFO
10:21 min:s
Intensity
Time (min)

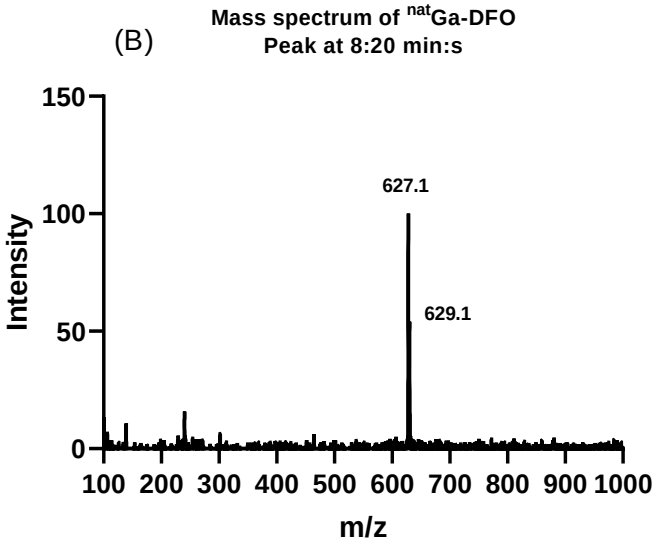
(B)
Mass spectrum of natGa-DFO
Peak at 8:20 min:s
627.1
629.1
Intensity
m/z

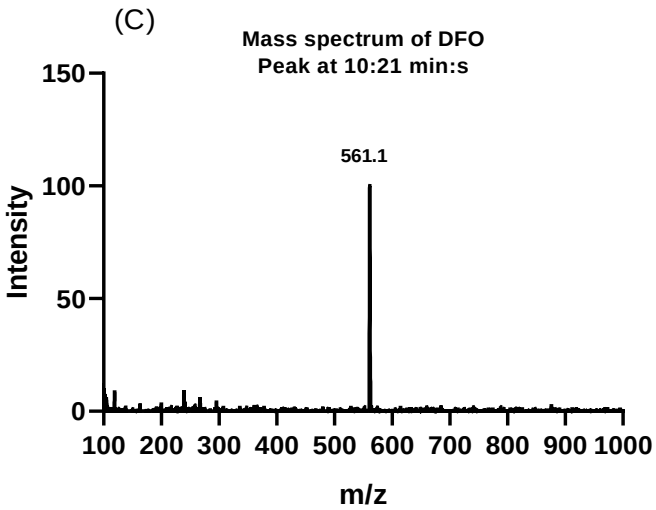
(C)
Mass spectrum of DFO
Peak at 10:21 min:s
561.1
Intensity
m/z

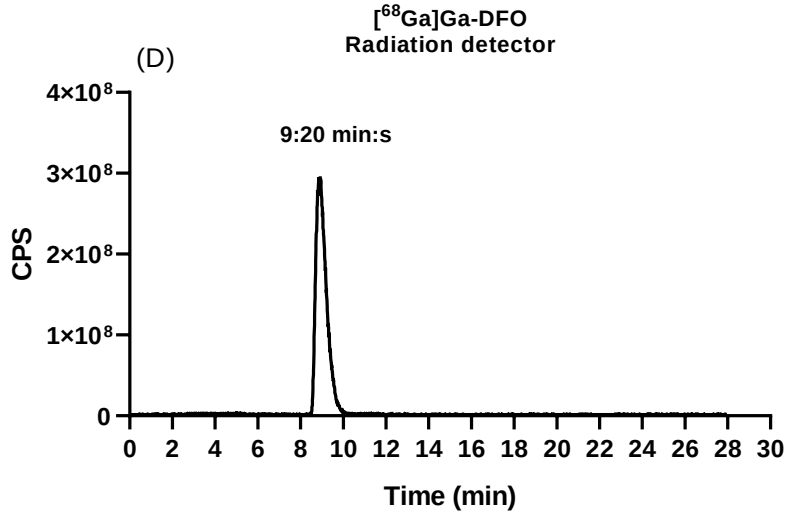

Figure 2.13: LC/MS analysis of ^{nat}Ga-DFO (A) represent two peaks at 8:20 and 10:21 min:s which correspond to ^{nat}Ga-DFO mass (627.1 and 629.1 m/z $[M+H]^+$, natural abundance isotopic pattern of gallium) (B) and DFO mass (561.1 m/z $[M+H]^+$) (C) respectively. LC/MS coupled with the radiation detector (D) shows similar elution time of [^{68}Ga]Ga-DFO (9:20 min:s) to that of ^{nat}Ga-DFO. Mobile phase: water (A) and acetonitrile (B), each containing 0.1%TFA

2.9.6 Serum stability study of [^{68}Ga]Ga-DFO

A serum stability test was performed as described in section 2.8.8. [^{68}Ga]Ga-DFO was incubated in human serum for 5 and 60 minutes. After adding acetonitrile to the sample mixture and centrifugation, <5% of the activity was in the precipitate, indicating low protein binding and that the supernatant samples used for iTLC and RP-HPLC analysis represent 95% of the total sample. On the contrary, [^{68}Ga]Ga-acetate showed 70% of activity in the precipitate, indicating high protein binding when DFO is absent (Figure 2.14 A). An iTLC analysis of [^{68}Ga]Ga-DFO incubated in human serum for 5 and 60 minutes showed high stability (> 97%) with Rf = 0.82 and 0.83 respectively, indicating the absence of free or protein-bound ^{68}Ga in the sample (Figure 2.14 B and C). However, [^{68}Ga]Ga-acetate incubated with human serum stayed in the origin with Rf = 0.03 (Figure 2.14 D). [^{68}Ga]Ga-DFO incubated in PBS and human serum showed similar retention times (10:50/11:00 min:s) even after 60 minutes of incubation as measured by RP-HPLC. On the contrary, [^{68}Ga]Ga-acetate incubated in human serum for 5 minutes eluted at 1:50/2:0 min:s (Figure 2.15).

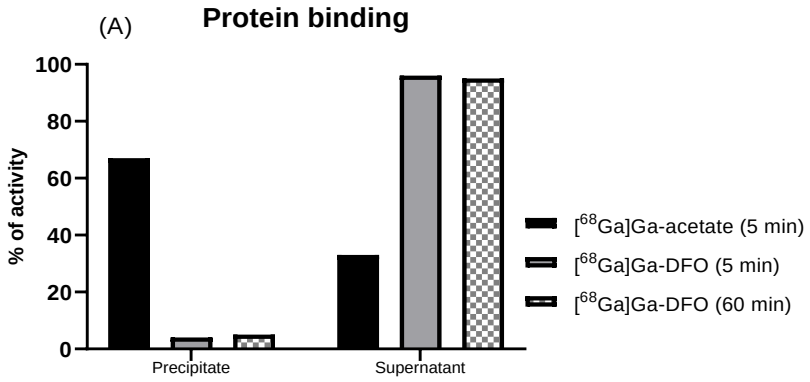

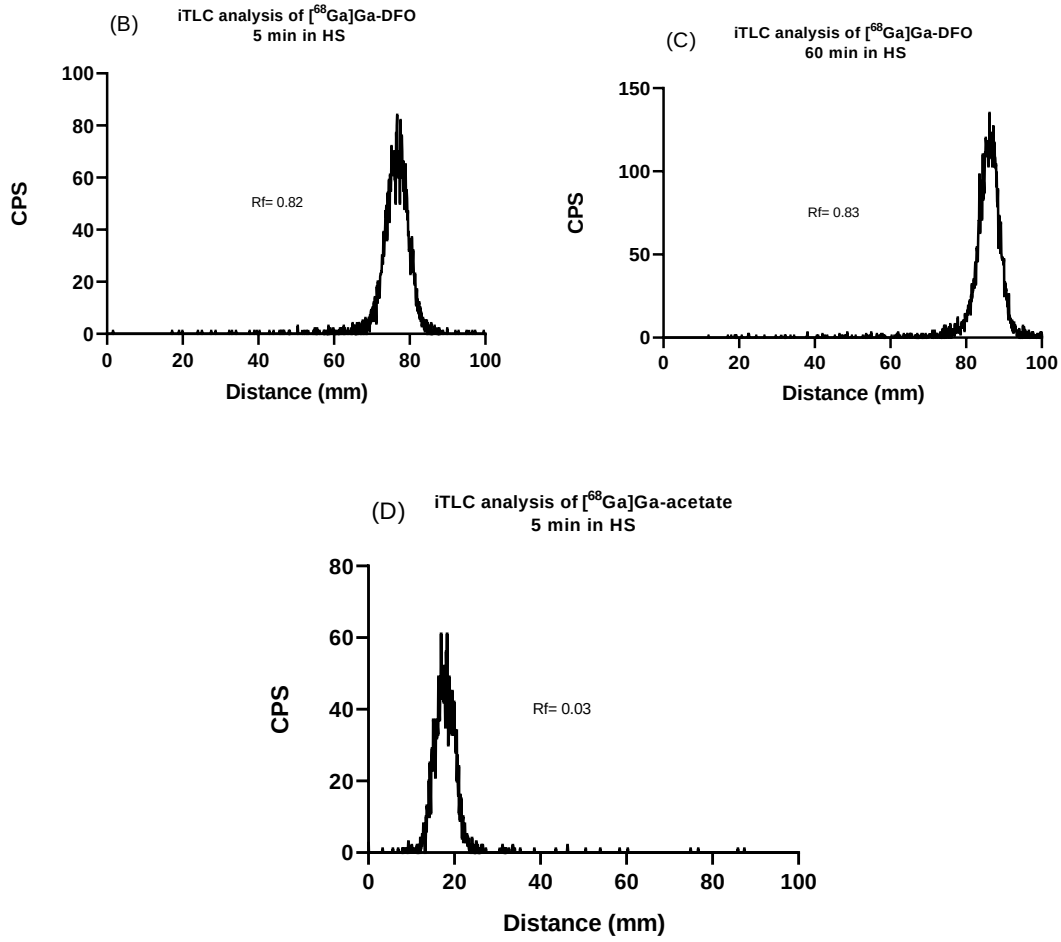

Figure 2.14: Panel A represents the percentage of activity in precipitate (protein binding) and supernatant after adding acetonitrile and centrifugation. Panel B and C represent the radioactivity distribution pattern on silica gel impregnated glass microfiber strips of [^{68}Ga]Ga-DFO after 5 minutes and 60 minutes of incubation in human serum respectively. Panel D represents the radioactivity distribution pattern of [^{68}Ga]Ga-acetate after 5 minutes of incubation in human serum. An iTLC analysis of the sample was done after the addition of ice-cold acetonitrile, centrifugation and five times dilution with water Mobile phase; 1M ammonium acetate in 1:1 v/v H_2O and methanol (pH=7). HS, human serum.

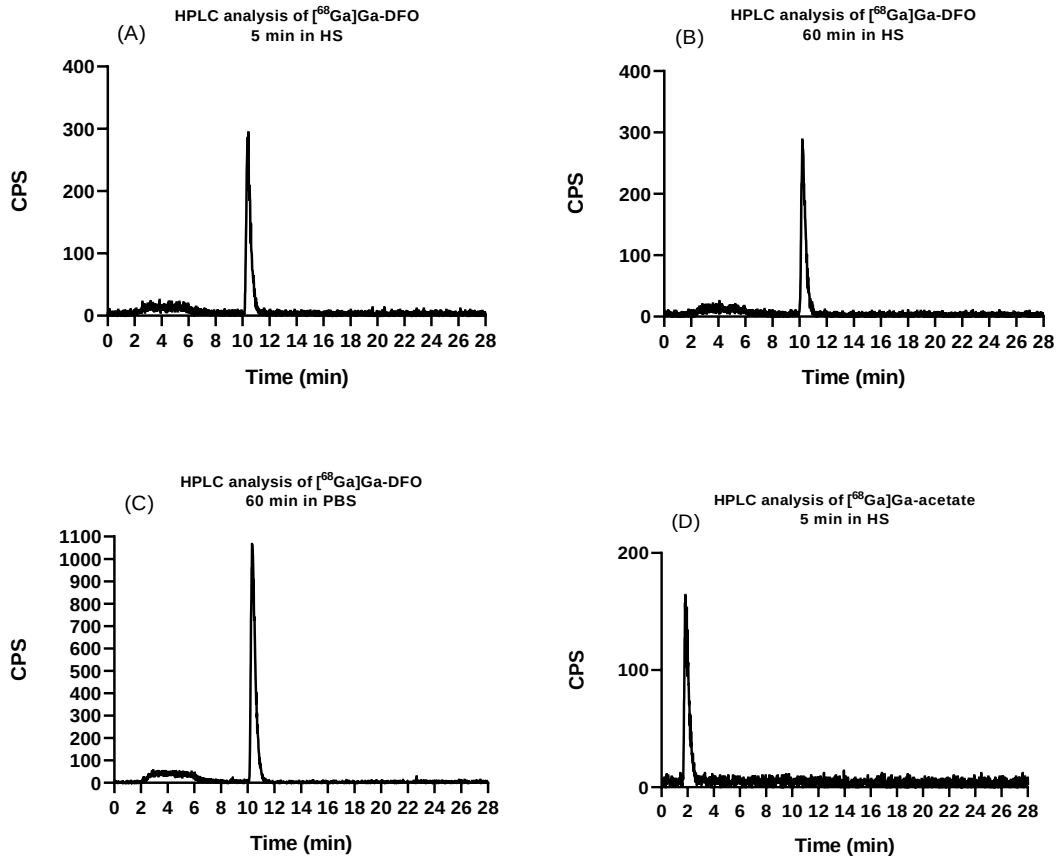

Figure 2.15: HPLC analysis of [^{68}Ga]Ga-DFO after 5 minutes (A), 60 minutes (B) incubation in human serum and 60 minutes incubation in PBS (C). [^{68}Ga]Ga-DFO chromatograms represent similar retention times when incubated in PBS and human serum (10:50/11:00 min:s). Panel D represents the HPLC analysis of [^{68}Ga]Ga-acetate (control) after 5 minutes of incubation in human serum with a retention time of 1:50/2:0 min:s. The HPLC analysis of the samples was done after the addition of ice-cold acetonitrile, centrifugation and five times dilution with water. HPLC mobile phase: water (A) and acetonitrile (B), each containing 0.1%TFA. HS, human serum.

2.9.7 *In vivo* study of [^{68}Ga]Ga-DFO after intravenous injection

PET/CT images showed a low blood pool and rapid renal excretion of [^{68}Ga]Ga-DFO after i.v. injection. Uptake was seen in kidneys at 2 minutes post injection and gradually decreased over time while activity in bladder increased. No uptake was seen in any organ except for the kidneys (minimal uptake) and bladder at 30- and 60-minutes post injection (Figure 2.16 A). *Ex vivo* biodistribution data at 60 minutes were consistent with the PET/CT results and showed 732.3 ± 244.7 %ID/g (62.1 ± 27.8 %ID) in the urine with less activity in the bladder (15.1 ± 4.3 %ID/g) and kidneys (8.36 ± 3.3 %ID/g) (Figure 2.16 B). Time-activity curves showed maximum uptake in kidneys at 2 minutes post injection (9.7 ± 5.4 %ID). Uptake in the heart (as a measure of blood activity) and liver showed maximum activity at 2-3 minutes post injection (2.45 ± 0.34 and 5.4 ± 1.68 %ID respectively) (Figure 2.17 A). Activity in the bladder accumulated gradually until 60 minutes with 87.1 ± 1.5 %ID (Figure 2.17 B). A RP-HPLC analysis of urine samples at 60 minutes revealed high and low abundant peaks at 2:00 and 17.50 min:s, respectively (Figure 2.16 C). While the peak that eluted at 17.50 min:s might be attributed to intact [^{68}Ga]Ga-DFO, the early eluted peak corresponded to the presence of another radioactive species in the sample and therefore the possibility of some level of [^{68}Ga]Ga-DFO dissociation or the presence of [^{68}Ga]Ga-DFO metabolites. However, it is not clear whether this metabolism occurs in plasma or urine.

Dynamic PET/CT maximum intensity projection (MIP) images after i.v. injection of [^{68}Ga]Ga-DFO

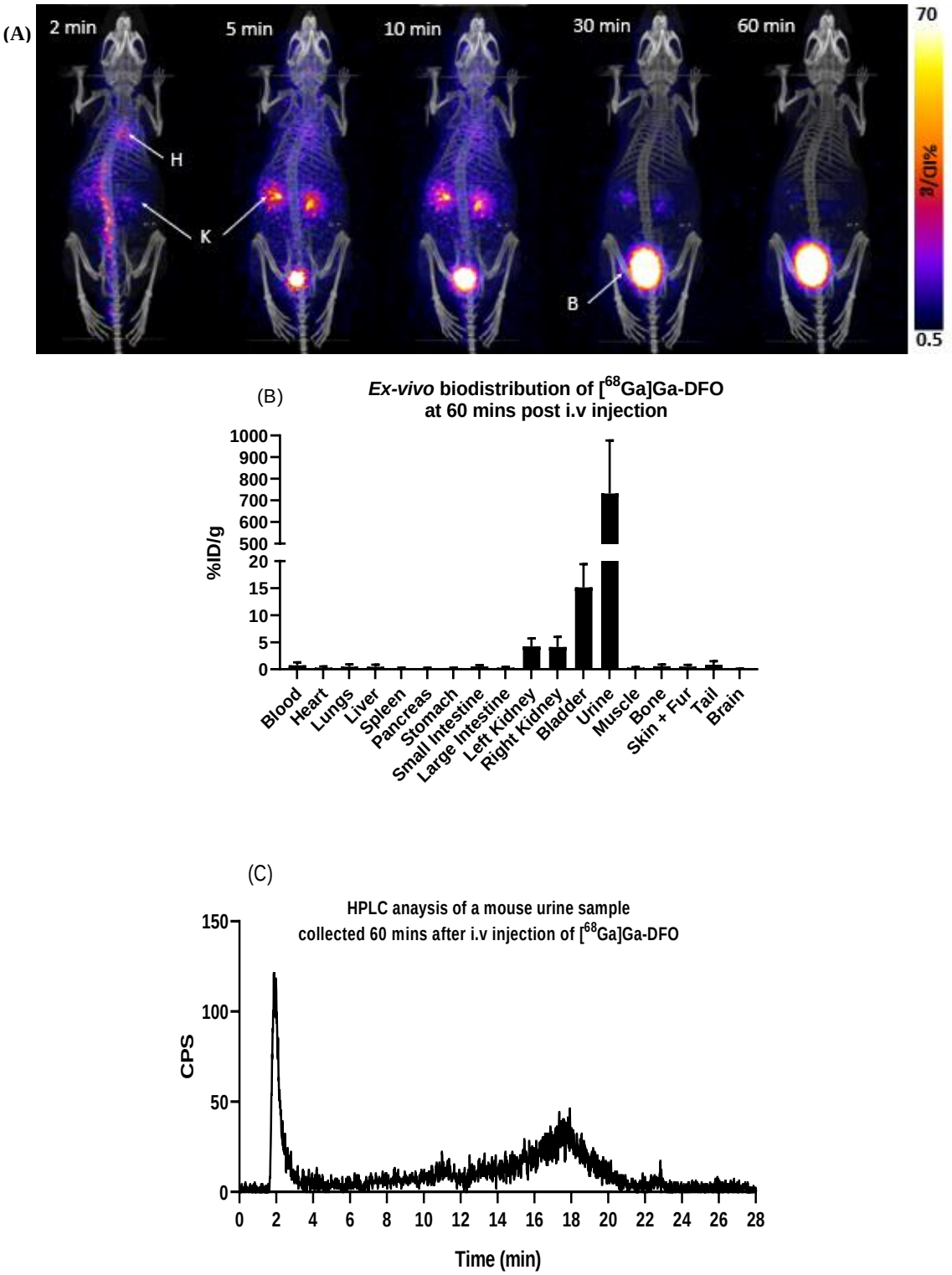

Figure 2.16: Dynamic PET/CT MIP images of healthy Balb/C mice (n=3) after an intravenous injection of [^{68}Ga]Ga-DFO (1.2–1.5 MBq, DFO concentration 0.2–0.3 µg) (A). PET/CT images shows fast renal excretion of [^{68}Ga]Ga-DFO. *Ex vivo* biodistribution data at 60 minutes post injection confirmed PET/CT results and showed most activity in urine. *Ex-vivo* data are expressed as mean ± SD of %ID/g. Panel C represent the RP-HPLC analysis of a mouse urine sample (n=1) collected at 60 minutes post injection. HPLC analysis of a mouse urine sample showed two peaks corresponding to two radioactive species in the sample. HPLC mobile phase: water (A) and acetonitrile (B), each containing 0.1%TFA. H: Heart, K: Kidney, B: Bladder.

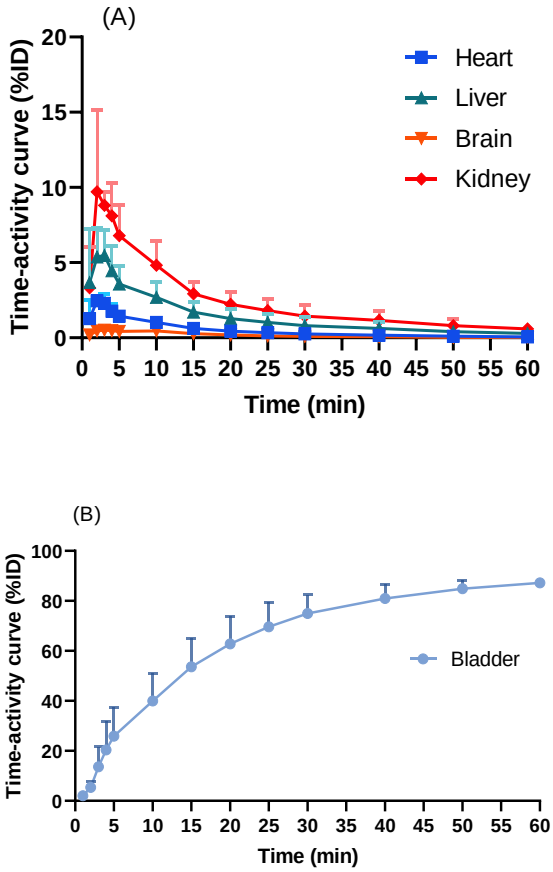

Figure 2.17: Time-activity curves of selected tissues after i.v. injection of [^{68}Ga]Ga-DFO. Panel A shows maximum uptake in liver, heart, and kidneys at 2-3 minutes, while activity in the bladder accumulated gradually until 60 minutes (B). The time-activity curve was obtained from generated ROI within the images of selected organs at each time point. Data expressed as mean ± SD of %ID

2.9.8 Stability of [^{68}Ga]Ga-DFO in human urine

To assess whether [^{68}Ga]Ga-DFO metabolism occurs in urine, [^{68}Ga]Ga-DFO and [^{68}Ga]Ga-acetate (control) were incubated in human urine for 5, 30 and 60 minutes and analysed by RP-HPLC. Incubation in PBS for 60 minutes was performed as a control. A RP-HPLC analysis of [^{68}Ga]Ga-acetate showed three different peaks at 2:15 (predominant peak), 4:00 and 7:20 min:s after 30 minutes of incubation in human urine. Although the earliest eluted peak at 2:15 min:s might represent the typical elution time of [^{68}Ga]Ga-acetate, the other two peaks eluted later, suggesting some binding of unchelated ^{68}Ga to some urine constituents (Figure 2.18 A). The HPLC analysis of [^{68}Ga]Ga-DFO incubated in human urine for 5 minutes showed a peak at 8:50 min:s, corresponding to intact [^{68}Ga]Ga-DFO in the sample and the absence of free ^{68}Ga (Figure 2.18 B). After 30 minutes of incubation in human urine, more activity (compared to the 5 minutes time point) was eluted at the early time point (2:50 min:s), while a small peak started to appear at 7:50/8:30 min:s (Figure 2.18 B). However, these peaks were more predominant after 60 minutes of incubation in human urine, and were not present in [^{68}Ga]Ga-DFO sample incubated in PBS for 60 minutes (Figure 2.18 C). Although the presence of these peaks at 2:50 and 7:50/8:30 min:s, which was also seen in the [^{68}Ga]Ga-acetate chromatogram sample incubated in urine, might indicate some level of dissociation occurring with time and that un-chelated ^{68}Ga bound to some urine constitutes, it might also indicate the formation of [^{68}Ga]Ga-DFO metabolites or degradation products.

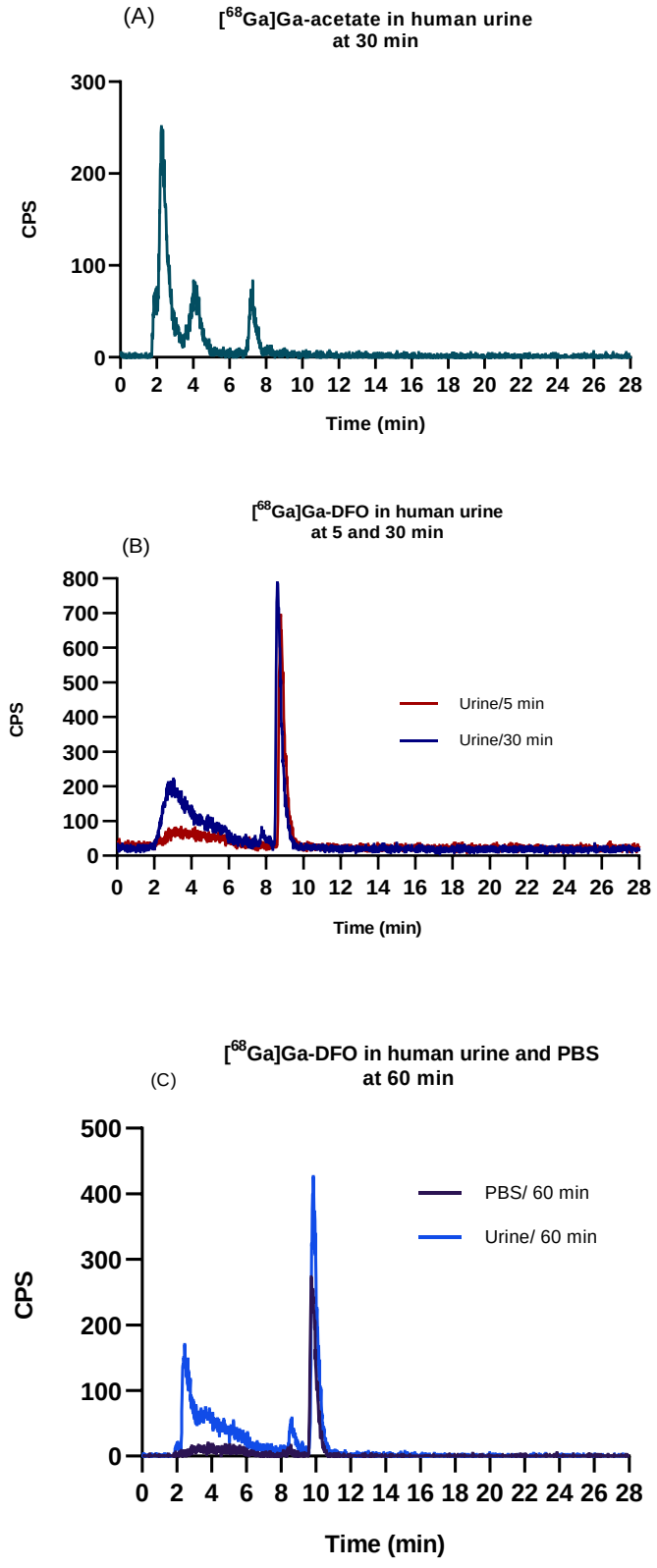

Figure 2.18: RP-HPLC analysis of [^{68}Ga]Ga-acetate after 30 minutes of incubation in human urine (A) shows three different peaks at 2:15, 4:0 and 7:20 min:s. Panel B represents HPLC analysis of [^{68}Ga]Ga-DFO incubated in human urine for 5 an 30 minutes. Panel C represents HPLC analysis of [^{68}Ga]Ga-DFO incubated in human urine and PBS for 60 minutes. [^{68}Ga]Ga-DFO radioactive chromatograms shows two radioactive species at 2:50 and 7:50/8:30 min:s at 30 minutes (B) which were more predominant at 60 minutes (C) of incubation in human urine. HPLC mobile phase: water (A) and acetonitrile (B), each containing 0.1% TFA

2.10 Discussion

In this work, we developed a simple GMP-compatible radiosynthesis of [^{68}Ga]Ga-DFO using GMP-grade reagents. After radiolabelling, [^{68}Ga]Ga-DFO was analysed *in vitro* and its serum and urine stability were studied. In addition, *in vivo* biodistribution of [^{68}Ga]Ga-DFO in healthy mice was investigated.

A RP-HPLC analysis of [^{68}Ga]Ga-DFO showed 95% of activity eluted at early time points, not consistent with the elution time of the DFO complex, when the sample was prepared with GMP-grade sodium bicarbonate (which was later found to contain 0.01 w/v EDTA). This suggests competition between EDTA and DFO for ^{68}Ga binding. Increasing DFO concentration in the sample to 150 µg/ml decreased the percentage of activity bound to EDTA to 38%. However, it did not prevent the binding completely. It was suggested that ^{68}Ga binding to EDTA might be a kinetic binding rather than thermodynamic, hence, adding a quick heating step might bring the desired equilibrium, favouring DFO binding. Although incubating [^{68}Ga]Ga-DFO for 10 minutes at 80°C did indeed improve the RCP, a small peak still eluted at 2:20 min:s, demonstrating that ^{68}Ga-EDTA was still present. Incubation for a longer time at a higher temperature might be used as an alternative. However, simplicity in the radiolabelling method is the main focus for the current work. In addition, obtaining EDTA free GMP-grade sodium bicarbonate was time consuming and expensive. Thus, it was decided to radiolabel [^{68}Ga]Ga-DFO using GMP-grade sodium acetate, which is free of EDTA instead.

An iTLC analysis of [^{68}Ga]Ga-DFO prepared with GMP-grade sodium acetate showed ≥ 95 of activity moved to the solvent front with Rf = 0.86, indicating good complexation. HPLC analysis showed a single peak at 11:50 min:s and an early elution of activity (tailing peak) between 3 and 6 minutes, which was also seen when sodium bicarbonate was used as a buffer but was not visible in the iTLC analysis. The shape of the peak suggested that it is not a single impurity and could be an artefact of the chosen mobile phase, e.g. due to a reaction between the TFA in the acetonitrile solvent and the pendant amino group of DFO in [^{68}Ga]Ga-DFO when they came in contact with each other as they enter the column. It was shown previously that TFA can react with amines on the column causing tailing peak.[175,176,177] When a small volume of TFA was added to [^{68}Ga]Ga-DFO before the RP-HPLC analysis, only 20% of activity eluted at 11:50 min:s. The rest of the activity was seen at 2:50 min:s, indicating the presence of a new radioactive species. This suggests that the early eluting radioactivity is indeed an artefact of the analytical method rather than a true impurity. In the absence of TFA in the mobile phase, a single radioactive species corresponding to [^{68}Ga]Ga-DFO was seen at 8:0 min:s with no visible impurities between 3 and 6 minutes. Unlike [^{68}Ga]Ga-acetate, washing the column with EDTA showed negligible activity eluted, indicating good complexation and the near-absence of free ^{68}Ga in the sample preparation. Unfortunately, the uncontrolled pH in the mobile phase in the absence of TFA or other buffer

cause the [^{68}Ga]Ga-DFO retention time to drift (range 8:0 to 11:50 min:s); however, by combining the two mobile phases we have confidence in the identity and radiochemical purity of the product.

As determined by the octanol extraction, the log *D* value of [^{68}Ga]Ga-DFO was -2.9 ± 0.4 and similar to the values measured by previous studies using ^{68}Ga and ^{67}Ga (-3.3 ± 0.19 and -3.0 ± 0.2 respectively), indicating its hydrophilic properties.[99,100] The LC/MS analysis (figure 2.13) showed that ^{nat}Ga-DFO and [^{68}Ga]Ga-DFO eluted simultaneously (8:20–9:20 min:s) and it confirms that HPLC peaks represents a 1:1 complex between Ga^{3+} and DFO. [^{68}Ga]Ga-DFO showed high serum (> 97%) and PBS stability with no change in chromatographic behaviour even after 60 minutes of incubation as determined by the iTLC and RP-HPLC analysis. The stability and low protein binding of [^{68}Ga]Ga-DFO were in agreement with previous studies that showed > 95% stability in PBS and human serum with ~20% of activity bound to protein at up to 120 minutes of incubation [100] and >95% stability in mouse serum with only 4.6% protein binding after 3 hours of incubation.[99]

The *in vivo* biodistribution study showed rapid renal excretion and low blood pool activity after intravenous injection of [^{68}Ga]Ga-DFO with no uptake seen in any organ except for the kidneys and bladder from 30 minutes onward. The fast renal excretion of [^{68}Ga]Ga-DFO is expected of a small molecule with short term resistance to metabolism or transchelation. Previous preclinical studies[99,100] using [$^{68/67}$Ga]Ga-DFO were consistent with the current study and showed uptake only in the kidneys and bladder at 60 minutes post injection. Despite the observed stability in plasma, RP-HPLC analysis of a mouse urine sample at 60 minutes post-injection showed two radioactive species, indicating the presence of some [^{68}Ga]Ga-DFO metabolites or degradation products. However, it was not clear whether this metabolism/degradation process occurs in plasma or urine. Although it is known that DFO can be metabolised in plasma, Fe^{3+}-DFO does not appear to metabolise in plasma to any considerable extent, and is rapidly excreted in urine.[178,179,180,181] Binding DFO to trivalent metal might thus protect the molecule against plasma degradation.[180] The presence of DFO metabolites in urine was also confirmed in a clinical study of post intramuscular injection of DFO in hemochromatosis patients. One of the metabolites was later confirmed to be Fe^{3+}-DFO.[179] Considering the ability of Fe^{3+}-DFO to be rapidly excreted unchanged, it is plausible to say that [^{68}Ga]Ga-DFO in the current study might have been excreted unchanged and chemical reaction might have occurred in urine over the period of 60 minutes. However, blood metabolites analysis post intravenous injection of [^{68}Ga]Ga-DFO (probably at early time points considering its fast excretion) must be performed to confirm the literature results and translate this theory to fact.

Although [^{68}Ga]Ga-DFO showed high stability in human serum *in vitro*, it showed some level of metabolism and/or degradation in mouse urine samples. It cannot be assumed that [^{68}Ga]Ga-DFO will show similar metabolic properties in animal and human urine samples. Thus, as a prelude to

PET imaging studies in humans, it was decided to further investigate [^{68}Ga]Ga-DFO metabolism post incubation in human urine. [^{68}Ga]Ga-acetate was incubated in human urine (control) and the two eluted peaks seen in the [^{68}Ga]Ga-acetate chromatograms at 4:0 and 7:20 min:s after 30 minutes of incubation in human urine might be an indication of un-chelated ^{68}Ga bound to urine constitutes. The early eluted peak at 2:15 min:s can be assigned to unchelated ^{68}Ga (typical elution time) or possibly another ^{68}Ga bound species eluted at the same elution time.[182,183] In addition, [^{68}Ga]Ga-DFO incubated in human urine for 5 minutes showed a single peak at 8:50 min:s, indicating the absence of metabolites and/or degradation products. However, after 30 and 60 minutes of incubation, new radioactive species were present in the radio-chromatograms. The two peaks that were seen in the [^{68}Ga]Ga-DFO chromatograms at 2:50 and 7:50/8:30 min:s after 30 and 60 minutes of incubation might indicate the degradation of [^{68}Ga]Ga-DFO in urine with time and binding of un-chelated ^{68}Ga to urine constituents. However, it might also indicate the presence of [^{68}Ga]Ga-DFO degradation products or metabolites due to reaction of the amino group in the DFO to urinary constituents.[182,184] These results do not prove the identity of these metabolites or degradation products since no attempts were made to further investigate the molecular weight of these species, and more studies can be done to further investigate the presence of [^{68}Ga]Ga-DFO or its stable compound (^{nat}Ga-DFO) metabolites or degradation products post incubation in human urine. However, these results clearly demonstrate the formation and presence of [^{68}Ga]Ga-DFO metabolites and/or degradation products in urine with time. As mentioned previously, more studies should be done to investigate the presence of [^{68}Ga]Ga-DFO metabolites in plasma post intravenous injection. However, with no current data to contradict this, our data indicate that [^{68}Ga]Ga-DFO is stable in plasma and observed degradation occurs in urine in the bladder and not in circulation.

2.11 Summary and conclusion

In this work we developed a simple GMP-compatible radiosynthesis method for [^{68}Ga]Ga-DFO using GMP-graded DFO and sodium acetate. Radiolabelling at room temperature for 10 minutes results in a preliminary product suitable for human use with RCP ≥ 95%. However, it must be noted that [^{68}Ga]Ga-DFO validation including sterility and pyrogen tests was conducted by the radiopharmaceutical scientists involved in the clinical study (not part of the current research).

In addition, [^{68}Ga]Ga-DFO chemical integrity and structure was confirmed with LC/MS of the non-radioactive complex which co-eluted with [^{68}Ga]Ga-DFO. The stability of [^{68}Ga]Ga-DFO in human serum (> 97%) was confirmed *in vitro* after 60 minutes of incubation. The preclinical study showed fast renal excretion and low blood pool after intravenous injection of [^{68}Ga]Ga-DFO, with only the kidneys and bladder visible at 30 minutes post injection. More than one radioactive species was seen in the urine samples either post intravenous injection or in the *in vitro* incubation of [^{68}Ga]Ga-DFO with urine at later time points, indicating the formation of metabolites and/or degradation products which increase with time on incubation in urine. Thus, We believe that [^{68}Ga]Ga-DFO is stable in blood over the expected time scale of imaging, and its degradation in urine occurs with time. Overall, [^{68}Ga]Ga-DFO can be easily radiolabelled to produce a radiopharmaceutical for evaluation clinically as a specific infection imaging agent.

3 *In vivo* trafficking of the anti-cancer drug tris(8-quinolinolato) gallium (III) (KP46) by gallium-68/67 PET/SPECT imaging

3.1 Gallium compounds as anti-cancer drugs

The potential anti-cancer activity of gallium compounds was triggered by the discovery of ^{67}Ga and its localisation into tumours, especially lymphoma.[4] Developing ^{67}Ga scans as a method for detecting tumours led researchers to investigate stable gallium salts for anti-cancer activity. Given the therapeutic potential of gallium, multiple gallium compounds are now in different phases of clinical trials.[4] Therapeutic gallium compounds in clinical trials can be grouped into two different generations of compounds which become more diverse with gallium binding to a wide variety of ligands.[46] Gallium nitrate represents the first generation of gallium compounds as it was the first gallium drug to enter clinical trials. With a relatively similar time frame, gallium chloride was reported in clinical trials in patients with lung cancer.[46] The second generation of gallium compounds in clinical trials was then developed, shifting from a simple gallium salt to gallium bound to multiple ligands to form specific compounds such as tris (8-quinolinolato) gallium (III) (KP46) and tris(3-hydroxy-2-methyl-4H-pyran-4-onato) gallium (gallium maltolate) to overcome some of the limitations of gallium salts.[46] Tris (8-quinolinolato) gallium (III) is the focus of this review, however, the nomenclature KP46 will be used instead in this chapter to refer specifically to the anti-cancer drug that was investigated previously in literature (as KP46) in preclinical and clinical studies. The current understanding of KP46 protein binding, mechanism of action, preclinical and clinical studies will be discussed in this chapter. However, it is important to discuss gallium nitrate and gallium chloride mechanism of action, preclinical and clinical studies as a foundation and comparator for KP46.

3.1.1 Gallium nitrate

Among group IIIa metals (thallium, indium, and aluminium) screened for anti-cancer activity in W256 (rat breast carcinoma) cell lines *in vitro*, gallium nitrate showed 30–38% growth inhibition after 72 hours' incubation.[185] *In vivo* studies supported these results and showed 61–92% inhibition of tumour volume in rats bearing W256 xenograft (subcutaneously injected) post intraperitoneal (i.p.) injection of 50–60 mg/kg of gallium nitrate.[185] The potential of the anti-cancer activity of gallium nitrate stimulated further evaluation of its mechanism of action, toxicity and anti-tumour activity in animals and humans.[4]

Further preclinical studies have been conducted to test the toxicity of gallium nitrate after i.p. administration. The LD50 of gallium nitrate administered i.p. daily for ten consecutive days was

80 mg/kg daily for CDF1 male mice and 67.6 mg/kg for Sprague-Dawley female rats. In the same study, the effect of high doses (≥ 85mg/kg) of gallium nitrate was also tested on mice and rats and showed weight change and more than 70% lethality. Microscopic and gross examination post toxic dose administration showed peritonitis in the lungs, pathologies in the liver and renal damage.[186] The toxicity of gallium (in the form of gallium lactate) was also investigated in an early preclinical study in rats and rabbits post i.v. injection. In both animal species, a dose of 45-47 mg/kg daily for 10 consecutive days produced 60-70% death while no effect was observed in control group (group injected with Na lactate). Autopsy after animal death showed multiple cortical haemorrhage in kidneys and haemorrhagic lungs.[187]

In addition to toxicity studies, the anti-tumour activity of gallium nitrate was tested preclinically. Multiple doses for ten days of i.p. injected gallium nitrate (≤ LD10, 50 mg/kg) into rats intraperitoneally transplanted with Walker carcinoma 256 showed a 138% increase in median survival time (MST) compared to the control group.[186] However, gallium nitrate showed no effect (0% increase in MST) in rats intraperitoneally transplanted with several leukaemia cell lines (PS88, K1964, and L1210). A possible explanation for the absence of gallium nitrate effect on leukaemia cells is that a higher concentration of the drug is needed (>LD10), which might be toxic to animals, or the resistance of this type of cells to gallium nitrate.[186]

Another preclinical study confirmed the dose-related anti-tumour activity of gallium nitrate. Intraperitoneal administration of 37.5 mg/kg/day of gallium nitrate for five days inhibited the tumour growth and development of metastasis in mice transplanted with Lewis lung carcinoma. The effect of gallium nitrate decreased with decreasing the dose administered. No change in primary tumour but a significant decrease in metastasis number was observed at 23.1 mg/kg/day. At 11.6 mg/kg/day, no change in primary tumour or metastases was seen.[188]

The bioavailability and plasma concentration of gallium nitrate post i.p., i.v., and oral administration was tested in an extended 24 h preclinical study in a rat model.[189] After intravenous injection of 0.13 mmol/kg (54.32 mg/kg) of gallium nitrate, 29,200 ng/ml of Ga^{3+} was seen immediately in plasma while 7,900 ng/ml (at 30 minutes) and 839 ng/ml (at three hours) was seen after i.p. and oral administration respectively.[189] The low plasma concentration observed from the previously mentioned preclinical study of orally administered gallium nitrate (compared to i.v. and i.p. administration) might be an indication of poor gallium absorption from the gut after oral administration. However, the previous preclinical studies demonstrated gallium concentration in plasma but did not demonstrate gallium uptake in tissues. The radioactive isotopes of gallium (^{67}Ga and ^{68}Ga) can be used with SPECT/PET imaging to measure gallium gut absorption and quantify tissue uptake after oral administration. In fact, a preclinical study investigated the absorption of gallium from the bowel on rats after oral administration of 3 MBq of ^{67}Ga citrate. Rats were placed in metabolic cages to monitor faeces and urine excretion for 72 hours. ^{67}Ga

citrate showed cumulative excretion of 97.2% of the administered dose in the faeces with only 0.1% seen in the urine. No imaging or information on ^{67}Ga citrate uptake in tissues were presented in the study.[190] The high level of ^{67}Ga excreted in the faeces indicated the poor gut absorption of gallium after oral administration. Another preclinical study on 14 Sprague-Dawley rats confirmed the poor gut absorption of gallium post oral administration of 1 MBq of ^{67}Ga citrate (no imaging was performed). Four rats excreted 100% of the administered dose in faeces at 72 hours while the rest excreted an average of 87%. In the same study, *ex vivo* biodistribution at 72 hours showed that the highest tissue concertation of gallium was in the liver – only 0.03% of the administered dose – compared to 8.7% in the control group (i.v. injection of ^{67}Ga citrate),[191] however, no data were presented on gallium uptake in other tissues. Although previously mentioned preclinical studies showed poor gut absorption of gallium post oral administration of ^{67}Ga citrate, therapeutic/large doses of orally administered gallium might have different gut absorption and biodistribution. It cannot be assumed that gut absorption and biodistribution of small amounts of radioactive gallium post oral administration of ^{67}Ga citrate would be similar to the large quantity of stable gallium when administered as therapeutic agents (see discussion section).

Based on previously mentioned preclinical toxicology studies and the potential of gallium nitrate as an anti-cancer drug, gallium nitrate was appointed as a National Cancer Institute (NCI) drug (NSC-15200) and phase I and II clinical trials followed.[105,106] In phase I clinical trial, gallium nitrate was given as 30 minutes intravenous infusion with subsequent treatments every three weeks. The maximum tolerated dose was 700 mg/m^2 at each administration. Doses above 700 mg/m^2 showed high renal toxicity and high peak plasma level of gallium. However, administering diuretics prior to gallium nitrate treatment showed less toxicity to the kidneys.[4,105,106,192] A different method of administration of gallium nitrate was used with 41 patients in another phase I clinical trial. Gallium nitrate was given as a short daily intravenous infusion for three consecutive days every 2–3 weeks. Daily doses of 300 mg/m^2 were well tolerated, however, doses above 300 mg/m^2 showed renal toxicity and anaemia that were found to be dose dependant.[105]

In phase II clinical trials conducted to test the spectrum of its anti-cancer activity, gallium nitrate was administered to patients with different cancer types either as a single dose of 700 mg/m^2 every 2–3 weeks or as a short daily intravenous infusion (300 mg/m^2) for three consecutive days every 2–3 weeks (recommended dose from phase I clinical trials). Gallium nitrate showed no complete response, defined as complete disappearance of the active tumour and tumour related symptoms, in breast, squamous, non-squamous, colorectal, and non-small lung cancer. Less than 8% of patients had a partial response (≥ 50% reduction in tumour size and no new lesions) and more than 50% of patients had disease progression.[193–197] Conversely, gallium nitrate showed antineoplastic activity against non-Hodgkin's lymphoma and bladder cancer. Regarding lymphoma, multiple phase II clinical trials have been conducted and shown an overall partial response rate of ≥ 10%. Interestingly, large cell lymphoma (40% response including two complete

remissions cases) and non-Hodgkin's lymphoma (63% of response) appeared to be more responsive to gallium nitrate compared to other lymphoma types. [2,4,105,198] It should be noted that most of the lymphoma phase II clinical trials were done in the 1980s. However, a more recent phase II clinical study on T and B cell lymphoma showed efficacy of this drug with ~ 30% response rate, 7% of which was a complete response.[46] In fact, these findings parallel the clinical results that showed ^{67}Ga citrate is best established in lymphomas diagnosis and treatment follow up.[199,200,201]

The activity of gallium nitrate in bladder cancer was confirmed in multiple phase II clinical trials. Complete remission was seen in patients with transitional cell carcinoma of the bladder.[2,202,203] Patients in phase II clinical trials tolerated the dose given and showed low to moderate renal toxicity, low-grade anaemia, nausea, and vomiting.[105,196,197] It should be noted that, while the anti-cancer activity of gallium nitrate has been tested in the previously mentioned malignancies, its effectiveness against other malignancies must be considered. Although renal toxicity of intravenously injected gallium nitrate has restricted the use of higher doses, it led to investigation of gallium salts toxicity and anti-cancer activity after prolonged (months) oral administration (more details in the next section).[107]

3.1.2 Gallium chloride

Gallium chloride is a gallium salt that was tested preclinically and clinically as an orally administered drug for a prolonged period of time hoping to provide activity against cancer and overcome the renal toxicity of intravenously injected gallium nitrate.[204] An early preclinical study investigated gallium toxicity, gut absorption, and tissue concentration in rats fed gallium chloride (10-1000 mg /kg of food) for 13 weeks. No weight loss, changes in behaviours, or death occurred during the entire experiment duration. Animals were culled at the end of the experiment and tissue gallium concertation was measured. No detectable gallium was measured in liver, spleen or kidneys, with traces found in bone.[187] In addition, preclinical studies were conducted to investigate gallium chloride toxicity, anti-tumour activity, and bioavailability after prolonged administration. A preclinical study on mice subcutaneously inoculated with C3HBA adenocarcinoma showed tumour accumulation of gallium (13.4 ± 7.3 nmol/g, ~ 0.9 µg/g) after 42 days treatment of 200 mg/kg/day of gallium chloride with no renal toxicity.[107] Two preclinical studies on dogs bearing mammary adenocarcinoma showed tumour accumulation of gallium (10–376 nmol/g, ~ 0.7–26 µg/g) after oral administration of an average of 5 mg/kg/day (1–10 mg/kg/day) gallium chloride for an average of seven months (2–13 months). The studies showed partial response and stabilisation of the tumour in some cases. However, progression of the disease in other cases was also noted.[205,206]

A clinical study on orally administered gallium chloride was conducted to investigate gallium toxicity and tumour delivery after administration of a daily dose for several months.[204] Gallium

concentration in tissues was assayed in two patients who died of cancer. One lung squamous cell carcinoma patient died after receiving a maximum dose of 600 mg/day for 6 months. In this patient, gallium concentration in tumour was 5.5 µg/g. Another lung adenocarcinoma patient died after receiving a maximum dose of 1200 mg/day for 8 months. Gallium concentration in tumour was 1.5 µg/g. No renal toxicities or other side effect was noticed except for diarrhoea.[204] Another clinical study investigated the toxicity and anti-cancer activity of gallium post prolonged oral administration of gallium chloride. Patients were orally administered with gallium chloride at doses gradually increased from 300-800 mg/day for a median time treatment of 4.5 months. For the entire duration of treatment, no renal toxicity was observed in any of the patients. Partial response was noticed in two ovarian adenocarcinoma and peritoneal carcinoses patients treated for 5-7 months with 200-600 mg/day. No response in seven patients with disease progression in 13 patients.[207]

All previously mentioned preclinical and clinical studies regarding gallium chloride showed no renal toxicity even after prolonged oral administration, unlike intravenously injected gallium nitrate. However, although prolonged oral administration of gallium chloride produced uptake in tumour, its anti-tumour effect is produced slowly and requires several months. The poor anti-neoplastic effect of gallium chloride might be related to the low sensitivity of the tumour type investigated to gallium or to the poor gut absorption of gallium post oral administration. However, studies on orally administered gallium salts have encouraged the development of other orally administered gallium compounds with possibly better gut absorption (more detail in section 3.3).[4,205] It would be desirable to develop gallium compounds that could be orally administered and at least have similar anti-neoplastic effect to intravenously injected gallium nitrate with less renal toxicity.[2,208] As mentioned previously, SPECT/PET imaging with ^{67}Ga/^{68}Ga can help with this task. ^{67}Ga/^{68}Ga can be radiolabelled with carrier-added gallium compounds and be used preclinically to investigate their gut absorption, and tissue biodistribution including trafficking to tumour cells (more detail later).

3.2 Gallium salts: mechanism of action

Although clinical trials have been conducted to study the antineoplastic activity of gallium salts, their mechanism of action is still only partly understood. It is worth mentioning some of the known molecular mechanisms behind the anti-cancer effect of gallium salt as a foundation for newer gallium compounds' mechanisms of action, including KP46.

A considerable body of evidence suggests that the central role of gallium as an anti-cancer drug is the interference with cellular iron haemostasis and interrupting tumour growth.[2,4,46,208,209] Gallium can inhibit cellular iron uptake by competing against transferrin binding and uptake through cellular transferrin receptors, consequently causing cellular iron deprivation, which was

proven to cause cell apoptosis.[2,4,46,208,209] *In vitro* studies on the effect of iron deprivation on cellular growth showed that adding iron chelators such as DFO and N, N-bis(2-hydroxybenzyl)ethylenediamine-N,N-diacetic acid (HBED) caused decrease in cell growth and viability, and DNA fragmentation in multiple cancer cell lines in a dose related manner.[210,211,212] In addition, *in vitro* studies on HL60 cell line in serum free media showed that incubating cells for 72 hours with 150 µg/ml of Ga-Tf results in a 75% decrease in cell growth compared to a control group. However, adding the same dose of Fe-Tf after 24 or 48 hours of the addition of Ga-Tf showed 55-75% restoration of cell growth after 72 hours of incubation.[213] Although adding iron does not induce complete restoration of cell growth, probably due to irreversible cytotoxic damage caused by gallium, partial restoration after adding iron suggest that gallium's mechanism of action is related to interference with iron metabolism causing iron deprivation. *In vitro* studies on HL60 and mouse sarcoma cells (EMT-6/UW) in media supplemented with fetal bovine serum (FBS) showed that pre-treating cells with iron-pyridoxal isonicotinoyl hydrazone (Fe-PIH) before gallium nitrate treatment or simultaneously adding Fe-citrate and gallium nitrate decreased cells' sensitivity to gallium nitrate. However, the effect of iron on cell growth and viability was only significant at low gallium nitrate concentration. At higher gallium nitrate concentration, the presence of iron provided only minor cell protection.[210,214] This indicates competition between gallium and iron for transferrin binding sites, and gallium interference with iron metabolism and consequently cell survival and proliferation. The high expression level of transferrin receptors in lymphoma and bladder cancer might explain on at least at some level the efficacy of gallium nitrate against these specific malignancies.[2] Gallium causing cellular iron deprivation was indeed seen clinically in patients treated with gallium nitrate and they developed anaemia and high levels of zinc protoporphyrin, a biomarker for iron insufficiency.[4,46]

Other studies have shown that gallium nitrate can interfere with the iron-containing enzyme ribonucleotide reductase (RNR), which is responsible for deoxyribonucleic acid (DNA) synthesis. RNR consists of R1 and R2 subunits where R2 consists of an iron binuclear centre that is essential for the enzyme function. Disturbing iron haemostasis with gallium can reduce available iron for R2 subunit activity and accordingly, DNA synthesis.[2,4,46,188,208,209,215] An early study on the HL60 cell line using electron spin resonance (ESR) spectroscopy showed a decrease of RNR levels after Tf-Ga incubation, however, it only became significantly different from the control group (no Tf-Ga added) after six hours of incubation. Only 30% signal of that in the control group was seen after 24 hours of incubation. Consistent with a decreased level of RNR, HL60 cells exhibited significantly less DNA synthesis compared to the control group.[215] Another early study on CCRF-CEM (T-cell) lymphoma cells showed that adding 120 µM gallium nitrate (IC50 dose for this cell line) plus 80 µg/ml apo-Tf decreased the percentage of cells in G1 phase from 36.1% (control group) to 22.5% and increased the percentage in S phase from 44.2% (control group) to 61.3%. The study suggested that the effect of gallium might be specific to killing cells at G1 phase; it can also mean that gallium affects the rate of DNA synthesis negatively and cells are trapped in S

phase, where chromosome duplication and DNA synthesis occurs.[216] Another study confirmed the possible selectivity of the antineoplastic effect of gallium in the G1 phase after three days incubation of Tf-Ga in a HL60 cell line. The study demonstrated that the ability of gallium to kill cells in G1 phase is dose related. Leukaemia cells treated with 150 µg/ml of Tf-Ga showed fewer cells in G1 phase (31%) and more cells in S phase (59%) compared to 40% and 48% in cells treated with 25 µg/ml and 78% and 14% in control cells (incubated with Tf-Fe) respectively.[217] The same results were also presented in other studies on human peripheral blood mononuclear cells (PBMCs) after incubation with gallium chloride.[218]

In addition to the indirect mechanism of action of gallium that is related to iron deprivation, a direct effect of gallium nitrate was found to induce cellular apoptosis through the mitochondrial pathway. Lymphoma cell lines CCRF-CEM (T-cell) and DoHH2 (B-cell) showed cell apoptosis by the activation of Bcl-2-associated X (BAX) protein, a proapoptotic protein that translocates from the cytoplasm to mitochondria and facilitates the loss of mitochondrial membrane and the release of cytochrome c to the cytoplasm.[2,4,209,219] Cytochrome c is a protein that can activate caspase 3, a protein responsible for death protease activation.[220,221,222] In the same study, the use of BAX and caspase 3 inhibitors decreased the percentage of cellular apoptosis by two and a half fold.[219]

Studies have been conducted to understand the possible mechanism of cells' resistance to gallium nitrate. Chitamber *et al.*[223] studied the possible mechanism behind resistance to gallium nitrate in a developed CCRF-CEM resistant to gallium nitrate cell line. The study showed a significantly diminished ferritin protein in resistant cells (only 9% that of sensitive cells) after 24 h incubation with gallium nitrate. Further experiments demonstrated that the binding activity of iron regulatory proteins (IRP) and iron-responsive elements (IRE) located in ferritin mRNA (a crucial binding step to decrease ferritin synthesis and increase transferrin receptor synthesis in iron-depleted cells) was higher in resistant cells. This result suggested that the minimal ferritin production in resistant cells is due to suppression of ferritin mRNA translation.[223,224] Another study confirmed the significantly lower ferritin protein content in HL60 resistant cells (5.0 ± 0.5 ng/mg protein) compared to HL60 sensitive cells (18.2 ± 3.8 ng/mg protein) after 24 h incubation with gallium nitrate.[225] In addition, CCRF-CEM resistant cells showed gallium nitrate uptake of only 34–36% of that into sensitive cells. However, uptake in resistant cells increased with the addition of transferrin and cells consequently became more sensitive to gallium nitrate ($0.75x10^6$ cell count compared to $2x10^6$ in the absence of transferrin post 72 h incubation).[223] Another *in vitro* study on the HL60 cell line confirmed the effect of transferrin in enhancing the cytotoxic effect of gallium nitrate.[213] These studies strongly suggest that the mechanism of developing gallium resistance is related on at least at some level to the degradation in cellular gallium transport. However, the specific transporting mechanism needs to be fully studied.[223] It is important to understand the basis behind some cells' resistance to gallium nitrate to allow better judgment of

which patients will benefit most from gallium nitrate treatment and to help develop newer gallium complexes that can overcome gallium nitrate resistance.[213]

The continuous research on the antineoplastic effect of gallium nitrate led to the discovery of its effect on decreasing blood calcium level, especially in hypercalcaemic-related malignancies.[209] A preclinical study on hypercalcaemic rat models showed that gallium nitrate significantly lowered blood calcium levels when administered intravenously or intraperitoneally compared to the control group (in which no gallium nitrate was administered) in a dose-related manner. However, even at the highest selected dose (0.45 mmol/kg), orally-administered gallium nitrate did not significantly decrease blood calcium level, which might be related to the low gut absorption and plasma level of gallium nitrate post oral administration.[189] In an early randomised blind study on patients with hypercalcaemic related malignancies (variable primary tumours) and bone metastasis, gallium nitrate showed that 75% of patients reached normal calcium level compared to only 27% in patients who were injected with calcitonin (a food and drug administration (FDA) approved hormonal drug to regulate blood calcium level).[226,227] In Paget's disease patients and patients with different primary tumour and bone metastasis, gallium nitrate was shown to reduce osteoclast activity, calcium urinary excretion and bone pain.[2,188,227,228] Due to its clinical effectiveness in regulating blood calcium level, gallium nitrate (Ganite) was approved in 2003 by the FDA for the treatment of malignancy-related hypercalcemia.[2,229]

3.3 Tris (8-hydroxyquinolinato) gallium (III) (KP46)

KP46 is an orally administered gallium compound that is currently being investigated as an anti-cancer drug (Figure 3.1). An attempt was made previously to crystalise KP46 using vapour diffusion of diethyl ether into a solution of KP46 in chloroform.[230] Although only meridional (mer) isomer was observed in the solid state, a mixture of facial (fac) and mer isomers was obtained in the chloroform solution indicating that KP46 can form different isomers.[230]

KP46 was developed with the rationale of making a stable drug that can be efficiently absorbed once administered orally and have higher bioavailability than orally administered gallium salts.[4,108] Despite the ongoing research on KP46 and indeed a clinical trial, its pharmacokinetics and biodistribution are yet to be fully understood.[231] KP46 is the main focus of this chapter. Hence, KP46 *in vitro*, *in vivo*, protein binding, and mechanism of action studies will be reviewed in the following sections due to their relevance to the current research project.

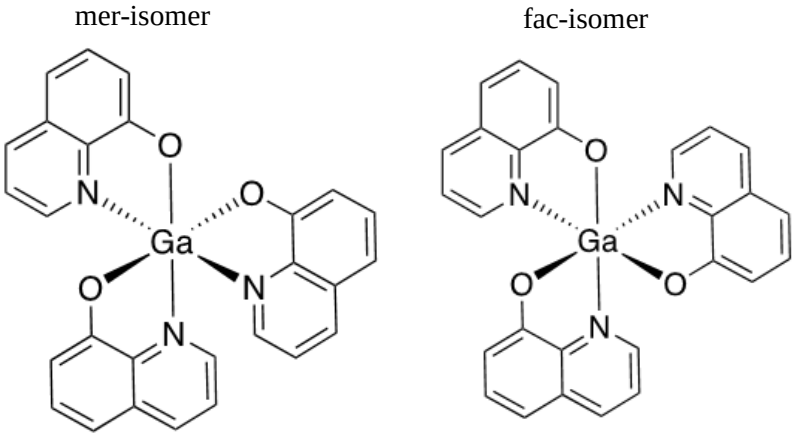

Figure 3.1: Tris (8-quinolinolato) gallium (III) (KP46) isomers.[230]

3.3.1 KP46 *in vitro* studies

Multiple reports studied the therapeutic potency of KP46 and showed that the range of the half-maximum inhibitory concentration (IC_{50}) of KP46 *in vitro* was between 0.85 and 10.4 μM in cell lines of lung, ovary, colon, kidney and breast cancer.[46,209,232,6,233] Furthermore, the IC50 of KP46 in melanoma cell lines is lower than that of gallium nitrate (0.85–2.5 and 20–72 μmol/L, respectively) indicating the susceptibility of melanomas cell lines to KP46 compared to gallium nitrate.[108] *In vitro* comparative studies revealed a potent inhibitory effect of KP46 on human lung adenocarcinoma cells that reached efficacy of up to ten-fold compared to the effects of gallium chloride.[233] However, no comparative studies have been conducted to demonstrate the difference in anticancer actions between KP46 and free 8HQ (without gallium). It has been reported that 8HQ and its derivatives have a pharmacological application as anti-cancer drugs and showed anticancer activity against human breast cancer cells (MCF-7) *in vitro* (more detail in chapter 4).[234,235]

3.3.2 KP46 preclinical studies

The toxicological profile and maximum tolerated dose (MTD, defined as the highest dose where organ toxicity is likely to occur without altering animal life span from any condition except carcinogenicity) of oral KP46 have been studied in healthy Swiss mice, showing a median lethal dose (LD50) of 2870 mg/kg in males and 2370 mg/kg in females following a single dose ranging between 464 and 4640 mg/kg.[236,237] Collery *et al*.[231] also conducted an *in vivo* study on NMRI BR mice and F344 rats that showed that the LD50 of a single dose of KP46 was 1742 mg/kg and 1352 mg/kg respectively, while the MTD was 900 mg/kg in both species.[231] Either mild or no renal toxicity was seen at the MTD. This indicates the well-tolerated nature of KP46 across different animal species. However, no pharmacokinetic studies after a single dose have been presented in the literature.

In addition to the single dose, studies have investigated the daily administration of KP46. For example, the following doses were administered via gavage to NMRI BR mice for 4 weeks: 5.5, 17.6, and 55 mg/kg/day. The highest dose caused severe toxicity, which was demonstrated as renal toxicity, a significant reduction of haemoglobin and toxic effects on the male reproductive system. Lower doses were well-tolerated with no toxicity observed.[231] In another experiment utilising 62.5, 125, 250, 500 and 750 mg/kg/day for two weeks in Swiss mice, the smallest dose was well-tolerated and did not negatively affect kidney function, nutrition, haematology, and organ weight. After 62.5 mg/kg daily oral doses (9 mg Ga/kg, accumulative dose of 126 mg/kg), the highest tissue concentration of gallium was reported in bone (7.02 ± 3.14 µg/g, 0.16 ± 0.07%ID/g) (more detail in discussion section). However, no gallium concentration data were presented in blood and the gastrointestinal system. Food consumption and body weight were affected in mice following the 125 mg/kg/day regimen and higher doses caused significant mortality.[236] Thus, only a daily dose of 62.5 mg/kg can be considered a safe dose for oral administration. Therefore, it seems that the single and low doses of daily administration of KP46 were well-tolerated with a low toxic profile, while toxicity and mortality increased with increasing the dose.[231,236] Although KP46 showed tolerability at a dose of 62.5 mg/kg administered daily for 14 days, the low concentration of gallium in tissues indicated the questionable bioavailability of the drug. For better gallium cytotoxic effect, prolonged KP46 treatment might be necessary to gain steady blood gallium concentration and progressive tumour accumulation and exposure to gallium.[204]

A preclinical study has been conducted on animals bearing tumours to test the antineoplastic effect of KP46 after oral administration. The anti-cancer activity of KP46 was investigated preclinically in hypercalcemia of malignancy in a rat model bearing Walker carcinosarcoma xenograft (WCS) subcutaneously inoculated.[238] A range of therapeutic doses (6, 12, 24 and 48 mg/kg) of orally administered KP46 were given to rats from day 3 to day 9 post inoculation. Two groups of rats were used as control; rats orally administered with gallium nitrate (25 mg/kg, equimolar to 48 mg/kg of KP46), and another group with no gallium administration. Blood samples from KP46 treated rats were taken on days 0, 6, 8, and 10 for calcium analysis. Animals were culled on day 10 and tumour weight was measured in all groups. No significant difference was seen in tumour weight between the control groups. However, rats treated with KP46 showed a significantly lower tumour weight compared to the control groups only at higher doses (24 and 48 mg/kg). No difference in blood calcium level was seen in rats treated with KP46 at 6 and 12 mg/kg compared to the control group (0 mg/kg, no KP46 administered) in all measured days. The group treated with 24 mg/kg of KP46 only showed a significant difference in blood calcium level at day 10 (3.5 ± 0.68 mmol/l) compared to the group treated with KP46 at 0, 6, and 12 mg/kg doses (4.25 ± 0.69 mmol/l).[238] No calcium analysis was done on the group treated with KP46 at 48 mg/kg dose.

Although KP46 at higher doses showed a significantly lower tumour weight compared to control groups, the data must be interpreted cautiously. The significant difference in tumour weight was seen only at higher doses and post 10 days of treatment, which might indicate that KP46 could be a possible anti-cancer drug, but that, like gallium chloride, high doses and relatively long periods of treatment must be applied for better antineoplastic effect.[238]

A limitation of the latter study is the oral use of gallium nitrate as a control. Gallium in the form of salts has proven to have low bioavailability after oral administration. However, using the same cell line (WCS), after subcutaneous inoculation into tumour-bearing Sprague-Dawley rats, a daily dose between 50 and 60 mg/kg of intraperitoneally administered gallium nitrate for 10 days showed 61–92% inhibition of tumour volume compared to the control group (no gallium nitrate administered).[185] The question that needs to be answered is not whether KP46 is a better anti-cancer drug compared to poorly bioavailable orally administered gallium salts, but whether orally administered KP46 can overcome gallium nitrate toxicity post intravenous injection and at the same time show efficient bioavailability and tumour response.

In addition, as mentioned previously, KP46 showed a decrease in blood calcium levels (3.5 ± 0.68 mmol/l) at 24 mg/kg dose suggesting that KP46 might be effective in hypercalcemia conditions and might share some of gallium nitrate's mechanism of action.[4,238] An early preclinical study investigated the effect of gallium nitrate on blood calcium level showed that a daily oral administration of 0.45 mmol/kg (~ 188 mg/kg) gallium nitrate for eight consecutive days into hypercalcaemic Sprague-Dawley rat model resulted in modest but significant ($p = 0.01$) decrease in blood calcium level. Although Ganite is an FDA approved intravenously administered drug for the treatment of malignancy-related hypercalcemia, its use is contraindicated in patients with impaired renal function due to its renal toxicity.[2,229] Hence, further research on orally administered gallium compounds should be carried out to find effective but less toxic compounds for the treatment of hypercalcemia in addition to their antineoplastic effect investigations.

The effect of KP46 against cancer was also tested in SCID Balb/C mice bearing HCT-116 (human colon cancer) after intraperitoneal administration. When the tumour was palpable, 15 mg/kg of KP46 was administered for two weeks (5 consecutive days/week). Tumour volume was measured from day 0 of KP46 administration to day 18, when mice were culled. The group treated with KP46 showed a lower tumour volume compared to the control group, however, it was only significantly different on day 15 onward. Tumour weight was measured on day 18 and showed that the group treated with KP46 had significantly lower tumour weight (0.4 g) compared to the control group (0.8g).[239] Although the current study showed a significant decrease in tumour weight after KP46 administration, this might not fully reflect the clinical study situation due to the different route of administration used (KP46 was administered orally in the clinical study). Absorption of drugs by a different route of administration depends on many different factors

including drug dosage, physiology and anatomy of the drug absorption site, and the chemical properties of the drug. In addition, the bioavailability of a drug is usually better when administered intraperitoneally compared to orally. The low bioavailability post oral administration is usually due to slow absorption from the gut.[240,241] The bioavailability of gallium nitrate post i.p and oral administration was tested and showed higher gallium plasma concentration post i.p injection, but no such studies have been conducted with KP46.[189] Nonetheless, results from preclinical studies of KP46 post oral and intraperitoneal administration were consistent regarding the need for daily doses and a long period of treatment for the drug to exhibit some efficacy.[238,239]

3.3.3 KP46 clinical studies

To test toxicity and safety in humans, a KP46 (as FFC11) phase I clinical trial was performed in Europe. KP46 was administered orally to seven patients as a tablet formulation over a 14-day period at doses ranging between 30 mg/m^2 and 480 mg/m^2, followed by another 14 days as a recovery period to assess drug toxicity (1 treatment cycle).[46,231] All patients received a total of 19 treatment cycles. No effect on the tumour was observed in a patient with ovarian cancer receiving 480 mg/m^2/day and she experienced fatigue and diarrhoea. Similarly, the lowest dose did not affect parotid gland cancer in a patient or stomach cancer in another patient when a dose of 30 mg/m^2/day was administered. Leukopenia was reported in the parotid gland cancer patient, however, no signs of toxicity in the stomach cancer patient were observed. Finally, some efficacy of KP46 was observed in three out of four patients with solid renal tumours (two disease stabilisations, one partial response), in which each patient received a different dose (30, 60, 120, or 240 mg/m^2/day). Regarding side effects, stomatitis was reported only in one patient.[231] Overall, the phase I clinical trial showed that KP46 is well tolerated with no renal toxicity. No pharmacokinetics or gallium concentration data were published in the phase I clinical study.

KP46 (as AP-002) is currently in phase I-II clinical trials (national clinical trial identifier number (NCT) 04143789) for patients with solid tumour (breast, lung, and prostate cancer) and bone metastasis.[242,243,244] The previously mentioned cancer types were probably chosen based on their resistance to gallium nitrate in clinical trials [196,245,246,247] and the ability of KP46 to induce cell death *in vitro* in these cell lines.[6,46,209,232,233] Surprisingly, no renal carcinoma was mentioned, even though the phase I clinical trial that was performed in Europe showed partial response in three out of four patients with renal carcinoma.[231] In addition, current AP-002 clinical trial is targeting patients with bone metastasis, which might be one step closer to understanding the effect of KP46 on cancer-related hypercalcemia and consequently, bone metastases.

3.3.4 KP46 chemical characteristics and protein binding studies

As mentioned in chapter 1, hydrated Ga^{3+} undergoes hydrolysis to insoluble $Ga(OH)_3$ at pH levels between 3–7 when stabilising ligands are not present. This might account for the poor absorption of gallium salts in the stomach's low pH environment after oral administration.[9] KP46 was developed on the rationale for more stable compound with efficient gut absorption.[4,108]

The stability of KP46 was measured in water (pH= 3.8) and a physiological buffer at pH 7.4. In both solutions, KP46 retained its chemical stability for several hours; decomposition occurred at a slower rate in the physiological buffer ($t_{1/2}$= 14.2 h) than in water ($t_{1/2}$= 4 h).[209,248,249] The Log *P* value (octanol/water) of KP46 using the shake flask method was 0.88, which indicates that KP46 is more soluble in octanol than water due to the chelation to lipophilic 8-hydroxyquinoline. However, it has been suggested that having a log *P* value of 0.88 might provide KP46 with a proper lipophilic/hydrophilic balance that might afford enough membrane permeability.[209] Although it was suggested that KP46 might have a balanced hydrophilic/lipophilic characteristic that can allow adequate membrane permeability, it should not be ignored that KP46 has low water solubility (4.4×10^{-5} M) which might be problematic and cause poor bioavailability after oral administration. Absorption from the gut is presumed to be affected by the water solubility of the drug, hence, enhancing the solubility of a hydrophobic drug can increase gut absorption and bioavailability.[248,250]

Moreover, to accomplish the desired clinical response, a drug must reach an adequate concentration and be sustained for an adequate time at its site of action. For oral administration, drugs must transfer from the gut to the blood circulation, where it may or may not bind to plasma proteins, before delivery to its target.[251] Studies have been published on the protein speciation of KP46 *in vitro* using capillary electrophoresis (CE) coupled with inductively coupled plasma mass spectrometry (ICP-MS).[252,253] The *in vitro* protein binding studies suggest the formation of KP46 adduct upon incubation with apo-Tf and human serum albumin (HSA) (at lesser extent),[252,253] however, the mechanism of binding was not identified.

Transferrin is an important competitor for gallium complexes, hence, it is crucial to understand the chemical form of KP46 once absorbed into blood circulation post oral administration.[254] More *in vitro* studies have been conducted to investigate the mechanism of KP46 binding to transferrin and HSA. HSA is the most abundant plasma protein and plays a major role in binding endogenous and exogenous ligands (e.g. pharmaceuticals). It possesses three domains that can provide a variety of binding sites for ligand binding and hydrophobic interaction. Based on the binding properties of HSA, it was expected that KP46 binds to HSA hydrophobically forming a metallodrug-protein complex.[254,255,256] A study has been conducted to measure the interaction of KP46 with HSA and apo-Tf using ^{1}H and saturation transfer difference (STD) nuclear magnetic resonance (NMR) spectroscopy after 24 h incubation. The similar NMR spectra of KP46 and

KP46 incubated with HSA suggested that KP46 does not dissociate in the presence of HSA and the ligand is not displaced, indicating hydrophobic binding.[254] In the same study using ^{1}H NMR spectroscopy, KP46 incubated with apo-Tf (in the presence of bicarbonate) showed a different spectrum compared to free KP46, and the presence of peaks between 8 and 8.2 ppm which corresponds the same peaks in the ligand NMR spectrum. This might indicate some level of dissociation which is not surprising considering the high affinity of transferrin to bind gallium. The author estimated that the partial release of the ligand in KP46 incubated with transferrin sample is approximately 30%. However, the method adopted for this estimation was not clearly explained.[254] In addition, KP46-apo-Tf and KP46 (control) was investigated by fluorescence spectrometry and showed that by monitoring the fluorescence intensities in the presence of apo-Tf, partial release of the ligand and consequently decreasing of the fluorescence signals was observed, however, these were qualitative observations rather than quantitative results. The author suggested a transferrin independent uptake mechanism of KP46 might occur parallel to or as an alternative to transferrin mediated uptake.[254] In contrast with previously mentioned research, another study using X-ray absorption near edge structure (XANES) supported the hydrophobic binding theory of KP46 to both HSA and apo-Tf. XANES analysis showed no change in KP46 spectra when incubated with apo-Tf and HSA for 30 minutes, suggesting the absence of coordination environment changes, no covalent binding of the metal to HSA and apo-Tf, and the possibility of hydrophobic binding.[249] Although literature provides some evidence suggesting the hydrophobic binding of KP46 to HSA, evidence regarding KP46 and apo-Tf mechanism of binding is contradictory. The reason for the contradictory results of KP46 and apo-Tf mechanism of binding might be related to the use of different methods of research and consequently different level of analysis and explanatory logics.

Although the previously mentioned protein binding studies did not give a conclusive explanation to the nature of KP46-apo-Tf binding, they have focused on KP46 protein binding and the mechanism of binding *in vitro* and overlooked the fact that KP46 is an orally administered drug and the important question that needs to be asked, therefore, is whether KP46 can primarily leave the gut as an intact form. A study was done to test the stability of KP46 in a simulated intestine juice (pH = 6.8) *in vitro* based on the observation that post oral administration, most drugs absorption in general occurs in the small intestine.[257] The electropherogram revealed no alteration (single peak) over four hours monitoring.[252] This study is considered important, but it lacks information on how KP46 behaves in the stomach (at low pH) before moving to the intestine, rendering the intestinal stability of KP46 potentially irrelevant. Drugs might go through dissolution and disintegration steps in the stomach which could affect the drug absorption and bioavailability.[258] Dissociation of a drug in the stomach is likely to be influenced by the physicochemical properties of the drug, pH at the site of administration, and additional physiological factors such as the presence of food. Another drawback of the previously mentioned *in vitro* approach is the absence of food particles which might induce changes to the administered

compound or adsorb it. Studies have shown that the presence of food can modulate drug metabolism and absorption, which consequently influence bioavailability.[251,258,257]

A study has been conducted to acquire information on the binding of KP46 to serum proteins in mouse tumour and liver tissues after oral administration of 200 mg/kg for 6 consecutive days, using µ-XAS (X-ray absorption spectroscopy) and XANES. The µ-XAS map showed different distribution of Ga to Fe but a similar pattern to Zn in tumour samples. Conversely, the distribution of Ga was similar to Fe and different to Zn in liver samples.[249] XANES analysis of the samples showed slight change in tumour and liver spectra compared to KP46 spectrum (control) in MEM (minimum essential media). The authors concluded that the change in XANES analysis might be a statistical error due to the low strength of the signals found in the tissues samples which also confirms the poor bioavailability of KP46 post oral administration. Based on their results, the authors have suggested that a hydrophobic interaction between KP46 and transferrin is conceivable post oral administration. However, the change in XANES analysis might also indicate possible coordinative binding (at least at some level) and some change in coordination environment of Ga atoms.[249] In addition, it is worth mentioning that due to the low concentration of KP46 found in tissue samples, the XANES spectra analyses were only performed at the highest Ga concentration focal spot that was seen in µ-XAS map and may not be representative of the whole sample. The difference in Ga distribution in tumour and liver tissues might suggest that the gallium may be in different coordination environments in the two organs which can also be the reason for the inconclusive XANES spectra.[249] Although µ-XAS map and XANES analysis study showed some possibility of hydrophobic binding to transferrin and consequently non-transferrin mediated tumour uptake of KP46 (or at least at some level) post oral administration,[249] the study (as mentioned previously) exhibited some limitations and inconclusive results. Thus, KP46 bioavailability, its stability in the gut, its mechanism of binding to proteins and delivery to normal tissues and cancer cells should not be overlooked and must be studied *in vivo* post oral administration. Imaging with ^{67}Ga/^{68}Ga using radiolabelled KP46 complex, as described later in this chapter, offers the potential to help with this task and provide new information.

3.3.5 KP46 mechanism of action

As mentioned previously, several cell lines showed more susceptibility to KP46 than to gallium salts. Hence, it was expected that KP46 might have some differences in its mechanisms of action compared to gallium salts owing to its ligand binding and the possibility that the ligand itself change the metal's mechanism of action.[46,2] Although KP46's exact mechanism of action is not fully understood, a considerable amount of literature reports insights into its cellular effects.[108,232,239,259,260]

A detailed study has been conducted *in vitro* on multiple cancer cell lines to understand the KP46 mechanism of action.[232] The study showed that KP46 induced cytotoxicity in HCT-116 cells with

positive p53 gene expression ($p53^{+/+}$) and in those with depleted p53 gene expression ($p53^{-/-}$). However, IC50 was less in $p53^{+/+}$ cells (4.4 µM) than $p53^{-/-}$ cells (7.78 µM) indicating that $p53^{+/+}$ cancer cells are more susceptible to KP46. In addition, western blotting in MCF-7 cells ($p53^{+/+}$) showed that p53 expression was significantly increased in cells treated with KP46 than control cells (no KP46 added). In the same study, the effect of KP46 on Ca^{2+} release in the cytoplasm was tested in MCF-7 cells ($p53^{+/+}$) and non-small lung carcinoma (H1299) ($p53^{-/-}$) after up to ten hours of incubation.[232] Unlike H1299 cells, which showed gradual Ca^{2+} release over time, MCF-7 showed the same gradual level of Ca^{2+} release, however, a significant burst was seen at 8 h post incubation. No Ca^{2+} release burst was seen when short-interfering RNA (siRNA), a p53 gene silencer, was used. Although Ca^{2+} release was not entirely dependent on p53 status in these cell lines, the Ca^{2+} burst release in MCF-7 might indicate a possible role of p53 in intracellular Ca^{2+} regulation. It should be remembered that Ca^{2+} release is one of the first steps in cell apoptosis.[232,188] Due to the general correlation between the induction of reactive oxygen species (ROS) and Ca^{2+} signalling, the effect of KP46 on cellular ROS was tested on MCF-7 ($p53^{+/+}$) and H1299 ($p53^{-/-}$) cell lines over 24 h. Interestingly, the increase of ROS profile followed the same pattern as Ca^{2+} release profile in both cell lines. However, using 8-(N,N-diethylamino)octyl-3,4,5-trimethoxybenzoatel (TMB-8), a calcium antagonist, an inhibition of ROS induction was seen in MCF-7 cells indicating cellular apoptosis by Ca^{2+} release and activation of ROS.[2,232,247,261] Another study confirmed that the apoptotic effect of KP46 on MCF-7 ($p53^{+/+}$) cells is due to Ca^{2+} release by transient receptor potential cation channel (TRPC6). KP46 treated cells showed higher expression of TRPC6 than untreated cells. However, silencing the p53 gene with siRNA showed downregulation in TRPC6 confirming the possible role of p53 in Ca^{2+} and TRPC6 expression.[259]

A study showed that, like gallium salts, KP46 induced the release of BAX and its translocation to mitochondria in HCT-116 ($p53^{+/+}$) cells. However, unlike gallium salts, using a caspase 3 inhibitor did not reduce the KP46 effect in non-small lung carcinoma (A427), indicating that the release of caspase 3 might not be one of the KP46 modes of action.[239] Although protein protease caspase 3 might not be involved in the KP46 mechanism of action, calpain, a Ca^{2+} dependant protease protein, was found to be involved in the KP46 apoptotic mechanism. Adding a calpain inhibitor (PD150606) to A427 cells resulted in significantly reduced KP46 cytotoxicity.[239,262] Due to the partial role of calpain in cell adhesion, the effect of KP46 in cellular adhesion was studied. Adding a calpain inhibitor showed a significant increase of cell adhesion by double compared to the control group (only KP46) in A427 cells.[239]

It is confirmed from the previously mentioned results that KP46 influences the upregulation of p53. However, recent data revealed that iron deprivation can upregulate p53 as well.[263,264] Hence, it was hypothesised that KP46 might upregulate p53 expression by causing cellular iron depletion.[260] After two hours incubation of KP46, HCT-116 ($p53^{+/+}$) cells showed 50% of the labile iron pool (LIP) of that in control cells (no KP46). In addition, LIP was measured 2 h after

adding ferric acetate in the presence and absence of KP46. In the absence of KP46, cells showed a more than two-fold higher level of LIP compared to cells exposed to KP46. The reduction of LIP in the presence of KP46 might be related to a possible transferrin binding competition and uptake by the transferrin mediated mechanism, which is counter to the hypothesis of KP46 cellular accumulation by non-transferrin mechanism.[260] However, another possible explanation is that KP46 enters the cells by the non-transferrin mediated mechanism; once inside the cells, gallium is released and cells cannot sufficiently distinguish gallium from iron, leading to less transferrin receptor synthesis and consequently less iron uptake. However, more experimental studies are needed to understand KP46 cellular/intracellular trafficking and protein binding. Finally, a study suggested that like gallium salts, KP46 might interfere with cell cycle development. An *in vitro* study of KP46 on multiple human melanoma cell lines exhibited fewer cells in the G1 phase and more cells in the S phase compared to the control group. An increased number of cells in the S phase might indicate the effect of KP46 in DNA synthesis.[108]

Overall, KP46 might be a potential anti-cancer drug. However, most of its protein binding and mechanism of action studies were done *in vitro.* As an orally administered drug, it is crucial to analyse the chemical form of KP46 in the gut, normal and cancer tissues in preclinical studies. Preclinical studies on KP46 protein binding after oral administration are lacking. Although a preclinical study provided some information regarding a possible hydrophobic interaction between KP46 and transferrin post oral administration, some of the study results were inconclusive and not representative of the whole samples.[249] Hence, it is not logical to assume that KP46 survives the harsh conditions encountered during digestion, reaches the circulation and binds to protein as an intact form based on the previously reviewed *in vitro* and *in vivo* protein binding studies. In addition, all preclinical studies regarding KP46 that have been reviewed so far did not assess KP46 pharmacokinetics and gallium biodistribution in tumour and plasma, which might be important assuming that delivery of gallium to tumour cells might be the major component of the mode of action of KP46. More comprehensive preclinical studies could be carried out on animals bearing tumour xenografts to investigate KP46 gut absorption, biodistibution, and chemical form after oral administration. Gallium radioisotopes (^{67}Ga and ^{68}Ga) are suitable for radiolabelling the drug complex, and SPECT/CT and PET/CT can be used no-invasively to image and facilitate this task.[209]

3.4 A pilot study

A pilot study has been conducted in our department by C. Imberti and J. Bartnicka (unpublished work), to study the biodistribution of KP46 in NSG mice bearing A375 human melanoma xenografts by using [^{68}Ga]KP46 and [^{68}Ga]Ga-acetate (control) after i.v. injection (Figure 3.2 and 3.3). PET/CT images of [^{68}Ga]Ga-acetate post i.v. injection showed visible tumour uptake, especially after one hour. In contrast, no visible tumour accumulation was observed during the four-hour PET/CT scan post i.v. injection of [^{68}Ga]KP46 (Figure 3.2). *Ex vivo* biodistribution of [^{68}Ga]Ga-acetate at four hours showed a significantly higher tumour uptake (6.1 ± 2.4%ID/g) compared to [^{68}Ga]KP46 (2.6 ± 0.9%ID/g) (Figure 3.3). The previously reviewed preclinical and clinical studies in literature suggested that KP46 has anti-cancer activity, therefore KP46 or a metabolite of it is likely to be delivered to tumour to some extent. The negligible tumour uptake of ^{68}Ga exhibited post i.v. injection of [^{68}Ga]KP46 in the pilot study might be due the different route of administration used (i.v. in the pilot study vs. oral in the clinical trial). Another reason might be related to the quantitative difference between the low concentration of radioactive Ga administered and the large concentration of stable/therapeutic dose of Ga. It cannot be assumed that tumour accumulation of pico/nano gram quantities of ^{68}Ga/^{67}Ga administered would be similar to the large quantities of Ga^{3+} administered seeking a therapeutic effect. This chapter is dedicated to investigating the *in vitro* protein binding, cellular uptake and whole body trafficking of KP46 in a cancer model (*in vitro* and *in vivo*), with the aim of evaluating the gut absorption, pharmacokinetics, and chemical form of KP46 after i.v. and oral administration of [$^{68/67}$Ga]KP46 as a tracer, or combined with a pharmacologically relevant dose of KP46.

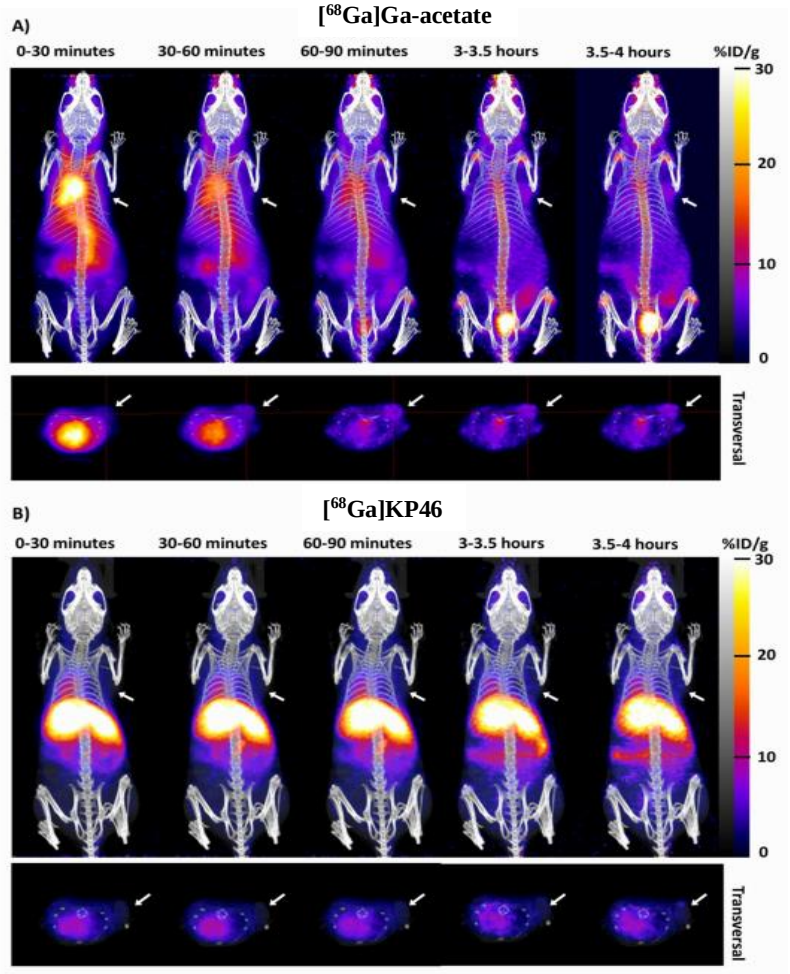

Figure 3.2: Dynamic MIP PET/CT images of [^{68}Ga]Ga-acetate (A), and [^{68}Ga]KP46 (B) at different time points post i.v. injection. For each image panel, MIP's are shown in the upper part of the image and transverse section images (axial) are showing in the lower part of the image. The white arrow represents the position of the tumour. Captured with permission from C. Imberti thesis (unpublished work).

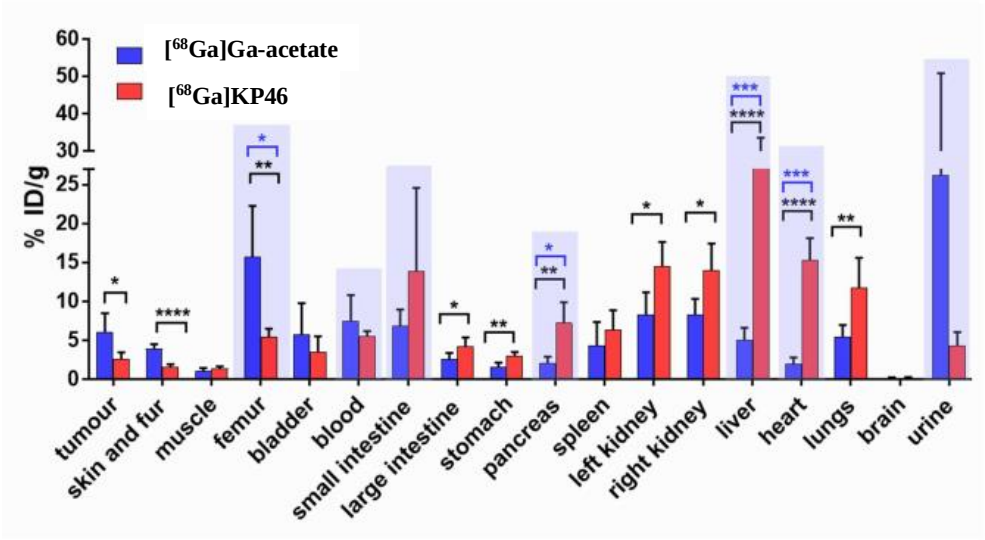

Figure 3.3: *Ex-vivo* bio distribution of [^{68}Ga]Ga-acetate and [^{68}Ga]KP46 at 4 hours post i.v. injection. Values are expressed as mean ± SD (n=5). P values are defined as follows: * = $P \leq 0.05$, ** = $P \leq 0.01$, *** = $P \leq 0.001$, **** = $P \leq 0.0001$. Captured with permission from C. Imberti thesis (unpublished work).

3.5 Aims

The experimental aims of this chapter are:

- Synthesis of KP46 by adopting the same method used in literature.
- Radiolabel [$^{68/67}$Ga]KP46 and assess the radiolabelling by iTLC and HPLC.
- Study the protein speciation of [$^{68/67}$Ga]KP46 and [$^{68/67}$Ga]Ga-acetate (control) *in vitro* using size exclusion chromatography.
- Investigate the cellular uptake mechanism of [$^{68/67}$Ga]KP46 and [$^{68/67}$Ga]Ga-acetate (control) in cultures using A375 human melanoma cell lines.
- Evaluate the biodistribution of [$^{68/67}$Ga]KP46 in animal models bearing A375 xenograft after i.v. injection
- Evaluate the biodistribution of [$^{68/67}$Ga]KP46 in animal models bearing A375 xenograft after oral administration as a tracer or combined with a pharmacologically relevant dose of KP46.
- Study the chemical form of [$^{68/67}$Ga]KP46 after oral administration in the gut and tissue samples by homogenisation and octanol extraction.
- Measure stable gallium concentration in normal and tumour tissues using ICP-MS.

3.6 Experimental

3.6.1 Equipment and consumables

All reagents and consumables were purchased from Fisher Scientific/Chemical, Crawford Scientific or Sigma Aldrich unless specified otherwise. Athymic nude nu/nu mice were purchased from Charles River UK Ltd. A375 human melanoma cell lines were purchased from the American Type Culture Collection (ATCC) and were then cultured and stocked in our department. ^{68}Ga was obtained from a ^{68}Ge/^{68}Ga generator (Eckert & Ziegler) and eluted with 5 ml of 0.1 M ultrapure HCl and collected in 5 x 1 ml fractions. [^{67}Ga]Ga-citrate was purchased from Mallinckrodt, The Netherlands. iTLC was carried out using Agilent's silica gel impregnated glass microfiber strips (10 cm in length). iTLC strips were scanned by a LabLogic mini scan TLC reader with positron (β^+) or gamma (γ) detectors for ^{68}Ga and ^{67}Ga, respectively, and analysed with Laura software or phosphor imager filmless autoradiography (Cyclone Plus). HPLC was implemented using an Agilent Eclipse XDB C_{18} 5 μm 4.6 × 150 mm reversed phase (RP) column and Agilent 1200 series HPLC with ultraviolet (UV) detection (220 nm) and radioactivity detection, using Gina Star ™ software version 5.8. PET/CT and SPECT/CT images were acquired on a nanoScan® PET/CT and a nanoScan® SPECT/CT (Mediso Medical Imaging System, Budapest, Hungary). Images were analysed by VivoQuant software (version 1.23). Gamma counting was performed using an LKB Wallac 1282 Compugamma Gamma Counter. Mass spectrometry analysis was conducted at King's College London using a Thermo Exactive HR mass spectrometer that used electrospray ionisation (ESI) and running Xcalibur version 2.2 software. Nuclear magnetic resonance (NMR) spectra were acquired on a Bruker Avance III HD NanoBay 400 MHz NMR spectrometer (Ascend™ magnet) and analysed with Topspin software. ICP-MS analysis was conducted in the London Metallomics Facility at King's College London using a PerkinElmer Flexar LC system linked to a PerkinElmer NexION 350D, with Syngistix version 1.0 and Chromera version 4.1.2 software. LC/MS was acquired through an Agilent Eclipse XDB C_{18} 5 μm 4.6 × 150 mm RP column on an Agilent liquid chromatograph (1200 Series) with UV detection at 254 nm, connected with Advion Expression LCMS mass spectrometer with electrospray ionisation source. Analysis was performed by Advion Mass Express software (version 6.4.16.1).

3.6.2 Synthesis and quality control of KP46

The synthesis of KP46 was based on a previous method by Collery et al.[236] In brief, 1.175 g (8 mmol) of 8-hydroxyquinoline (dissolved in 10% acetic acid) was added to 0.559 g (2 mmol) of gallium (III) nitrate [Ga $(NO_3)_3.H_2O$]. The mixture was heated under reflux to 80° C for one hour before being filtered and the residue washed with both hot and cold water and diethyl ether. The final compound was dried overnight at 100° C in a drying oven. The final yield of KP46 produced 0.6232 g (1.2 mmol) of a bright yellow powder compound.

3.6.3 Elemental analysis

A 5 mg sample of KP46 and 8-hydroxyquinoline (control) was sent for elemental analysis to London Metropolitan University's elemental analysis service for the determination of carbon, hydrogen, and nitrogen content in the samples. Measured analysis of 8-hydroxyquinoline (74.30 %C, 4.85 %H, 9.75 %N) showed negligible deviation from theoretical analysis (74.47 %C, 4.86 %H, 9.65 %N). However, measured analysis of KP46 (61.50 %C, 3.30 %H, 7.60 %N) showed a considerable deviation from theoretical analysis (64.56 %C, 3.61 %H, 8.38 %N).

3.6.4 NMR analysis

Five mg of KP46 and 8-hydroxyquinoline (control) was dissolved in 0.5 ml deuterated dimethyl sulfoxide (DMSO) and placed in NMR tubes (5 mm in diameter) for NMR analysis at a frequency of 400 MHz. ^{1}H NMR of 8-hydroxyquinoline: (DMSO-d6 400 MHz) δ: 8.84 (dd, J = 4.1, 1.5 H_Z, 1H), 8.30 (dd, J = 8.3, 1.5 H_Z, 1H), 7.52 (dd, J = 8.3, 4.1 H_Z, 1H), 7.43 (t, J = 8.0 H_Z, 1H), 7.38 (dd, J = 8.1, 1.1 H_Z, 1H), 7.11 (dd, J = 7.4, 1.2 H_Z, 1H). ^{1}H NMR of KP46; (DMSO-d6 400 MHz) δ: 8.71 (0.63 H), 8.57 (1H), 7.65 (0.68 H), 7.50 (1.67 H), 7.18 (1H), 6.88 (1H). In the KP46 sample, three peaks were observed at 1.9 ppm, 2.5 ppm and 3.4 ppm, corresponding to acetic acid, DMSO-d6 and H_2O, respectively.

3.6.5 Mass spectrometry

Five mg of KP46 was dissolved in 1 ml ethanol before being diluted 10 times with 0.1% formic acid in 50% methanol and was used for mass spectrometry. Mass spectrometry analysis of KP46 showed a peak at 502.0677 m/z $[M+H]^+$, corresponding to the desired compound (KP46, calculated: 502.4498 for $C_{27}H_{18}GaN_3O_3 + H^+$). Mass spectrometry analysis of KP46 displayed the regular isotopic pattern of the natural gallium complex: 502.0677 m/z and 504.0667 m/z, correlating to MW $[M+H]^+$ of ^{69}Ga and ^{71}Ga isotopes, respectively. Additional peaks at 503.071 m/z and 505.0701 m/z correlated to ^{69}Ga and ^{71}Ga MW $[M+H]^+$ incorporating one ^{13}C, respectively.

3.6.6 LC/MS

KP46 and 8-hydroxyquinoline (control) were dissolved in ethanol and diluted with water to bring the final concentration to 250/350 µM. Mobile phase: H_2O (A) and acetonitrile (B). Gradient: 0–2 minutes: 5% B, 2–17 minutes: 60% B, 17–18 minutes: 100% B, 18–24 minutes: 100% B, 24–26 minutes: 5% B and 26–30 minutes: 5% B. LC/MS analysis of 8-hydroxyquinoline showed a single peak at 14:03 min:s, which corresponded to the ligand mass seen in the mass spectrometry analysis at 146 m/z $[M+H]^+$. LC/MS analysis of KP46 showed one peak at 16:02 min:s, which gave a molecular ion in the mass spectrometry analysis at 501.75 and 503.77 m/z $[M+H]^+$ (regular isotopic pattern of natural gallium, corresponding to KP46), and another peak at 14:04 min:s corresponded to the free ligand.

3.6.7 Radiolabelling of [^{68}Ga]KP46

The ^{68}Ga complex formation with 8-hydroxyquinoline was prepared according to a modified method used by Yano *et al.*[265] In brief, 8-hydroxyquinoline was dissolved in ethanol (1 mg/ml). 200 µl of the ligand solution was mixed with 200 µl of sodium acetate (0.5 M in sterile H_2O, pH = 9) and 100 µl (8-10 MBq) of ^{68}Ga from most radioactive fraction (see materials section for ^{68}Ga elution method) to bring the final mixture to 2:2:1 v/v respectively (final mixture pH = 5.5/6). The final mixture comprised 2.76 mM 8-hydroxyquinoline and approximately 0.98 nM ^{68}Ga (see the following section for calculation method) at the time of preparation. [^{68}Ga]Ga-acetate (control) was prepared following the [^{68}Ga]KP46 method (except that no ligand was added; the ligand solution was replaced with ethanol only). RCP was evaluated by iTLC after 10 minutes of incubation at room temperature ($CHCl_3$:CH_3OH, 95:5%, v/v) and showed a retention factor (Rf) of 1 for [^{68}Ga]KP46. In comparison, a Rf of 0 was observed for [^{68}Ga]Ga-acetate.

3.6.8 Calculation method for ^{68}Ga concentration

^{68}Ga concentration at the time of preparation was calculated following Brown *et al.*[266] method.

$$Decay\ constant\ (disintegration\ per\ atom\ per\ second) = Ln\ 2/\ half\ life\ in\ seconds\ (4080\ s) = 1.7E-04$$

$$Number\ of\ atoms = desintegration\ per\ second\ (Bq)\ \ at\ the\ time\ of\ preparation\ /decay\ constant$$

$$Number\ of\ atoms = 1.0E+07\ Bq\ (10\ MBq)/1.7E-04 = 5.89E+10$$

$$Number\ of\ moles = number\ of\ atoms/\ Avagadro's\ constant$$

$$Number\ of\ moles = 5.89E + 10/\ 6.023E + 23 = 9.77E - 14$$

$$Concentration\ (M) = number\ of\ moles\ (9.77E - 14)/\ volume\ used\ (0.0001\ (100\ \mu l))$$
$$= 9.77E - 10\ M (= 0.98\ nM)$$

3.6.9 Determination of the distribution/partition coefficients (log*D* and log*P)* of [^{68}Ga]KP46

Lipophilicity determination was performed using the shake flask method. Between 5–20 µl (0.3–0.5 MBq) of [^{68}Ga]KP46 and [^{68}Ga]Ga-acetate mixtures (see section 3.6.7 for radiolabelling method) was added to a pre-equilibrated mixture of octanol/water (500 µl/500 µl [for log*P* measurement]) or octanol/PBS (500 µl/500 µl [for log$D_{7.4}$ measurement]). Samples were vortexed for two minutes in a Multi Vortex Mixer V-32 (Grant Bio). From each layer, 200 µl was taken and analysed separately using a gamma counter.

3.6.10 *In vitro:* [$^{68/67}$Ga]KP46 binding to serum proteins

Human apo-Tf (2 mg/ml) and HSA (50 mg/ml) (purchased from Sigma Aldrich) were dissolved in aqueous $NaHCO_3$ (5 mM, pH = 8) and PBS (pH = 7.4), respectively. [^{68}Ga]KP46 and [^{68}Ga]Ga-acetate were prepared following the methods described in section 3.6.7. One MBq (13–20 µl) of [^{68}Ga]KP46 was either added to 1.2 ml of $NaHCO_3$, containing apo-transferrin and apo-transferrin-free $NaHCO_3$ (control), or 1.5 ml PBS, containing HSA or HSA-free PBS (control), and was incubated for 60 minutes at 37° C (pH = 7-7.5). One MBq (20–25 µl) of [^{68}Ga]Ga-acetate was used as a control to obtain standard elution profiles of ^{68}Ga in buffers in both the presence and absence of the proteins. From both mixtures, 0.5 ml was loaded into PD MidiTrap G-25 tubes that were preconditioned with 8 ml of $NaHCO_3$ (5 mM) (for apo-Tf binding) or PBS (for albumin binding). Radioactive fractions (0.5 ml) were measured by a Wallac gamma counter. The protein absorbance at 280 nm was measured using a nanodrop spectrophotometer. PD MidiTrap G-25 tubes were counted by a gamma counter to determine how much radioactivity remained in the columns. Owing to the longer half-life of ^{67}Ga (78.3 hours) compared to that of ^{68}Ga (68 minutes), [^{67}Ga]KP46 was radiolabelled following the radiolabelling methods for [^{68}Ga]KP46 (see section 3.6.7) (see the following section for ^{67}Ga citrate to ^{67}Ga chloride conversion method) to investigate [^{67}Ga]KP46 protein speciation at longer time points. For [^{67}Ga]KP46, only binding to apo-transferrin was performed following the method mentioned previously. However, the incubation of different periods (0, 1, 3, 5, 24 and 48 hours) was investigated. In addition, the elution profiles of [^{67}Ga]KP46 in apo-transferrin-free $NaHCO_3$ (control) were completed after 24 and 48 hours of incubation.

3.6.11 ^{67}Ga citrate to ^{67}Ga chloride conversion method

^{67}Ga was provided as [^{67}Ga]Ga-citrate, usually 418-430 MBq in 5.5 ml at the time of receipt (76-78 MBq/ml). ^{67}Ga citrate was passed through a Sep-Pak plus light silica cartridge (part number WAT023537) at 1 ml/min to trap the radio-metal on the silica cartridge. The eluate was passed through again to capture 80% of the activity on the cartridge. The cartridge was washed twice with 5 ml of H_2O, then eluted with 600 µl of 0.1 M HCl in 50 µl fractions. Fractions with the highest activity (fraction 4, 5, and 6) were used for experiments.

3.6.12 Cellular uptake of [^{68}Ga]KP46

The uptake was evaluated by placing 0.5 ml of Dulbecco's Modified Eagle Medium (DMEM) – low glucose media – (10% FBS, 5 ml of L-glutamine and 5 ml of penicillin and streptomycin) that contained 1 x 10^6 A375 (human melanoma) cells in suspension into 1.5 ml Eppendorf tubes. [^{68}Ga]KP46 and [^{68}Ga]Ga-acetate were radiolabelled using the method mentioned in section 3.6.7. 10 MBq of each mixture was transferred to Eppendorf tubes and diluted with sodium acetate (0.5 M in sterile H_2O, pH = 9) to 1 ml to obtain the activity concentration of 100 kBq/10 µl, pH = 7. ^{68}Ga mixtures were tested for radiochemical purity by iTLC prior to the uptake studies. Ten µl of each mixture was added to cells/control (no cells to correct for non-specific binding to plastic) and incubated for 60 minutes (37^o C and 5% CO_2). Following incubation, samples were centrifuged (Sci Spin Mini) for three minutes at 1,500 RPM. Then, the supernatant was removed and transferred to another Eppendorf tube. Following the same centrifuging method, cell samples were washed twice with 0.5 ml PBS, and washes were added to the supernatant tubes. All samples were measured using a gamma counter. The average percentage uptake of [^{68}Ga]KP46, [^{68}Ga]Ga-acetate, and corresponding controls was calculated by dividing the activity obtained for the pellet/control-containing tubes by the sum of activity for pellet/control, supernatant and washes tubes combined, then multiplying by 100. Control corrected was calculated by correcting the percentage cell uptake for corresponding control.

In addition, to correct for the different volume between cell pellets and supernatant, ratio of intracellular (IC) and extracellular (EC) concentration of ^{68}Ga was calculated for [^{68}Ga]KP46 and [^{68}Ga]Ga-acetate. IC (control corrected activity associated with the cell pellets) and EC (supernatant + washes) activity was divided by their volumes (2.804 µl and 1500 µl respectively). The volume of 1 x 10^6 A375 cells (2.804 µl) was calculated based on an estimated diameter of 17.5 µm for a A375 cell from literature.[267] The formula $V=4/3 \prod r^3$ (considering A375 cells as spheres) was used to find the volume of a A375 cell (2804.73 μm^3 which corresponds to 2.804 $x10^{-6}$ µl).

3.6.13 Preparation and quality control of [$^{68/67}$Ga]KP46 and KP46 for *in vivo* studies

To obtain the highest radioactivity yield and purity, [^{68}Ga]KP46 radiolabelling was modified slightly by using a Sep-Pak Light C-18 cartridge (part number WAT 023501). One ml of the highest ^{68}Ga elution fraction was added to a mixture of 2 ml of freshly dissolved 8-hydroxyquinoline in ethanol (1 mg/ml) and 1 ml of sodium acetate (0.5 M in sterile H_2O, pH = 9), final mixture pH = 5.5. For [^{67}Ga]KP46 radiolabelling, after ^{67}Ga citrate to ^{67}Ga chloride conversion, 0.5 ml of ^{67}Ga chloride was added to a mixture of 1 ml of freshly dissolved 8-hydroxyquinoline in ethanol (1 mg/ml) and 0.5 ml sodium acetate (0.5 M in sterile H_2O, pH = 9), final mixture pH = 5.5. The mixtures were diluted (1:2 v/v) with sterile water and loaded into a C-18 cartridge (preconditioned with 5 ml of water and 5 ml of ethanol). The C-18 cartridge was eluted with 500 µl of ethanol into 5 x 100 µl fractions. For RP-HPLC analysis, samples from the [^{67}Ga]KP46 C-18 eluted fraction in ethanol (diluted 1:2 v/v with water, 20–30 µl, 2 MBq) and KP46 (preparation method detailed in LC/MS section 3.6.6) were used.

Volumes of [^{68}Ga]KP46 administered intravenously (10 ml/kg) (no preclinical study of [^{67}Ga]KP46 was performed post i.v. injection) and [$^{68/67}$Ga]KP46 administered orally (20 ml/kg) were based on the maximum administered volume allowed by the project licence. Mice were weighed before dose administration. As the lowest measured weight was 20 g, it was decided to base the dose volume calculation on this weight (200 µl for i.v. injection and 400 µl for oral administration). 10 µl of the [^{68}Ga]KP46 C-18-eluted hottest fraction (10% ethanol – the maximum % allowed by the project registration licence) was added to 180 µl of PBS to bring the final volume to 200 µl for i.v. injection. The same method was used for the oral administration of [^{68}Ga]KP46 as a tracer; however, 40 µl of the hottest fraction (10% of ethanol) was added to 360 µl of PBS to bring the final volume to 400 µl. Unlike in the literature, where high volumes of dissolved KP46 in DMSO were used for preclinical studies,[249,236] the co-administration of [^{68}Ga]KP46 and KP46 for oral administration in this study was performed by adding 20 µl of KP46 dissolved in DMSO (20 mM) (only 5% DMSO of the final volume was allowed by the project licence) to 40 µl of [^{68}Ga]KP46 from the hottest fraction (10% of ethanol). Due to the hydrophobic behaviour of KP46, 180 µl of polyethylene glycol (PEG) (0.4 g/ml in water) was added before diluting the sample further with water to avoid precipitation. Distilled water was added to bring the final volume to 400 µl. Oral administration of [^{67}Ga]KP46 and KP46 was performed following the same dose preparation method as [^{68}Ga]KP46 and KP46. However, for the orally administered [^{67}Ga]KP46 used as a tracer without the bulk drug, DMSO (KP46-free), PEG and water were used as vehicles (instead of PBS). iTLC was performed (see section 3.6.7 for iTLC method) after mixing [$^{68/67}$Ga]KP46 and KP46 and adding the vehicle. iTLC strips were analysed by a LabLogic mini scan TLC reader for [$^{68/67}$Ga]KP46 and by UV lamp (Analytik Jena, 254/365 nm) for KP46.

3.6.14 *In vivo* studies

All *in vivo* studies were completed in accordance with the project and personal licence that was approved by the British Home Office under regulations governing animal experimentation. All animal-bearing tumour xenograft studies were performed on female athymic nude mice after injecting them subcutaneously in the right shoulder with 2.5 x 10^6 A375 cells in 100 µl of PBS. Tumour growth was monitored regularly so as not to exceed the maximum volumetric size limit (1.2 cm^3), as per the project and personal licence. All *in vivo* studies were conducted between 14- and 24-days post cell inoculation with a minimum and maximum tumour volume of 100 mm^3 and 580 mm^3, respectively (Figure 3.4).

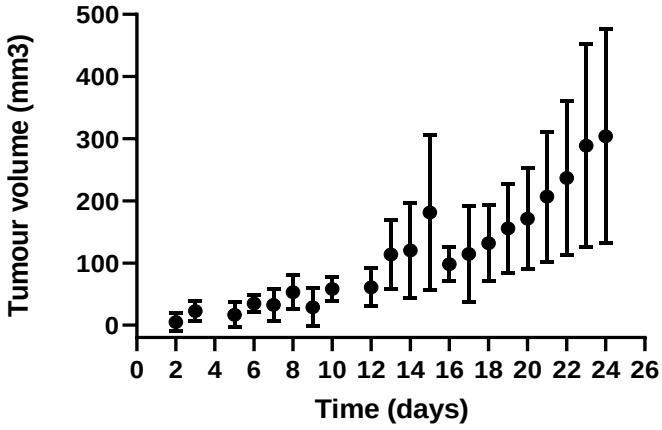

Figure 3.4: Tumour growth graph of A375 human melanoma cells in female athymic nude mice (2.5 x 10^6 cells). Data are reported as mean ± SD (n=24).

3.6.15 *Ex vivo* biodistribution after intravenous injection of [^{68}Ga]KP46

With the aim of uniting the variables between intravenously and orally administered preclinical studies, mice bearing an A375 xenograft (n = 3) fasted for 12-14 hours before the start of the experiment. Mice were anaesthetised and then injected with [^{68}Ga]KP46 (2.3–2.5 MBq) via their tail vein. Mice were kept under anaesthesia before they were culled at two hours post injection, and the organs were harvested, weighed and gamma counted.

3.6.16 *In vivo*: Developing a method for oral administration of [^{68}Ga]KP46

The method for the oral administration of [^{68}Ga]KP46 was based on two pilot studies that were performed to find the best (i.e. with transit through the gastrointestinal tract least affected by anaesthesia) method for obtaining maximum absorption of [^{68}Ga]KP46 post oral administration. In the first pilot study, mice bearing a tumour xenograft (A375) were anaesthetised, orally

administered with [^{68}Ga]KP46 (10 MBq) and PET scanned (no CT scan was performed) for four hours (n = 1), or orally administered with [^{68}Ga]KP46 (1–2 MBq) and kept anaesthetised for four hours (n = 3), before being culled for organ harvesting and gamma counting. To enhance the gastrointestinal motility, in the second pilot study, healthy mice (n = 3) were anaesthetised, orally administered with [^{68}Ga]KP46 (6–8.5 MBq) and allowed to recover for three hours before being re-anaesthetised and PET scanned for one hour. In both studies, mice fasted for no more than 18 hours during the entire study.

3.6.17 *In vivo*: Oral administration of [^{68}Ga]KP46 in the presence and absence of a pharmacologically relevant dose of KP46

Athymic nude nu/nu mice bearing an A375 xenograft were divided into two groups: A (n = 3) and B (n = 3). Mice in both groups fasted for no more than 18 hours over the entire study. Awake (non-anaesthetised) mice were orally administered with [^{68}Ga]KP46 (5–13 MBq) (group A) or with [^{68}Ga]KP46 and KP46 (5–8.5 MBq) (group B) (see section 3.6.13 for dose preparation) and kept fasting in a cage for three hours before being anaesthetised and PET/CT scanned dynamically for one hour. Mice in both groups were culled four hours post oral administration for organ harvesting and gamma counting. Blood, urine, stomach content, small intestine and large intestine content samples from the mice in group A were used for octanol extraction (shake flask method, Log $P_{\text{octanol/water}}$) to measure the lipophilicity of ^{68}Ga in the samples. No octanol extraction was performed on the tumours due to the absence of tumour activity (due to decay) at the time of experiment. Blood samples were placed in a serum separator tube (Fisher Scientific Ltd VS367954) and centrifuged at 3,000 rpm for 10 minutes. Serum (200–300 µl) and urine samples (150–180 µl) from each mouse were directly and equally added to three different Eppendorf tubes containing a pre-equilibrated mixture of octanol (500 µl) and water (500 µl). Serum and urine samples were vortexed for two minutes by a Multi Vortex Mixer V-32 (Grant Bio). From each layer, 400 µl was transferred separately into Eppendorf tubes and analysed by a gamma counter. Stomach content (72–77 mg), small intestine content (35–88 mg) and large intestine content (86–100 mg) samples from each mouse were added equally to three different Eppendorf tubes containing a pre-equilibrated mixture of octanol (500 µl) and water (500 µl) before being vortexed for two minutes by a Multi Vortex Mixer V-32 (Grant Bio) and centrifuged at 10,000 rpm for 10 minutes at 4^{o} C. From each layer, 430 µl was removed post centrifuging, transferred separately into Eppendorf tubes, and analysed by gamma counter. Precipitation remaining in Eppendorf tubes was also analysed by a gamma counter to measure the activity bound to samples. [^{68}Ga]KP46 (see section 3.6.13 for radiolabelling method) and [^{68}Ga]Ga-acetate (see section 3.6.7 for radiolabelling method) log *P* values were measured on each experimental day as controls. To measure how much natural gallium was in the tissue samples using ICP-MS, samples were left to decay at –20° C, then liver, stomach, tumour, heart, small intestine, large intestine (after being sliced into small pieces), blood and urine from the mice in

group B were transferred to 15 ml metal-free centrifuge tubes (Elkay Laboratories, 2086-500). Metal-free HNO_3 (68%) (Fisher Scientific, 10098862*)* was added to all samples (0.5–3 ml) in addition to two–four drops of 30% hydrogen peroxide (Sigma Aldrich H1009). Samples were digested for four days (and vortexed daily) before being centrifuged at 2,000 rpm for five minutes. At this point, only the small and large intestine samples had visible precipitation. Of the samples, 0.5 ml was transferred into new 15 ml metal-free falcon tubes, diluted with distilled water to 5 ml (10 times dilution) and centrifuged at 2,000 rpm for five minutes. Aliquots (4 ml) of samples were transferred to new 15 ml metal-free tubes and sent for analysis.

3.6.18 In vivo: Oral administration of [^{67}Ga]KP46 in the presence and absence of a pharmacologically relevant dose of KP46

Athymic nude nu/nu mice bearing an A375 xenograft were divided in two groups: A (n = 4) and B (n = 4). Mice in group A fasted for 11–14 hours, while the mice in group B fasted for 7–10 hours prior to the experiment. Awake (non-anaesthetised) mice were orally administered with [^{67}Ga]KP46 (2–11 MBq) (group A) or with [^{67}Ga]KP46 and KP46 (1–11 MBq) (group B) (see section 3.6.13 for dose preparation) and remained fasting in a cage for three hours before being placed under anaesthesia and SPECT/CT scanned dynamically for one hour (first time point). Mice were allowed to eat after the first time point scan. Group A mice were re-scanned 24 hours post oral administration, followed by *ex vivo* biodistribution, organ harvesting and gamma counting. Blood, urine, tumours, stomach wall/content, small and large intestine wall/content and faeces samples from each mouse in group A were used for an octanol extraction study. Following the method mentioned in section 3.6.17, serum (30–120 µl) and urine samples (60–100 µl) from each mouse were directly and equally added to three different Eppendorf tubes that contained a pre-equilibrated mixture of octanol and water. However, the tumours, stomach wall/content, small and large intestine wall/content and faeces samples were homogenised by slicing into small pieces, adding 1–2 ml of EDTA-free RIPA lysis and an extraction buffer (Thermo scientific, 89900) containing a freshly added EDTA-free Halt Protease and Phosphatase Inhibitor Cocktail (10–20 µl) (Thermo Scientific, 78441). Samples were homogenised by passing them through an 18-gauge needle that was attached to a plastic syringe at least 10 times before repeating the same process with a 21-gauge needle until homogenates were achieved. Homogenates (supernatant) were removed by centrifugation at 10,000 rpm for 20 minutes at 4°C. Both supernatants and precipitation were analysed by a gamma counter to measure the activity of the supernatant and the activity bound to the samples. Equal volumes from each sample homogenate were added to three different Eppendorf tubes that contained a pre-equilibrated mixture of octanol and water. Samples were vortexed for two minutes before 200 µl was taken from each layer and transferred to separate Eppendorf tubes for gamma counting. Group B mice were re-scanned 24 and 48 hours post oral administration, which was followed by *ex vivo* biodistribution, organ harvesting and gamma counting. An octanol extraction study for group B tissue samples was only performed on

the liver, large intestine content and tumour following the exact method used on the mice in group A. Tissue samples from the mice in group B were left to decay at –20° C for further ICP-MS analysis. The liver, stomach, small intestine, large intestine, and tumour (after being sliced into small pieces), urine, blood, faeces, and heart samples were transferred to 15 ml metal-free centrifuge tubes (Elkay Laboratories, 2086-500). Samples were digested by adding optima grade concentrated HNO_3 (67–68%, Fisher Scientific*)* (3–5 ml) and being left to stand at room temperature for 24 hours. Samples were transferred to acid-cleaned 7–15 ml PTFE microwave digestor vessels and placed in a Milestone UltraWAVE microwave digestion system, which was heated to 220° C over the course of a 15-minute period and was maintained at that temperature for a further 10 minutes to complete the digestion process. Sample aliquots of 0.5 ml were transferred to acid-cleaned trace metal grade HDPE centrifuge tubes (purchased from VWR) and diluted to 10 ml (factor of x20 dilution) using purified water from an Elga PureLab purification system and then analysed by ICP-MS. PET/CT images were used for the delineation of the region of interest (ROI) and quantification of distributed activity in selected organs. The time–activity curve was obtained from the generated ROI within the selected organs.

3.7 Results

3.7.1 Synthesis and quality control of KP46

KP46 was synthesised by following a method reported by Colley *et al.*[236] Table 3.1 represents the measured and theoretical elemental percentages in the 8-hydroxyquinoline and KP46 samples. Elemental analysis of 8-hydroxyquinoline showed negligible deviation from theoretical analysis. However, a measured analysis of KP46 showed a considerable deviation from theoretical analysis. The deficiency noticed in the percentage of nitrogen and carbon in the measured analysis is probably related to the presence of residual acetic acid from KP46 preparation related to increase oxygen percentage in the sample. Theoretical elemental percentages of KP46 combined with one mole of acetic acid showed similar elemental percentages to that of measured KP46 sample (Table 3.1 bottom row). In addition, the presence of acetic acid was also observed later in NMR at 1.9 ppm (Figure 3.5 C), confirming the possibility of acetic acid impurities. Attempts at purification by crystallisation by vacuum sublimation and liquid diffusion were made but did not improve the elemental analysis results (data not shown).

Sample	%C	%H	%N	%O	%Ga
8HQ (T)	74.47	4.86	9.65	11.02	N/A
8HQ (M)	74.30	4.85	9.75	N/M	N/A
KP46 (T)	64.56	3.61	8.38	9.56	13.89
KP46 (M)	61.50	3.30	7.60	N/M	N/M
KP46 + CH_3COOH (T)	61.95	3.94	7.47	14.23	12.41

Table 3.1: CNM elemental analysis of KP46 and 8-hydroxyquinoline: a comparison between theoretical and measured analysis. 8HQ, 8-hydroxyquinoline: T, theoretical: M, measured: N/A, not applicable: N/M, not measured.

3.7.2 NMR analysis

Figure 3.5A represents the NMR spectrum of 8-hydroxyquinoline. The assessment seen in Figure 3.5 A is consistent with previously assigned 8-hydroxyquinoline from literature.[268] Figure 3.5 B represents the NMR spectrum of KP46 (see method section 3.6.4 for chemical shifts and integration) and shows the absence of free ligand in the sample. However, signals of not equivalent ligand protons were detected indicating the possible coexistent of KP46 structure isomers in the solution. The COSY spectrum of KP46 (Figure 3.6) is generally in agreement with the proposed assignment seen in figure 3.5 B.

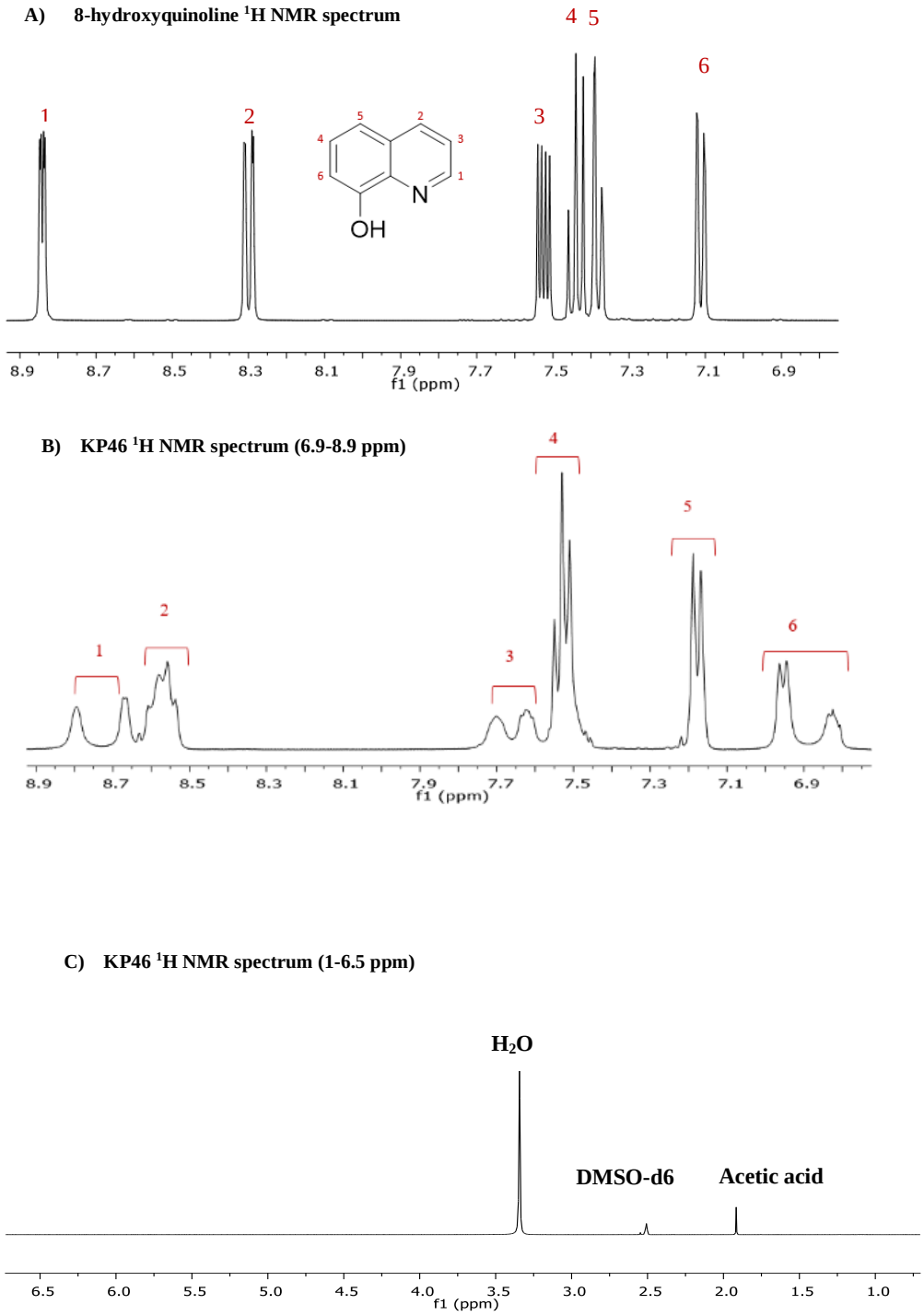

Figure 3.5: 400 MHz ¹H NMR spectra of 8-hydroxyquinoline (A) and KP46 (B and C).

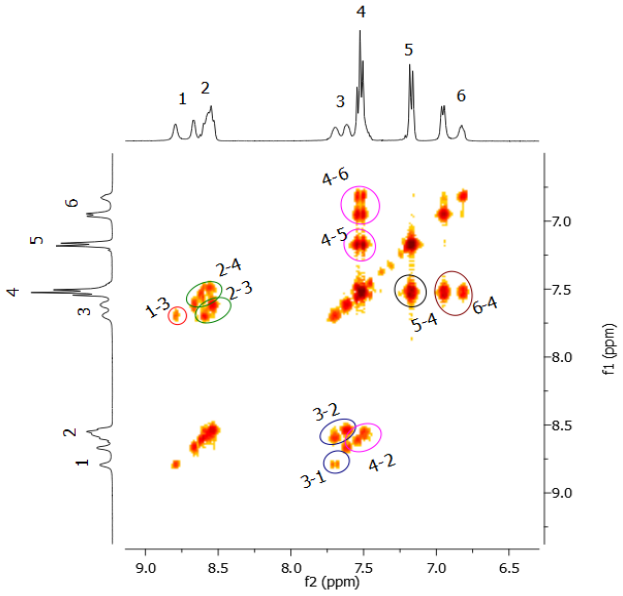

Figure 3.6: 400 MHz ^{1}H COSY spectrum of KP46 demonstrates the coupling between the protons.

3.7.3 Mass spectrometry

Figure 3.7 represents the mass spectrum of KP46, showing a peak of 502.0677 m/z $[M+H]^+$, which corresponds to the desired compound (KP46, calculated: 502.4498 for $C_{27}H_{18}GaN_3O_3$+ H^+) (Figure 3.7 A). Figure 3.7 B represents the peak at 502.0677 m/z and shows the regular isotopic pattern of the natural gallium complex. Four additional peaks were observed (m/z) in the mass spectrum of KP46: 357.0148 $[M]^+$, which corresponds to Ga^{3+} binding to two 8-hydroxyquinolinate ligands (calculated: 357.2998 for $C_{18}H_{12}GaN_2O_2$), 733.0324 $[M+H]^+$, which correlates to the mass of two Ga^{3+} binding to four 8-hydroxyquinolinate ligands and OH group (calculated: 732.6071 for $C_{36}H_{25}Ga_2N_4O_5$ + H^+), 761.0273 $[M+H]^+$, which corresponds to the mass of two Ga^{3+} binding to four 8-hydroxyquinolinate ligands and formate group (CHO_2) (calculated: 760.6167 for $C_{37}H_{25}Ga_2N_4O_6$ + H^+), and 860.0750 $[M+H]^+$, which correlates to the mass of two Ga^{3+} binding to five 8-hydroxyquinolinate ligands (calculated: 859.7497 for $C_{45}H_{30}Ga_2N_5O_5$ + H^+). However, peaks assignments (except 502.0677) are suggestions and subject to confirmation based on the isotope distribution pattern. The presence of other species in the mass spectrometry may be instrumentally related to the compound dissociating in the gas phase. Mass spectrometry analysis of KP46 was performed previously by Groessl *et al.*,[253] and the presence of a species at 357.1 m/z was also noticed in the sample. However, the highest m/z value included in the spectrum was 600 m/z. Hence, the presence or absence of another species at 733.0324, 761.0273, and 860.0750 m/z cannot be confirmed.[253]

3.7.4 LC/MS

LC/MS presented 8-hydroxyquinoline with a single peak at 14:04 min:s and KP46 with two peaks, which corresponded to the desired compound (16:02 min:s) and excess-free ligand (14:04 min:s) (Figure 3.8). The presence of excess 8-hydroxyquinoline in the sample may be due to the dissociation of the compound under analytical conditions which was not seen in HPLC analysis of the same sample (HPLC results are presented in section 3.7.9). Although no acid was used in the mobile phase, residual acid in the LC/MS line might be present causing some level of dissociation.

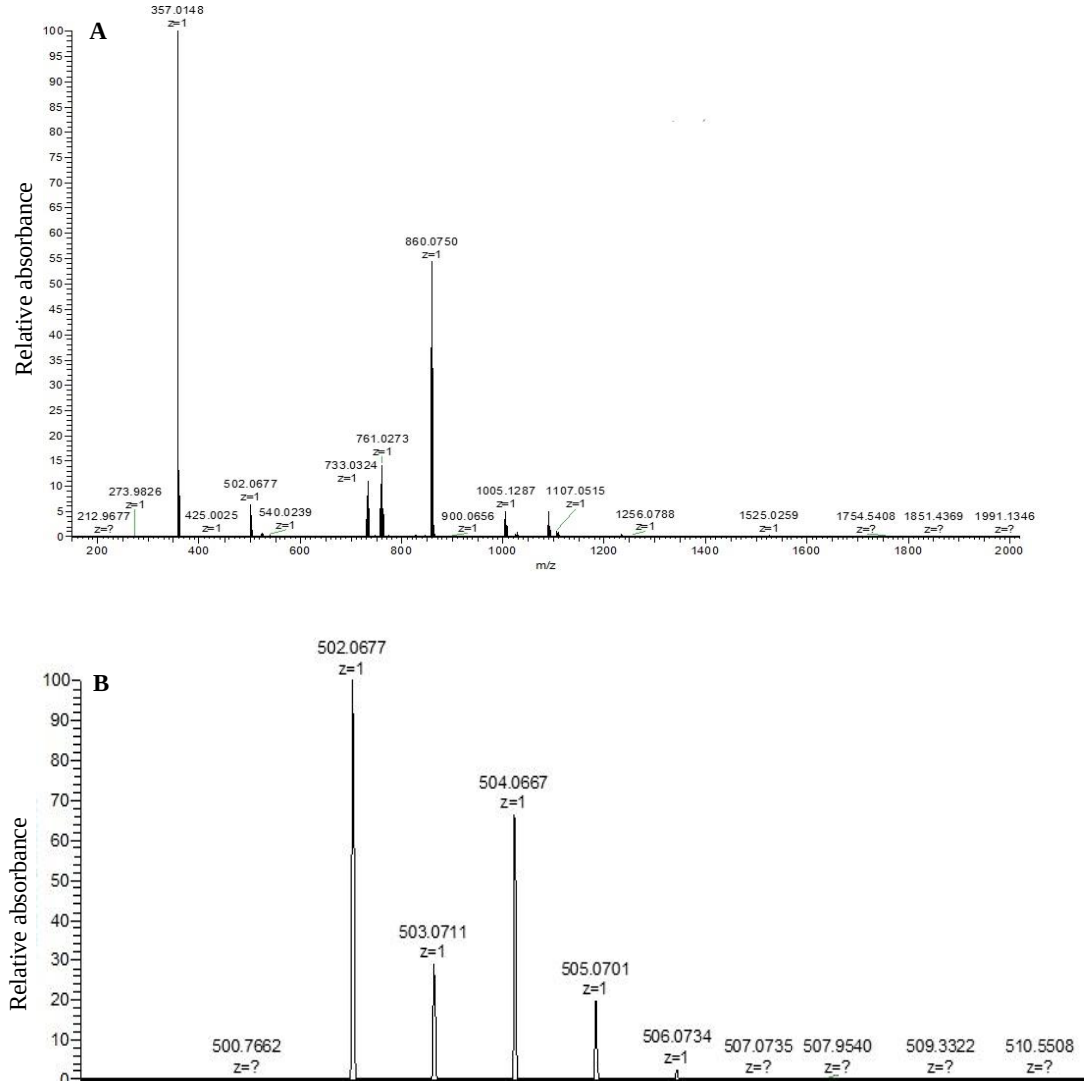

Figure 3.7: High resolution mass spectrometry of KP46 from 200 to 2000 m/z (A), and 499 to 511 m/z (B). The peak at 502.0677 m/z represents KP46 and shows the regular isotopic patten of natural gallium complex. Peak at 357.0148 m/z corresponds to Ga^{3+} binding to two 8-hydroxyquinolinate ions (calculated: 357.2998 for $C_{18}H_{12}GaN_2O_2$). Peak at 733.0324 m/z correlates to the mass of two Ga^{3+} binding to four 8-hydroxyquinolinate ions and OH group (calculated: 732.6071 for $C_{36}H_{25}Ga_2N_4O_5 + H^+$). Peak at 761.0273 m/z corresponds to the mass of two Ga^{3+} binding to four 8-hydroxyquinolinate ions and CHO_2 group (calculated: 760.6167 for $C_{37}H_{25}Ga_2N_4O_6 + H^+$). Peak at 860.0750 m/z represents the mass of two Ga^{3+} binding to five 8-hydroxyquinolinate ions (calculated: 859.7497 for $C_{45}H_{30}Ga_2N_5O_5 + H^+$). Peak's assignments (except 502.0677) are suggestions and subject to confirmation based on the isotope distribution pattern.

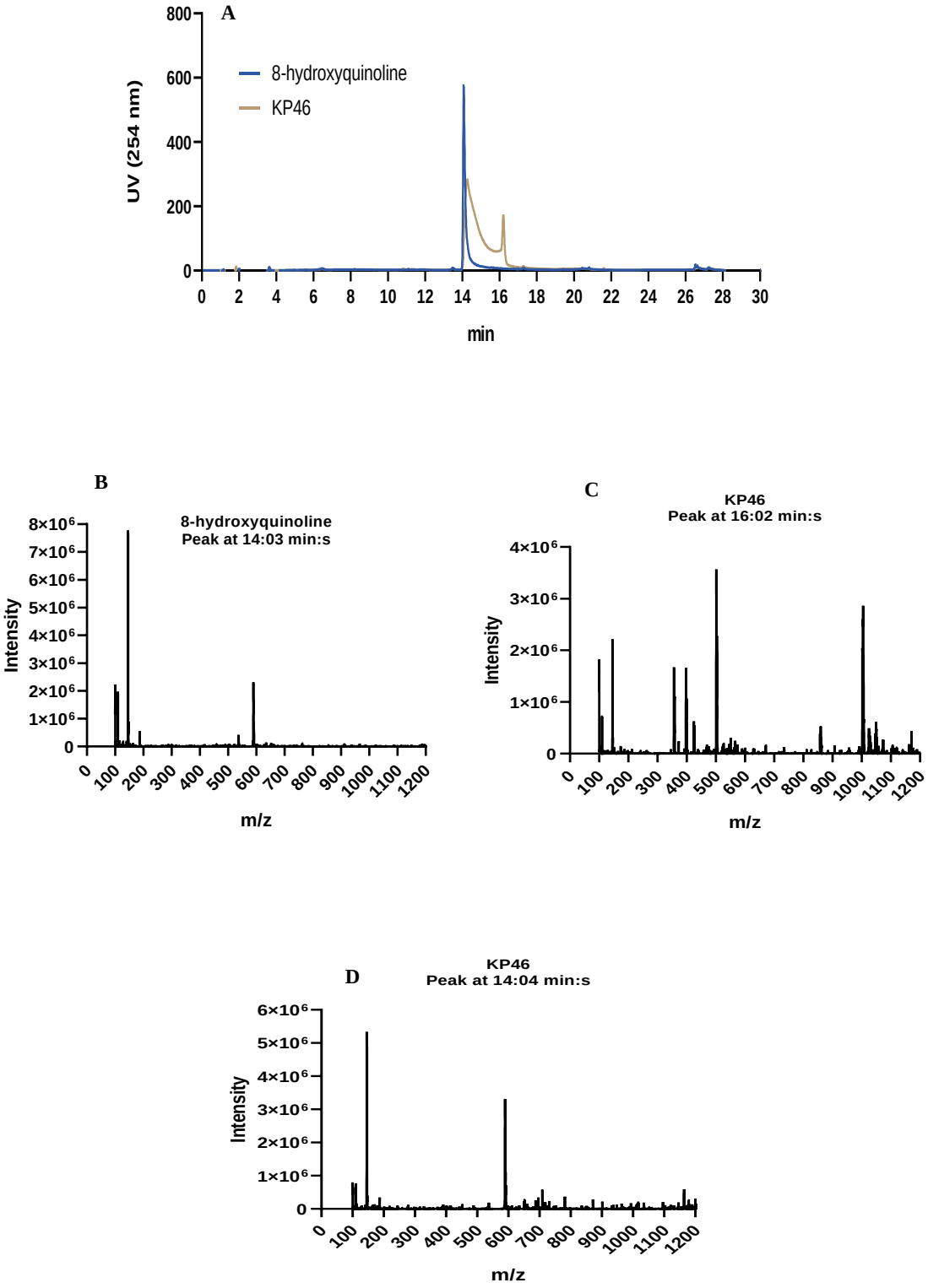

Figure 3.8: LC/MS analysis of 8-hydroxyquinoline represents a single peak at 14:03 min:s (A) corresponds to the ligand mass seen (146 m/z $[M+H]^+$) in panel B. LC/MS analysis of KP46 shows two peaks at 16:02 and 14.04 min:s (A) which correspond to KP46 mass (501.75 and 503.77 m/z $[M+H]^+$, regular isotopic pattern of natural gallium) (C) and the free ligand mass (146 m/z $[M+H]^+$) (D) respectively. H_2O (A) and acetonitrile (B) were used as mobile phase. Gradient: 0-2 minutes: 5% B, 2-17 minutes: 60% B, 17-18 minutes: 100% B, 18-24 minutes: 100% B, 24-26 minutes: 5% B, 26-30 minutes: 5% B).

3.7.5 Radiolabelling of [^{68}Ga]KP46

Mixing 8-hydroxyquinoline with ^{68}Ga chloride in an acetate buffer results in the efficient chelation of ^{68}Ga to form a lipophilic complex with high RCP (98%), as determined by iTLC ($CHCl_3$: CH_3OH, 95:5%, v/v) with Rf = 1. Using the same iTLC conditions, [^{68}Ga]Ga-acetate showed Rf = 0 (Figure 3.9).

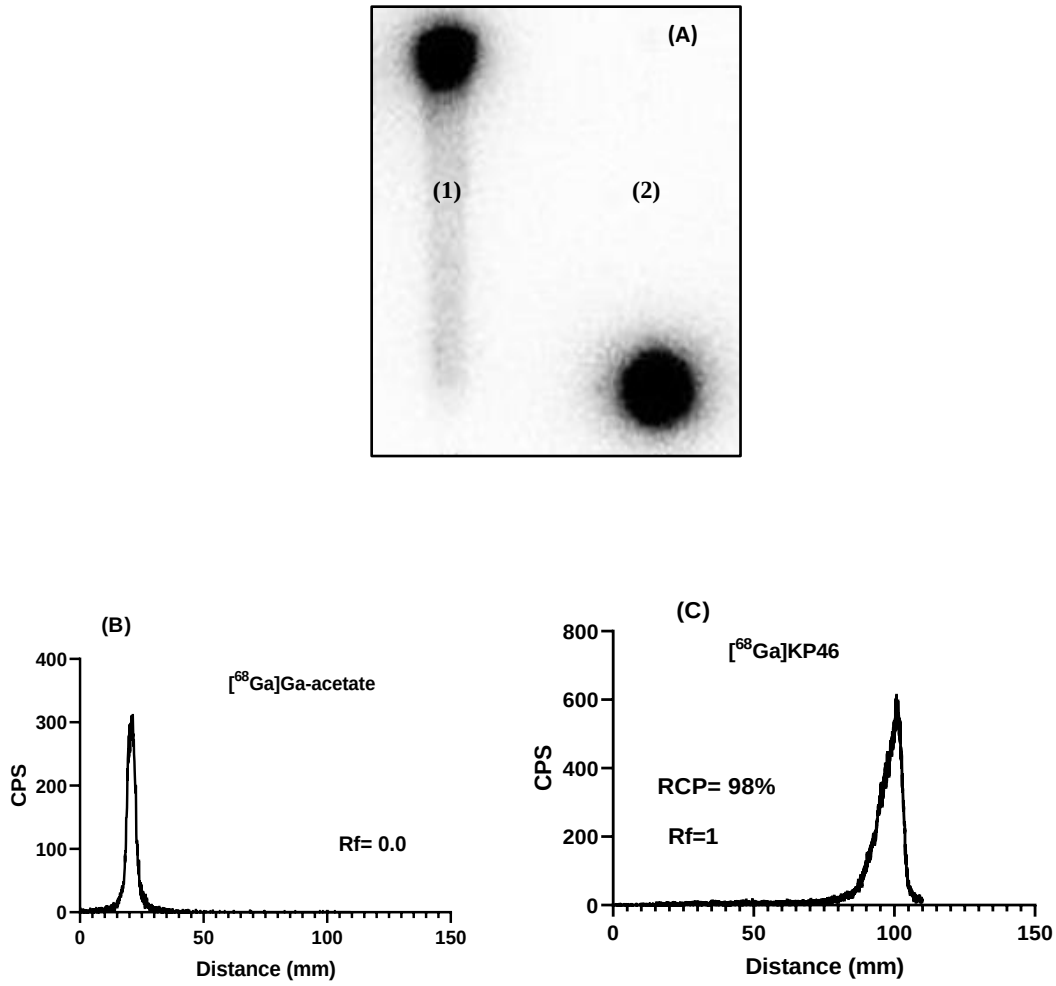

Figure 3.9: Radioactivity distribution on silica gel impregnated glass microfiber strips using phosphor imager (A) and Lablogic mini scan TLC reader with β^+ detection (B). [^{68}Ga]KP46 moved to the solvent front with Rf=1 (A1 and C), while [^{68}Ga]Ga-acetate stayed in the origin with Rf= 0 (A2 and B).

3.7.6 Determination of the distribution/partition coefficients (Log D/P) of [^{68}Ga]KP46

As expected, [^{68}Ga]KP46 is highly lipophilic, with log $D_{(octanol/PBS)}$ and log $P_{(octanol/water)}$ values of 1.9 ± 0.19 and 2.33 ± 0.28, respectively. [^{68}Ga]Ga-acetate is highly hydrophilic due to the absence of a lipophilic chelating agent, with log *D* and log *P* values of –3 ± 0.3 and –3.2 ± 0.48, respectively (Figure 3.10).

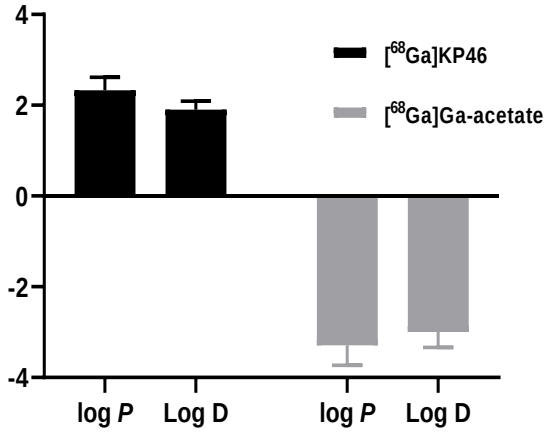

Figure 3.10: Log $D_{(octanol/PBS)}$ and log $P_{(octanol/water)}$ analysis of [^{68}Ga]KP46 and [^{68}Ga]Ga-acetate (control) using shake flask method. Results are reported as mean ± SD.

3.7.7 *In vitro:* [$^{68/67}$Ga]KP46 binding to serum proteins

In vitro protein binding studies for [$^{68/67}$Ga]KP46 and [^{68}Ga]Ga-acetate were performed using PD MidiTrap G-25 tubes. Tubes were counted by gamma counter to measure activity and nanodrop spectrometer to measure protein absorbance. The nanodrop spectrometer showed that apo-Tf and HSA eluted at fractions 3, 4 (highest absorbance) and 5 (Figure 3.11 A and B). [$^{68/67}$Ga]KP46 showed a similar elution profile in the presence and absence of apo-Tf in $NaHCO_3$ (Figure 3.12 A and B), indicating the absence of trans-chelation to apo-Tf even after a 48-hour incubation. The elution was at fractions 18, 19 and 20 (13.6 ± 3.8%, 14.7 ± 3.8% and 12.3 ± 32.6% of activity, respectively), which corresponds to small molecular weight compounds. An increase in column residual activity was noticed with time. This might be related to the formation of insoluble gallium hydroxide with time (at pH <7.4, the prepared mixture pH) that were retained in the column. [^{68}Ga]KP46 showed binding to HSA in fractions 3, 4 and 5 (~16% of total activity) (Figure 3.12 C). The low efficiency of [^{68}Ga]KP46 to bind to serum proteins is an indication of the stability of the compound. In contrast, in the presence of apo-Tf, [^{68}Ga]Ga-acetate eluted in fractions 3, 4 and 5, (24.1%, 69.65% and 5.2% of activity, respectively) (Figure 3.12 D), indicating the behaviour of a large molecule and suggesting a complete binding to apo-Tf. In the presence of HSA,

[^{68}Ga]Ga-acetate showed less binding (< 50% in fractions 3, 4 and 5) compared to its binding to apo-Tf (Figure 3.12 E).

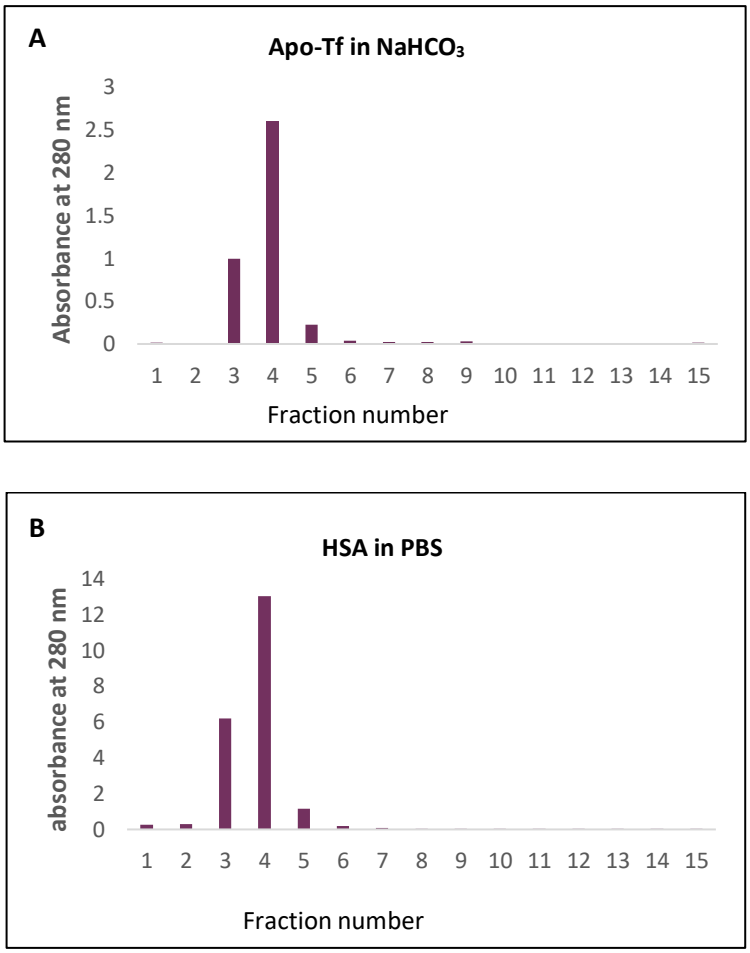

Figure 3.11**:** Elution profile of apo-Tf in $NaHCO_3$ (A) and HSA in PBS (B). Absorbance of each fraction at 280 nm was measured using nanodrop spectrophotometer.

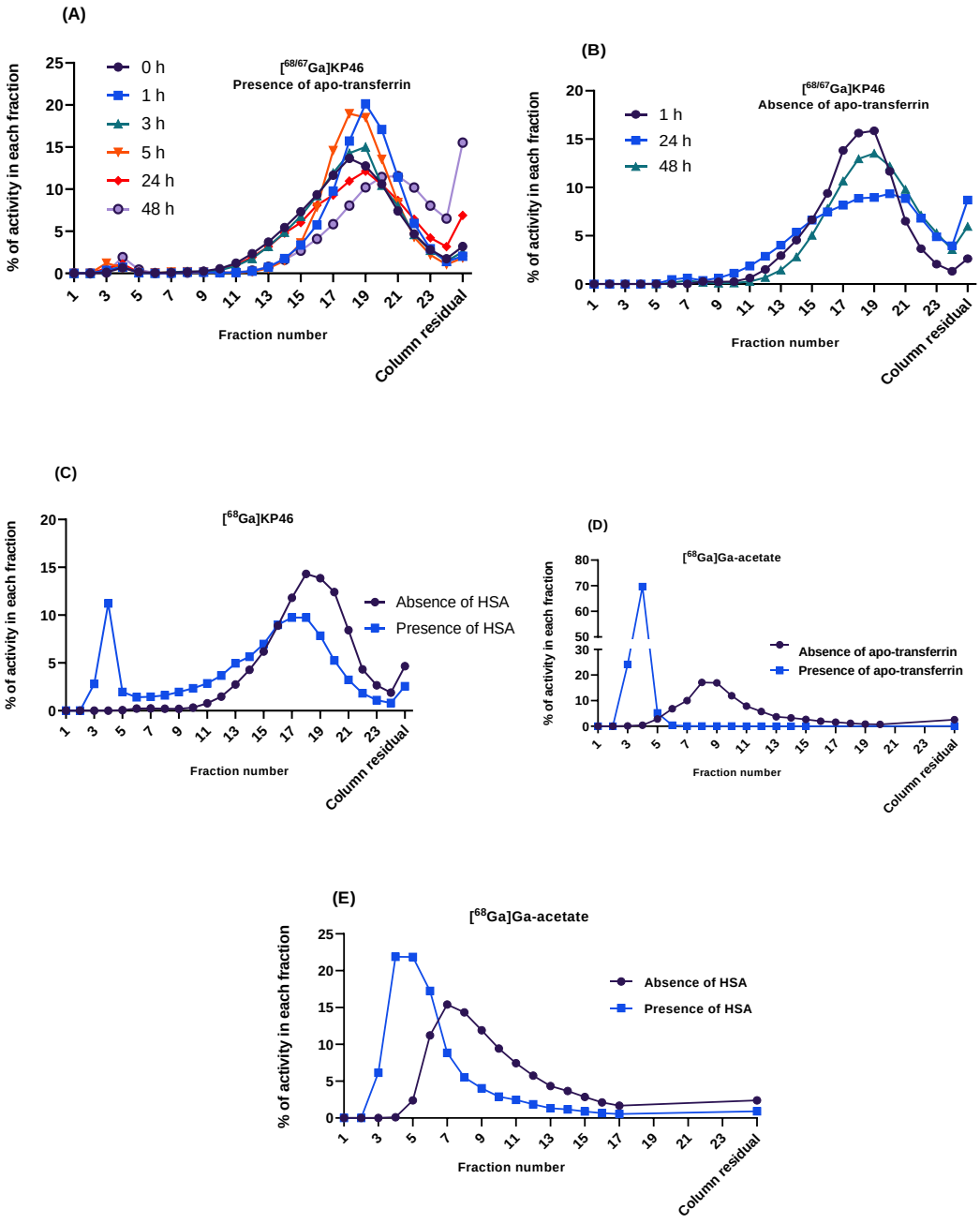

Figure 3.12: Elution profiles of [$^{68/67}$Ga]KP46 in a $NaHCO_3$ buffer in the presence (A) and absence (B) of apo-Tf at multiple time points and in PBS (C) in the presence and absence of HSA at one hour. Panel (D) represents the elution profiles of [^{68}Ga]Ga-acetate in the $NaHCO_3$ buffer in the presence and absence of apo-Tf. Panel (E) represents the elution profiles of [^{68}Ga]Ga-acetate in PBS in the presence and absence of HSA at one hour. This study was performed using size exclusion chromatography in PD MidiTrap G-25 tubes. Activity of fractions was measured using a gamma counter.

3.7.8 Cellular uptake of [^{68}Ga]KP46

[^{68}Ga]KP46 exhibited a significantly higher cellular uptake (3% ± 1%) and control corrected (specific binding) cellular uptake (2.55% ± 1%) than [^{68}Ga]Ga-acetate (1.6% ± 0.9% and 1% ± 0.08%, respectively) ($p < 0.01$) in A375 cells after one hour of incubation in DMEM media containing fetal bovine serum (FBS) (Figure 3.13 A). The IC/EC concentration ratio of [^{68}Ga]KP46 was almost twice (14.14 ± 6.47) that of [^{68}Ga]Ga-acetate (6.01 ± 3.76) (Figure 3.13 B).

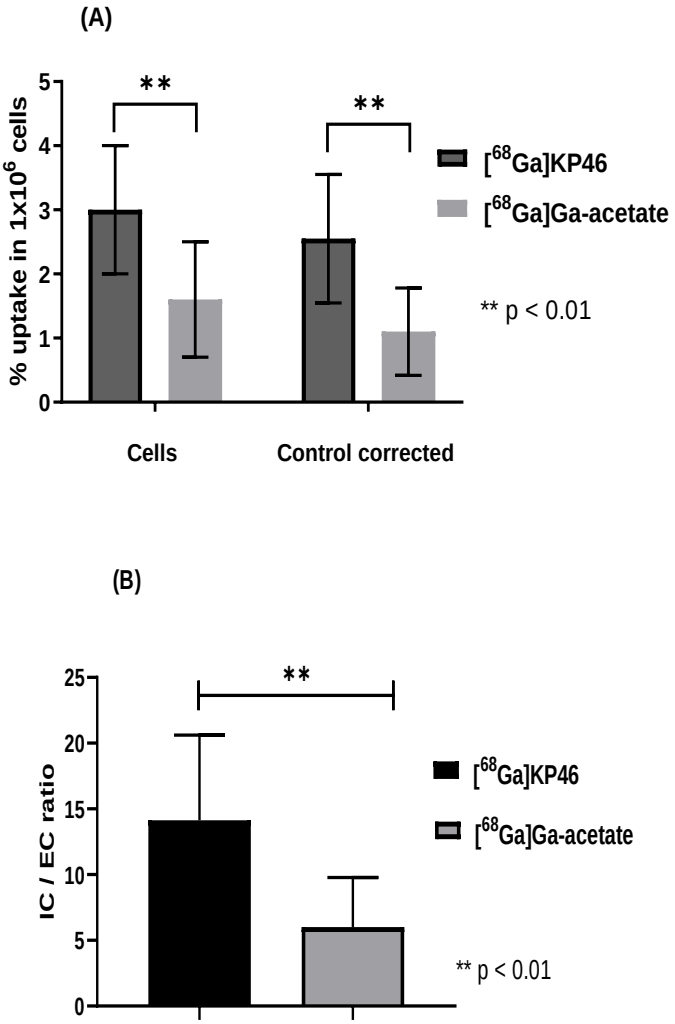

Figure 3.13: Cellular uptake, control corrected (cells – controls/no cells) (A) and ratio of IC/EC concentration (B) of [^{68}Ga]KP46 and [^{68}Ga]Ga-acetate in A375 cells after one hour of incubation in DMEM media containing FBS (n = 3, independent experiments). A significant difference between the study groups was noticed. Data are reported as mean ± SD. A t-test was performed to evaluate the difference between [^{68}Ga]KP46 and [^{68}Ga]Ga-acetate in each group.

3.7.9 Preparation and quality control of [$^{68/67}$Ga]KP46 and KP46 for *in vivo* studies

Samples from the [^{67}Ga]KP46 C-18 eluted fraction in ethanol (diluted 1:2 v/v with water, 20–30 µl, 2 MBq) and KP46 (preparation method detailed in LC/MS section 3.6.6) were used for RP-HPLC analysis. Both [^{67}Ga]KP46 and KP46 presented a similar elution time (16:03–16:35 min:s) (Figure 3.14 A), which was consistent with LC/MS analysis results (Figure 3.8 A). The 30-second delay was due to the serial configuration between the UV and radiation detectors. HPLC analysis of KP46 sample showed a low abundant peak at 21:50 min:s which was also seen in the blank sample (Figure 3.14 B), indicating column related impurity. In addition, iTLC analysis confirmed HPLC results and showed that [$^{67/68}$Ga]KP46 and KP46 had the same Rf (Figure 3.15).

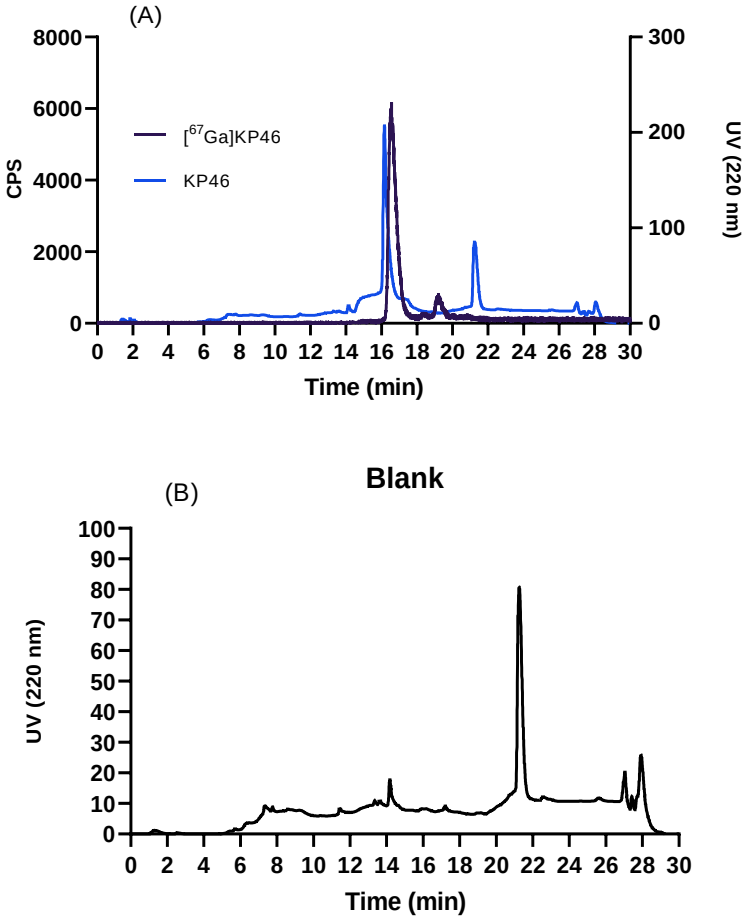

Figure 3.14: HPLC analysis of [^{67}Ga]KP46 and KP46 samples (A) shows two peaks at 16:03 and 16:35 min:s which correspond to KP46 and [^{67}Ga]KP46 respectively. Panel A shows a low abundant peak at 21:50 min:s which was also seen in a blank (B). HPLC mobile phase used: H_2O (A) and acetonitrile (B). Gradient: 0-2 minutes: 5% B, 2-17 minutes: 60% B, 17-18 minutes: 100% B, 18-24 minutes: 100% B, 24-26 minutes: 5% B, 26-30 minutes: 5% B).

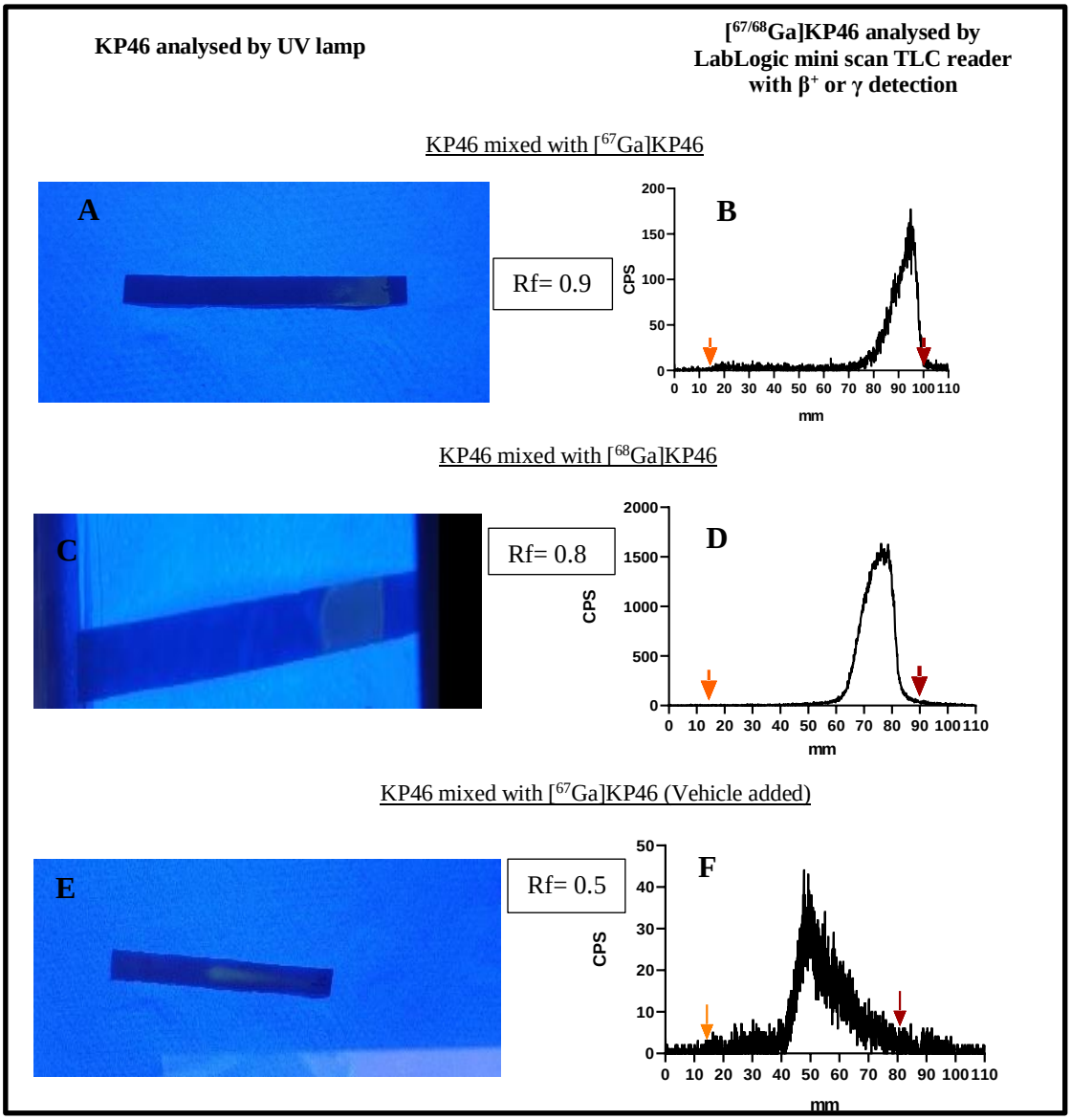

Figure 3.15**:** iTLC analysis of KP46 (dissolved in DMSO) mixed with ethanol solution of [$^{67/68}$Ga]KP46 before (A-D) and after (E and F) diluting the sample with PEG and water (vehicle). iTLC strips were analysed by UV lamp (Analytik Jena, 254/365 nm) for KP46 (A, C, and E) and LabLogic mini scan TLC reader with β^+ or γ detection for [$^{68/67}$Ga]KP46 (B, D, and F). iTLC analysis showed that KP46 and [$^{67/68}$Ga]KP46 had the same Rf. Red arrows represent the solvent front while orange arrows represent the origin.

3.7.10 *Ex vivo* biodistribution after intravenous injection of [^{68}Ga]KP46

Mice were intravenously injected with [^{68}Ga]KP46 and culled two hours post injection for organ harvesting and gamma counting. Consistent with the previous study conducted in our department (Figure 3.2 and 3.3), 31.4 ± 3.8%ID/g was seen in the liver two hours after the i.v. injection of [^{68}Ga]KP46. Activity was observed in the kidneys (30%ID/g for both kidneys) and urine, indicating excretion through urinary system. Less activity was seen in the lungs, heart, and small intestine (14.3 ± 0.6, 12.6 ± 1.7 and 12 ± 2.6%ID/g, respectively), with minimal activity accumulating in the tumour (3.4 ± 0.4%ID/g) (Figure 3.16).

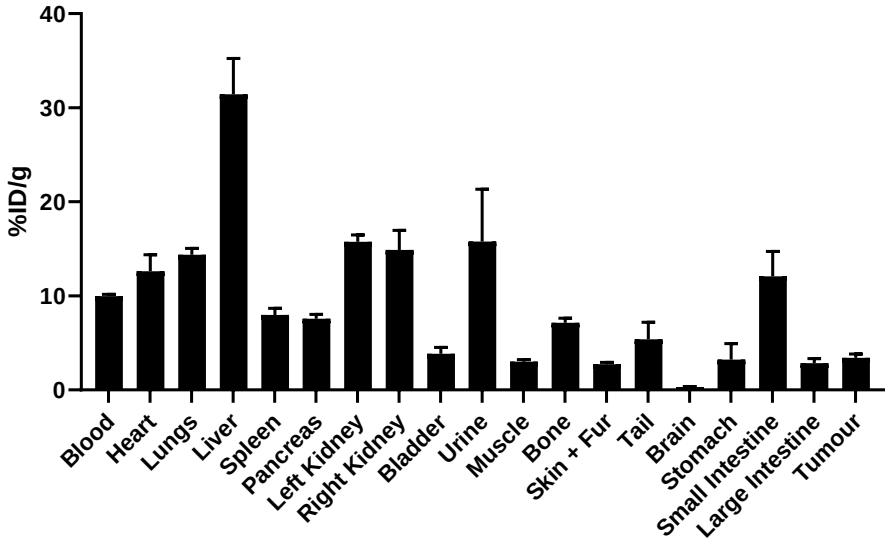

Figure 3.16: *Ex vivo* biodistribution of [^{68}Ga]KP46 at two hours post i.v. tail injection. [^{68}Ga]KP46 experienced hepatic and renal clearance. Minimal uptake was observed in tumours. Values are expressed as mean ± SD (n=3).

3.7.11 *In vivo:* Developing a method for the oral administration of [^{68}Ga]KP46

PET imaging from the first pilot study group revealed that most of the uptake was in the stomach, with minimal uptake in the small intestine. The *ex vivo* biodistribution data confirmed the PET image results and showed 324.4 ± 75.6 %ID/g in the stomach (77.6 ± 31.7 %ID), with less activity seen in the small intestine (33.4 ± 8.3%ID/g, 30.07 ± 9.8 %ID). Tumours could not be localised in the PET images due to the absence of a CT scan. However, from *ex vivo* biodistribution data, negligible activity was observed in the tumour (0.6 ± 0.3%ID/g) (Figure 3.17 A and C). The low absorption and low translocation from stomach to small intestine of [^{68}Ga]KP46 indicates the negative effect of anaesthesia on bowel motility. However, following the addition of a three-hour recovery period prior to scanning, the PET images showed the most activity in the large intestine. *Ex vivo* data supported the PET scan results and showed less activity in the stomach (27.5 ± 43.2%ID/g, 5.07 ± 7.88 %ID) and more activity in the large intestine (62.3 ± 35.4%ID/g, 50.09 ± 19.6 %ID) compared to first group. More activity was also noticed in the blood, liver, and urine (Figure 3.17 B and D), indicating improved absorption. Due to the better bowel motility observed post three-hour recovery, it was decided that this method would be applied in further [$^{68/67}$Ga]KP46 preclinical studies.

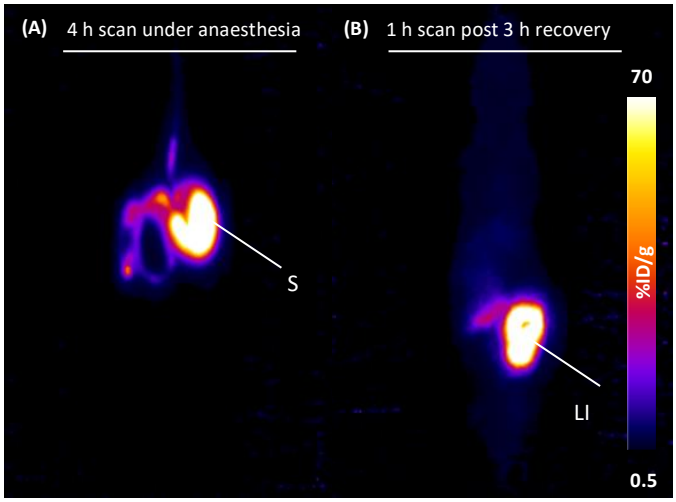

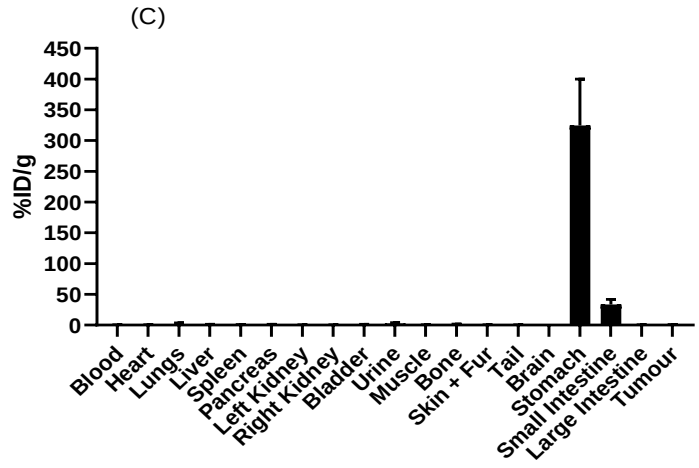

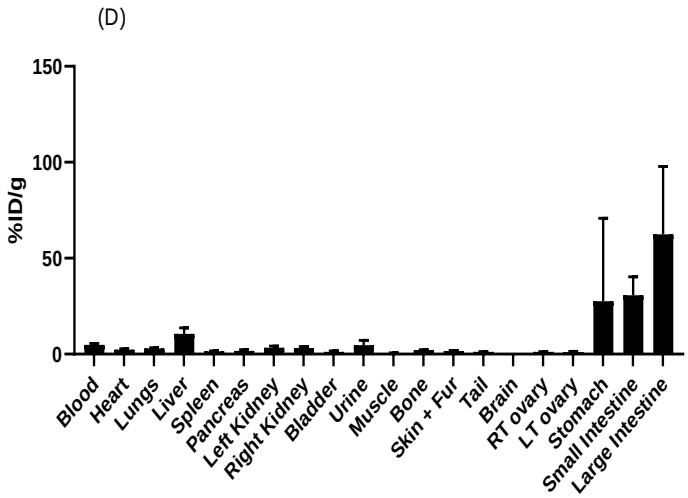

Figure 3.17: MIP PET image (A) and *ex vivo* bio distribution (C) conducted post 4 hours scan of mice being under anaesthesia (n=4) after oral administration of [^{68}Ga]KP46. MIP PET image (B) and *ex vivo* bio distribution (D) conducted for 1-hour post 3 hours recovery (n=3) after oral administration of [^{68}Ga]KP46. *Ex vivo* bio distribution values are expressed in mean ± SD. S: stomach and LI: large intestine.

3.7.12 *In vivo*: Oral administration of [^{68}Ga]KP46 in the presence and absence of a pharmacologically relevant dose of KP46

After the oral administration of [^{68}Ga]KP46 as a tracer (see section 3.6.13 for dose preparation), PET/CT images showed that uptake was mostly seen in the large intestine (Figure 3.18 A). *Ex vivo* biodistribution results (Figure 3.18 B) supported these PET/CT results, showing the highest uptake in the large intestine (61.7 ± 21.5%ID/g), followed by the small intestine (12.8 ± 4.1%ID/g) and stomach (11.1 ± 10%ID/g). Some uptake was observed in the blood, liver, and urine. Negligible activity was delivered to the tumour (0.8 ± 0.6%ID/g).

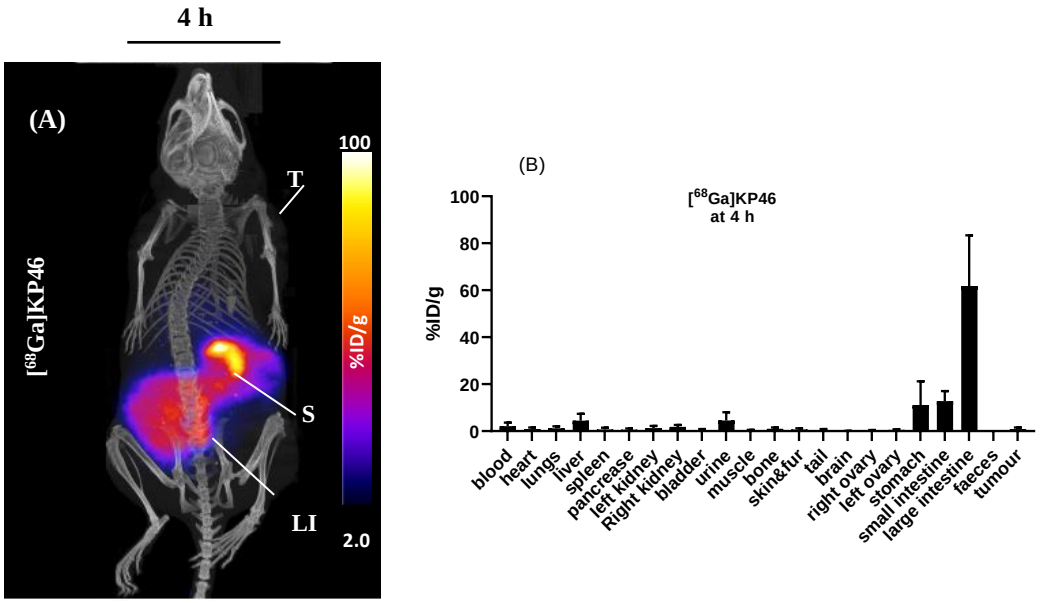

Figure 3.18: MIP whole-body PET/CT coronal image and *ex vivo* biodistribution of A375 xenograft animal model four hours after the oral administration of [^{68}Ga]KP46 as a tracer (A and B). *Ex vivo* bio distribution values are expressed as mean ± SD (n=3). T: tumour, S: stomach and LI: large intestine.

To measure the lipophilicity of ^{68}Ga in the tissues, octanol extraction was performed on tissue samples (Figure 3.19 A) post *ex vivo* biodistribution (see section 3.6.17 for octanol extraction method), and this showed 97.7% ± 1.2% of [^{68}Ga]KP46 (control) due to its lipophilicity in the octanol phase, while 99.3% ± 0.7% of [^{68}Ga]Ga-acetate (control) was observed in the water phase. ^{68}Ga in the serum and urine samples displayed hydrophilic behaviour, and almost all activity was seen in the water phase (98.6% ± 1.5% and 98.2% ± 1.7%, respectively). Most of the activity in the stomach (82.9% ± 10.7%), small intestine (80.7% ± 19.4%) and large intestine contents (83.7% ± 8.8%) was retained in the precipitate (Figure 3.19 B). However, post centrifugation, most of extracted activity from the precipitate (76.8% ± 8.7% for stomach, 95% ± 2.5% for small intestine and 95.5% ± 4.2% for large intestine) was seen in the aqueous phase (Figure 3.19 A), suggesting that activity was no longer in the form of [^{68}Ga]KP46 in these tissues.

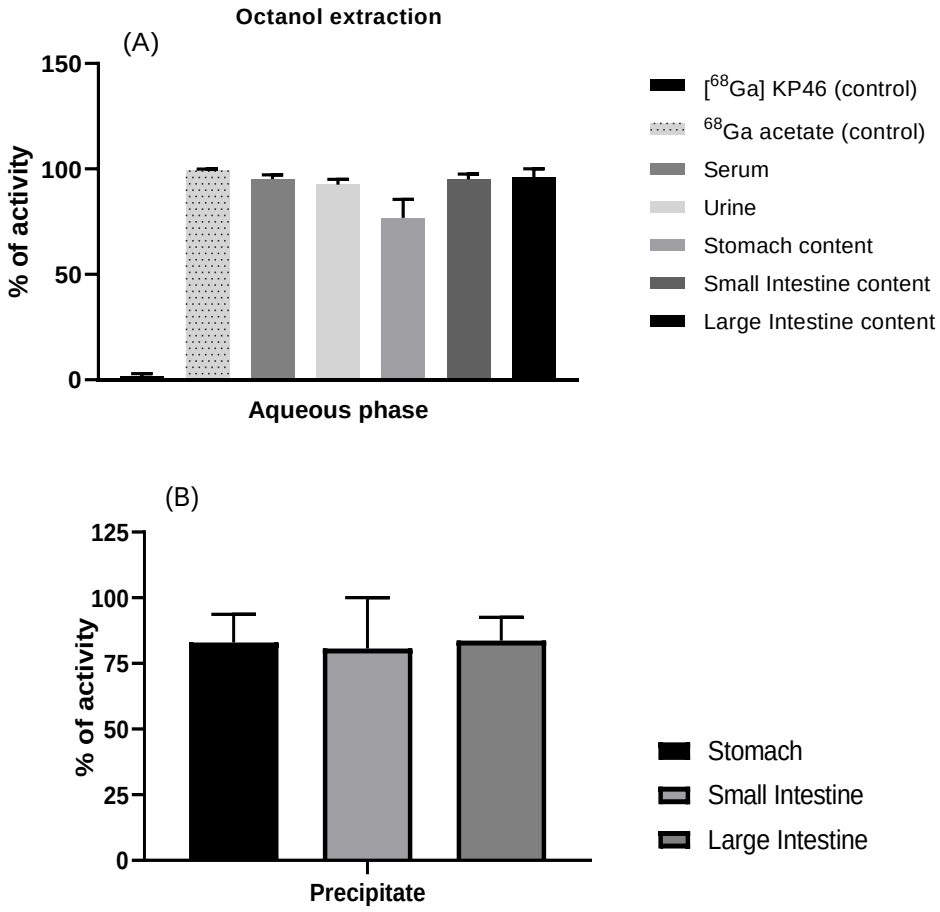

Figure 3.19: Panel A represents the percentage of activity in the aqueous phase in tissue samples post oral administration of [^{68}Ga]KP46 using octanol extraction (shake flask method). Panel B represents the percentage of activity remained in the precipitate in stomach, small intestine and large intestine samples post centrifugation of the samples at 10,000 rpm for 10 minutes (n=3). Values are expressed as mean ± SD.

In addition, after the oral administration of [^{68}Ga]KP46 combined with KP46, the PET/CT images showed uptake mostly in the large intestine (Figure 3.20 A). *Ex vivo* biodistribution (Figure 3.20 B) showed high activity in the large intestine (56.5 ± 21.4%ID/g), while the small intestine (18.4 ± 5%ID/g) and stomach (11.9 ± 8.1%ID/g) showed less activity. Negligible activity was delivered to the tumour (0.5 ± 0.3%ID/g). An ICP-MS measurement of ^{69}Ga in the tissue samples (Figure 3.20 C) was consistent with, and followed a similar biodistribution pattern to that of, the ^{68}Ga trafficking results (Figure 3.20 B). ^{69}Ga was seen mostly in the large intestine (23.7 ± 9.2%ID/g). Less ^{69}Ga was observed in the small intestine (6.7 ± 1.0%ID/g) and stomach (6.3 ± 4.7%ID/g). A negligible amount of ^{69}Ga was absorbed from the gut and delivered to the tumour (0.17 ± 0.1%ID/g).

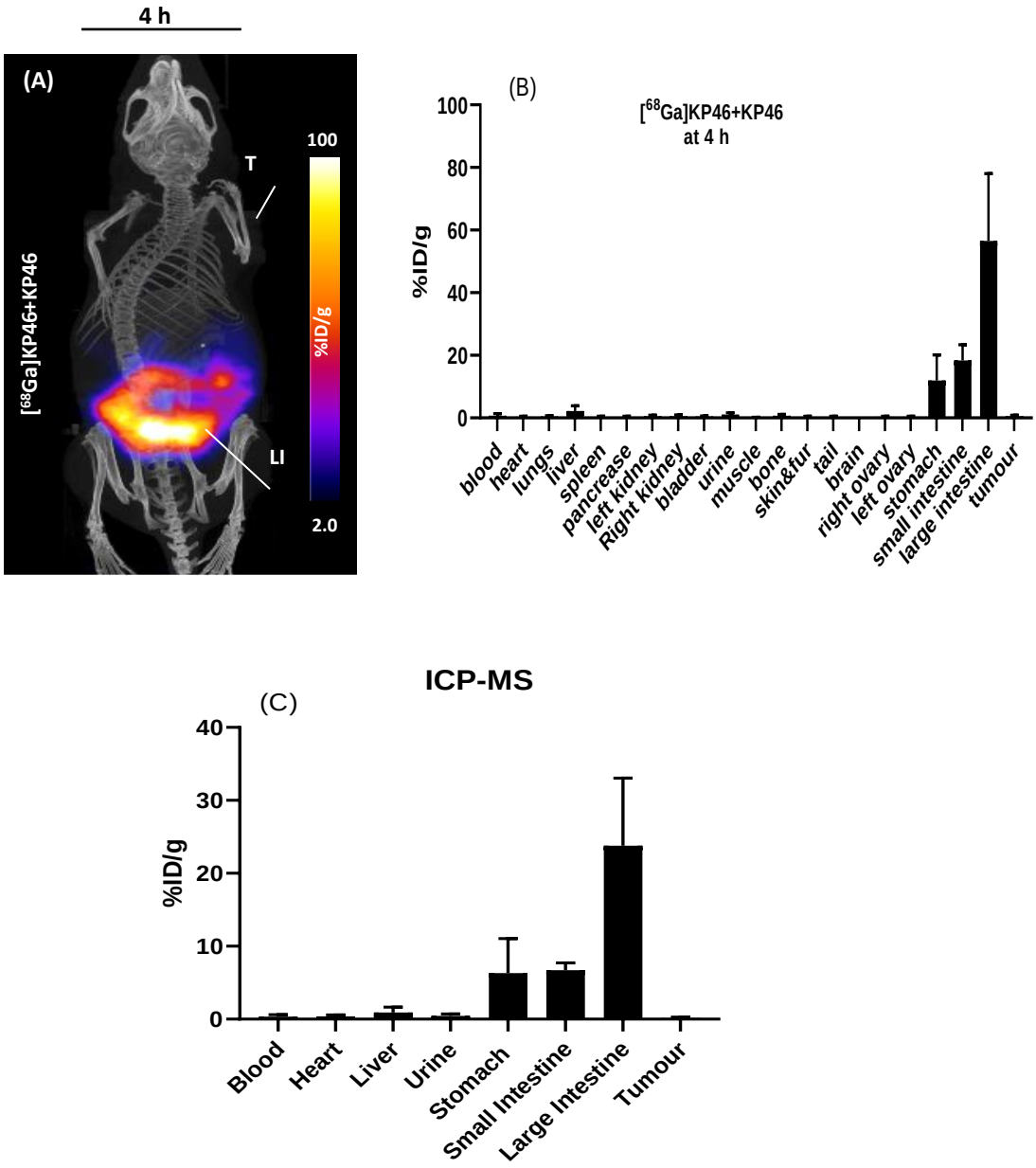

Figure 3.20: MIP whole-body PET/CT coronal image and *ex vivo* biodistribution of A375 xenograft animal model four hours after the oral administration of [^{68}Ga]KP46 combined with KP46 (A and B). Panel C represents ICP-MS analysis of ^{69}Ga in tissue samples post oral administration of [^{68}Ga]KP46 combined with KP46. *Ex vivo* bio distribution values are expressed in mean ± SD (n=3). T: tumour, and LI: large intestine.

3.7.13 *In vivo*: Oral administration of [^{67}Ga]KP46 in the presence and absence of a pharmacologically relevant dose of KP46

^{67}Ga was used (owing to its longer half-life) instead of ^{68}Ga to study KP46 biodistribution in a prolonged study. After the oral administration of [^{67}Ga]KP46 as a tracer (group A) or combined with KP46 (group B) (see section 3.6.13 for dose preparation), SPECT/CT images at the four-hour time point showed most activity occurring in the large intestine, which was consistent with the previous [^{68}Ga]KP46 study. However, uptake in the liver and heart was significantly higher in the presence of a pharmacological dose of KP46 (Figure 3.21 and figure 3.22), suggesting that adding a pharmacological dose of KP46 may increase [^{67}Ga]KP46 absorption. At 24 hours, a SPECT/CT image of the mice in group A exhibited no uptake in any organ, indicating that almost all activity was excreted before the 24-hour time point (Figure 3.23). It is worth mentioning that the mice's cage was monitored with a LB 124 scintillation monitor and exhibited approximately 4,000 cps, indicating the presence of large amount of activity in the cage – probably in the faeces. However, metabolic cages were not used and, consequently, the accumulative %ID of the faeces were not calculated. For the mice in group B, SPECT/CT images at 24 hours showed significantly higher tissue uptake in the liver and tumour compared to that of the mice in group A, thus demonstrating the effects of a pharmacological dose of KP46 on delaying [^{67}Ga]KP46 excretion and increasing absorption (Figure 3.22 and figure 3.23). *Ex vivo* biodistribution of group A mice at 24 hours confirmed the SPECT/CT results and showed that a considerable amount of activity was in faeces (3.0 ± 2.9 %ID/g) with minimal activity delivered to the tumour (0.3 ± 0.11%ID/g) (Figure 3.24). To measure the lipophilicity of ^{67}Ga in tissues post oral administration of [^{67}Ga]KP46 (group A), octanol extraction was done on tissue samples following the method described in section 3.6.18. Octanol extraction study showed that 20-35% of activity was extracted from stomach, small intestine, large intestine, and faeces samples after the homogenisation step indicating that large percentage of activity remained in the precipitate. Regarding tumour, 68% ± 31.8% of activity was extracted (Figure 3.25). The octanol extraction of homogenates in all tested tissue samples showed minimal activity in the organic phase (approximately < 5%) while most of the activity was seen in the aqueous phase (≥ 95%), demonstrating the hydrophilic behaviours of ^{67}Ga in these tissue samples (Figure 3.26) and indicating that it is not in the form of [^{67}Ga]KP46.

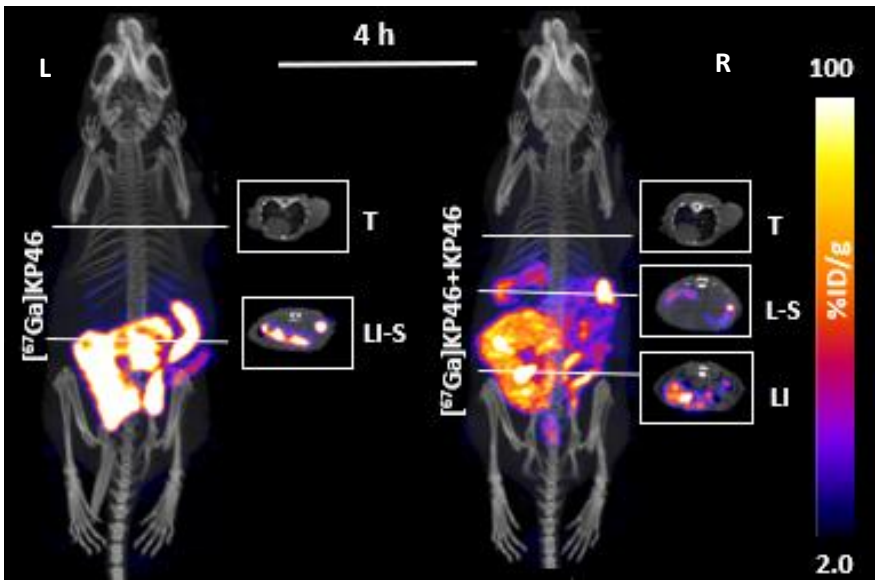

Figure 3.21: MIP whole body SPECT/CT coronoal image of A375 xenograft animal model at 4 hours post oral administration of [^{67}Ga]KP46 as a tracer (L) or combined with KP46 (R). T; Tumour, L; liver, S; stomach, SI; small intestine, and LI; large intestine (n=4).

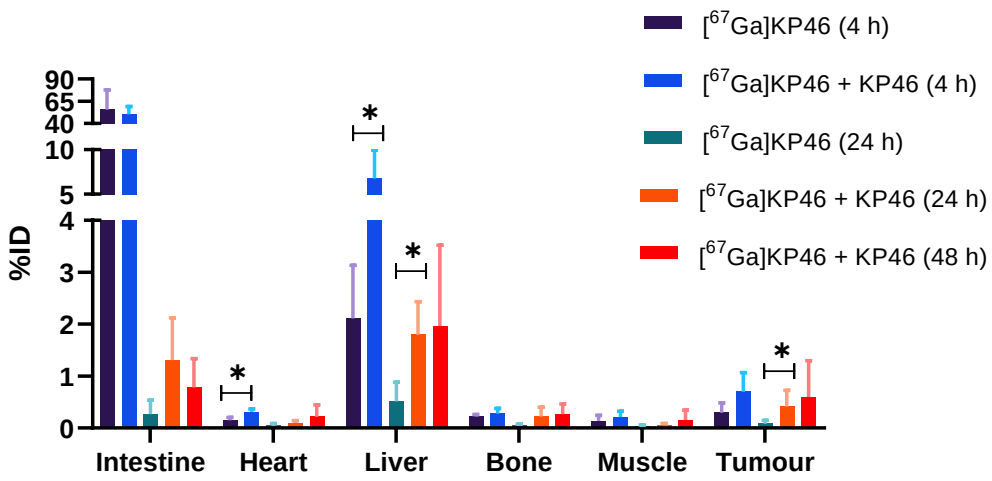

Figure 3.22: Region of interest (ROI) manually drawn on multiple tissue samples. Values are expressed in mean ± SD (n=4). *P* value; * ($p< 0.05$). Test used: one-way ANOVA, Tukey post-hoc test for multiple comparison analysis to evaluate the difference between [^{67}Ga]KP46 and [^{67}Ga]KP46 combined with KP46 groups at 4 and 24 hours.

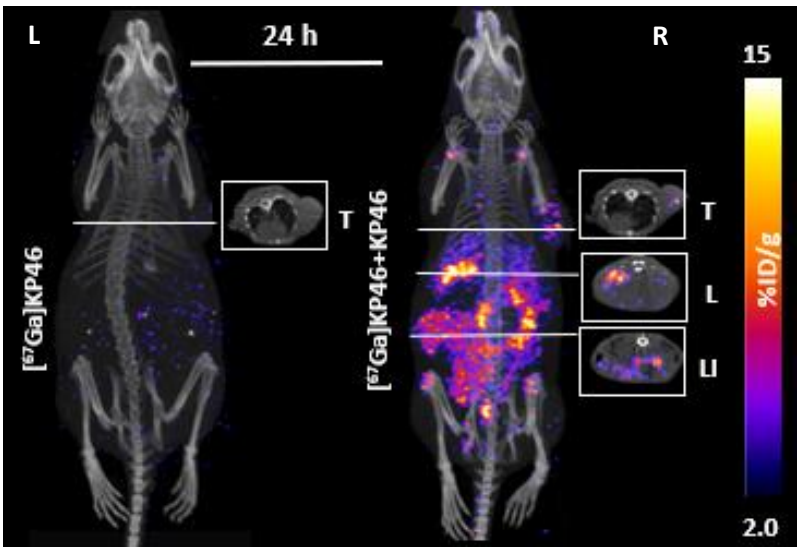

Figure 3.23: MIP whole body SPECT/CT coronoal image of A375 xenograft animal model at 24 hours post oral administration of [^{67}Ga]KP46 as a tracer (L) or combined with KP46 (R). T; Tumour, L; liver, S; stomach, SI; small intestine, and LI; large intestine (n=4).

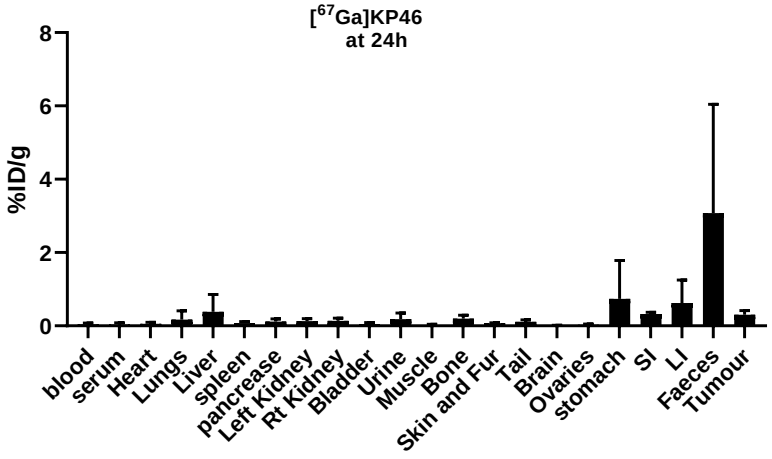

Figure 3.24: *Ex vivo* biodistribution of A375 xenograft animal model at 24 hours after the oral administration of [^{67}Ga]KP46 as a tracer. *Ex vivo* bio distribution values are expressed in mean ± SD (n=4). SI: small intestine, and LI: large intestine.

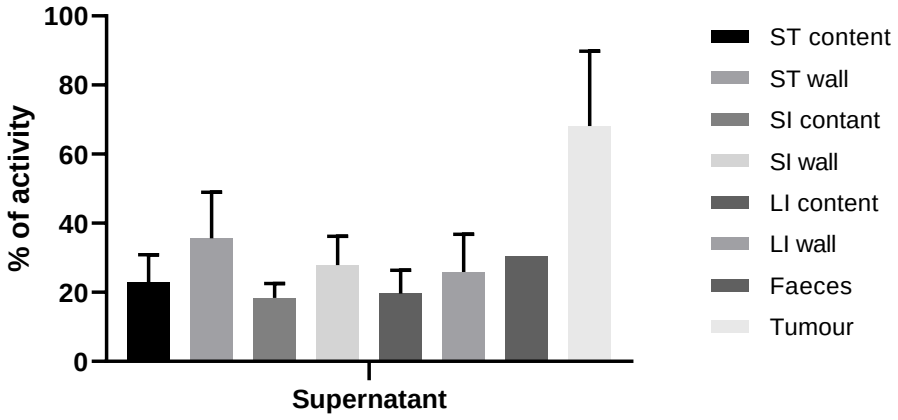

Figure 3.25: Percentage of activity in supernatant of multiple tissue samples post homogenisation using RIPA lysis buffer and Halt protease and phosphatase inhibitor cocktails and centrifugation at 10,000 rpm for 20 minutes. All data are represented as mean ± SD, n=4. S: stomach, SI: small intestine, and LI: large intestine.

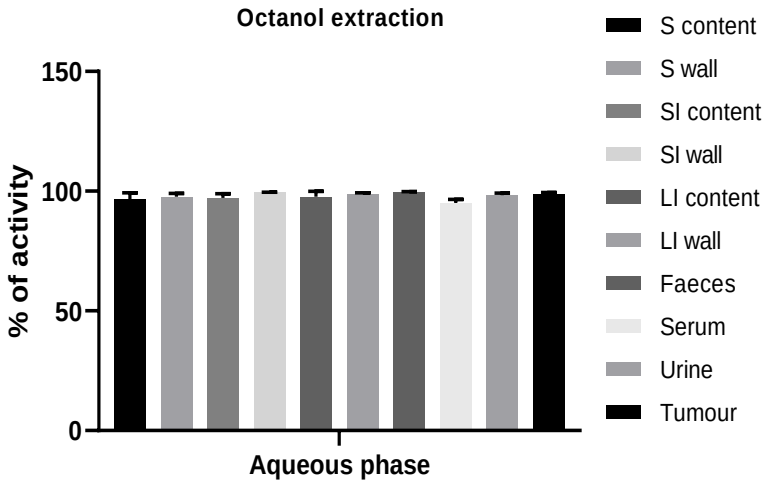

Figure 3.26: Percentage of activity in the aqueous phase in tissues samples post oral administration of [^{68}Ga]KP46 using octanol extraction (shake flask method). S: stomach, SI: small intestine, and LI: large intestine.

At 48 hours, SPECT/CT images of mice in group B showed some uptake in tumour, liver, and bone (Figure 3.27 A and figure 3.22). The *ex vivo* biodistribution at 48 hours supported the SPECT/CT results and showed some uptake in faeces (5.1 %ID/g), bone (2.55 ± 1.82 %ID/g), liver (1.34 ± 1.01% ID/g), and tumour (1.57 ± 0.48 %ID/g) (Figure 3.27 B). Octanol extraction analysis after the homogenisation step showed 27% of activity was extracted from the large intestine content while 64% and 85% was extracted from liver and tumour samples, respectively (Figure 3.28 A). Octanol extraction of homogenates in all samples showed 99% of activity in the aqueous phase, indicating that activity in these samples was not in the form of [^{67}Ga]KP46 (Figure 3.28 B). The ICP-MS measurement of ^{69}Ga in the tissue samples (Figure 3.29) was consistent and followed a similar biodistribution pattern to ^{67}Ga trafficking results at 48 hours seen in figure 3. 27 B. ^{69}Ga was seen mostly in the faeces (4.39%ID/g). ^{69}Ga was observed in liver, stomach, and small and large intestine with 0.39 ± 0.34%ID/g of ^{69}Ga was absorbed from the gut and delivered to tumour.

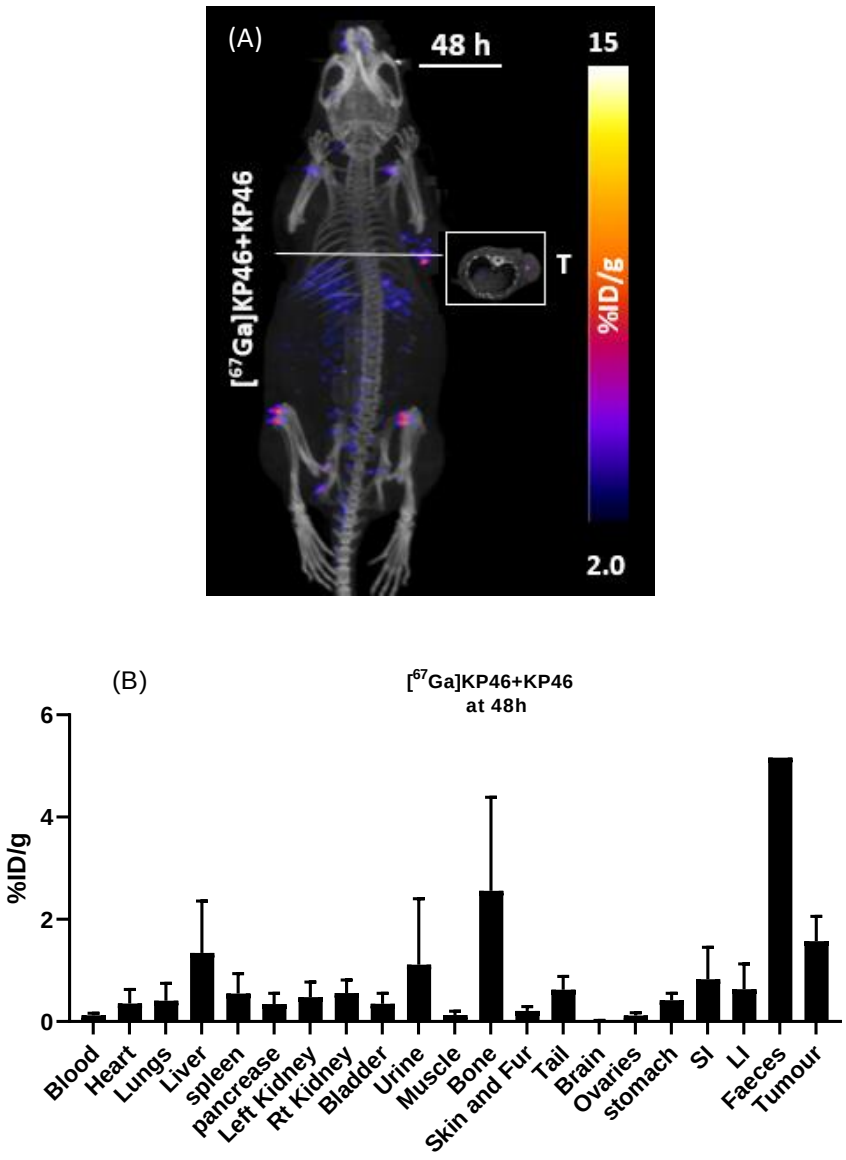

Figure 3.27: MIP whole body SPECT/CT coronoal image and *ex vivo* biodistribution of A375 xenograft animal model at 48 hours post oral administration of [^{67}Ga]KP46 combined with KP46 (A and B respectively). All data are represented as mean ± SD (n=4, except for faeces (n=1)). T: tumour, SI: small intestine, and LI: large intestine.

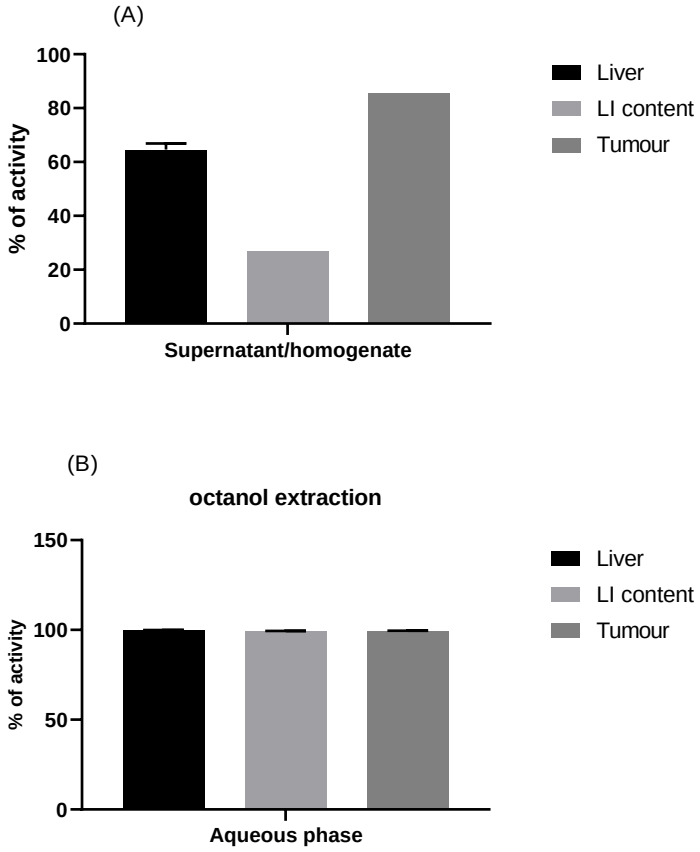

Figure 3.28: Panel A represents the percentage of activity in supernatant of multiple tissue samples after homogenisation using RIPA lysis buffer and Halt protease and phosphatase inhibitor cocktails and centrifugation at 10,000 rpm for 20 minutes (n=1 for large intestine and tumour samples, n=2 for liver sample). Panel B represents the percentage of activity in the aqueous phase in tissue samples using octanol extraction (shake flask method). All data is represented as mean ± SD. LI: large intestine.

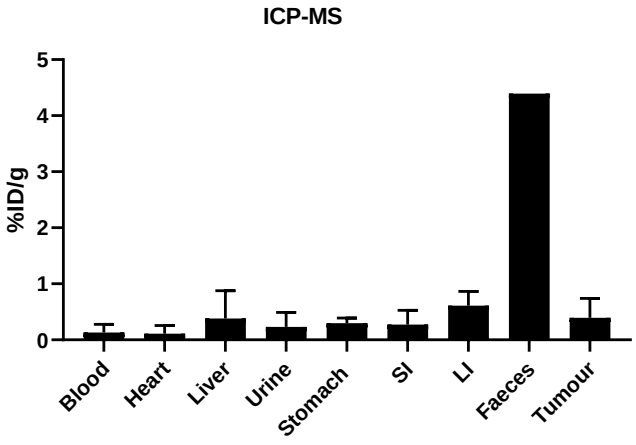

Figure 3.29: ICP-MS analysis of ^{69}Ga in tissue samples post oral administration of [^{67}Ga]KP46 combined with KP46 at 48 hours. All data are represented as mean ± SD (n=4, except for faeces (n=1)). SI: small intestine and LI: large intestine.

3.8 Discussion

In this work, we investigated KP46 *in vitro* protein binding and trafficking in a cancer model (*in vitro* and *in vivo*) using [$^{68/67}$Ga]KP46. Based on the chromatography methods used, radiolabelled [$^{68/67}$Ga]KP46 exhibited similar chemical properties as stable KP46, with the exception of being radioactive. Thus, with no reason to contradict this, [$^{68/67}$Ga]KP46 can be used in principle to study the delivery of gallium by KP46. Notably, the best way to synthesise radiolabelled bulk KP46 is probably by performing the entire synthesis in the presence of $^{67/68}$Ga; however, this method was not feasible as KP46 quality controls must be completed and cannot be performed on radioactive samples. However, radioisotopic compounds are usually used in very low concentrations compared to the corresponding stable pharmacological compounds; they can provide useful information owing to their radioactive property. This includes the ability to measure *in vivo* biodistribution, tissue accumulation and excretion and the use of dynamic/static images provided by SPECT/PET scanners.[269]

3.8.1 Partition coefficient and protein binding studies of [$^{68/67}$Ga]KP46

For orally administered compounds, adequate penetration through the gastrointestinal tract is required.[209] A compound's ability to cross the gastrointestinal barrier is frequently predicted by octanol extraction (distribution/partition coefficient) to measure the lipophilicity of the compound.[248,209] Lipophilic molecules can penetrate the lipid cellular membrane, including enterocytes. Accordingly, it is generally believed that lipophilicity is an essential characteristic of orally administered drugs as it means they can achieve good absorption,[270] which affects their pharmacokinetics and trafficking *in vivo.* KP46 is a lipophilic bulk drug. KP46 lipophilicity was measured in literature ($\log P_{(octanol/water)} = 0.88$) by shake flask method.[209,248] Although the log *P* study in the current study confirmed the lipophilicity of tracer [^{68}Ga]KP46 with a log *P* value of 2.33 ± 0.28, it showed a much higher value compared to measurement with bulk KP46. A possible reason for this is that, unlike bulk KP46, which has a 1:3 complex of Ga^{3+} with 8-hydroxyquinoline, tracer [^{68}Ga]KP46 possesses a large concentration of excess-free ligand ($> 10^6$ fold) compared to ^{68}Ga concentration. Hence, during octanol extraction, some dissociation of bulk KP46 may occur, causing free Ga^{3+} to be present in the aqueous phase. However, in the case of tracer [^{68}Ga]KP46, the excess concentration of 8-hydroxyquinoline in the sample might minimise the dissociation by binding again to free ^{68}Ga. This theory may also explain the difference in behaviour between bulk KP46 and tracer [$^{68/67}$Ga]KP46 in binding to apo-Tf. In literature, bulk KP46 was found to bind to apo-Tf more favourably compared to binding to HSA.[252,253,254] As mentioned in the introduction section, the mechanism of bulk KP46 binding to apo-Tf is rather controversial with one study producing evidence of the hydrophobic binding of bulk KP46 to apo-Tf with no ligand release *in vitro* using XANES, and another study showing some ligand release using NMR and spectrofluorometric measurements, which is not surprising considering the high

affinity of transferrin to bind gallium.[249,254] However, in the current study, using a G-50 gel filtration chromatography column and $NaHCO_3$ buffer, tracer [$^{68/67}$Ga]KP46 showed no trans-chelation to apo-Tf at any time points, which indicates the stability of the compound. In agreement with the previously mentioned theory, even in the presence of apo-Tf, the excess concentration of 8-hydroxyquinoline in [$^{68/67}$Ga]KP46 samples may compete with apo-Tf for $^{68/67}$Ga binding. In addition, tracer [$^{68/67}$Ga]KP46 showed similar binding behaviours to HSA as bulk KP46. Both compounds expressed binding to HSA one hour after incubation.[252,253] Based on the binding properties of HSA, including the variety of binding sites and hydrophobic interaction, it was suggested that bulk KP46 binds hydrophobically to HSA.[254,255,256] Studies using NMR and XANES identify the hydrophobic binding mechanism of bulk KP46 to HSA *in vitro*.[254,12] In the current study, tracer [^{68}Ga]KP46 binding to HSA (~16% of total activity) is consistent with those of KP46 from literature studies. Hence, it is plausible to conclude that tracer [^{68}Ga]KP46 might just as well bind to HSA hydrophobically. Unlike [^{68}Ga]KP46, [^{68}Ga]Ga-acetate showed complete binding to apo-Tf, indicating the behaviour of a large molecule. [^{68}Ga]Ga-acetate can also bind to HSA but at lesser extent. The current results on [^{68}Ga]Ga-acetate binding to apo-Tf and HSA confirm the previous literature studies on free radioisotopic gallium binding to apo-Tf more favourably than albumin.[64,83,271]

3.8.2 Cellular uptake study of [$^{68/67}$Ga]KP46

Cellular uptake of [^{68}Ga]KP46 was evaluated *in vitro* in an A375 cell line, the xenograft of which was previously used for studying the biodistribution of [^{68}Ga]KP46 post i.v. injection in our department by C. Imberti and J. Bartnicka (unpublished) (Figure 3.2 and Figure 3.3). A375 cell line was chosen in the current studies because it is known to express high levels of transferrin receptors and is consequently able to take up gallium by transferrin-mediated mechanisms.[272] In addition, an A375 cell line was among other human melanoma cell lines that showed a lower IC50 of KP46 than that of gallium nitrate, indicating the susceptibility of melanoma cell lines to KP46 compared to gallium nitrate.[108] [^{68}Ga]Ga-acetate cellular uptake was assessed as a control in the same cell line. [^{68}Ga]KP46 showed a significantly higher uptake ($p < 0.01$) compared to [^{68}Ga]Ga-acetate, which could be attributed to the lipophilicity of [^{68}Ga]KP46 and cell entry by passive diffusion. However, it does not bind to apo-transferrin or enter the cells by a transferrin-dependant mechanism. In addition, although the presence of transferrin in a culture medium is known to show a relatively high cellular uptake of ^{67}Ga citrate by transferrin-mediated mechanisms,[61,273] the presence of FBS (containing transferrin) in the current study may actually compromise [^{68}Ga]Ga-acetate uptake into A375 human cancer cells. Bovine transferrin has a similar affinity for gallium to human transferrin but does not bind efficiently to transferrin receptor in human cancer cells.[274,275] Hence, [^{68}Ga]Ga-acetate may bind to transferrin in the media without entering the cells, which can diminish the amount of activity entering the cells by a

transferrin-independent pathway. Another cellular uptake approach can be obtained using cell culture media supplemented with human serum.

3.8.3 *Ex vivo* biodistribution post intravenous injection of [^{68}Ga]KP46

According to unpublished work by C. Imberti and J. Bartnicka, the preclinical study of [^{68}Ga]Ga-acetate post i.v. injection showed a visible tumour uptake in PET/CT images – especially after one hour. In contrast, no visible tumour accumulation was observed during the four-hour PET/CT scan post i.v. injection of [^{68}Ga]KP46 (Figure 3.2). *Ex vivo* biodistribution of [^{68}Ga]Ga-acetate at four hours presented a significantly higher tumour uptake (6.1 ± 2.4%ID/g) compared to [^{68}Ga]KP46 (2.6 ± 0.9%ID/g) (Figure 3.3). In the current study, even when a different strain of mouse was used (athymic nude mice), *ex vivo* biodistribution showed similar tumour accumulation of [^{68}Ga]KP46 at two hours post i.v. injection (3.4 ± 0.4%ID/g). In addition, the biodistribution of different tissues was also noticed between the two tracers. While [^{68}Ga]Ga-acetate showed the highest uptake in bone, [^{68}Ga]KP46 accumulated in the liver (31.4 ± 3.8%ID/g) and, interestingly, in the myocardium (12.6 ± 1.7%ID/g). A high myocardium accumulation of [^{68}Ga]KP46 might be interesting for the design of new radioisotopes for myocardial imaging application. The difference in tumour uptake between the two tracers suggests different uptake mechanisms. [^{68}Ga]Ga-acetate may bind to transferrin and be delivered to the tumour in the form of a Ga-Tf complex. However, when administered intravenously, [^{68}Ga]KP46 is stable and does not release ^{68}Ga to transferrin but rather, owing to its lipophilicity, accumulates in the liver.

3.8.4 *In vivo*: Oral administration of [^{68}Ga]KP46 in the presence and absence of a pharmacologically relevant dose of KP46

Due to the lack of accumulation of [^{68}Ga]KP46 in the tumour post i.v. injection, we decided to mimic the route of administration used in the clinical trial and investigate [^{68}Ga]KP46 pharmacokinetics post oral administration as well as investigate the effects of adding a pharmacological dose of KP46 to [^{68}Ga]KP46 biodistribution. Orally administering [^{68}Ga]KP46 as a tracer showed a negligible amount of gallium being absorbed from the gut and delivered to tumour within four hours (Figure 3.18). Adding a therapeutic dose of KP46 showed no trafficking change during the same time frame (Figure 3.20). An ICP-MS measurement of ^{69}Ga in tissue samples was consistent with ^{68}Ga trafficking results. Octanol extraction showed that most of the activity in tissue samples was in a hydrophilic form (i.e. no longer in the form of [^{68}Ga]KP46).

3.8.5 *In vivo*: Oral administration of [^{67}Ga]KP46 in the presence and absence of a pharmacologically relevant dose of KP46

Due to most of the activity remaining in the gut and the absence of tumour uptake during the short timescale investigated, it was decided that ^{67}Ga should be used (owing to its longer half-life) to study KP46 biodistribution at later time points. The oral administration of [^{67}Ga]KP46 as a tracer or combined with KP46 showed that most of the activity remained in the gut, with minimal tissue trafficking at four hours (consistently with the study of [^{68}Ga]KP46) (Figure 3.21). However, at the 24-hour time point, the group administered with [^{67}Ga]KP46 as a tracer showed no visible uptake in any organ in SPECT/CT images (Figure 3.23). *Ex vivo* biodistribution at 24 hours showed low uptake in tissues with 0.3 ± 0.11%ID/g of activity in tumour (Figure 3.24). The low uptake in tissues and tumour 24 hours after administration indicated that most of the activity had been excreted before the 24-hour timepoint, with no sufficient time for absorption. In fact, these results were consistent with a couple of preclinical studies that investigated the absorption of gallium from the bowel of rats after the oral administration of ^{67}Ga citrate. These studies showed between 87%–100% of ^{67}Ga excreted in the faeces at 72 hours post oral administration (see introduction section).[190,191] In the current study, octanol extraction analysis of all tissue samples at 24 hours post [^{67}Ga]KP46 administration as a tracer showed ≥ 95% of activity was no longer in the form of [^{67}Ga]KP46.

On the contrary, the presence of a therapeutic dose of KP46 delayed bowel excretion, which allowed more time for absorption at the 24-hour time point (Figure 3.22 and figure 3.23). The fact that the presence of a therapeutic dose of KP46 increases ^{67}Ga absorption may be related to some level of alteration in gastric emptying and excretion rate, which allows more time for absorption. Although the presence of a therapeutic dose of KP46 increased gut absorption compared to the group of mice administered with tracer [^{67}Ga]KP46, delivery to tissues was still low with 1.57 ± 0.48%ID/g of activity in tumour at 48 hours, indicating that a large amount of activity was excreted before that time point. The measurement of ^{69}Ga in the tissue samples at 48 hours was consistent with ^{67}Ga trafficking results. Generally, the *in vivo* trafficking of tracer [^{67}Ga]KP46 in the presence of bulk KP46 showed poor gut absorption similar to results obtained from literature on ^{67}Ga citrate post oral admisntation,[190,191] which raise a question on whether KP46 can enhance gallium gut absorption compared to gallium salts which it was developed to accomplish. In addition, the current study results were also consistent with an early preclinical study in mice investigated gallium gut absorption post simultaneous single oral administration of bulk gallium chloride (100 nmol) and 0.037 MBq of ^{67}Ga citrate. Using a large volume scintillation counter, 0.3 ± 0.08 % of the original measured counts remained in mice five days after oral administration. However, the percentage of counts remained in mice at earlier time points or excreted in faeces were not reported in the study.[276] From the literature and the current study, results suggest that

KP46 does not enhance gallium absorption compared to gallium salts after oral administration of a single dose.

In addition, the low concentration of gallium in normal tissue in the current study is consistent with a previous preclinical study conducted by Collery *et al.*,[236] who measured gallium concentration in healthy animal tissues. The study reported low gallium concentration in bone (7.02 ± 3.14 µg/g, 0.16 ± 0.07 % ID/g), liver (3.55 ± 2.10 µg/g, 0.08 ± 0.04 % ID/g), spleen (1.77 ± 1.45 µg/g, 0.04 ± 0.03% ID/g), and kidneys (1.81 ± 0.24 µg/g, 0.04 ± 0.005 % ID/g)– even after a daily oral administration of KP46 (62.5 mg/kg, 9 mg Ga/kg) over two weeks.[236] In the current study, similar concentration in bone (2.5 ± 1.8 % ID/g), liver (1.3 ± 1.0 % ID/g), spleen (0.54 ± 0.39 % ID/g), and kidneys (1.0 ± 0.55 % ID/g) were noticed post oral administration of [^{67}Ga]KP46 combined with bulk KP46. However, gallium concentration in tumours post oral administration of KP46 as a single dose or in multiple doses was not studied in literature for comparison with the current study. In the KP46 clinical study, KP46 was administered over a prolonged period, which might be necessary to gain steady blood gallium concentration, progressive tumour accumulation and exposure to gallium and, consequently, improved cytotoxic effects.[231] Hence, [^{67}Ga]KP46 can be combined with KP46 to study the biodistribution of KP46 in animal models bearing xenografts after prolonged daily oral administration. In addition, gallium might not be the only active component for KP46 cytotoxicity. 8-hydroxyquinoline has shown cytotoxic effect against multiple cancer cell lines,[234,277] and can be investigated in the future as an active component for KP46 mode of action.

In the current study, octanol extraction analysis showed that even after adding a therapeutic dose of KP46, activity in analysed tissue samples was in a hydrophilic form. Although all performed octanol extraction studies on tissue samples showed a high percentage of activity in the aqueous phase, it does not represent the whole sample, for some activity was still retained in precipitate. However, 68%–85% of activity was extracted from tumour samples and found in the aqueous phase. Hence, it is plausible to conclude that, unlike the i.v. injection of [^{68}Ga]KP46, when [^{67}Ga]KP46 is administered orally, 8-hydroxyquinoline releases gallium in the gut that then likely travels to the tumour as a Ga-Tf complex. We propose that if [^{67}Ga]KP46 were to reach the tumour intact, it would be in a small concentration.

3.9 Summary and conclusion

In this work, we used [$^{68/67}$Ga]KP46 to study *in vitro* protein binding and trafficking of KP46 in a cancer model *in vitro* and *in vivo* post i.v. and oral administration. We have provided supporting evidence that [$^{68/67}$Ga]KP46, unlike [$^{68/67}$Ga]Ga-acetate, does not release gallium to transferrin *in vitro* and is therefore likely to be stable in blood, although it does exhibit some HSA binding (probably hydrophobic binding of the intact complex). Although studies from literature showed

that bulk KP46 binds to transferrin *in vitro*, the stability of tracer [$^{68/67}$Ga]KP46 against binding to transferrin *in vitro* in the current study is probably due to the present of excess ligand in the sample competing with apo-Tf for $^{68/67}$Ga binding.

[^{68}Ga]KP46 showed a significantly higher *in vitro* uptake ($p < 0.01$) compared to [^{68}Ga]Ga-acetate, which could be attributed to the lipophilicity of [^{68}Ga]KP46 and cell entry by passive diffusion. However, it does not bind to apo-transferrin or enter the cells by a transferrin-dependant mechanism. The difference in tumour uptake between [^{68}Ga]KP46 and [^{68}Ga]Ga-acetate post i.v. injection suggests the different uptake mechanism. While [^{68}Ga]Ga-acetate is delivered to tumour as a transferrin complex, [^{68}Ga]KP46 does not release ^{68}Ga to transferrin, but rather, accumulated in liver owing to its lipophilicity.

Most activity was retained in the gut with low activity delivered to the tumour after the oral administration of [^{68}Ga]KP46, either as tracer or combined with KP46 at four hours (0.8± 0.6 and 0.5 ± 0.3 %ID/g respectively). However, at 24 hours, a different biodistribution was observed between the group administered with [^{67}Ga]KP46 as a tracer and the group administered with [^{67}Ga]KP46 combined with KP46. While the former group showed low tissue uptake with 0.3 ± 0.11 %ID/g in tumour, the latter showed delayed bowel excretion at 24 hours with 1.57 ± 0.48%ID/g activity in tumour at 48 hours post administration. Although the presence of a therapeutic dose of KP46 increased gut absorption and tissue accumulation of activity compared to the group of mice administered with tracer [^{67}Ga]KP46, ^{67}Ga delivery to tissues and tumour was generally low. We conclude that a large amount of activity is excreted after oral dose of [^{67}Ga]KP46 as a tracer or combined with KP46, indicating that KP46 does not enhance gallium gut absorption compared to gallium salts after a single dose. However, gallium tumour uptake and *in vivo* trafficking can be investigated in the future in animal model bearing xenograft post prolonged oral administration of [^{67}Ga]KP46 combined with KP46. In addition, the delivery of 8-hydroquinoline to tumour by KP46 could also be investigated in the future as an alternative hypothesis for KP46 mode of action.

The octanol extraction results of the *in vivo* samples suggest that [$^{68/67}$Ga]KP46 does not survive intact in the gut. However, since the octanol extraction does not represent all of the tumour samples, it is safe to say that if any [^{67}Ga]KP46 were to reach the tumour intact, it would be in a small concentration.

4 8-hydroxyquinoline derivatives as ionophores for gallium-68 cell delivery

4.1 Introduction

Metal ions are essential for biological process and metal homeostasis.[278] Indeed, the interaction with metal ions is important, since several diseases arise from the loss of metal balance, including abnormal absorption or metabolism.[279] The biological activities of 8-hydroxyquinoline (8HQ, oxine) and its derivatives are at least partly attributable to their ability to form complexes with metal ions in the body through chelation.[278,280] For example, 8HQ can be used as a potent chelator for the treatment of metal related diseases by restoring the metal imbalance as observed in neurodegenerative diseases, such as Parkinson's disease, Alzheimer's disease, and multiple sclerosis.[278,281]

In addition to their anti-neurodegenerative application, 8HQ and its derivatives have a pharmacological application as anti-cancer agents.[235] A study investigating the anti-cancer activity of 8HQ showed 30% reduction in MCF-7 cell line proliferation at 5 μM concentration. In the same study, a dose of 20 mg/kg of intravenously injected 8HQ showed decrease in tumour growth in mice inoculated with MCF-7 or MDA-MB-435 (human breast cancer) xenograft compared to control groups; however, the difference was not significant. Nonetheless, co-administration of 8HQ and 10 mg/kg paclitaxel (a chemotherapy drug) showed significantly less tumour volume compared to either 8HQ or paclitaxel alone.[234] In another *in vitro* study, 8HQ was shown to inhibit DNA synthesis in a rat hepatoma cell line (A5-30D). At 48 hours, 8HQ was more effective at DNA synthesis inhibition (IC50 = 9.69 μM) than at 24 hours (IC50 = 20.88 μM).[277]

The role of transition metal ions such as iron and copper in cancer cells has been described when they are chelated with 8HQ. For example, the cytotoxic effect of $Fe(oxinate)_3$ complex has been previously observed in cultured lung cells, causing major cell growth inhibition (90% inhibition) and breakage of the DNA-strands compared to minor inhibition in cells treated with only 8HQ (15% inhibition).[282] The cytotoxic effect of $Cu(oxinate)_2$ was studied *in vitro* in HeLa and PC3 (human prostatic adenocarcinoma). The IC50 of $Cu(oxinate)_2$ was lower than that of the oxine ligand (13.5 c.f. 1.9 μM in Hela cells, and 8.6 c.f. 1.3 μM in PC3 cells).[283] Therefore, it seems that the therapeutic and anticancer actions of 8HQ are significantly increased via its delivery into the body in the form of metal complexes.[284]

5-chloro-8-hydroxy-7-iodoquinoline (CQ, Clioquinol), 5, 7-dichloro-8-quinolinol (Chloroxine), and 5-chloro-8-hydroxyquinoline (Cloxyquin) (Figure 4.1) are 8HQ derivatives that exhibited cytotoxicity in multiple cancer cell lines such as prostate, breast, bladder and cervical cell lines.[283,285–287] However, like 8HQ , copper complexation with these ligands decreased their IC50

from 15.6-26.1 to 3.1-8.9 μM in Hela cells, and from 12.3-23.7 to 2.3-9.0 μM in PC3 cells, indicating that these cell lines were more susceptible to the therapeutic effect of 8HQ derivatives when they were delivered as metal complexes.[283] Studies have showed that clioquinol can also act as ionophore for zinc, inducing a cellular apoptotic effect.[288,289,290] *In vitro* studies on A2780 (human ovarian cancer) and DU145 (prostate cancer) cell lines exhibited significant increase in cell apoptosis and decrease in cell viability after $Zn(oxinate)_2$ incubation compared to cells incubated with either $ZnCl_2$ or clioquinol.[289,290]

8-Hydroxy-5-nitroquinoline (Nitroquinoline) (Figure 4.1), another 8HQ derivative, was found to exert a similar anti-cancer effect to that of clioquinol in HuCCT1 and Huh28 (human hepatic cholangiocarcinoma) cells line. In HuCCT1 and Huh28 cells, nitroquinoline showed an IC50 of 3.69 and 4.49 μM while clioquinol showed 2.84 and 4.69 μM, respectively.[285] However, in Raji cells (human lymphoma), nitroquinoline showed a more potent anti-cancer effect with a 5 fold lower IC50 value than clioquinol. In fact, in the same cell line, nitroquinoline exerted the best anti-cancer activity compared to other 8HQ derivatives used including chloroxine, cloxyquin and 8HQ.[278,291] It is noteworthy that $Cu(nitroquinolinate)_2$ (10 μM) and $Zn(nitroquinolinate)_2$ (50 μM) had greater toxicity than nitroquinoline in Raji cells.[291] Other cell lines such as A2780, DHL-4 (human lymphoma), HL60 and Panc-1 (human pancreatic cancer) exhibited lower IC50 values for the metal complex $zinc(nitroquinolinate)_2$ (1.15-5.22 μM) and $Cu(nitroquinolinate)_2$ (0.07-0.19 μM) compared to clioquinol metal complexes (2.07-8.60 and 0.69-7.5 μM respectively) indicating that a variety of cell lines are more susceptible to nitroquinoline complexes than clioquinol metal complexes.[291]

Gallium shares multiple characteristics with iron that enables it to form complexes with iron-binding proteins and ligands. Given the vital role of iron as an essential nutrient for the growth of cancer cells, the development of gallium compounds as anticancer agents seems to be of a clinical relevance (see chapter 3).[6] As mentioned previously, the lipophilic complex $Fe(oxinate)_3$ is capable of growth inhibition and breakage of the DNA-strands. Therefore, it is important to investigate the possible role of gallium complexes with such chelating agents.[282]

^{67}Ga has potential as anti-cancer agent due to its ability to emit Auger electrons. Auger electrons deposit their energy over a short distance (ca. 1 μm). Hence it is crucial for ^{67}Ga electrons to be in close proximity to the target to cause damage.[14] Although ^{67}Ga produces fewer auger electrons (average of 4.7) per decay compared to ^{111}In (average of 14.7), the average energy release of ^{67}Ga (6.3 keV) per decay is similar to that of ^{111}In (6.8 keV). In fact, ^{67}Ga is one of Auger electron emitters that produces the highest energy Auger electrons (7-9 keV) and longest range in water (up to 2.4 μm). [26,292]

Owing to the ability of ^{67}Ga to emit Auger electrons, the potential of carrier free [^{67}Ga]Ga-citrate was investigated previously, to a limited extent, as a radionuclide for therapeutic application. *In*

vitro studies on the therapeutic effect of [^{67}Ga]Ga-citrate in human U937 lymphoma cells and myeloid leukemic blasts were promising and showed 36% growth inhibition post 3 days of incubation, and 20-51% clonogenic capacity after 3-4 days of incubation at doses between 0.75-1.5 MBq/ml. However, low uptake values (1.7-1.8%) were noticed even after 72 hours of incubation.[293,294] [^{67}Ga]Ga-citrate might have some potential as a therapeutic radionuclide but with some limitations. ^{67}Ga might not be substantially toxic unless its incorporated into cells. The oxine complexes of gallium radioisotopes can be used to incorporate ^{67}Ga into cells and evaluate their radiobiological toxicity.

An attempt was made to investigate the ability of 8HQ derivatives; oxine, 2-hydroxy-2,4,6-cycloheptatrien-1-one (tropolone), and mercaptopyridine n-oxide (MPO) (Figure 4.1) to incorporate ^{67}Ga into a MDA-MB-231 cell line and investigate its therapeutic effect as an Auger electron emitter radionuclide.[26] Oxine showed superiority in incorporating ^{67}Ga into cells (7.5 ± 1.3% uptake) compared to tropolone and MPO (1% uptake) after 1 hour of incubation.[26] [^{67}Ga]Ga-oxine showed similar cellular uptake in DU145 and HCC1954 (human breast cancer) cells to that in MDA-MB-231 cells. Due to the higher cellular uptake of [^{67}Ga]Ga-oxine compared to its other derivatives, [^{67}Ga]Ga-oxine was used for the rest of the cellular studies. For [^{67}Ga]Ga-oxine, the percentage of cellular activity at 1 hour post incubation was set at 100% in previously mentioned cell lines and the percentage of retained activity in the cells was calculated for 72 hours. At 72 hours, 38.8% ± 0.7% of activity remained in the cells.[26] The viability assay after 72 hours of incubation of [^{67}Ga]Ga-oxine in DU145 cells showed reduction in cell viability to 17.4 ± 6.6% (compared to 100% viability in untreated cell) at a concentration of 1.5 Bq/cell (occurred at incubation of 15 MBq/ml). For control studies, DU145 cells were either incubated with [^{67}Ga]Ga-citrate (15 MBq/ml, no significant cell uptake) or decayed [^{67}Ga]Ga-oxine at concentration equal to decayed 20 MBq/ml. Both control groups showed 53% cell viability at 72 hours post incubation.[26] Although [^{67}Ga]Ga-citrate showed some level of toxicity without being significantly taken up by cells, high toxicity was induced only when ^{67}Ga incorporated into the cells by using [^{67}Ga]Ga-oxine.[26] Hence, it was suggested that ^{67}Ga originates high toxicity only if absorbed into cells. In addition, the decayed oxine complex showed similar toxicity to the citrate complex which might be related to the toxicity of oxine or the presence of other metals from decayed ^{67}Ga, i.e. zinc, that could have affected the viability.[26] It is worth investigating ^{67}Ga as a therapeutic radionuclide especially in the context with 8HQ as a carrying agent. Although tropolone and MPO was investigated and showed lower cellular uptake compared to oxine, further development of 8HQ derivatives complexes of gallium radioisotopes may generate improved methods of controlled loading of cells with ^{67}Ga for these purposes.

In this chapter, we examine multiple conditions for radiolabelling 8HQ and its analogues with ^{68}Ga first, aiming to find the best chemical form to deliver ^{67}Ga to cells and study its radiobiology. The following ligands were used for these purposes: oxine, tropolone, nitroquinoline, 8-

mercaptoquinoline hydrochloride (thiooxine hydrochloride), Chloroxine, Cloxyquin, Clioquinol, 2-hydroxyquinoline, 3-hydroxyisoquinoline, MPO (Figure 4.1). In addition, protein speciation studies of selected ^{68}Ga-8HQ derivatives were performed *in vitro* aiming to investigate their possible cell uptake pathway.

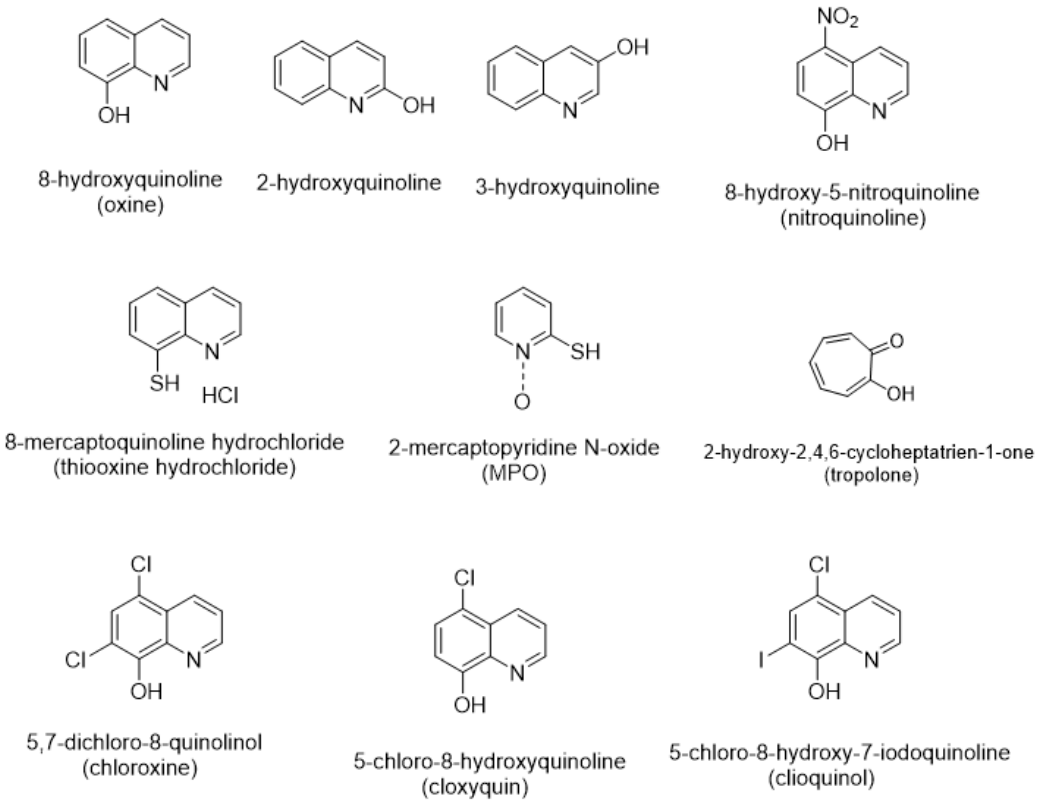

Figure 4.1: Chemical structure of 8HQ derivatives

4.2 Experimental

4.2.1 Equipment and consumables

All reagents and consumables were purchased from Fisher Scientific/Chemicals and Sigma Aldrich unless specified otherwise. ^{68}Ga was obtained from a ^{68}Ge/^{68}Ga generator (Eckert & Ziegler) and eluted with 5 ml of 0.1 M ultrapure HCl and collected in 5 x 1 ml fractions. Activity was measured using a Captintec, INC (CRC-25R) dose calibrator. The two highest 1 ml activity fractions were used to prepare all complexes. iTLC was carried out using Agilent's silica gel impregnated glass microfiber strips (10 cm in length). iTLC strips were analysed with phosphor imager filmless autoradiography (Cyclone Plus). Gamma counting was performed using an LKB Wallac 1282 Compugamma Gamma Counter. A375 human melanoma cell lines were purchased from the American Type Culture Collection (ATCC), and then cultured and stocked in our department.

4.2.2 Radiolabelling of ^{68}Ga with 8HQ derivatives

Two radiolabelling methods were performed to find the best suitable conditions for radiolabelling ^{68}Ga with different 8HQ derivatives.

4.2.2.1 First radiolabelling method

The first method that has been used for radiolabelling was adapted from J. Bartnicka, unpublished work. Oxine, tropolone, nitroquinoline, thiooxine hydrochloride, 2-hydroxyquinoline, and 3-hydroxyisoquinoline were tested using this method. The ligands were dissolved in ethanol (0.5 mg/ml). 200 µl of the ligand solutions were mixed with 100 µl of ammonium acetate (0.5 M ammonium acetate in sterile H_2O, pH= 7.5) and 100 µl of ^{68}Ga to bring the final mixture to 2:1:1 volume ratio respectively (final mixture pH= 5.5). The solutions were heated in a heating block for 5 minutes at 50º C. [^{68}Ga]Ga-acetate was used as a control and was prepared following the same method, but no ligand was added; the ligand solution was replaced with ethanol only. 3 µl was used for iTLC analysis. Mobile phase was chloroform ($CHCl_3$): methanol (CH_3OH) (95:5%, v/v).

4.2.2.2 Second radiolabelling method

This method was done to increase yield of [^{68}Ga]Ga-thiooxine by increasing the concentration of the ligand and increasing the pH of the final complex. In addition, Oxine, tropolone, nitroquinoline, chloroxine, cloxyquin, clioquinol, and MPO were also radiolabelled with ^{68}Ga using this method to compare the iTLC results of the first and seconds radiolabelling methods. All ligands were dissolved in ethanol (1 mg/ml). 200 µl of the ligand solutions were mixed with 200 µl of sodium acetate (0.5 M sodium acetate in sterile H_2O, pH=9) and 100 µl ^{68}Ga to bring

the final mixture to 2:2:1 volume ratio respectively (final mixture pH= 6). Aqueous solution of sodium hydroxide (0.1 M, pH=13, 70 µl) was added to adjust the final solution to pH 7. The complexes were incubated at room temperature for 10 minutes. [^{68}Ga]Ga-acetate was used as a control and was prepared following the same method, but no ligand was added; the ligand was replaced with ethanol only. 3 µl was used for iTLC analysis. Mobile phase was chloroform ($CHCl_3$): methanol (CH_3OH) (95:5%, v/v) for all ^{68}Ga complexes, plus 50 µl of the freshly prepared ligand (1 mg/ml) for [^{68}Ga]Ga-thiooxine only.

4.2.3 Determination of distribution coefficient (Log *D* octanol/PBS) of ^{68}Ga 8HQ derivatives complexes

Lipophilicity determination was performed using shake flask method. [^{68}Ga]Ga-acetate was utilised as a control. All ^{68}Ga complexes were prepared using the second radiolabelling method (see section 4.2.2.2). Log *D* of [^{68}Ga]Ga-thiooxine was also measured using the first radiolabelling method (see section 4.2.2.1) to test if using the second radiolabelling method will increase the radiolabelling yield of [^{68}Ga]Ga-thiooxine and consequently its apparent lipophilicity. Log *D* was measured by adding 20 µl of ^{68}Ga complexes to pre-equilibrated mixture of octanol/PBS = 500 µl/500µl. The final solutions were mixed for 5 minutes by Multi Vortex Mixer V-32 (Grant bio). 200 µl were taken from each layer and placed separately in Eppendorf tubes.

4.2.4 Cellular uptake studies

4.2.4.1 Cell culturing

A375 human melanoma cells were used in all *in vitro* studies. T-75 and T-150 flasks were used to grow the cells in Dulbecco's Modified Eagle Medium (DMEM) containing 50 ml of fetal bovine serum (FBS, 10% of the medium), 5 ml of L-glutamine and 5 ml of penicillin and streptomycin. After cells reached confluence, cell dissociation was attained by adding trypsin and incubation for 5 minutes in 37ºC under 5% CO_2. DMEM medium with FBS serum was added to inactivate trypsin. Cell suspension was transferred to a 50 ml Falcon tube and centrifuged for 5 minutes at 1300 RPM. The supernatant was removed, and relevant medium was added.

4.2.4.2 Cellular uptake of [^{68}Ga]Ga-oxine, [^{68}Ga]Ga-thiooxine, and [^{68}Ga]Ga-acetate in A375 cells in the presence of FBS in the media

^{68}Ga complexes were prepared following the second radiolabelling method (see section 4.2.2.2). Sodium hydroxide was not used to increase the pH of the solution, however, 10 MBq (50 to 70 µl) of ^{68}Ga complexes were then diluted with 0.5 M sodium acetate to 1 ml to obtain the activity of 100 kBq/ 10 µl, pH = 7. iTLC was used to test the radiochemical purity of ^{68}Ga complexes before all *in vitro* studies. Cell uptake study was done in suspension in 1.5 ml Eppendorf tubes

which contained one million cells in 0.5 of DMEM media. Three samples of cells (cell pellet) and controls (no cells to correct for non-specific uptake) were used for each complex. Samples were incubated in DMEM media containing FBS for 60 minutes in 37º C and 5% CO2. Following the incubation, samples were centrifuged (Sci Spin Mini) for 3 minutes at 1500 RPM, the supernatant was removed and transferred to another Eppendorf tube. Two 0.5 ml PBS washes were performed, and the washings added to the supernatant Eppendorf's. The activity of tubes (cells/ control) was measured by Wallac gamma counter after removing the media, first wash and second wash. The average percentage uptake of ^{68}Ga complexes and corresponding controls was calculated by dividing the activity obtained for pellet/control-containing tubes by the sum of activity for pellet/control, supernatant and washes tubes combined, then multiplying by 100. Control corrected was calculated by correcting the percentage of cell uptake for corresponding controls.

4.2.4.3 Cellular uptake of [^{68}Ga]Ga-thiooxine in A375 cells incubated with 0.9% saline

Saline was used instead of full cell culture media to test if the presence of media can compromise [^{68}Ga]Ga-thiooxine cellular uptake. Cell uptake and [^{68}Ga]Ga-thiooxine preparation were performed using the same method discussed in section 4.2.4.2. However, 0.9% saline solution was used instead of media and PBS washes. Cells and control samples were incubated for 10, 30, 60, and 90 minutes and the activity of tubes (cells/controls) were measured by Wallac gamma counter.

4.2.4.4 Cellular uptake of ^{68}Ga HQ derivatives in A375 cells incubated in the presence of human serum in media

One million cells in 1 ml of media (DMEM media + 10% human serum, purchased from Sigma Aldrich, H4522) were put in 6-well plates one day before use. On the same day of the experiment, old media was removed and replaced with 1 ml fresh media. ^{68}Ga complexes (oxine, thiooxine, tropolone, clioquinol, chloroxine, cloxyquin, nitroquinoline, and acetate) were prepared following the same method discussed in section 4.2.4.2. The experiment was done in triplicate for each complex. Cells and controls were incubated with 100 KBq/10 µl of ^{68}Ga complexes in each well for 60 minutes. The supernatant was then removed and transferred to Eppendorf tubes. Wells were washed twice with PBS (0.5 ml each) and washings added to the supernatant Eppendorf tubes. 0.5 ml of trypsin was added to both cells and control wells (incubated for 5 minutes) then transferred to a new Eppendorf tube; 0.5 ml of PBS was used to wash the well plates after trypsin and then added to trypsin (with cells/ control) Eppendorf. Eppendorf tube activity was measured by Wallac gamma counter and the average percentage uptake of each complex was calculated as described in section 4.2.4.2.

4.2.5 Protein binding studies

Size exclusion chromatography was done to study ^{68}Ga complex binding to human apo-transferrin (purchased from Sigma Aldrich T1147). ^{68}Ga complexes (oxine, thioooxine, nitroquinoline) were radiolabelled by mixing 1 MBq (13 to 20 µl) of ^{68}Ga with the ligands (1mg/ml of ethanol) to achieve 1:2 volume ratio of ^{68}Ga and the ligands. 600 µl of sodium bicarbonate in distilled water ($NaHCO_3$, 5 mM, pH = 8) was used as a buffer and added to all ^{68}Ga complexes. Post 10 minutes incubation at room temperature, 600 µl of $NaHCO_3$ (control) or $NaHCO_3$ containing apo-transferrin (2 mg/ml) was added to each mixture. Final solution pH = 7-7.5. Complexes were incubated for 60 minutes then 0.5 ml of each sample (0.2 -0.5 MBq) was eluted from PD midiTrap G-25 tubes (equilibrated by 8 ml of $NaHCO_3$) with $NaHCO_3$ into 0.5 ml fractions and radioactivity of each fraction was measured using Wallac gamma counter. Uncomplexed ^{68}Ga (control) was prepared following the same method (ligand solution was replaced with ethanol) in just $NaHCO_3$ and in apo-transferrin dissolved in $NaHCO_3$ to obtain standard elution profiles of ^{68}Ga in the buffer in the presence and absence of apo-transferrin. The protein absorbance at 280 nm was measured using a nanodrop spectrophotometer. ^{68}Ga complexes were tested for radiochemical purity by iTLC before size exclusion studies.

4.3 Results

4.3.1 Radiolabelling of ^{68}Ga with 8HQ derivatives

Different radiolabelling methods were adopted to find the most suitable conditions for radiolabelling ^{68}Ga with different complexes. Analyses of the first radiolabelling method are presented in Figure 4.2. [^{68}Ga]Ga-tropolone (1), [^{68}Ga]Ga-oxine (2), and [^{68}Ga]Ga-nitroquinoline (6) moved to solvent front (R_f = 1), leaving no residual ^{68}Ga in the solvent origin. On the other hand, no move to the solvent front was observed for either [^{68}Ga]Ga-2-hydroxyquinoline (4) or [^{68}Ga]Ga-3-hydroxy-isoquinoline (5). Their radioactivity remained at the origin (R_f = 0) similar to [^{68}Ga]Ga-acetate (3). [^{68}Ga]Ga-thiooxine (7) showed a partial migration or smearing (R_f = 0 - 0.3).

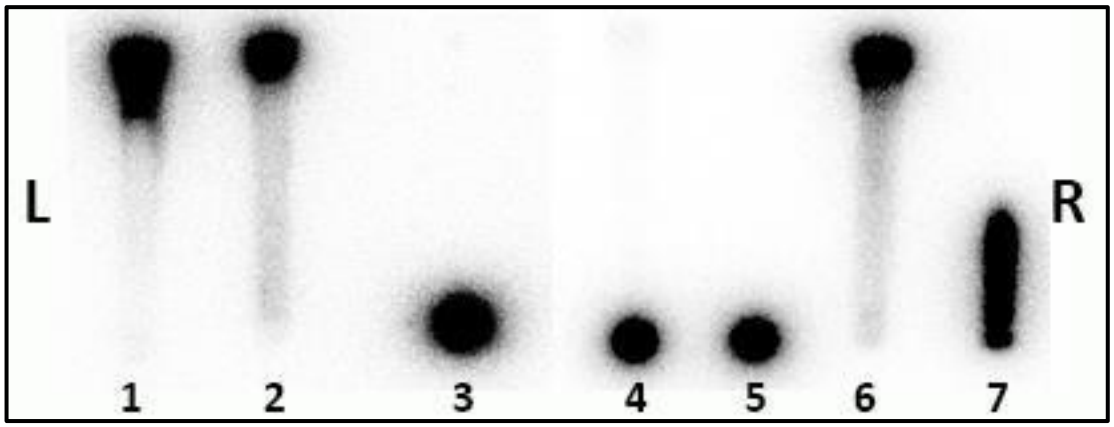

Figure 4.2: Radioactivity distribution on silica gel impregnated glass microfiber strips (iTLC-SG) using phosphor imager. From left to right [^{68}Ga]Ga-tropolone(1), [^{68}Ga]Ga-oxine (2), [^{68}Ga]Ga-acetate (control) (3), [^{68}Ga]Ga-2-hydroxyquinoline (4), [^{68}Ga]Ga-3-hydroxyisoquinoline (5), [^{68}Ga]Ga-nitroquinoline (6), and [^{68}Ga]Ga-thiooxine (7), all samples were done in quadruplicates.

Figure 4.3 presents the results of the second radiolabelling method and figure 4.4 shows the comparative behaviours of [^{68}Ga]Ga-thiooxine using the first versus second radiolabelling methods. Like the first method, results from the second method showed that [^{68}Ga]Ga-tropolone (1), [^{68}Ga]Ga-oxine (2), and [^{68}Ga]Ga-nitroquinoline (3) moved to solvent front ($R_{f=}1$), without residual ^{68}Ga in the solvent origin. Similarly, halogenated derivatives of 8HQ including [^{68}Ga]Ga-chloroxine (5), [^{68}Ga]Ga-cloxyquin (6), and [^{68}Ga]Ga-clioquinol (7) moved to the solvent front. Regarding [^{68}Ga]Ga-thiooxine (4), a short move from the solvent origin was observed (arrow figure 4.3), along with smearing from the stationary phase (R_f = 0.5) after using the second radiolabelling method (Figure 4.4, top-right panel, R). By adding 50 µl of thiooxine to the mobile phase, we observed an additional lift of the complex toward the solvent front as shown in figure 4.3.B and figure 4.4 bottom panel: (R_f=0.6). [^{68}Ga]Ga-MPO (8) remained in solvent origin (R_f = 0) identical to [^{68}Ga]Ga-acetate (control) (9), which indicated poor complexation.

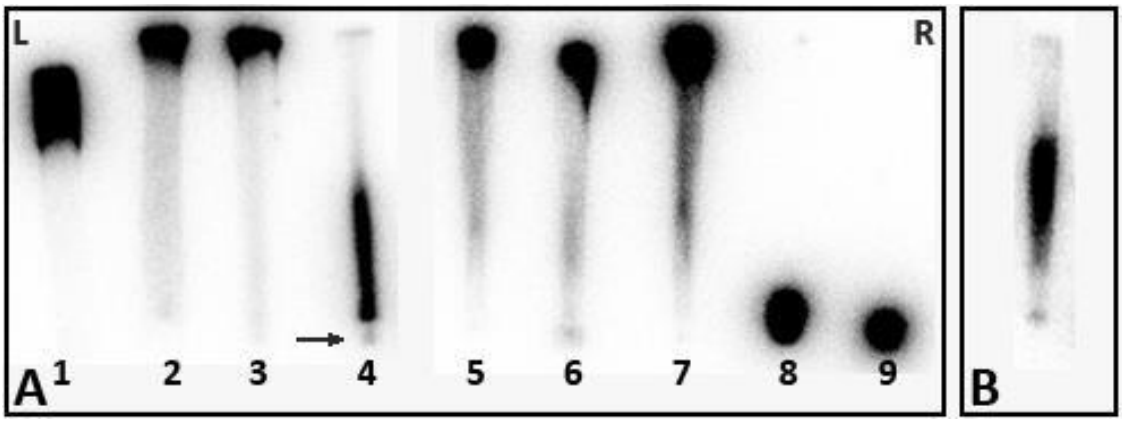

Figure 4.3: Panel A represents the radioactivity distribution on silica gel impregnated glass microfiber strips using Phosphor Imager. From left to right: [^{68}Ga]Ga-tropolone (1), [^{68}Ga]Ga-oxine (2), [^{68}Ga]Ga- nitroquinoline (3), [^{68}Ga]Ga-thiooxine (4), [^{68}Ga]Ga-chloroxine (5), [^{68}Ga]Ga-cloxyquin (6), [^{68}Ga]Ga-clioquinol (7), [^{68}Ga]Ga-MPO (8), [^{68}Ga]Ga-acetate (control) (9). (B) Radioactivity distribution of [^{68}Ga]Ga-thiooxine on silica gel impregnated glass microfiber strips using Phosphor Imager after adding 50 µl of the freshly dissolved thiooxine to the mobile phase. All samples were done in triplicates.

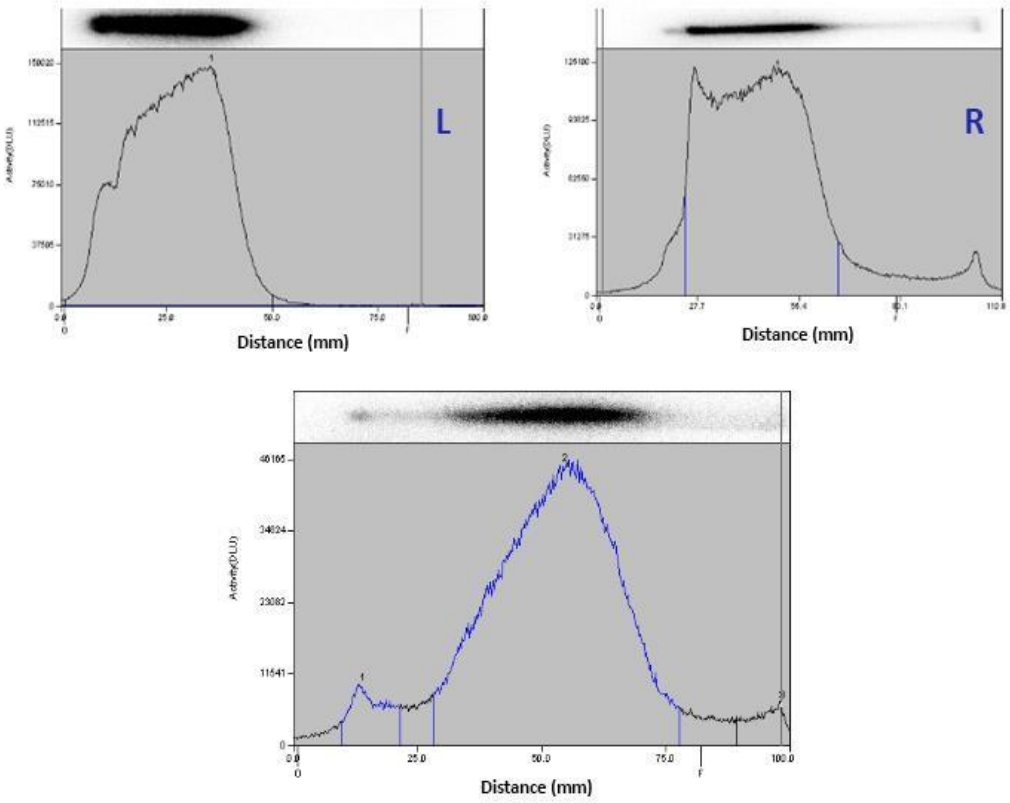

Figure 4.4: Radioactivity distribution analysed by Phosphor Imager of [^{68}Ga]Ga-thiooxine using the first (top-left panel, L) and second (top right panel, R) radiolabelling methods, and after adding 50 µl of thiooxine to the mobile phase (bottom panel).

4.3.2 Determination of distribution coefficient (Log *D* octanol/PBS) of ^{68}Ga 8HQ derivatives complexes

Determination of distribution coefficient (octanol/PBS) showed that [^{68}Ga]Ga-oxine (Log *D* ± SD=1.75±0.3) and tropolone (Log *D* ± SD = 1.67± 0.2) were highly lipophilic, which supports the iTLC results. By contrast with iTLC results, [^{68}Ga]Ga-MPO was shown to be lipophilic (Log *D* ± SD = 1.4 ± 0.2). On the other hand, both [^{68}Ga]Ga-2-hydroxyquinoline (Log *D* ± SD= -1±0.1) and [^{68}Ga]Ga-3-hydroxyisoquinoline (Log *D* ± SD = -1 ± 0.2) were hydrophilic suggesting poor complexation; consequently, they were excluded from further experiments. Halogenated hydroxyquinoline derivatives and nitroquinoline showed lesser log *D* values compared to [^{68}Ga]Ga-oxine and tropolone. [^{68}Ga]Ga-thiooxine log *D* value increased from 0.5 ± 0.2 to 0.9 ± 0.2 after increasing the concentration of the ligands in ethanol by two fold (Table 4.1).

^{68}Ga HQ derivatives	Log *D* (0.5 mg/ml)	Log *D* (1 mg/ml)
Oxine		1.75 ± 0.34
Tropolone		1.67 ± 0.2
chloroxine		0.9 ± 0.2
cloxyquin		1.3 ± 0.3
clioquinol		1 ± 0.0
MPO		1.4 ± 0.2
Thiooxine	0.5 ± 0.2	0.9 ± 0.2
Nitroquinoline		1.1 ± 0.06
2-hydroxyquinolinee		-1 ± 0.1
3-hydroxy-isoquinoline		-1 ± 0.2
Acetate (control)		-2.7 ± 0.62

Table 4.1: Log D value of ^{68}Ga chelators. values represent an average of three replicates and ± standard deviation

4.3.3 Cellular uptake of [^{68}Ga]Ga-oxine, [^{68}Ga]Ga-thiooxine, and [^{68}Ga]Ga-acetate in A375 cells in the presence of FBS in the media

Comparative analysis between the three complexes showed that thiooxine had the highest cellular uptake throughout all washes including after media removal, after first and second wash as demonstrated by table 4.2. Analysis of gallium uptake over the three phases showed uptake decreasing significantly after first PBS wash for all three ligands, while no difference in cellular uptake was noticed between the first and second wash (Figure 4.5). However, [^{68}Ga]Ga-thiooxine was the most retained in cells after the second wash compared to [^{68}Ga]Ga-oxine and [^{68}Ga]Ga-acetate. Figure 4.6 represent gallium uptake between cells and controls (no cells) after the second wash versus control-corrected (cells – controls/no cells) values. Control-corrected uptake was calculated as the difference of activity in cells and in the corresponding control. The results show that control corrected values were not different from cell activity for both [^{68}Ga]Ga-oxine and [^{68}Ga]Ga-thiooxine, indicating minimal plastic binding occurred and activity accumulated in cells, whereas control value was high for [^{68}Ga]Ga-acetate, indicating most activity bound to plastic and minimal amount incorporated into cells.

Time	Oxine		Thiooxine		Acetate		p-value
	Mean	SD	Mean	SD	Mean	SD	
After media removal	3.61	0.48	6.30	0.79	2.45	0.28	<0.01*
After first wash	0.89	0.03	2.92	0.40	0.71	0.17	≤0.001**
After second wash	0.68	0.15	2.86	0.64	0.46	0.19	≤0.001**

Table 4.2: Comparing percentage cellular uptake of ^{68}Ga between oxine, thiooxine and acetate after media removal, first wash and second wash. Values are percentage uptake (mean and standard deviation). SD: Standard deviation. *P* value; * ($p< 0.01$), and ** (≤ 0.001). *P* values represent the significant difference of [^{68}Ga]Ga-thiooxine to [^{68}Ga]Ga-oxine and [^{68}Ga]Ga-acetate after media removal, first wash, and second wash. Test used: One-way ANOVA + Tukey HSD.

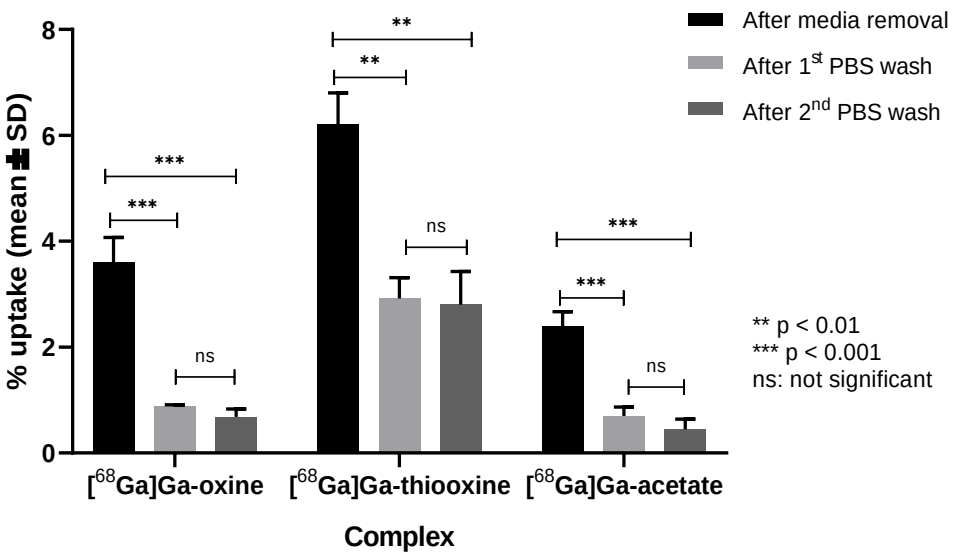

Figure 4.5: Comparing ^{68}Ga cellular uptake after removing the media, 1st, and 2nd PBS wash in oxine, thiooxine, and acetate. Cellular uptake study showed significant decrease in cells uptake after the first wash, while no significant difference was seen between the first and second wash for all three complexes. [^{68}Ga]Ga-thiooxine showed the highest retention in cells throughout the washes. Bars represent mean ± standard deviation of percentage uptake. Test used: One-way ANOVA + Tukey HSD.

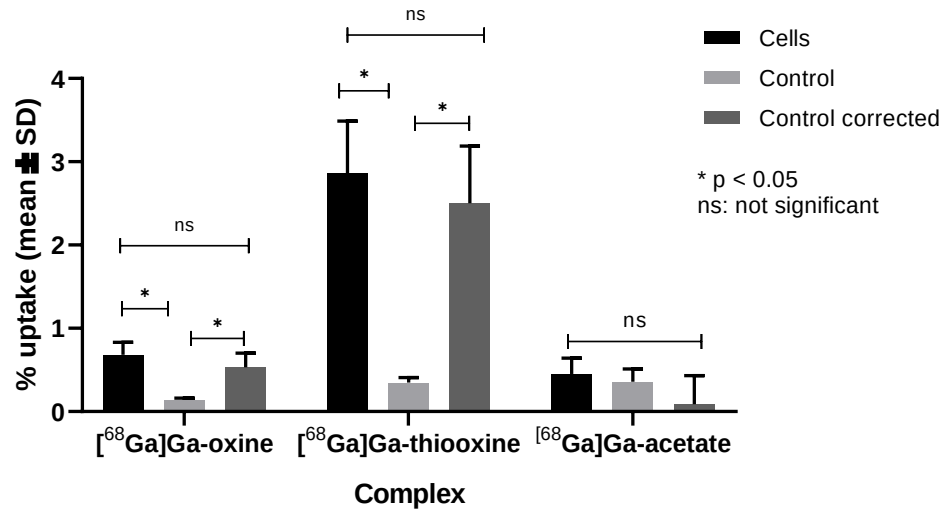

Figure 4.6: Effect of ligand on cellular uptake. Figure compares ^{68}Ga uptake between cells and controls after the second wash versus control-corrected values (activity in cell – activity in control) in oxine, thiooxine, and acetate. [^{68}Ga]Ga-oxine and [^{68}Ga]Ga-thiooxine showed no significant difference between cells and control corrected values. [^{68}Ga]Ga-acetate showed no significant difference between cells, control, and control corrected values. Test used: One-way ANOVA + Tukey HSD.

4.3.4 Cellular uptake of [^{68}Ga]Ga-thiooxine in A375 cells incubated with 0.9% saline

Due to its optimal uptake characteristics, [^{68}Ga]Ga-thiooxine was selected for cellular uptake study using saline as an incubation media. Figure 4.7 shows that using saline for cell incubation is likely to increase [^{68}Ga]Ga-thiooxine uptake; for example, after 60 minutes, mean ± SD percentage of [^{68}Ga]Ga-thiooxine concentration in cells was 20.19 ± 3.17 (Figure 4.7), compared to 2.8 ± 0.6 measured after incubation in DMEM media (contain FBS) for a similar time (Figure 4.6). However, no difference was observed in [^{68}Ga]Ga-thiooxine uptake between cells and controls at any time of the incubation; this indicated that more activity bound to the plastic compared to previous study when DMEM media was used. [^{68}Ga]Ga-thiooxine control corrected values were relatively similar whether incubated in DMEM media (2.50 ± 0.69) or saline (3.70 ± 1.7) for 60 minutes. The higher plastic binding activity in saline compared to DMEM media condition might be related to the lipophilicity of the compound and its preference to adsorb to the plastic rather than stay in the aqueous saline solution (more details in the discussion section). This indicates that saline incubation is not efficient for [^{68}Ga]Ga-thiooxine cellular uptake based on the high plastic binding activity noticed.

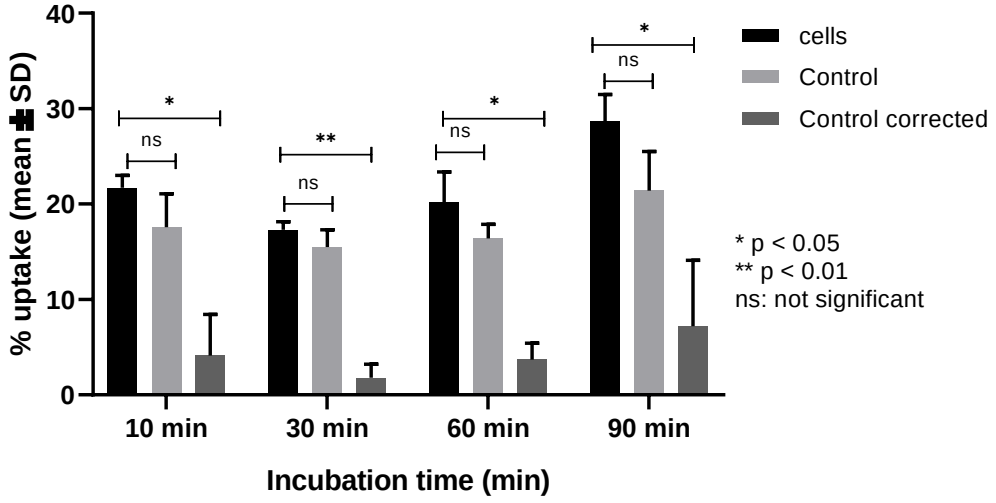

Figure 4.7: Evaluation of [^{68}Ga]Ga-thiooxine cellular uptake in 0.9% saline over time. No significant difference was seen between cells and control values at all time points. Test used: One-way ANOVA + Tukey HSD.

4.3.5 Cellular uptake of ^{68}Ga HQ derivatives in A375 cells incubated in the presence of human serum in media

According to unpublished experimental data by F. Al-Salemee, an increase of [^{68}Ga]Ga-acetate uptake in A375 melanoma cell line is observed in the presence of human serum compared to fetal bovine serum. Incubation with human serum in media was performed in the current study to investigate the uptake difference between ^{68}Ga complexes. Figure 4.8 represents gallium uptake differences between cells and control for each ^{68}Ga complex used in the presence of human serum. The results showed that cells and control values were significantly different in all ^{68}Ga complexes indicating minimal plastic binding occurred and activity accumulated in cells. [^{68}Ga]Ga-thiooxine showed the highest cellular uptake (23.2 ± 3.3 %) compared to other ligands used (Figure 4.8), while some similarities were evident between the other ligands (see appendix section for comparison of ^{68}Ga cellular uptake using different ligands). [^{68}Ga]Ga-oxine and [^{68}Ga]Ga-tropolone showed minimal cellular uptake compared to other ligands, 0.2 ± 0.02% and 3.9 ± 0.4% respectively. Consistent with the F. Al-Salemee study, [^{68}Ga]Ga-acetate cellular uptake increased from 0.45 ±0.19 (in the presence of FBS in the media, Figure 4.6) to 11.2 ± 2.4 in the current experiment when human serum was used instead (Figure 4.8).

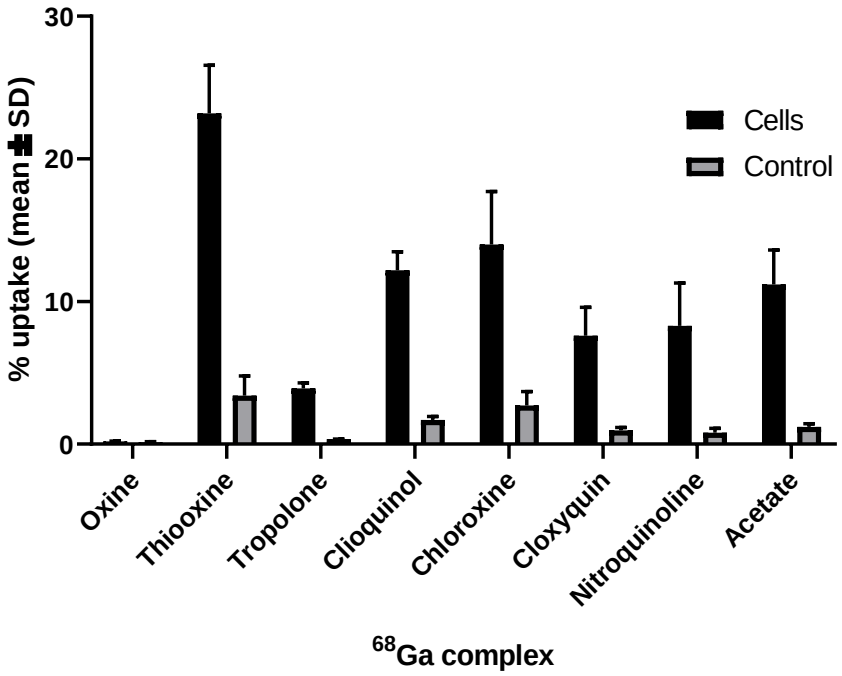

Figure 4.8: Gallium cellular uptake after incubation in DMEM media with human serum using different ligands. Bars are means ± standard deviation of percentage uptake in 10^6 cells. Values are percentage uptake (mean and standard deviation). The difference between cells and controls for all ^{68}Ga complexes was significant ($p<0.001$), except for [^{68}Ga]Ga-acetate ($p<0.01$). A t-test was performed to evaluate the difference between cells and control values for each ^{68}Ga complex.

4.3.6 Protein binding studies

Figure 4.9 represents the elution profile of *apo*-transferrin in sodium bicarbonate, showing that apo transferrin elution in bicarbonate occurs in fractions 3, 4 and 5. Elution profiles of unchelated ^{68}Ga and [^{68}Ga]Ga-oxine in sodium bicarbonate, in the presence versus absence of apo transferrin are presented in figure 4.10 and 4.11, respectively. In the presence of apo transferrin, unchelated ^{68}Ga was eluted in fractions 3, 4, and 5, which corresponds to large MW compound, indicating binding to apo transferrin. In absence of apo transferrin, unchelated ^{68}Ga eluted in middle fractions (fractions 7-11) (Figure 4.10). By contrast, [^{68}Ga]Ga-oxine showed a similar elution profile in both presence and absence of apo transferrin, indicating absence of binding of [^{68}Ga]Ga-oxine to apo transferrin. [^{68}Ga]Ga-oxine eluted in the latter fractions, corresponding to small MW compounds (Figure 4.11). Figure 4.12 represent the elution profile of [^{68}Ga]Ga-thiooxine. [^{68}Ga]Ga-thiooxine showed similar elution profiles in presence versus absence of apo transferrin. [^{68}Ga]Ga-thiooxine eluted in fractions 3-5, behaving like a large MW compound, and in fractions 13-15 fractions behaving like a small molecular compound (see discussion section). Similar to un-chelated ^{68}Ga, [^{68}Ga]Ga-nitroquinoline was eluted in fractions 3, 4 and 5 in presence of apo transferrin; thus corresponding to large MW compound and indicating effective binding to apo transferrin (Figure 4.13).

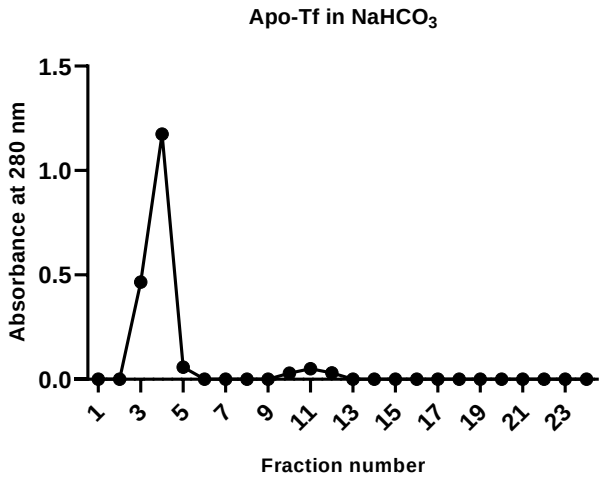

Figure 4.9: Elution profile of apo transferrin in $NaHCO_3$ measured using nanodrop spectrophotometer.

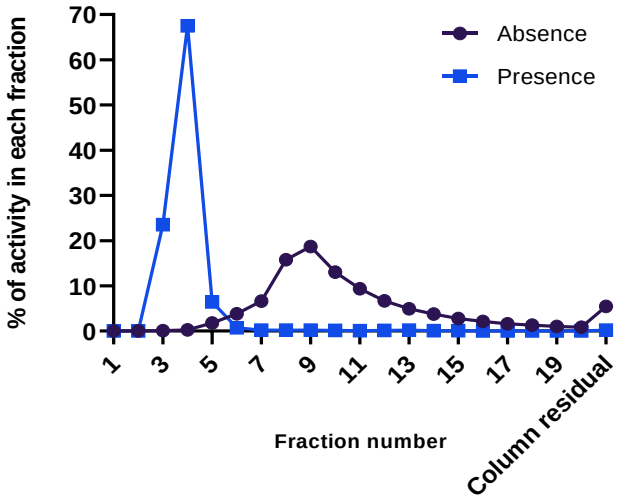

Figure 4.10: Elution profile of unchelated ^{68}Ga in $NaHCO_3$ in the presence and absence of apo transferrin using PD midiTrap G-25 tubes post 60 minutes of incubation.

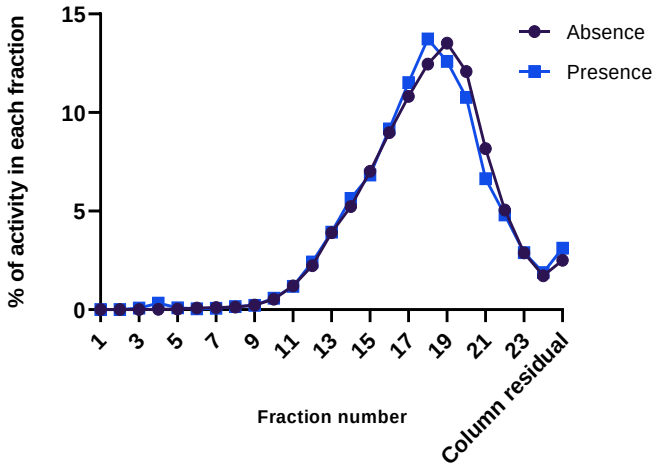

Figure 4.11: Elution profile of [^{68}Ga]Ga-oxine in $NaHCO_3$ in the presence and absence of apo transferrin using PD midiTrap G-25 tubes post 60 minutes of incubation.

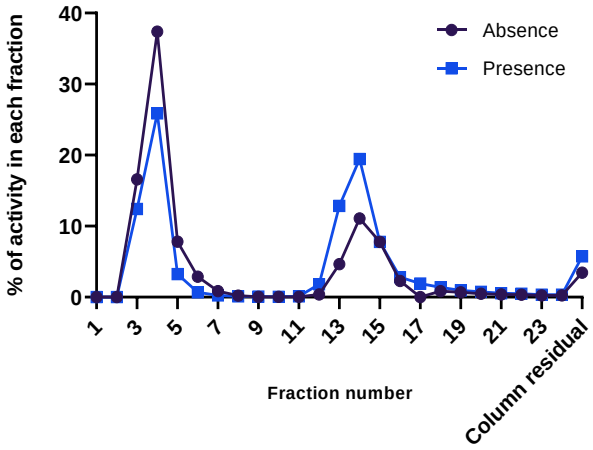

Figure 4.12: Elution profile of [^{68}Ga]Ga-thiooxine in $NaHCO_3$ in the presence and absence of apo transferrin using PD midiTrap G-25 tubes post 60 minutes of incubation.

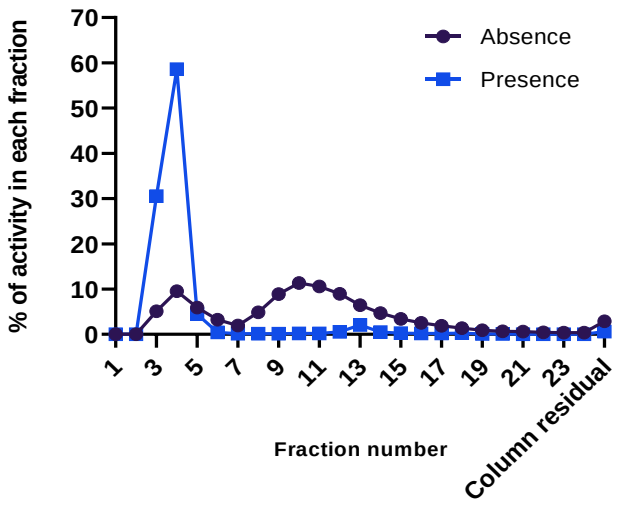

Figure 4.13: Elution profile of [^{68}Ga]Ga-nitroquinoline in $NaHCO_3$ in the presence and absence of apo transferrin using PD midiTrap G-25 tubes post 60 minutes of incubation.

4.4 Discussion

Using the first radiolabelling method, [^{68}Ga]Ga-2-hydroxyquinoline and [^{68}Ga]Ga-3-hydroxyisoquinoline showed the same iTLC results as [^{68}Ga]Ga-acetate (R_f= 0). The log *D* values of [^{68}Ga]Ga-2-hydroxyquinoline and [^{68}Ga]Ga-3-hydroxyisoquinoline were -1.0 ± 0.1 and -1.0 ± 0.2 respectively, suggesting poor complexation, that matching iTLC results. Hence, they were excluded from further experiment. These results were not surprising as these ligands (based on their chemical structure) were not expected to be suitable for chelation (Figure 4.1) and were used effectively as controls.

Due to weak [^{68}Ga]Ga-thiooxine formation when the first radiolabelling method was used, the thiooxine concentration in ethanol solution was increased from 0.5 mg/ml (first method) to 1 mg/ml (second method) in order to maximise the radiochemical yield. Doubling the concentration of ligands showed the R_f value changing from 0.3 to 0.5. Further moving towards the solvent front was noticed by the addition of 50 µl of thiooxine to the mobile phase (Figure 4.4 top right panel, R, and bottom panel). This can be due to the instability of the [^{68}G]Ga-thiooxine complex and dissociation of ^{68}Ga from the ligand as it migrates up the strip and the ligand and metal is becoming separated. Adding extra ligand to the mobile phase results in more thiooxine being available to bind gallium and help move the complex further, indicating greater complexation of the complex. An increase in apparent log *D* value of [^{68}G]Ga-thiooxine from 0.5 ± 0.2 to 0.9 ± 0.2 after increasing the concentration of the ligands in ethanol by two fold is consistent with the greater complexation of the complex in iTLC. For [^{68}Ga]Ga-MPO, the log *D* value indicated that the complex is lipophilic, but iTLC results showed poor complexation. Due to the discrepancy between log *D* and iTLC results with no further experiment being performed to explain this discrepancy, [^{68}Ga]Ga-MPO was excluded from cell uptake and protein binding studies.

[^{68}Ga]Ga-oxine, and [^{68}Ga]Ga-tropolone showed higher apparent log *D* value compared to all other ^{68}Ga complexes tested (Table 4.1). This could indicate higher stability of the first two with minimal free ^{68}Ga available, while the latter complexes are less stable and consist of larger amount of free ^{68}Ga. It was supported by cellular uptake study in the presence of human serum in the media, as [^{68}Ga]Ga-oxine, and [^{68}Ga]Ga-tropolone exhibited less cellular uptake in comparison to other ligands, indicating that [^{68}Ga]Ga-oxine and [^{68}Ga]Ga-tropolone might form more stable compounds compared to other 8HQ derivatives, and ^{68}Ga might diffuse in cells but gets trapped to a lesser extend due to slower dissociation.[26] While no protein binding studies were performed for [^{68}Ga]Ga-tropolone, [^{68}Ga]Ga-oxine showed no binding to human apo-transferrin using size exclusion chromatography, which is also an indication for the stability of the complex and cell uptake by passive diffusion. It does not bind to apo-transferrin or enter the cells by transferrin medicated mechanism.

Cellular uptake study in the presence of FBS in the media showed no significant difference between cells and control corrected (cells – controls/no cells) values for [^{68}Ga]Ga-oxine and [^{68}Ga]Ga-thiooxine indicating low plastic binding (low control values), and that cell uptake value represents activity incorporated into cells. However, plastic binding was high for [^{68}Ga]Ga-acetate and the result showed no difference between cells and control, indicating poor cellular uptake occurred. These results are consistent with a literature study[26] (see introduction section) that showed higher ^{67}Ga cell incorporation and cytotoxic effect when oxine was used as a chelating agent compared to ^{67}Ga citrate.[26]

Incubation with saline increased the cellular uptake of [^{68}Ga]Ga-thiooxine in comparison to DMEM media contain FBS. However, due to the high activity in control tubes in saline condition, control corrected samples in both conditions showed similar values. This indicates that in the presence of FBS, a large amount of [^{68}Ga]Ga-thiooxine binds to serum proteins and gets removed with the supernatant, providing minimal plastic binding. However, in the absence of serum proteins (incubation in saline) the majority of activity bound to the plastic rather than remain in the aqueous saline solution (owing to [^{68}Ga]Ga-thiooxine lipophilicity).[295,296] In this specific setting, saline incubation is not efficient for cellular uptake due the difficulties to recognise the difference between cellular uptake and plastic binding activity rendering high cellular uptake of [^{68}Ga]Ga-thiooxine potentially irrelevant. Using glass bottom wells instead of plastic could minimize the plastic binding.

[^{68}Ga]Ga-thiooxine exhibited the highest cellular uptake compared to all ligands in the presence of human serum in the media. In addition, cells incubated with [^{68}Ga]Ga-thiooxine showed higher uptake in the presence of human serum (23.2 ± 3.3) compared to FBS (2.86 ± 0.64) in the media, suggesting that [^{68}Ga]Ga-thiooxine is possibly dissociated (at least at some level) and enters the cells by transferrin mediated mechanism. Bovine transferrin has a similar affinity to human transferrin for gallium, however, it doesn't bind efficiently to TfR1 in human cancer cells.[274,275] Thus, in the presence of FBS, a large amount of ^{68}Ga might binds to bovine transferrin in the media without entering the cells causing low cellular uptake value. However, in the presence of human serum, ^{68}Ga binds to human apo-transferrin in the media and enters the cells by transferrin mediated mechanism.[274,275] However, protein binding result of [^{68}Ga]Ga-thiooxine using size exclusion chromatography did not confirm or reject binding of [^{68}Ga]Ga-thiooxine to serum proteins. The experiment was only done using apo-transferrin in sodium bicarbonate solution, and the results exhibited similar elution profiles in the presence and absence of apo-transferrin. This experiment must be repeated using higher concentration of the ligand or else the addition of a small amount of surfactant to the mixture to increase the complex solubility.[250] Thus, [^{68}Ga]Ga-thiooxine cellular uptake pathway cannot be explained due to the inconclusive results of [^{68}Ga]Ga-thiooxine protein binding study and with no further research being undertaken. Like [^{68}Ga]Ga-thiooxine, [^{68}Ga]Ga-acetate had higher cellular uptake in the presence of human serum

than bovine serum in the media, which also can be explained based on the low binding efficiency of bovine transferrin to TfR1 in human cancer cells.[274,275]

[^{68}Ga]Ga-nitroquinoline exhibited similar cellular uptake as [^{68}Ga]Ga-acetate in human serum, along with complete binding to apo-transferrin by size exclusion chromatography. This suggest that the complex is not stable and ^{68}Ga dissociates from the ligand, binds to apo-transferrin, and enter the cells by transferrin mediated mechanism. However, [^{68}Ga]Ga-nitroquinoline is a lipophilic complex that showed good complexation by iTLC. Hence, binding to apo-transferrin might not occur at the same speed as [^{68}Ga]Ga-acetate. In the current study, [^{68}Ga]Ga-nitroquinoline incubated with apo-transferrin for 60 minutes, and different incubation times might be required to test the duration need for transferrin binding. In addition, protein binding studies must be done to other 8HQ derivatives including tropolone, clioquinol, chloroxine, and cloxyquin to investigate their protein binding mechanism and cellular uptake pathway.

As mentioned previously (see introduction section), [^{67}Ga]Ga-oxine showed higher cellular uptake and cytotoxicity against DU145 cells compared to [^{67}Ga]Ga-citrate, suggested that ^{67}Ga might cause radiotoxicity only if absorbed into cells.[26] Thus, developing 8HQ derivative complexes might generate better methods for delivering ^{67}Ga in order to investigate the radiobiology of its therapeutic effect. From the current studies, results showed that [^{68}Ga]Ga-thiooxine has the highest cellular uptake compared to all other ^{68}Ga complexes tested when incubated using DMEM media containing human serum, however more experiments are needed to understand its protein binding mechanism. Thiooxine could be a promising ligand to radiolabel ^{67}Ga, deliver it to cancer cells, and study its radiobiology as an Auger electron emitter. In addition, cellular efflux studies of [^{68}Ga]Ga-thiooxine along with the other ligands are required to measure their cellular washout over time. The therapeutic potential of radionuclides is likely to be dependent on their distribution and accumulation in cancer cells.[26,297] Thus, finding the best chemical form to deliver ^{67}Ga into cells and be sustained for adequate time is desired for better cytotoxic effect, and radiobiological investigation.

4.5 Summary and conclusion

[^{68}Ga]Ga-thiooxine exhibited unstable behaviours in iTLC results. However, the complexation was increased by doubling the concentration of the ligand. [^{68}Ga]Ga-thiooxine showed high cellular uptake compared to other ligands in the presence of human serum in the media, however, its protein speciation study was inconclusive, and more experiments are needed for more understanding of the complex biological behaviour. [^{68}Ga]Ga-oxine showed stability in iTLC results with no binding to apo-transferrin by size exclusion chromatography, indicating cellular uptake by non-transferrin pathway. [^{68}Ga]Ga-nitroquinoline showed relatively high percentage of uptake, with complete binding to apo-transferrin as determined by size exclusion chromatography, indicating cellular uptake by transferrin mediated mechanism. However, protein binding studies at different time points are required to measure the time needed for [^{68}Ga]Ga-nitroquinoline to bind to transferrin. [^{68}Ga]Ga-tropolone, -chloroxine, -cloxyquin, and -clioquinol protein binding studies should be performed to investigate their possible cellular uptake pathways. Further experiments including efflux studies of ^{68}Ga-8HQ complexes can be performed to measure their cellular washout over time. Finally, selected 8HQ derivatives can be radiolabelled with ^{67}Ga in the future and used to study the radiobiology of ^{67}Ga as an Auger electron emitter radionuclide. Among tested 8HQ derivatives in the current study, thiooxine was the best chelator for delivering gallium into cells when incubated in DMEM media containing human serum.

5 Conclusion, challenges, and future work

This chapter will explore some opportunities for future work on $^{68}Ga/^{67}Ga$. Some of these opportunities are natural extensions of the work in this thesis, while others are recommendations for future work and challenges in the field in general.

5.1 Introduction

Over the past decades, Ga^{3+} applications in medicine have become significant due to its similarity, in some aspects, to Fe^{3+}.[2] The similarities between the two metals permit gallium to bind to iron-binding proteins and biomolecules and be taken up by tumours and microorganisms as an iron analogue.[3,5] However, gallium cannot be considered an ideal analogue for iron based on their differences in other aspects, such as the inability of Ga^{3+} to be reduced under physiological conditions to Ga^{2+} or be accumulated in hematopoietic tissues (like iron). In fact, studies have shown different cellular trafficking mechanisms and pharmacokinetics *in vivo* between the two metals.[3,78] In addition, the differences between the two metals render gallium compounds to be of interest as potential therapeutic agents for disturbing the role of iron in cancer cells and bacteria.[5] The availability of gallium radioisotopes has facilitated the understanding of gallium cellular trafficking and biodistribution. It has also allowed the use of gallium as a partial iron analogue for imaging purposes.

5.2 Un-chelated gallium radioisotopes

Gallium radioisotopes (^{68}Ga and ^{67}Ga) play a significant role in modern medicine and are likely to gain more popularity in the next decade. The advantage of ^{68}Ga over other PET radioisotopes is primarily based on ^{68}Ga generator production from its long-lived mother radioisotope (t½ (^{68}Ge) = 270.95 days).[12] Generator-based production allows for the continued presence of radionuclide and onsite radiolabelling. However, some failings of the ^{68}Ga generator include impurities in the elution that can reduce radiolabelling yields.[1,30] On the contrary, ^{67}Ga is a cyclotron produced radionuclide.[10] ^{67}Ga (in citrate complex form) has been extensively studied and used clinically as a cancer (especially lymphoma) and infection imaging agent.[5,94,95,96] The ^{67}Ga citrate uptake mechanism is based on transchelation to transferrin (subsequent binding to sites with high transferrin receptor expression), lactoferrin (especially in neutrophil leukocytes), and macrophages, which can be observed in tumours, infections, and inflammation sites. Thus, ^{67}Ga citrate has low specificity and cannot be considered as a specific imaging agent.[9,95,96,132,133,134] However, ^{67}Ga citrate's non-specific activity can be an advantage for localising possible causes of fever of unknown origin (FUO) due to the extensive disease spectrum causing FUO.[96,142]

5.3 Gallium labelled siderophores

As mentioned previously, microorganisms can secrete siderophores and sequester gallium as gallium–siderophores complex. This permits the use of the radioactive gallium-siderophore complexes as specific infection imaging agents, unlike ^{67}Ga citrate.[98] Recent studies on ^{68}Ga and ^{67}Ga radiolabelled with different siderophores showed promising results *in vitro* and *in vivo*, suggesting these compounds might have sensitivity and specificity as infection imaging agents and potential for clinical translation.[97–103] Studies have shown the selectivity of different gallium siderophore complexes to individual pathogens. Thus, selecting the relevant siderophore before imaging might be a crucial step for a better diagnosis. Siderophore selectivity to specific pathogens is an advantage if bacterial species causing an infection are known. However, it can also be a limitation if bacterial species are unknown, leading to false-negative results. For example, $^{68/67}$Ga siderophores might not be the best approach for imaging patients with FUO.

^{68}Ga and ^{67}Ga radiolabelled with DFO showed high specificity and sensitivity for imaging an animal model infected with *P. aeruginosa* and *S. aureus*[99,100] and can be used to investigate animal models bearing infections with fungal and bacteria that utilise ferrioxamine. In the current study, we provided a simple radiosynthesis of [^{68}Ga]Ga-DFO using GMP-grade reagents as a foundation for imaging graft infection in humans. To the best of our knowledge, no clinical studies have been conducted to investigate the sensitivity and specificity of $^{68/67}$Ga siderophores in imaging graft infection. In addition, studies that investigated the sensitivity and specificity of DFO radiolabelled with ^{68}Ga and ^{67}Ga used a relatively high pathogen burden (CFU > 10^8) in lung infection and myositis animal models.[99,100] However, a graft can be infected with lower bacterial densities. For example, a preclinical study showed that the threshold for bacteria to cause graft infection in more than 50% of aortic grafts in canine models could be as low as 10^2 for *P. aeruginosa*.[298] The rapid renal excretion of [^{68}Ga]Ga-DFO might be a limitation in patients with a low-grade infection. However, the high selectivity of [^{68}Ga]Ga-DFO to specific pathogens combined with its low background activity might render infection sites sufficient uptake compared to surrounding tissues. The ability of [^{68}Ga]Ga-DFO in detecting graft infection cannot be predicted since no studies have been conducted to investigate that. However, this could be a step towards an early graft infection diagnosis that can reduce morbidity and mortality.

5.4 Gallium as anti-cancer drugs

KP46 is an anti-cancer drug developed based on the rationale of making a stable compound that can be absorbed efficiently from the gut. Consequently, it has better anti-cancer activity compared to orally administered gallium salts.[4,108] Although KP46 showed some efficacy against renal cell carcinoma in phase I clinical trial, studies on its *in vivo* trafficking and tumour accumulation are lacking. In the current study, we investigated the *in vivo* behaviour of KP46 after oral

administration of [$^{68/67}$Ga]KP46 as a tracer or combined with a pharmacologically relevant dose of KP46. We provided supporting evidence that the presence of a pharmacological dose of KP46 increased gut absorption compared to orally administered [$^{68/67}$Ga]KP46 as a tracer. However, delivery of gallium to tissues and tumour was still low. Based on studies from literature that showed poor gut absorption after oral administration of ^{67}Ga citrate, even in the presence of a high dose of a single oral administration of gallium chloride,[190,191,276] and the current study results, we concluded that KP46 does not enhance gut absorption compared to gallium salts after a single oral administration. However, the *in vivo* trafficking of KP46 using [$^{68/67}$Ga]KP46 can be investigated in the future after prolonged oral administration to mimic the method used in the clinical trial. A prolonged period of time might be necessary for progressive tumour uptake and cytotoxicity.[231]

We have also investigated the chemical form of [$^{68/67}$Ga]KP46 in the gut and organs. We showed that the majority of activity is no longer in a form of [$^{68/67}$Ga]KP46, indicating that KP46 does not survive the gut intact. Our studies show that KP46 is a poor vehicle for delivering gallium to tumours. However, due to the anti-cancer activity of 8-hydroxyquinoline *in vitro,*[234,277] its contribution to the KP46 cytotoxic mode of action cannot be ignored. Nothing is known of the role of KP46 as a vehicle for delivery of 8-hydroxyquinoline to tumours *in vivo* or cancer cells *in vitro*. The *in vivo* trafficking of 8-hydroxyquinoline could be investigated in the future as an active component for the KP46 mode of action. For example, 8-hydroxyquinoline can be radiolabelled with carbon-11, and its trafficking and anti-cancer activity can be studied post oral administration and compared to KP46 in a head-to-head study.

In addition to investigating KP46 activity against cancer, a preclinical study in hypercalcemia of malignancy rats model showed a decrease in blood calcium levels post oral administration of 24 mg/kg of KP46 for ten days, indicating the possible effect of KP46 on blood calcium levels and suggesting that KP46 might share some of gallium nitrate mechanism of actions.[238] However, more research could be carried out to investigate the ability of KP46 as a hypercalcemia treatment agent to overcome gallium nitrate (Ganite) renal toxicity post intravenous injection, especially in patients with impaired renal function.[229]

5.5 ^{67}Ga as a potential therapeutic agent

As mentioned previously, ^{67}Ga emits Auger electrons (in addition to its gamma emissions) and is as a potential therapeutic radionuclide.[26] The final chapter of this work was inspired by a previous study that showed the ability of 8-hydroxyquinoline to increase ^{67}Ga cell incorporation and, consequently, the ^{67}Ga therapeutic effect.[26] We investigated multiple 8-hydroxyquinoline derivatives as a delivery vehicle for ^{68}Ga into A375 cells. ^{68}Ga showed the highest cellular incorporation when radiolabelled with thiooxine compared to other derivatives. However, further

cellular work and protein binding studies can be done to find the best chelator for delivering ^{67}Ga into cells and studying its radiobiology. It should be noted that 8-hydroxyquinoline and its derivatives might not be the best chelators for delivering ^{67}Ga into cells,[26] and other chelators could be tested. The continuous development of gallium chelators might renew the ^{67}Ga opportunity as a therapeutic radionuclide.

In conclusion, this work explored gallium-essential applications of ^{67}Ga and ^{68}Ga in cancer therapeutics, infections, and cell biology. ^{67}Ga and ^{68}Ga (as radioactive isotopes) can provide quantitative information on certain pharmacological compounds stability, biodistribution, tissue accumulation, and route of excretion, via the use of imaging by SPECT and PET scanners. Studying KP46 with radioactive gallium, as described in this work, can be one of many ways to investigate gallium compounds as anti-cancer drugs. In addition, different siderophores can be radiolabelled with radioactive gallium as an iron analogue to image infection. [^{68}Ga]Ga-DFO has a low regulatory barrier to clinical translation, and it can encourage the clinical translation of other ^{68}Ga siderophores complexes.

References

1 M. D. Bartholomä, A. S. Louie, J. F. Valliant and J. Zubieta, Technetium and Gallium Derived Radiopharmaceuticals: Comparing and Contrasting the Chemistry of Two Important Radiometals for the Molecular Imaging Era, *Chem. Rev.*, 2010, **110**, 2903–2920.

2 C. R. Chitambar, Medical Applications and Toxicities of Gallium Compounds, *Int. J. Environ. Res. Public Health*, 2010, **7**, 2337–2361.

3 L. R. Bernstein, Gallium, Therapeutic Effects, *Encycl. Met.*, 1997, **140**, 29–34.

4 C. R. Chitambar, Gallium-Containing Anticancer Compounds, *Future Med. Chem.*, 2012, **4**, 1257–1272.

5 C. R. Chitambar, Gallium and its Competing Roles with Iron in Biological Systems, *Biochim. Biophys. Acta - Mol. Cell Res.*, 2016, **1863**, 2044–2053.

6 C. R. Chitambar and W. E. Antholine, Iron-Targeting Antitumor Activity of Gallium Compounds and Novel Insights into Triapine-Metal Complexes, *Antioxid. Redox Signal.*, 2013, **18**, 956–972.

7 R. E. Weiner, The Mechanism of 67Ga Localization in Malignant Disease, *Nucl. Med. Biol.*, 1996, **23**, 745–751.

8 W. R. Harris and V. L. Pecoraro, Thermodynamic Binding Constants for Gallium Transferrin, *Biochemistry*, 1983, **22**, 292–299.

9 L. R. Bernstein, Mechanisms of Therapeutic Activity for Gallium, *Pharmacol. Rev.*, 1998, **50**, 665–682.

10 M. A. Green and M. J. Welch, Gallium Radiopharmaceutical Chemistry, *Int. J. Radiat. Appl. Instrumentation.*, 1989, **16**, 435–448.

11 W. R. Harris and L. Messori, A comparative Study of Aluminum (III), Gallium (III), Indium (III), and Thallium (III) Binding to Human Serum Transferrin, *Coord. Chem. Rev.*, 2002, **228**, 237–262.

12 I. Velikyan, Prospective of 68Ga-Radiopharmaceutical Development, *Theranostics*, 2014, **4**, 47–80.

13 M. C. Graham, K. S. Pentlow, O. Mawlawi, R. D. Finn, F. Daghighian and S. M. Larson, An Investigation of the Physical Characteristics of 66Ga as an Isotope for PET Imaging

and Quantification, *Med. Phys.*, 1997, **24**, 317–326.

14 R. W. Howell, Radiation Spectra for Auger-Electron Emitting Radionuclides: Report No.2 of AAPM Nuclear Medicine Task Group No.6, *Med.Phys*, 1992, **19**, 1371–1383.

15 M. Brucer, G. A. Andrews and H. D. Bruner, A Study of Gallium72, *Radiology*, 1951, **61**, 534–612.

16 K. Duncan, Radiopharmaceuticals in PET Imaging, *J. Nucl. Med. Technol.*, 1998, **26**, 228–234.

17 S. Shahhosseini, PET Radiopharmaceuticals, *Iran. J. Pharm. Res.*, 2011, **10**, 1–2.

18 M. M. Khalil, J. L. Tremoleda, T. B. Bayomy and W. Gsell, Molecular SPECT Imaging: An Overview, *Int. J. Mol. Imaging*, 2011, **2011**, 1–15.

19 J. Cal-Gonzalez, I. Rausch, L. K. S. Sundar, M. L. Lassen, O. Muzik, E. Moser, L. Papp and T. Beyer, Hybrid Imaging: Instrumentation and Data Processing, *Front. Phys.*, 2018, **6**, 47.

20 G. J. R. Cook and V. Goh, Molecular Imaging of Bone Metastases and Their Response to Therapy, *J. Nucl. Med.*, 2020, **61**, 799–806.

21 C. L. Edwards and R. L. Hayes, Tumor Scanning with 67Ga Citrate, *SNM Journals*, 1969, **10**, 103–106.

22 T. H. Farncombe, H. C. Gifford, M. V. Narayanan, P. H. Pretorius, P. Bruyant, M. Gennert and M. A. King, An Optimization of Reconstruction Parameters and Investigation into the Impact of Photon Scatter in 67Ga SPECT, *IEEE Trans. Nucl. Sci.*, 2002, **49 I**, 2148–2154.

23 J. Okada, Y. Imai, H. Tamada, O. Kawashiro, N. Yui, T. Togawa, F. Kinoshita and H. Ito, 67Ga Planar Imaging With a Low-Energy Collimator and Scatter Correction Using the Triple Energy Window Method, *Nucl. Med. Commun.*, 1999, **20**, 647–657.

24 E. Bombardieri, C. Aktolun, R. P. Baum, A. Bishof-Delaloye, J. Buscombe, J. F. Chatal, L. Maffioli, R. Moncayo, L. Mortelmans and S. N. Reske, 67Ga Scintigraphy: Procedure Guidelines for Tumour Imaging, *Eur. J. Nucl. Med. Mol. Imaging*, 2003, **30**, 125–131.

25 P. L. Esquinas, C. Rodríguez-Rodríguez, T. V. F. Esposito, J. Harboe, M. Bergamo, A. Celler, K. Saatchi, V. Sossi and U. O. Häfeli, Dual SPECT Imaging of 111In and 67Ga to Simultaneously Determine In Vivo the Pharmacokinetics of Different Radiopharmaceuticals: A Quantitative Tool in Pre-Clinical Research, *Phys. Med. Biol.*, 2018, **63**, 647–657.

26 M. F. bi. Othman, N. R. Mitry, V. J. Lewington, P. J. Blower and S. Y. A. Terry, Re-assessing Gallium-67 as a Therapeutic Radionuclide, *Nucl. Med. Biol.*, 2017, **46**, 12–18.

27 A. Ku, V. J. Facca, Z. Cai and R. M. Reilly, Auger Electrons for Cancer Therapy – A Review, *EJNMMI Radiopharm. Chem.*, 2019, **4**, 1–36.

28 M. F. bin Othman, E. Verger, I. Costa, M. Tanapirakgul, M. S. Cooper, C. Imberti, V. J. Lewington, P. J. Blower and S. Y. A. Terry, In Vitro Cytotoxicity of Auger Electron-Emitting [67Ga]Ga-Trastuzumab, *Nucl. Med. Biol.*, 2020, **80**–**81**, 57–64.

29 I. Velikyan, 68Ga-Based Radiopharmaceuticals: Production and Application Relationship, *Molecules*, 2015, **20**, 12913–12943.

30 R. Cusnir, A. Cakebread, M. S. Cooper, J. D. Young, P. J. Blower and M. T. Ma, The Effects of Trace Metal Impurities on Ga-68-Radiolabelling with a Tris(3-hydroxy-1,6-dimethylpyridin-4-one) (THP) Chelator, *RSC Adv.*, 2019, **9**, 37214–37221.

31 A. Ghai, B. Singh, M. Li, T. A. Daniels, R. Coelho, K. Orcutt, G. L. Watkins, J. P. Norenberg, D. Cvet and M. K. Schultz, Optimizing the Radiosynthesis of [68Ga]DOTA-MLN6907 Peptide Containing Three Disulfide Cyclization Bonds – A GCC Specific Chelate for Clinical Radiopharmaceuticals, *Appl. Radiat. Isot.*, 2018, **140**, 333–341.

32 B. Bumbaca, Z. Li and D. K. Shah, Pharmacokinetics of Protein and Peptide Conjugates, *Drug Metab. Pharmacokinet.*, 2019, **34**, 42–54.

33 N. K. Pianou, P. Z. Stavrou, E. Vlontzou, P. Rondogianni, D. N. Exarhos and I. E. Datseris, More Advantages in Detecting Bone and Soft Tissue Metastases from Prostate Cancer Using (18)F-PSMA PET/CT, *Hell. J. Nucl. Med.*, 2019, **22**, 6–9.

34 P. Sharp and S. K. Srai, Molecular Mechanisms Involved in Intestinal Iron Absorption, *World J. Gastroenterol.*, 2007, **13**, 4716–4724.

35 A. R. West and P. S. Oates, Mechanisms of Heme Iron Absorption : Current Questions and Controversies, *World J. Gastroenterol.*, 2008, **14**, 4101–4110.

36 B. Silva and P. Faustino, An Overview of Molecular Basis of Iron Metabolism Regulation and the Associated Pathologies, *Biochim. Biophys. Acta*, 2015, **1852**, 1347–1359.

37 M. Shayeghi, G. O. Latunde-Dada, J. S. Oakhill, A. H. Laftah, K. Takeuchi, N. Halliday, Y. Khan, A. Warley, F. E. McCann, R. C. Hider, D. M. Frazer, G. J. Anderson, C. D. Vulpe, R. J. Simpson and A. T. McKie, Identification of an Intestinal Heme Transporter, *Cell*, 2005, **122**, 789–801.

38 G. O. Latunde-Dada, K. Takeuchi, R. J. Simpson and A. T. McKie, Haem Carrier Protein 1 (HCP1): Expression and Functional Studies in Cultured Cells, *FEBS Lett.*, 2006, **580**, 6865–6870.

39 B. K. Fuqua, C. D. Vulpe and G. J. Anderson, Intestinal Iron Absorption, *J. Trace Elem. Med. Biol.*, 2012, **26**, 115–119.

40 S. Le Blanc, M. D. Garrick and M. Arredondo, Heme Carrier Protein 1 Transports Heme and is Involved in Heme-Fe Metabolism, *Am. J. Physiol. - Cell Physiol.*, 2012, **302**, 1780–1785.

41 N. C. Andrews, The Iron Transporter DMT1, *Int. J. Biochem. Cell Biol.*, 1999, **31**, 991–994.

42 D. Frazer and G. Anderson, The Orchestration of Body Iron Intake: How and Where Do Enterocytes Receive their Cues?, *Blood Cells, Mol. Dis.*, 2003, **30**, 288–297.

43 J. Wang and K. Pantopoulos, Regulation of Cellular Iron Metabolism, *Biochem. J.*, 2011, **434**, 365–381.

44 C. M. Craven, J. Alexander, M. Eldridge, J. P. Kushner, S. Bernstein and J. Kaplan, Tissue Distribution and Clearance Kinetics of Non-Transferrin-Bound Iron in the Hypotransferrinemic Mouse: A Rodent Model for Hemochromatosis, *Proc. Natl. Acad. Sci. U. S. A.*, 1987, **84**, 3457–3461.

45 C. E. Peterson and R. H. Ettinger, Radioactive Iron Absorbtion in Siderosis (Hemochromatosis) of the Liver, *Am. J. Med.*, 1953, **15**, 518–524.

46 C. R. Chitambar, The Therapeutic Potential of Iron-Targeting Gallium Compounds in Human Disease: From Basic Research to Clinical Application, *Pharmacol. Res.*, 2017, **115**, 56–64.

47 D. R. Richardson and P. Ponka, The Molecular Mechanisms of the Metabolism and Transport of Iron in Normal and Neoplastic Cells, *Biochim. Biophys. Acta*, 1997, **1331**, 1–40.

48 H. Sun, H. Li and P. J. Sadler, Transferrin as a Metal Ion Mediator, *Chem. Rev.*, 1999, **99**, 2817–2842.

49 H. Huebers, B. Josephson, E. Huebers, E. Csiba and C. Finch, Uptake and Release of Iron from Human Transferrin, *Proc. Natl. Acad. Sci. U. S. A.*, 1981, **78**, 2572–2576.

50 K. Thorstensen and I. Romslo, The Role of Transferrin in the Mechanism of Cellular Iron

Uptake, *Biochem. J.*, 1990, **271**, 1–9.

51 H. Shi1, K. Bencze, T. Stemmler and C. Philpott, A Cytosolic Iron Chaperone that Delivers Iron to Ferritin, *Science.*, 2008, **320**, 1207–1210.

52 D. R. Richardson, D. J. R. Lane, E. M. Becker, M. L. H. Huang, M. Whitnall, Y. S. Rahmanto, A. D. Sheftel and P. Ponka, Mitochondrial Iron Trafficking and the Integration of Iron Metabolism Between the Mitochondrion and Cytosol, *Proc. Natl. Acad. Sci. U. S. A.*, 2010, **107**, 10775–10782.

53 K. J. Logan, P. K. Ng, C. J. Turner, R. P. Schmidt, U. K. Terner, J. R. Scott, B. C. Lentle and A. A. Noujaim, Comparative Pharmacokinetics of 67Ga and 59Fe in Humans, *Int. J. Nucl. Med. Biol.*, 1981, **8**, 271–276.

54 L. Hayes and E. Hartman, The Binding of Gallium by Blood Serum, *J. Pharmacol. Exp. Ther.*, 1969, **168**, 193–198.

55 A. W. Harris and R. G. Sephton, Transferrin Promotion of 67 Ga and 59 Fe Uptake by Cultured Mouse Myeloma Cells, *Cancer Res.*, 1977, **37**, 3634–3638.

56 S. Vallabhajosula, J. Harwig and J. Siemsen, Radiogallium Localization in Tumors : Blood Binding and Transport and the Role of Transferrin, *J. Nucl. Med.*, 1980, **21**, 650–656.

57 J. Clausen, C. J. Edeling and J. Fogh, 67Ga Binding to Human Serum Proteins and Tumor Components, *Cancer Res.*, 1974, **34**, 1931–1937.

58 K. Y. Tzen, Z. H. Oster, H. N. Wagner and M. F. Tsan, Role of Iron-Binding Proteins and Enhanced Capillary Permeability on the Accumulation of Gallium-67, *J. Nucl. Med.*, 1979, **21**, 31–36.

59 Z. Chikh, N. T. Ha-Duong, G. Miquel and J. M. El Hage Chahine, Gallium Uptake by Transferrin and Interaction with Receptor 1, *J. Biol. Inorg. Chem.*, 2007, **12**, 90–100.

60 J. M. El Hage Chahine, M. Hémadi and N. T. Ha-Duong, Uptake and Release of Metal Ions by Transferrin and Interaction with Receptor 1, *Biochim. Biophys. Acta*, 2012, **1820**, 334–347.

61 C. R. Chitambar and Z. Zivkovic, Uptake of Gallium-67 by Human Leukemic Cells: Demonstration of Transferrin Receptor-Dependent and Transferrin-Independent Mechanisms, *Cancer Res.*, 1987, **47**, 3929–3934.

62 C. A. Luttropp, J. A. Jackson, B. J. Jones, M. H. Sohn, R. E. Lynch and K. A. Morton, Uptake of Gallium-67 in Transfected Cells and Tumors Absent or Enriched in the

Transferrin Receptor, *J. Nucl. Med.*, 1998, **39**, 1405–1411.

63 S. M. Chan, P. B. Hoffer, N. Maric and P. Duray, Inhibition of Gallium-67 Uptake in Melanoma by an Anti-Human Transferrin Receptor Monoclonal Antibody, *J. Nucl. Med.*, 1987, **28**, 1303–1307.

64 S. R. Vallabhajosula, J. F. Harwig and W. Wolf, The Mechanism of Tumor Localization of Gallium-67 Citrate: Role of Transferrin Binding and Effect of Tumor pH, *Int. J. Nucl. Med. Biol.*, 1981, **8**, 363–370.

65 S. J. McGregor and J. H. Brock, Effect of pH and Citrate on Binding of Iron and Gallium by Transferrin in Serum, *Clin. Chem.*, 1992, **38**, 1883–1885.

66 A. C. Illing, A. Shawki, C. L. Cunningham and B. Mackenzie, Substrate Profile and Metal-Ion Selectivity of Human Divalent Metal-Ion Transporter-1, *J. Biol. Chem.*, 2012, **287**, 30485–30496.

67 M. Tumors, Gallium-67 Localization in Rat and Mouse Tumors, *Science.*, 1970, **167**, 289–290.

68 N. P. Davies, Y. S. Rahmanto, C. R. Chitambar and D. R. Richardson, Resistance to the Antineoplastic Agent Gallium Nitrate Results in Marked Alterations in Intracellular Iron and Gallium Trafficking : Identification of Novel Intermediates, *J. Pharmacol. Exp. Ther.*, 2006, **317**, 153–162.

69 H. G. Sherman, C. Jovanovic, S. Stolnik, K. Baronian, A. J. Downard and F. J. Rawson, New Perspectives on Iron Uptake in Eukaryotes, *Front. Mol. Biosci.*, 2018, **5**, 97.

70 J. P. Liuzzi, F. Aydemir, H. Nam, M. D. Knutson and R. J. Cousins, Zip14 (Slc39a14) Mediates Non-Transferrin-Bound Iron Uptake into Cells, *Proc. Natl. Acad. Sci. U. S. A.*, 2006, **103**, 13612–13617.

71 B. Sturm, U. Lassacher, N. Ternes, A. Jallitsch, H. Goldenberg and B. Scheiber-Mojdehkar, The Influence of Gallium and Other Metal Ions on the Uptake of Non-Transferrin-Bound Iron by Rat Hepatocytes, *Biochimie*, 2006, **88**, 645–650.

72 W. H. Koppenol and R. H. Hider, Iron and Redox Cycling. Do's and Don'ts, *Free Radic. Biol. Med.*, 2019, **133**, 3–10.

73 P. Brissot, M. Ropert, C. Le Lan and O. Loréal, Non-Transferrin Bound Iron: A Key Role in Iron Overload and Iron Toxicity, *Biochim. Biophys. Acta*, 2012, **1820**, 403–410.

74 C. R. Chitambar and D. Sax, Regulatory Effects of Gallium on Transferrin-Independent

Iron Uptake by Human Leukemic HL60 Cells, *Blood*, 1992, **80**, 505–511.

75 A. Sturrock, J. Alexander, J. Lamb, C. M. Craven and J. Kaplan, Characterization of a Transferrin-Independent Uptake System for Iron in HeLa Cells, *J. Biol. Chem.*, 1990, **265**, 3139–3145.

76 T. L. Wright, P. Brissot, Wei-Lan Ma and R. A. Weisiger, Characterization of Non-Transferrin-Bound Iron Clearance by Rat Liver, *J. Biol. Chem.*, 1986, **261**, 10909–10914.

77 J. Kaplan, I. Jordan and A. Sturrock, Regulation of the Transferrin-Independent Iron Transport System in Cultured Cells, *J. Biol. Chem.*, 1991, **266**, 2997–3004.

78 R. G. Sephton, G. S. Hodgson, S. D. Abrew and A. W. Harris, Ga-67 and Fe-59 Distribution in Mice, *J. Nucl. Med.*, 1978, **19**, 930–935.

79 D. C. Swartzendruber, B. L. Byrd, R. L. Hayes, B. Nelson and R. L. Tyndall, Preferential Localization of Gallium-67 Citrate in Tissues of Leukemic Mice, *J Natl Cancer Inst*, 1970, **44**, 695–700.

80 M. Petrik, A. Vlckova, Z. Novy, L. Urbanek, H. Haas and C. Decristoforo, Selected 68Ga-Siderophores Versus 68Ga-Colloid and 68 Ga-Citrate: Biodistribution and Small Animal Imaging in Mice, *Biomed Pap Med Fac Univ Palacky Olomouc Czech Repub*, 2014, **159**, 60–66.

81 T. Ujula, S. Salomäki, A. Autio, P. Luoto, T. Tolvanen, P. Lehikoinen, T. Viljanen, H. Sipilä, P. Härkönen and A. Roivainen, 68Ga-Chloride PET Reveals Human Pancreatic Adenocarcinoma Xenografts in Rats-Comparison with FDG, *Mol. Imaging Biol.*, 2010, **12**, 259–268.

82 A. Autio, H. Virtanen, T. Tolvanen, H. Liljenbäck, V. Oikonen, T. Saanijoki, R. Siitonen, M. Käkelä, A. Schüssele, M. Teräs and A. Roivainen, Absorption, Distribution and Excretion of Intravenously Injected 68Ge/68Ga Generator Eluate in Healthy Rats, and Estimation of Human Radiation Dosimetry, *EJNMMI Res.*, 2016, **6**, 1–11.

83 S. M. Larson, Mechanisms of Localization of Gallium-67 in Tumors, *Semin. Nucl. Med.*, 1978, **8**, 193–203.

84 R. Sephton, Relationships between the Metabolism of 67Ga and Iron, *Int. J. Nucl. Med. Biol.*, 1981, **8**, 323–331.

85 L. Hayes, J. Rafter and B. Byrd, Studies of the In Vivo Entry of Ga-67 into Normal and Malignant Tissue, *J. Nucl. Med.*, 1981, **22**, 325–332.

86 M. F. Tsan, L. J. Anghileri and V. Scheffel, Mechanism of Gallium-67 Accumulation in Tumors, *J. Nucl. Med.*, 1986, **27**, 1215–1219.

87 W. P. Bradley and J. F. Weiss, Effect of Iron Deficiency on the Biodistribution and Tumor Uptake of Ga-67 Citrate in Animals: Concise Communication, *J. Nucl. Med.*, 1979, **20**, 243–247.

88 R. L. Hayes, J. E. Carlton and B. L. Byrd, Bone Scanning with Gallium-68: A Carrier Effect, *J. Nucl. Med.*, 1965, **6**, 605–610.

89 K. Schomäcker, W. G. Franke, E. Henke, W. D. Fromm, G. Maka and G. J. Beyer, The Influence of Isotopic and Nonisotopic Carriers on the Biodistribution and Biokinetics of M3+-Citrate Complexes, *Eur. J. Nucl. Med.*, 1986, **11**, 345–349.

90 M. H. Sohn, B. J. Jones, J. H. Whiting, F. L. Datz, R. E. Lynch and K. A. Morton, Distribution of Gallium-67 in Normal and Hypotransferrinemic Tumor-Bearing Mice, *J. Nucl. Med.*, 1993, **34**, 2135–2143.

91 L. H. Raymond, B. L. Byrd, J. J. Rafter and J. E. Carlton, The Effect of Scandiumon the Tissue Distribution of Ga-67 in Normal and Tumor-Bearing Rodents, *J. Nucl. Med.*, 1980, **21**, 361–365.

92 A. W. Ford-Hutchinson and D. J. Perkins, The Binding of Scandium Ions to Transferrin In Vivo and In Vitro, *J. Chem. Inf. Model.*, 1971, **21**, 55–59.

93 A. B. Kelson, M. Carnevali and V. Truong-Le, Gallium-Based Anti-Infectives: Targeting Microbial Iron-Uptake Mechanisms, *Curr. Opin. Pharmacol.*, 2013, **13**, 707–716.

94 F. Mota, A. A. Ordonez, G. Firth, C. A. Ruiz-Bedoya, M. T. Ma and S. K. Jain, Radiotracer Development for Bacterial Imaging, *J. Med. Chem*, 2020, **63**, 1964–1977.

95 T. Xu and Y. Chen, Research Progress of [68Ga]Citrate PET's Utility in Infection and Inflammation Imaging: A Review, *Mol. Imaging Biol.*, 2020, **22**, 22–32.

96 A. A. Ordonez and S. K. Jain, Pathogen-Specific Bacterial Imaging in Nuclear Medicine, *Semin Nucl Med*, 2018, **48**, 182–194.

97 M. Petrik, H. Haas, G. Dobrozemsky, C. Lass-fl, A. Helbok, M. Blatzer, H. Dietrich and C. Decristoforo, 68Ga-Siderophoresfor PET Imaging of Invasive Pulmonary Aspergillosis : Proof of Principle, *J Nucl Med*, 2010, **51**, 639–645.

98 M. Petrik, H. Haas, M. Schrettl, A. Helbok, M. Blatzer and C. Decristoforo, In Vitro and In Vivo Evaluation of Selected Ga-Siderophores for Infection Imaging, *Nucl. Med. Biol.*,

2012, **39**, 361–369.

99 J. A. Ioppolo, D. Caldwell, O. Beiraghi, L. Llano, M. Blacker, J. F. Valliant and P. J. Berti, Ga-Labeled Deferoxamine Derivatives for Imaging Bacterial Infection: Preparation and Screening of Functionalized Siderophore Complexes, *Nucl. Med. Biol.*, 2017, **52**, 32–41.

100 M. Petrik, E. Umlaufova, V. Raclavsky, A. Palyzova, V. Havlicek, J. Pfister, C. Mair, Z. Novy, M. Popper, M. Hajduch and C. Decristoforo, 68Ga-Labelled Desferrioxamine-B for Bacterial Infection Imaging, *Eur. J. Nucl. Med. Mol. Imaging*, 2021, **48**, 372–382.

101 M. Petrik, G. M. Franssen, H. Haas, P. Laverman, C. Hörtnagl, M. Schrettl, A. Helbok and C. Lass-flörl, Preclinical Evaluation of Two 68Ga-Siderophores as Potential Radiopharmaceuticals for Aspergillus Fumigatus Infection Imaging, *Eur J Nucl Med Mol Imaging*, 2012, **39**, 1175–1183.

102 M. Petrik, H. Haas, P. Laverman, M. Schrettl, G. M. Franssen, M. Blatzer and C. Decristoforo, 68Ga-Triacetylfusarinine C and 68Ga-Ferrioxamine E for Aspergillus Infection Imaging: Uptake Specificity in Various Microorganisms, *Mol. Imaging Biol.*, 2014, **16**, 102–108.

103 M. Petrik, E. Umlaufova, V. Raclavsky, A. Palyzova, V. Havlicek, H. Haas, Z. Novy, D. Dolezal, M. Hajduch and C. Decristoforo, Imaging of Pseudomonas Aeruginosa Infection with Ga-68 Labelled Pyoverdine for Positron Emission Tomography, *Sci. Rep.*, 2018, **8**, 15698.

104 M. Naser, S. Mehrnoosh, E. Hassan, N. Hajar, S. Mehdi, S. Mohsen, G. Mehdi, P. Hoda and A. Mehdi, A Review on Iron Chelators in Treatment of Iron Overload Syndromes., *Int. J. Hematol. stem cell Res.*, 2016, **10**, 239–247.

105 C. R. Chitambar, Gallium Nitrate for the Treatment of Non-Hodgkin's Lymphoma, *Expert Opin. Investig. Drugs*, 2004, **13**, 531–541.

106 M. K. Samson, R. J. Fraile, L. H. Baker and R. O'Bryan, Phase I-II Clinical Trial of Gallium Nitrate (NSC-15200), *Cancer Clin. Trials*, 1980, **3**, 131–136.

107 P. Collery, H. Millart, M. Pluot and L. J. Anghileri, Effects of Gallium Chloride Oral Administration on Transplanted C3HBA Mammary Adenocarcinoma: Ga, Mg, Ca and Fe Concentration and Anatomopathological Characteristics, *Anticancer Res.*, 1986, **6**, 1085–1088.

108 S. M. Valiahdi, P. Heffeter, M. A. Jakupec, R. Marculescu, W. Berger, K. Rappersberger and B. K. Keppler, The Gallium Complex KP46 Exerts Strong Activity Against Primary

Explanted Melanoma Cells and Induces Apoptosis in Melanoma Cell Lines, *Melanoma Res.*, 2009, **19**, 283–293.

109 W. C. Strahle and J. C. Handley, Iron in Infection and Immunity, *Cell Host Microbe*, 2013, **13**, 509–519.

110 C. Wandersman and I. Stojiljkovic, Bacterial Heme Sources: The Role of Heme, Hemoprotein Receptors and Hemophores, *Curr. Opin. Microbiol.*, 2000, **3**, 215–220.

111 N. D. Hammer and E. P. Skaar, Molecular Mechanisms of Staphylococcus Aureus Iron Acquisition, *Annu. Rev. Microbiol.*, 2011, **65**, 129–147.

112 P. Lisiecki, Transferrin and Lactoferrin-Human Iron Sources for Enterococci, *Polish J. Microbiol.*, 2017, **66**, 419–425.

113 T. C. Johnstone and E. M. Nolan, Beyond Iron: Non-Classical Biological Functions of Bacterial Siderophores, *Dalt. Trans.*, 2015, **44**, 6320–6339.

114 E. Ahmed and S. J. M. Holmström, Siderophores in Environmental Research: Roles and Applications, *Microb. Biotechnol.*, 2014, **7**, 196–208.

115 G. Majka, K. Śpiewak, K. Kurpiewska, P. Heczko, G. Stochel, M. Strus and M. Brindell, A High-Throughput Method for the Quantification of Iron Saturation in Lactoferrin Preparations, *Anal. Bioanal. Chem.*, 2013, **405**, 5191–5200.

116 S. Abdollahi and W. R. Harris, Determination of the Binding Constant of Terbium-Transferrin, *Iran. J. Chem. Chem. Eng.*, 2006, **25**, 45–52.

117 R. C. Hider and X. Kong, Chemistry and Biology of Siderophores, *Nat. Prod. Rep.*, 2010, **27**, 637–657.

118 B. R. Wilson, A. R. Bogdan, M. Miyazawa, K. Hashimoto and Y. Tsuji, Siderophores in Iron Metabolism : From Mechanism to Therapy Potential, *Trends Mol. Med.*, 2016, **22**, 1077–1090.

119 N. Noinaj, N. C. Easley, M. Oke, N. Mizuno, J. Gumbart, E. Boura, A. N. Steere, O. Zak, P. Aisen, E. Tajkhorshid, R. W. Evans, A. R. Gorringe, A. B. Mason, A. C. Steven and S. K. Buchanan, Structural Basis for Iron Piracy by Pathogenic Neisseria, *Nature*, 2012, **483**, 53–58.

120 M. Caza and J. W. Kronstad, Shared and Distinct Mechanisms of Iron Acquisition by Bacterial and Fungal Pathogens of Humans, *Front. Cell. Infect. Microbiol.*, 2013, **4**, 80.

121 D. Perkins-balding, M. Ratliff-Griffin and I. Stojiljkovic, Iron Transport Systems in Neisseria Meningitidis, *Microbiol. Mol. Biol. Rev.*, 2004, **68**, 154–171.

122 R. Pandey and G. M. Rodriguez, A Ferritin Mutant of Mycobacterium Tuberculosis Is Highly Susceptible to Killing by Antibiotics and Is Unable to Establish a Chronic Infection in Mice, *Infect. Immun.*, 2012, **80**, 3650–3659.

123 P. Arosio, L. Elia and M. Poli, Ferritin, Cellular Iron Storage and Regulation, *IUBMB Life*, 2017, **69**, 414–422.

124 M. Rivera, Bacterioferritin: Structure, Dynamics, and Protein-Protein Interactions at Play in Iron Storage and Mobilization, *Acc. Chem. Res.*, 2017, **50**, 331–340.

125 N. Noinaj, M. Guillier, T. J. Barnard and S. K. Buchanan, TonB-Dependent Transporters: Regulation, Structure, and Function, *Annu. Rev. Microbiol.*, 2010, **64**, 43–60.

126 M. M. Welling, A. W. Hensbergen, A. Bunschoten, A. H. Velders, M. Roestenberg and F. W. B. van Leeuwen, An Update on Radiotracer Development for Molecular Imaging of Bacterial Infections, *Clin. Transl. Imaging*, 2019, **7**, 105–124.

127 S. S. Ali and N. N. Vidhale, Bacterial Siderophore and their Application : A review, *Int. J. Curr. Microbiol. App. Sci*, 2013, **2**, 303–312.

128 M. Petrik, C. Zhai, H. Haas and C. Decristoforo, Siderophores for Molecular Imaging Applications, *Clin. Transl. Imaging*, 2017, **5**, 15–27.

129 E. A. Weinstein, A. A. Ordonez, V. P. DeMarco, A. M. Murawski, S. Pokkali, E. M. MacDonald, M. Klunk, R. C. Mease, M. G. Pomper and S. K. Jain, Imaging Enterobacteriaceae Infection In Vivo with 18F-Fluorodeoxysorbitol Positron Emission Tomography, *Sci. Transl. Med.*, 2014, **6**, 259ra146.

130 M. Bray, J. Lawler, J. Paragas, P. B. Jahrling and D. J. Mollura, Molecular Imaging of Influenza and other Emerging Respiratory Viral Infections, *J. Infect. Dis.*, 2011, **203**, 1348–1359.

131 V. Kumar and D. K. Boddeti, in *Theranostics, Gallium-68, and Other Radionuclides: A Pathway to Personalized Diagnosis and Treatment*, eds. R. Baum and F. Rosch, Springer, Berlin, Heidelberg, 2013, vol. 194, chap.2, pp. 189–219.

132 P. Lankinen, T. Noponen, A. Autio, P. Luoto, J. Frantzèn, E. Löyttyniemi, A. J. Hakanen, H. T. Aro and A. Roivainen, A Comparative 68Ga-Citrate and 68Ga-Chloride PET/CT Imaging of Staphylococcus Aureus Osteomyelitis in the Rat Tibia, *Contrast Media Mol.*

Imaging, 2018, **2018**, 9892604.

133 A. Roivainen, S. Jalkanen and C. Nanni, Gallium-Labelled Peptides for Imaging of Inflammation, *Eur. J. Nucl. Med. Mol. Imaging*, 2012, **39**, 68–77.

134 S. P. Salomäki, J. Kemppainen, U. Hohenthal, P. Luoto, O. Eskola, P. Nuutila, M. Seppänen, L. Pirilä, J. Oksi and A. Roivainen, Head-to-Head Comparison of 68Ga-Citrate and 18F-FDG PET/CT for Detection of Infectious Foci in Patients with Staphylococcus Aureus Bacteraemia, *Contrast Media Mol. Imaging*, 2017, **2017**, 3179607.

135 D. C. Swartzendruber, B. Nelson and R. L. Hayes, Gallium-67 Localization in Lysosomal-Like Granules of Leukemic and Nonleukemic Murine Tissues, *J. Natl. Cancer Inst.*, 1971, **46**, 941–952.

136 S. M. Kennedy, D. C. Walker, A. S. Belzberg and J. C. Hogg, Macrophage Accumulation of Inhaled Gallium-67 Citrate in Normal Lungs, *J. Nucl. Med.*, 1985, **26**, 1195–1201.

137 R. Codd, T. Richardson-Sanchez, T. J. Telfer and M. P. Gotsbacher, Advances in the Chemical Biology of Desferrioxamine B, *ACS Chem. Biol.*, 2018, **13**, 11–25.

138 D. K. Hughes, B. A. Sci and N. Med, Nuclear Medicine and Infection Detection : The Relative Effectiveness of Imaging with 99mTc-Stannous Fluoride Colloid – Labeled Leukocytes and with 67Ga-Citrate, *J. Nucl. Med. Technol.*, 2003, **31**, 196–201.

139 V. Kumar, D. K. Boddeti, S. G. Evans and S. Angelides, 68Ga-Citrate-PET for Diagnostic Imaging of Infection in Rats and for Intra-Abdominal Infection in a Patient, *Curr. Radiopharm.*, 2012, **5**, 71–75.

140 C. Nanni, C. Errani, L. Boriani, L. Fantini, V. Ambrosini, S. Boschi, D. Rubello, C. Pettinato, M. Mercuri, A. Gasbarrini and S. Fanti, 68Ga-Citrate PET/CT for Evaluating Patients with Infections of the Bone: Preliminary Results, *J. Nucl. Med.*, 2010, **51**, 1932–1936.

141 O. L. Nielsen, P. Afzelius, D. Bender, H. C. Schønheyder, P. S. Leifsson, K. M. Nielsen, J. O. Larsen, S. B. Jensen and A. K. Alstrup, Comparison of Autologous (111)In-Leukocytes, (18)F-FDG, (11)C-Methionine, (11)C-PK11195 and (68)Ga-Citrate for Diagnostic Nuclear Imaging in a Juvenile Porcine Haematogenous Staphylococcus Aureus Osteomyelitis Model, *Am. J. Nucl. Med. Mol. Imaging*, 2015, **5**, 169–182.

142 N. Ergül and T. F. Çermik, FDG-PET or PET/CT in Fever of Unknown Origin: The Diagnostic Role of Underlying Primary Disease, *Int. J. Mol. Imaging*, 2011, **2011**, 318051.

143 H. Haas, Fungal Siderophore Metabolism with a Focus on Aspergillus Fumigatus, *Nat. Prod. Rep.*, 2014, **31**, 1266–1276.

144 D. Pucar and M. M. Sadeghi, 18F-Fluorodeoxyglucose PET Imaging in Aortic Graft Infection: Many more Questions than Answers, *J. Nucl. Cardiol.*, 2021, **28**, 1017–1020.

145 Y. Tokuda, H. Oshima, Y. Araki, Y. Narita, M. Mutsuga, K. Kato and A. Usui, Detection of Thoracic Aortic Prosthetic Graft Infection with 18F-Fluorodeoxyglucose Positron Emission Tomography/Computed Tomography, *Eur. J. Cardio-thoracic Surg.*, 2013, **43**, 1183–1187.

146 C. Lauri, R. Iezzi, M. Rossi, G. Tinelli, S. Sica, A. Signore, A. Posa, A. Tanzilli, C. Panzera, M. Taurino, P. A. Erba and Y. Tshomba, Imaging Modalities for the Diagnosis of Vascular Graft Infections: A Consensus Paper amongst Different Specialists, *J. Clin. Med.*, 2020, **9**, 1510.

147 C. J. Palestro, C. Love, G. G. Tronco and M. B. Tomas, Role of Radionuclide Imaging in the Diagnosis of Postoperative Infection, *Radiographics*, 2000, **20**, 1649–1660.

148 W. Dong, Y. Li, J. Zhu, J. Xia, L. He, M. Yun, J. Jiao, G. Zhu, M. Hacker, Y. Wei, X. Zhang and X. Li, Detection of Aortic Prosthetic Graft Infection with 18F-FDG PET/CT Imaging, Concordance with Consensus MAGIC Graft Infection Criteria, *J. Nucl. Cardiol.*, 2021, **28**, 1005–1016.

149 A. A. Ordonez, M. A. Sellmyer, G. Gowrishankar, C. A. Ruiz-Bedoya, E. W. Tucker, C. J. Palestro, D. A. Hammoud and S. K. Jain, Molecular Imaging of Bacterial Infections: Overcoming the Barriers to Clinical Translation, *Sci. Transl. Med.*, 2019, **11**, aax8251.

150 H. Al-Khayyat, N. Toussaint, S. Holt and P. Hughes, Gram-Negative Sepsis Following Biopsy of a Transplant Recipient with Asymptomatic Allograft Pyelonephritis, *CEN Case Reports*, 2017, **6**, 46–49.

151 M. Liberatore, A. P. Iurilli, F. Ponzo, D. Prosperi, C. Santini, P. Baiocchi, L. Rizzo, F. Speziale, P. Fiorani and A. C. Colella, Clinical Usefulness of Technetium-99m-HMPAO-Labeled Leukocyte Scan in Prosthetic Vascular Graft Infection, *J. Nucl. Med.*, 1998, **39**, 875–879.

152 M. Liberatore, A. P. Lurilli, F. Ponzo, D. Prosperi, C. Santini, P. Baiocchi, P. Serra, L. Rizzo, F. Speziale, P. Fiorani and A. C. Colella, Aortofemoral Graft Infection: The Usefulness of 99mTc-HMPAO-Labelled Leukocyte Scan, *Eur. J. Vasc. Endovasc. Surg.*, 1997, **14**, 27–29.

153 P. A. Erba, G. Leo, M. Sollini, C. Tascini, R. Boni, R. N. Berchiolli, F. Menichetti, M. Ferrari, E. Lazzeri and G. Mariani, Radiolabelled Leucocyte Scintigraphy versus Conventional Radiological Imaging for the Management of Late, Low-Grade Vascular Prosthesis Infections, *Eur. J. Nucl. Med. Mol. Imaging*, 2014, **41**, 357–368.

154 A. K. Buck, S. Nekolla, S. Ziegler, A. Beer, B. J. Krause, K. Herrmann, K. Scheidhauer, H. J. Wester, E. J. Rummeny, M. Schwaiger and A. Drzezga, SPECT/CT, *J. Nucl. Med.*, 2008, **49**, 1305–1319.

155 A. S. Mark, S. M. McCarthy, A. A. Moss and D. Price, Detection of Abdominal Aortic Graft Infection : Comparison of CT and In-Labeled White Blood Cell Scans, *AJR Am J Roentgenol*, 1985, **144**, 315–318.

156 M. C. Brunner, R. S. Mitchell, J. C. Baldwin, D. R. James, C. Olcott, J. T. Mehigan, I. R. McDougall and D. C. Miller, Prosthetic Graft Infection: Limitations of Indium White Blood Cell Scanning, *J. Vasc. Surg.*, 1986, **3**, 42–48.

157 L. Malone, M. B. A. Cm, E. Grigorenko and D. Stalons, Clinical Utility of Indium 111–Labeled White Blood Cell Scintigraphy for Evaluation of Suspected Infection, *open forum Infect. Dis.*, 2014, **1**, ofu089.

158 M. S. Khaja, O. Sildiroglu, K. Hagspiel, P. K. Rehm, K. J. Cherry and U. C. Turba, Prosthetic Vascular Graft Infection Imaging, *Clin. Imaging*, 2013, **37**, 239–244.

159 I. Banzo, R. Quirce, J. Serrano, J. Jimenez, O. Tabuenca and J. M. Carril, Ga-67 Citrate Scan in Vascular Graft Infection, *Ann. Nucl. Med.*, 1992, **6**, 235–239.

160 D. A. Causey, W. A. Fajman, G. D. Perdue, M. J. Constantino, P. J. Sones and Y. A. Tarcan, 67Ga Scintigraphy in Postoperative Synthetic Graft Infections, *AJR Am J Roentgenol*, 1980, **134**, 1041–1045.

161 P. Thivolle, L. Varenne, Y. Heyden and M. Berger, Gallium-67 Citrate Whole Body Scanning for the Localization of Inected Vascular Synthetic Grafts, *Clin. Nucl. Med.*, 1985, **10**, 330–332.

162 A. J. Simpson, K. Astin, Jan and M. R. Peck, Diagnosis of an Abdominal Aortic Graft Abscess, *Clin. Nucl. Med.*, 1979, **4**, 338–340.

163 J. R. Haaga, G. N. Baldwin, N. E. Reich, E. Beven, A. Kramer, A. Weinstein, T. R. Havrilla, F. E. Seidelmann, A. H. Namba and C. M. Parrish, CT Detection of Infected Synthetic Grafts: Preliminary Report of a New Sign, *AJR Am J Roentgenol*, 1978, **131**, 317–320.

164 Z. Keidar, A. Engel, A. Hoffman, O. Israel and S. Nitecki, Prosthetic Vascular Graft Infection: The Role of 18F-FDG PET/CT, *J. Nucl. Med.*, 2007, **48**, 1230–1236.

165 B. R. Sah, L. Husmann, D. Mayer, A. Scherrer, Z. Rancic, G. Puippe, R. Weber and B. Hasse, Diagnostic Performance of 18F-FDG-PET/CT in Vascular Graft Infections, *Eur. J. Vasc. Endovasc. Surg.*, 2015, **49**, 455–464.

166 M. Spacek, O. Belohlavek, J. Votrubova, P. Sebesta and P. Stadler, Diagnostics of 'Non-Acute' Vascular Prosthesis Infection Using 18F-FDG PET/CT: Our Experience with 96 Prostheses, *Eur. J. Nucl. Med. Mol. Imaging*, 2008, **36**, 850–858.

167 K. Fukuchi, Y. Ishida, M. Higashi, T. Tsunekawa, H. Ogino, K. Minatoya, K. Kiso and H. Naito, Detection of Aortic Graft Infection by Fluorodeoxyglucose Positron Emission Tomography: Comparison with Computed Tomographic Findings, *J. Vasc. Surg.*, 2005, **42**, 919–925.

168 P. Berger, I. Vaartjes, A. Scholtens, F. L. Moll, G. J. De Borst, B. De Keizer, M. L. Bots and J. D. Blankensteijn, Differential FDG-PET Uptake Patterns in Uninfected and Infected Central Prosthetic Vascular Grafts, *Eur. J. Vasc. Endovasc. Surg.*, 2015, **50**, 376–383.

169 E. I. Reinders Folmer, G. C. I. Von Meijenfeldt, M. J. Van der Laan, A. W. J. M. Glaudemans, R. H. J. A. Slart, B. R. Saleem and C. J. Zeebregts, Diagnostic Imaging in Vascular Graft Infection: A Systematic Review and Meta-Analysis, *Eur. J. Vasc. Endovasc. Surg.*, 2018, **56**, 719–729.

170 E. Banin, A. Lozinski, K. M. Brady, E. Berenshtein, P. W. Butterfield, M. Moshe, M. Chevion, E. P. Greenberg and E. Banin, The Potential of Desferrioxamine-Gallium as an Anti-Pseudomonas Therapeutic Agent, *Proc. Natl. Acad. Sci. U. S. A.*, 2008, **105**, 16761–16766.

171 J. R. Dilworth and S. I. Pascu, The Chemistry of PET Imaging with Zirconium-89, *Chem. Soc. Rev.*, 2018, **47**, 2554–2571.

172 H. Kornreich-Leshem, C. Ziv, E. Gumienna-Kontecka, R. Arad-Yellin, Y. Chen, M. Elhabiri, A. M. Albrecht-Gary, Y. Hadar and A. Shanzer, Ferrioxamine B Analogues: Targeting the FoxA Uptake System in The Pathogenic Yersinia Enterocolitica, *J. Am. Chem. Soc.*, 2005, **127**, 1137–1145.

173 B. Gaurav, W. H. Jung and J. w. Kronstad, Iron Acquisition in Fungal Pathogens of Humans, *Physiol. Behav.*, 2017, **9**, 215–227.

174 D. H. Howard, Acquisition, Transport, and Storage of Iron by Pathogenic Fungi, *Clin.*

Microbiol. Rev., 1999, **12**, 394–404.

175 C. Denekamp and E. Egbaria, Remarkable Amine-TFA Self Assembly, *J. Am. Soc. Mass Spectrom.*, 2004, **15**, 356–362.

176 A. I. Gasco-López, A. Santos-Montes and R. Izquierdo-Hornillos, The Effect of Different Amines Added to Eluents as Silanol Masking Agents on the Chromatographic Behavior of Some Diuretics in Reversed-Phase High-Performance Liquid Chromatography Using C18 Packings, *J. Chromatogr. Sci.*, 1997, **35**, 525–535.

177 J. Nawrocki, The Silanol Group and Its Role in Liquid Chromatography, *J. Chromatogr. A*, 1997, **779**, 29–71.

178 Y. Bentur, M. McGuigan and G. Koren, Deferoxamine (Desferrioxamine): New Toxicities for an Old Drug, *Drug Saf.*, 1991, **6**, 37–46.

179 W. D. Lehmann and H. C. Heinrich, Ferrioxamine and its Hexadentate Iron-Chelating Metabolites in Human Post-Desferal Urine Studied by High-Performance Liquid Chromatography and Fast Atom Bombardment Mass Spectrometry, *Anal. Biochem.*, 1990, **184**, 219–227.

180 G. Peters, H. Keberle, K. Schmid and H. Brunner, Distribution and Renal Excretion of Desferrioxamine and Ferrioxamine in the Dog and in the Rat, *Biochem. Pharmacol.*, 1966, **15**, 93–109.

181 H. Keberle, The Biochemistry of Desferrioxamine and its Relation to Iron Metabolism, *Ann. N. Y. Acad. Sci.*, 1964, **119**, 758—768.

182 M. . A. Zivanovic, D. M. Taylor and V. R. McCready, The Chemical Form of Gallium-67 in Urine, *Int. J. Nucl. Med. Biol.*, 1978, **5**, 97–100.

183 J. Fielding and G. M. Brunstrom, Estimation of Ferrioxamine and Desferrioxamine in Urine., *J. Clin. Pathol.*, 1964, **17**, 395–398.

184 M. K. van Gelder, J. A. W. Jong, L. Folkertsma, Y. Guo, C. Blüchel, M. C. Verhaar, M. Odijk, C. F. Van Nostrum, W. E. Hennink and K. G. F. Gerritsen, Urea Removal Strategies for Dialysate Regeneration in a Wearable Artificial Kidney, *Biomaterials*, 2020, **234**, 119735.

185 M. M. Hart and R. H. Adamson, Antitumor Activity and Toxicity of Salts of Inorganic Group 3A Metals: Aluminum, Gallium, Indium, and Thallium, *Proc. Natl. Acad. Sci. U. S. A.*, 1971, **68**, 1623–1626.

186 M. M. Hart, C. F. Smith, S. T. Yancey and R. H. Adamson, Toxicity and Antitumor Activity of Gallium Nitrate and Periodically Related Metal Salts, *J. Natl. Cancer Inst.*, 1971, **47**, 1121–1127.

187 H. C. Dudley and M. D. Levine, Studies of the Toxic Action of Gallium, *J. Pharmacol. Exp. Ther.*, 1948, **95**, 487–493.

188 P. Collery, B. Keppler, C. Madoulet and B. Desoize, Gallium in Cancer Treatment, *Crit. Rev. Oncol. / Hematol.*, 2002, **42**, 283–296.

189 J. . Lin, I. Bekersky, N. S. Brown, S. Mong, F. Lee, R. A. Newman and D. H. Ho, Normocalcemic Effect of Gallium Nitrate in a Hypercalcemic Rat Model, *Cancer Res.*, 1995, **55**, 307–311.

190 J. C. Bellen, B. Chatterton, S. Pengjis and C. Tsopelas, Gallium-67 Complexes as Radioactive Markers to Assess Gastric and Colonic Transit, *J Nucl Med*, 1995, **36**, 513–517.

191 A. Taylor, N. Chafetz, J. Hollenbeck and W. Hooser, The Source of Fecal Gallium-Clinical Implications: Concise Communication, *J Nucl Med*, 1978, **19**, 1214–1216.

192 I. H. Krakoff, R. A. Newman and R. S. Goldberg, Clinical Toxicologic and Pharmacologic Studies of Gallium Nitrate, *Cancer*, 1979, **44**, 1722–1727.

193 J. H. Malfetano, J. A. Blessing, H. D. Homesley and P. Hanjani, A phase II Trial of Gallium Nitrate (NSC 15200) in Advanced or Recurrent Squamous Cell Carcinoma of the Cervix, *Invest. New Drugs*, 1991, **9**, 109–111.

194 L. K. Webster, I. N. Olver, K. H. Stokes, R. G. Sephton, B. L. Hillcoat and J. F. Bishop, A Pharamacokinetic and Phase II Study of Gallium Nitrate in Patients with Non-Small Cell Lung Cancer, *Cancer Chemother. Pharmacol.*, 2000, **45**, 55–58.

195 J. H. Malfetano, J. A. Blessing and H. D. Homesley, A Phase II Trial of Gallium Nitrate (NSC 15200) in Nonsquamous Cell Carcinoma of the Cervix, *Am J Clin Oncol*, 1995, **18**, 495–497.

196 K. Jabboury, D. Frye, F. A. Holmes, G. Fraschini and G. Hortobagyi, Phase II Evaluation of Gallium Nitrate by Continuous Infusion in Breast Cancer, *Invest. New Drugs*, 1989, **7**, 225–229.

197 V. A. Canfield and A. P. Lyss, A Phase II Trial of Gallium Nitrate in Advanced Previously Untreated Colorectal Cancer, *Invest. New Drugs*, 1993, **11**, 335–336.

198 R. P. Warrell, C. J. Coonley, D. J. Straus and C. W. Young, Treatment of Patients with Advanced Malignant Lymphoma Using Gallium Nitrate Administered as a Seven-Day Continuous Infusion, *Cancer*, 1983, **51**, 1982–1987.

199 E. Even-sapir and O. Israel, Gallium-67 Scintigraphy : A Cornerstone in Functional Imaging of Lymphoma, *Eur J Nucl Med Mol Imaging*, 2003, **30**, S65–S81.

200 K. A. Morton, J. Jarboe and E. M. Burke, Gallium-67 Imaging in Lymphoma : Tricks of the Trade, *J. Nucl. Med. Technol.*, 2000, **28**, 221–232.

201 M. Gasparini, E. Bombardieri, M. Castellani, C. Tondini, L. Maffioli and L. Devizzi, Gallium-67 Scintigraphy Evaluation of Therapy in Non-Hodgkin's Lymphoma chemotherapy, *J. Nucl. Med.*, 1998, **39**, 1586–1590.

202 E. D. Crawford, J. H. Saiers, L. H. Baker, J. H. Costanzi and R. M. Bukowski, Gallium Nitrate in Advanced Bladder Carcinoma: Southwest Oncology Goup Study, *Urology*, 1991, **38**, 355–357.

203 P. A. Seligman and E. D. Crawford, Treatment of Advanced Transitional Cell Carcinoma of the Bladder with Continuous-Infusion Gallium Nitrate, *J. Natl. Cancer Inst.*, 1991, **83**, 1582–1584.

204 P. Collery, H. Millart, D. Lamiable, R. Vistelle, P. Rinjard, G. Tran, B. Gourdier, C. Cossart, J. C. Bouana, C. Pechery, J. C. Etienne, H. Choisy and J. M. Dubois De Montreynaud, Clinical Pharmacology of Gallium Chloride After Oral Administration in Lung Cancer Patients, *Anticancer Res.*, 1989, **9**, 353–356.

205 P. Collery, H. Millart and J. P. Simoneau, Experimental Treatment of Mammary Carcinomas by Gallium Chloride After Oral Administration: Intratumor Dosages of Gallium, Anatomopathologic Study and Intracellular Microanalysis, *Trace Elem. Med.*, 1984, **1**, 159–161.

206 P. Collery, H. Millart, J. P. Simoneau, M. Pluot, S. Halpern, R. Vistelle, D. Lamiable, H. Choisy, P. Coudoux and J. C. Etienne, in *Proceeding of the 13th International Congress of Chemotherapy*, eds. K. H. Spitzy and K. Karrer, H. Egermann, Vienna, 1983.

207 P. Collery, H. Millart, O. Ferrand, J. B. Jouet, J. P. Dubois, G. Barthes, C. Pourny, C. Pechery, H. Choisy, A. Cattan, J. M. Dubios De Montreynaud and J. C. Etienne, Gallium Chloride Treatment of Cancer Patients After Oral Administration: A Pilot Study, *Chemiotherapia*, 1985, **4**, 1165–1166.

208 M. A. Jakupec, M. Galanski, V. B. Arion, C. G. Hartinger and B. K. Keppler, Antitumour

Metal Compounds: More Than Theme and Variations, *Dalt. Trans.*, 2008, **14**, 183–194.

209 A. R. Timerbaev, Advances in Developing Tris(8-quinolinolato)gallium(iii) as an Anticancer Drug: Critical Appraisal and Prospects, *Metallomics*, 2009, **1**, 193–198.

210 J. H. Lundberg and C. R. Chitambar, Interaction of Gallium Nitrate with Fludarabine and Iron Chelators: Effects on the Proliferation of Human Leukemic HL60 Cells, *Cancer Res.*, 1990, **50**, 6466–6470.

211 X. Sun, R. Ge, Z. Cai, H. Sun and Q. Y. He, Iron Depletion Decreases Proliferation and Induces Apoptosis in a Human Colonic Adenocarcinoma Cell Line, Caco2, *J. Inorg. Biochem.*, 2009, **103**, 1074–1081.

212 K. Fukuchi, S. Tomoyasu, N. Tsuruoka and K. Gomi, Iron Deprivation-Induced Apoptosis in HL-60 Cells, *FEBS Lett.*, 1994, **350**, 139–142.

213 C. R. Chitambar and P. A. Seligman, Effects of Different Transferrin Forms on Transferrin Receptor Expression, Iron Uptake, and Cellular Proliferation of Human Leukemic HL60 Cells, *J. Clin. Invest.*, 1986, **78**, 1538–1546.

214 J. S. Rasey, N. J. Nelson and S. M. Larson, Tumor Cell Toxicity of Stable Gallium Nitrate: Enhancement by Transferrin and Protection by Iron, *Eur. J. Cancer Clin. Oncol.*, 1982, **18**, 661–668.

215 C. R. Chitambar, W. G. Matthaeus, W. E. Antholine, K. Graff and W. J. O'Brien, Inhibition of Leukemic HL60 Cell Growth by Transferrin-Gallium: Effects of Ribonucleotide Reductase and Demonstration of Drug Synergy with Hydroxyurea, *Blood*, 1988, **72**, 1930–1936.

216 D. W. Hedley, E. H. Tripp, P. Slowiaczek and G. J. Mann, Effect of Gallium on DNA Synthesis by Human T-Cell Lymphoblasts, *Cancer Res.*, 1988, **48**, 3014–3018.

217 C. R. Chitambar, E. J. Massey and P. A. Seligman, Regulation of Transferrin Receptor Expression on Human Leukemic Cells During Proliferation and Induction of Differentiation, *J. Clin. Invest.*, 1983, **72**, 1314–1325.

218 K. L. Chang, W. T. Liao, C. L. Yu, C. C. E. Lan, L. W. Chang and H. S. Yu, Effects of Gallium on Immune Stimulation and Apoptosis Induction in Human Peripheral Blood Mononuclear Cells, *Toxicol. Appl. Pharmacol.*, 2003, **193**, 209–217.

219 C. R. Chitambar, J. P. Wereley and S. Matsuyama, Gallium-Induced Cell Death in Lymphoma: Role of Transferrin Receptor Cycling, Involvement of Bax and the

Mitochondria, and Effects of Proteasome Inhibition, *Mol. Cancer Ther.*, 2006, **5**, 2834–2843.

220 W. Gao, Y. Pu, K. Q. Luo and D. C. Chang, Temporal Relationship Between Cytochrome C Release and Mitochondrial Swelling During UV-Induced Apoptosis in Living HeLa Cells, *J. Cell Sci.*, 2001, **114**, 2855–2862.

221 Y. L. P. Ow, D. R. Green, Z. Hao and T. W. Mak, Cytochrome C: Functions Beyond Respiration, *Nat. Rev. Mol. Cell Biol.*, 2008, **9**, 532–542.

222 A. G. Porter and R. U. Jänicke, Emerging Roles of Caspase-3 in Apoptosis, *Cell Death Differ.*, 1999, **6**, 99–104.

223 C. R. Chitambar and J. P. Wereley, Resistance to the Antitumor Agent Gallium Nitrate in Human Leukemic Cells is Associated with Decreased Gallium/Iron Uptake, Increased Activity of Iron Regulatory Protein-1, and Decreased Ferritin Production, *J. Biol. Chem.*, 1997, **272**, 12151–12157.

224 P. Ponka, Cellular Iron Metabolism, *Kidney Int.*, 1999, **55**, 2–11.

225 C. R. Chitambar, Z. Zivkovic-Gilgenbach, J. Narasimhan and W. E. Antholine, Development of Drug Resistance to Gallium Nitrate through Modulation of Cellular Iron Uptake, *Cancer Res.*, 1990, **50**, 4468–4472.

226 R. P. Warrell, R. Israel, M. Frisone, T. Snyder, J. J. Gaynor and R. S. Bockman, Gallium Nitrate for Acute Treatment of Cancer-Related Hypercalcemia: A randomized, Double-Blind Comparison to Calcitonin, *Ann. Intern. Med.*, 1988, **108**, 669–674.

227 R. P. Warrell, Gallium Nitrate for the Treatment of Bone Metastases, *Cancer*, 1997, **80**, 1680–1685.

228 R. T. Warrell, N. W. Alcock and R. S. Bockman, Gallium Nitrate Inhibits Accelerated Bone Turnover in Patients with Bone Metastases, *J. Clin. Oncol.*, 1987, **5**, 292–298.

229 M. Smith, FDA Approves Ganite for Hypercalcemia, *Oncol. Times*, 2003, **25**, 24.

230 Y. Wang, W. Zhang and Y. Li, X-ray Crystal Structure of Gallium Tris- (8-hydroxyquinoline): Intermolecular π - π Stacking Interactions in the Solid State, *Chem. Mater*, 1999, **11**, 530–532.

231 K. B. Collery P, Jakupec MA, Kynast B, Preclinical and Early Clinical Development of the Oral Gallium Complex KP46 (FFC11), *Met. Ions Biol. Med.*, 2006, **46**, 521–524.

232 R. Gogna, E. Madan, B. Keppler and U. Pati, Gallium Compound GaQ 3-Induced Ca 2+ Signalling Triggers p53-Dependent and -Independent Apoptosis in Cancer Cells, *Br. J. Pharmacol.*, 2012, **166**, 617–636.

233 J. A. Lessa, G. L. Parrilha and H. Beraldo, Gallium Complexes as New Promising Metallodrug Candidates, *Inorganica Chim. Acta*, 2012, **393**, 53–63.

234 J. Zhou, H. Zhang, P. Gu, J. B. Margolick, D. Yin and Y. Zhang, Cancer Stem/Progenitor Cell Active Compound 8-Quinolinol in Combination with Paclitaxel Achieves an Improved Cure of Breast Cancer in the Mouse Model, *Breast Cancer Res Treat*, 2009, **115**, 1–7.

235 H. A. Saadeh, K. A. Sweidan and M. S. Mubarak, Recent Advances in the Synthesis and Biological Activity of 8-Hydroxyquinolines, *Molecules*, 2020, **25**, 4321.

236 P. Collery, J. L. Domingo and B. K. Keppler, Preclinical Toxicology and Tissue Gallium Distribution of a Novel Antitumour Gallium Compound: Tris (8-quinolinolato) gallium (III), *Anticancer Res.*, 1996, **16**, 687–692.

237 H. G. Stampfer, G. M. Gabb and S. B. Dimmitt, Why Maximum Tolerated Dose?, *Br. J. Clin. Pharmacol.*, 2019, **85**, 2213–2217.

238 M. Thiel, T. Schilling, D. C. Gey, R. Ziegler, P. Colley and B. K. Keppler, in *Relevance of Tumor Models for Anticancer Drug Development*, eds. H. H. Fiebing and A. M. Burger, Karger, Basel, 1999, vol.54, chap.9, pp. 439–443.

239 U. Jungwirth, J. Gojo, T. Tuder, G. Walko, M. Holcmann, T. Schöfl, K. Nowikovsky, N. Wilfinger, S. Schoonhoven, C. R. Kowol, R. Lemmens-Gruber, P. Heffeter, B. K. Keppler and W. Berger, Calpain-Mediated Integrin Deregulation as a Novel Mode of Action for the Anticancer Gallium Compound KP46, *Mol. Cancer Ther.*, 2014, **13**, 2436–49.

240 M. R. Gerasimov, M. Franceschi, N. D. Volkow, A. Gifford, S. J. Gatley, D. Marsteller, P. E. Molina and S. L. Dewey, Comparison Between Intraperitoneal and Oral Methylphenidate Administration: A Microdialysis and Locomotor Activity Study, *J. Pharmacol. Exp. Ther.*, 2000, **295**, 51–57.

241 K. B. Nemes, M. Abermann, E. Bojti, G. Grézal, S. Al-behaisi and I. Klebovich, Oral, Intraperitoneal and Intravenous Pharmacokinetics of Deramciclane and its N-desmethyl Metabolite in the Rat, *J. Pharm. Pharmacol.*, 2000, **52**, 47–51.

242 B. K. Keppler, *presented in part at the 1st Metals in Medicine Workshop, Paris, November*, 2019.

243 Clinicaltrials.gov, https://clinicaltrials.gov/ct2/show/NCT04143789, (accessed 24 March 2021).

244 Y. Wang, Y. Mei, Y. Song, C. Bachus, C. Sun, H. Sheshbaradaran and M. Glogauer, AP-002: A Novel Inhibitor of Osteoclast Differentiation and Function without Disruption of Osteogenesis, *Eur. J. Pharmacol.*, 2020, **889**, 173613.

245 J. Baselga, M. G. Kris, H. I. Scher, M. Phillips and R. T. Heelan, Phase II Trial of Gallium Nitrate in Previously Treated Patients with Small Cell Lung Cancer, *Invest. New Drugs*, 1993, **11**, 85–86.

246 A. M. Senderowicz, R. Reid, D. Headlee, T. Abornathy, R. M. Lush, E. Reed, W. D. Figg and E. A. Sausville, A Phase II Trial of Gallium Nitrate in Patients with Androgen-Metastatic Prostate Cancer, *Urol. Int.*, 1999, **63**, 120–125.

247 F. Trudu, F. Amato, P. Vaňhara, T. Pivetta, E. M. Peña-Méndez and J. Havel, Coordination Compounds in Cancer: Past, Present and Perspectives, *J. Appl. Biomed.*, 2015, **13**, 79–103.

248 A. V. Rudnev, L. S. Foteeva, C. Kowol, R. Berger, M. A. Jakupec, V. B. Arion, A. R. Timerbaev and B. K. Keppler, Preclinical Characterization of Anticancer Gallium(III) Complexes: Solubility, Stability, Lipophilicity and Binding to Serum Proteins, *J. Inorg. Biochem.*, 2006, **100**, 1819–1826.

249 A. A. Hummer, C. Bartel, V. B. Arion, M. A. Jakupec, W. Meyer-Klaucke, T. Geraki, P. D. Quinn, A. Mijovilovich, B. K. Keppler and A. Rompel, X-ray Absorption Spectroscopy of an Investigational Anticancer Gallium(III) Drug: Interaction with Serum Proteins, Elemental Distribution Pattern, and Coordination of the Compound in Tissue, *J. Med. Chem.*, 2012, **55**, 5601–5613.

250 S. Jatwani, A. C. Rana, G. Singh and G. Aggarwal, An Overview on Solubility Enhancement Techniques for Poorly Soluble Drugs and Solid Dispersion as an Eminent Strategic Approach, *Int. J. Pharm. Sci. Res.*, 2012, **3**, 942–956.

251 P. Winstanley and M. Orme, The Effects of Food on Drug Bioavailability, *Br. J. Clin. Pharmacol.*, 1989, **28**, 621–628.

252 J. K. Abramski, L. S. Foteeva, K. Pawlak, A. R. Timerbaev and M. Jarosz, A versatile Approach for Assaying In Vitro Metallodrug Metabolism Using CE Hyphenated with ICP-MS, *Analyst*, 2009, **134**, 1999–2002.

253 M. Groessl, A. Bytzek and C. G. Hartinger, The Serum Protein Binding of

Pharmacologically Active Gallium(III) Compounds Assessed by Hyphenated CE-MS Techniques, *Electrophoresis*, 2009, **30**, 2720–2727.

254 É. A. Enyedy, O. Dömötör, K. Bali and B. K. Keppler, Interaction of the Anticancer Gallium (III) Complexes of 8 - Hydroxyquinoline and Maltol with Human Serum Proteins, 2015, **20**, 77–88.

255 D. Zhong, A. Douhal and A. H. Zewail, Femtosecond Studies of Protein-Ligand Hydrophobic Binding and Dynamics: Human Serum Albumin, *Proc. Natl. Acad. Sci. U. S. A.*, 2000, **97**, 14056–14061.

256 S. Fatima, P. Sen, P. Sneha and C. G. Priyadoss, Hydrophobic Interaction Between Domain I of Albumin and B Chain of Detemir may Support Myristate-Dependent Detemir-Albumin Binding, *Appl. Biochem. Biotechnol.*, 2017, **182**, 82–96.

257 M. Koziolek, S. Alcaro, P. Augustijns, A. W. Basit, M. Grimm, B. Hens, C. L. Hoad, P. Jedamzik, C. M. Madla, M. Maliepaard, L. Marciani, A. Maruca, N. Parrott, P. Pávek, C. J. H. Porter, C. Reppas, D. van Riet-Nales, J. Rubbens, M. Statelova, N. L. Trevaskis, K. Valentová, M. Vertzoni, D. V. Čepo and M. Corsetti, The Mechanisms of Pharmacokinetic Food-Drug Interactions – A Perspective from the UNGAP group, *Eur. J. Pharm. Sci.*, 2019, **134**, 31–59.

258 S. S. Jambhekar and P. J. Breen, *Basic Pharmacokinetics*, Pharmaceutical Press, London, 2012.

259 E. Madan, R. Gogna, B. Keppler and U. Pati, p53 Increases Intra-Cellular Calcium Release by Transcriptional Regulation of Calcium Channel TRPC6 in GaQ3-Treated Cancer Cells, *PLoS One*, 2013, **8**, e71016.

260 N. Wilfinger, S. Austin, B. Scheiber-Mojdekhar, W. Berger, S. Reipert, M. Praschberger, J. Paur, R. Trondl, B. K. Keppler, C. C. Zielinski and K. Nowikovsky, Novel p53-Dependent Anticancer Strategy by Targeting Iron Signaling and BNIP3L-Induced Mitophagy, *Oncotarget*, 2016, **7**, 1242–1261.

261 M. D. Brand and S. M. Felber, The Intracellular Calcium Antagonist TMB-8 18-(NN-diethylamino) octyl-3,4,5- trimethoxybenzoatel Inhibits Mitochondrial ATP Production in Rat Thymocytes, *Biochem. J.*, 1984, **224**, 1027–1030.

262 M. V. Sa, E. Alberdi, E. Pe, J. Alberch and C. Matute, Bax and Calpain Mediate Excitotoxic Oligodendrocyte Death Induced by Activation of Both AMPA and Kainate Receptors, 2011, **31**, 2996–3006.

263 J. Shen, X. Sheng, Z. N. Chang, Q. Wu, S. Wang, Z. Xuan, D. Li, Y. Wu, Y. Shang, X. Kong, L. Yu, L. Li, K. Ruan, H. Hu, Y. Huang, L. Hui, D. Xie, F. Wang and R. Hu, Iron Metabolism Regulates p53 Signaling through Direct Heme-p53 Interaction and Modulation of p53 Localization, Stability, and Function, *Cell Rep.*, 2014, **7**, 180–193.

264 J. Zhang and X. Chen, p53 Tumor Suppressor and Iron Homeostasis, *FEBS J.*, 2019, **286**, 620–629.

265 Y. Yano, T. F. Budinger, S. N. Ebbe, C. A. Mathis, M. Singh, K. M. Brennan and B. R. Moyer, Gallium-68 Lipophilic Complexes for Labeling Platelets., *J. Nucl. Med.*, 1985, **26**, 1429–1437.

266 T. Brown, H. E. Lemay, B. E. Bursten, C. J. Murphy and P. M. Woodward, *Chemistry the Central Science*, Pearson, Glenview, 2012.

267 M. A. Gonda, S. A. Aaronson, N. Ellmore, V. H. Zeve and K. Nagashima, Ultrastructural Studies of Surface Features of Human Normal and Tumor Cells in Tissue Culture by Scanning and Transmission Electron Microscopy, *J. Natl. Cancer Inst.*, 1976, **56**, 245–263.

268 J. Kidriz and D. Hadii, 1H and 13C NMR Study of 8-Hydroxyquinoline and some of its 5-Substituted Analogues, *Org. Magn. Reson.*, 1981, **15**, 280–284.

269 J. G. Hamilton, The Use of Radioactive Tracers in Biology and Medicine, *Radiology*, 1942, **39**, 541–572.

270 Z. Liu, S. Wang and M. Hu, in *Developing Solid Oral Dosage Forms: Pharmaceutical Theory and Practice*, ed. Y. Qiu, Y. Chen, G. Zhang, L. Yu, V. Rao, Elsevier Inc, USA, 2009, vol. 1, chap. 11, pp. 265–288.

271 R. A. Gams and J. D. Glickson, Serum Inhibition of Ga 67 Binding by L1210 Leukemic Cells, *Cancer Res.*, 1975, **35**, 1422–1426.

272 X. Shen, G. Bin Hu, S. J. Jiang, F. R. He, W. Xing, L. Li, J. Yang, H. F. Zhu, P. Lei and G. X. Shen, Engineering and Characterization of a Baculovirus-Expressed Mouse/Human Chimeric Antibody Against Transferrin Receptor, *Protein Eng. Des. Sel.*, 2009, **22**, 723–731.

273 S. M. Larson, J. S. Rasey, D. R. Allen and N. J. Nelson, A Transferrin-Mediated Uptake of Gallium-67 in Tissue Culture by EMT-6 Sarcoma. I. Studies in Tissue Culture, *J Nucl Med*, 1979, **20**, 837–842.

274 S. P. Young and C. Garner, Delivery of Iron to Human Cells by Bovine Transferrin, *Biochem. J.*, 1990, **265**, 587–591.

275 R. G. Sephton and A. W. Harris, Brief Communication : Gallium-67 Citrate Uptake by Cultured Tumor Cells , Stimulated by Serum Transferrin, *J. Natl. Cancer Inst*, 1974, **54**, 1263–1266.

276 L. S. Valberg, P. R. Flanagan, J. Haist, J. V Frei and M. J. Chamberlain, Gastrointestinal Metabolism of Gallium and Indium: Effect of Iron Deficiency, *Clin. Investig. Med.*, 1981, **4**, 103–108.

277 S. Xiao, Z. Lin, X. Wang, J. Lu and Y. Zhao, Synthesis and Cytotoxicity Evaluation of Panaxadiol Derivatives, *Chem. Biodivers.*, 2020, **17**, 543–548.

278 V. Prachayasittikul, S. Prachayasittikul, S. Ruchirawat and V. Prachayasittikul, 8-Hydroxyquinolines: A Review of their Metal Chelating Properties and Medicinal Applications, *Drug Des. Devel. Ther.*, 2013, **7**, 1157–1178.

279 R. R. Crichton, D. T. Dexter and R. J. Ward, Brain Iron Metabolism and its Perturbation in Neurological Diseases, *J. Neural Transm.*, 2011, **118**, 301–314.

280 A. Rubbo, A. Albert and M. I. Gibson, The Influence of Chemical Constitution on Anti-Bacterial Activity. Part V: The Anti-Bacterial Action of 8-Hydroxyquinoline (oxine), *Br. J. Exp. Pathol.*, 1950, **31**, 425–441.

281 B. R. D. Short, M. A. Vargas, J. C. Thomas, S. O'Hanlon and M. C. Enright, In Vitro Activity of a Novel Compound, the Metal Ion Chelating Agent AQ+, Against Clinical Isolates of Staphylococcus Aureus, *J. Antimicrob. Chemother.*, 2006, **57**, 104–109.

282 P. Leanderson and C. Tagesson, Iron Bound to the Lipophilic Iron Chelator, 8-Hydroxyquinoline, Causes DNA Strand Breakage in Cultured Lung Cells, *Carcinogenesis*, 1996, **17**, 545–550.

283 S. Tardito, A. Barilli, I. Bassanetti, M. Tegoni, O. Bussolati, R. Franchi-Gazzola, C. Mucchino and L. Marchiò, Copper-Dependent Cytotoxicity of 8-Hydroxyquinoline Derivatives Correlates with Their Hydrophobicity and Does Not Require Caspase Activation, *J. Med. Chem.*, 2012, **55**, 10448–10459.

284 S. Zhai, L. Yang, Q. Cindy Cui, Y. Sun, Q. P. Dou and B. Yan, Tumor Cellular Proteasome Inhibition and Growth Suppression by 8-Hydroxyquinoline and Clioquinol Requires their Capabilities to Bind Copper and Transport Copper into Cells, *J Biol Inorg Chem*, 2010, **15**, 259–269.

285 W. Chan-On, N. T. B. Huyen, N. Songtawee, W. Suwanjang, S. Prachayasittikul and V. Prachayasittikul, Quinoline-Based Clioquinol and Nitroxoline Exhibit Anticancer Activity Inducing FoxM1 Inhibition in Cholangiocarcinoma Cells, *Drug Des. Devel. Ther.*, 2015, **9**, 2033–2047.

286 D. Chen, Q. C. Cui, H. Yang, R. A. Barrea, F. H. Sarkar, S. Sheng, B. Yan, G. P. V. Reddy and Q. P. Dou, Clioquinol, a Therapeutic Agent for Alzheimer's Disease, Has Proteasome-Inhibitory, Androgen Receptor-Suppressing, Apoptosis-Inducing, and Antitumor Activities in Human Prostate Cancer Cells and Xenografts, *Cancer Res.*, 2007, **67**, 1636–1644.

287 W. Q. Ding, B. Lin, J. L. Vaught, H. Yamauchi and S. E. Lind, Anticancer Activity of the Antibiotic Clioquinol, *Cancer Res.*, 2005, **65**, 3389–3395.

288 H. Yu, Y. Zhou, S. E. Lind and W. Q. Ding, Clioquinol Targets Zinc to Lysosomes in Human Cancer Cells, *Biochem. J.*, 2009, **417**, 133–139.

289 W. Q. Ding, H. J. Yu and S. E. Lind, Zinc-Binding Compounds Induce Cancer Cell Death via Distinct Modes of Action, *Cancer Lett.*, 2008, **271**, 251–259.

290 H. Yu, J. R. Lou and W. Q. Ding, Clioquinol Independently Targets NF-κB and Lysosome Pathways in Human Cancer Cells, *Anticancer Res.*, 2010, **30**, 2087–2092.

291 H. Jiang, J. E. Taggart, X. Zhang, D. M. Benbrook, S. E. Lind and W. Q. Ding, Nitroxoline (8-Hydroxy-5-nitroquinoline) Is more a Potent Anti-Cancer Agent than Clioquinol (5-Chloro-7-iodo-8-quinoline), *Cancer Lett.*, 2011, **312**, 11–17.

292 F. Buchegger, F. Perillo-Adamer, Y. M. Dupertuis and A. Bischof Delaloye, Auger Radiation Targeted into DNA: A Therapy Perspective, *Eur. J. Nucl. Med. Mol. Imaging*, 2006, **33**, 1352–1363.

293 A. R. Jonkhoff, P. C. Huijgens, R. T. Versteegh, E. B. van Dieren, G. J. Ossenkoppele, H. J. M. Martens and G. J. J. Teule, Gallium-67 Radiotoxicity in Human U937 Lymphoma Cells, *Br. J. Cancer*, 1993, **67**, 693–700.

294 A. R. Jonkhoff, P. C. Huijgens, R. T. Versteegh, A. van Lingen, G. J. Ossenkoppele, A. M. Dräger and G. J. J. Teule, Radiotoxicity of 67-Gallium on Myeloid Leukemic Blasts, *Leuk. Res.*, 1995, **19**, 169–174.

295 A. Egger, C. Rappel, M. A. Jakupec, C. G. Hartinger, P. Heffeter and B. K. Keppler, Development of an Experimental Protocol for Uptake Studies of Metal Compounds in Adherent Tumor Cells, *J. Anal. Spectrom*, 2009, **24**, 51–61.

296 J. J. Palmgrén, J. Mönkkönen, T. Korjamo, A. Hassinen and S. Auriola, Drug Adsorption to Plastic Containers and Retention of Drugs in Cultured Cells under In Vitro Conditions, *Eur. J. Pharm. Biopharm.*, 2006, **64**, 369–378.

297 E. B. Van Dieren, M. A. B. D. Plaizier, A. Van Lingen, J. C. Roos, G. W. Barendsen and G. J. J. Teule, Absorbed Dose Distribution of the Auger Emitters 67Ga and 125I and the β-emitters 67Cu, 90Y, 131I, and 186Re as a Function of Tumor Size, Uptake, and Intracellular Distribution, *Int. J. Radiat. Oncol. Biol. Phys.*, 1996, **36**, 197–204.

298 M. Vicaretti, in *Mechanims of vascular disease*, eds. R. Fitridge and M. Thompson, Adelaide, Australia, 2011, chap. 29, pp. 537–547.

Table of Figures

Table of Tables

Appendix

Table A1: Multiple comparison of ^{68}Ga cellular uptake after incubation in human serum using different ligands (one-way ANOVA followed by post hoc analysis)

Group (i)	Group (j)	Difference (i-j)		p-value
		Mean	SE	
Oxine	Thiooxine	-23.00	1.50	<0.001*
	Tropolone	-3.72	1.84	0.481
	Clioquinol	-11.94	1.84	<0.001*
	Chloroxine	-13.78	1.50	<0.001*
	Cloxyquin	-7.37	1.50	0.001*
	Nitroquinoline	-8.10	1.50	<0.001*
	Acetate	-10.97	1.84	<0.001*
Thiooxine	Tropolone	19.27	1.84	<0.001*
	Clioquinol	11.06	1.84	<0.001*
	Chloroxine	9.22	1.50	<0.001*
	Cloxyquin	15.63	1.50	<0.001*
	Nitroquinoline	14.90	1.50	<0.001*
	Acetate	12.03	1.84	<0.001*
Tropolone	Clioquinol	-8.22	2.12	0.011*
	Chloroxine	-10.05	1.84	<0.001*
	Cloxyquin	-3.64	1.84	0.509
	Nitroquinoline	-4.37	1.84	0.285
	Acetate	-7.24	2.12	0.034*
Clioquinol	Chloroxine	-1.84	1.84	0.971
	Cloxyquin	4.57	1.84	0.237
	Nitro	3.84	1.84	0.442
	Acetate	0.97	2.12	1.000
Chloroxine	Cloxyquin	6.41	1.50	0.004*
	Nitroquinoline	5.68	1.50	0.013*
	Acetate	2.81	1.84	0.787
Cloxyquin	Nitroquinoline	-0.73	1.50	1.000
	Acetate	-3.60	1.84	0.523
Nitroquinoline	Acetate	-2.87	1.84	0.768

SE: Standard error of mean; * statistically significant result. Values are in percentages